




ADVERTIMENT. L'accés als continguts d'aquesta tesi queda condicionat a l'acceptació de les condicions d'ús establertes per la següent llicència Creative Commons:  <https://creativecommons.org/licenses/?lang=ca>

ADVERTENCIA. El acceso a los contenidos de esta tesis queda condicionado a la aceptación de las condiciones de uso establecidas por la siguiente licencia Creative Commons:  <https://creativecommons.org/licenses/?lang=es>

WARNING. The access to the contents of this doctoral thesis it is limited to the acceptance of the use conditions set by the following Creative Commons license:  <https://creativecommons.org/licenses/?lang=en>



Mechanisms of androgen metabolism reprogramming in aggressive prostate cancer models and the association between androgens and COVID-19

Doctoral thesis presented by

Emily Toscano Guerra

To obtain the degree of

PhD. In biochemistry, molecular biology, and biomedicine

Universitat Autònoma de Barcelona

PhD Thesis carried out in the Cell Signaling and Cancer Progression laboratory of the
Clinical Biochemistry Group at the Vall d'Hebron Research Institute (VHIR)

Director:

Dra. Rosanna Paciucci Barzanti

Tutor:

Ibane Abasolo Olaortua

Dedicatoria

Esta dedicatoria la voy a escribir en castellano para que mis seres amados a quien debo tanto la puedan leer.

No puedo estar más orgullosa de tener unos padres ejemplares a quien debo lo que soy. Luz Guerra y Bernardo (Julio) Toscano, cada paso que doy es gracias a ustedes, por enseñarme a no rendirme jamás, cada día que lucharon para darme un techo, un alimento y una educación, han forjado en mi un espíritu de trabajo que ha sido y será mi mayor herencia. Los amo con todo mi corazón, sé que cosas buenas llegarán.

A mi adorado Junior, más que mi hermano, mi “hijastro”. Eres un ejemplo de constancia, fuerza y lucha constante, nos enseñas que una discapacidad no es una incapacidad. Has sido mi inspiración y te agradezco lo que soy.

A Arnau Bosch, quien estuvo a mi lado en este recorrido, quien me daba aliento cuando los días eran tan largos y no podía más. Quien cree en mí, incluso más que yo misma. Gracias por compartir tus días conmigo. Este trabajo también te lo dedico a ti.

Por último, a mi abuelito Federico Guerra. Donde quiera que estés... ¡por fin seré tu científica! Gracias hasta el infinito.

Agradecimientos

Primero que todo quiero agradecer a mi directora de tesis, **Rosanna Paciucci**, por darme la oportunidad de venir a Barcelona a empezar mis estudios del doctorado. Gracias por la confianza que depositaste en mí y sobre todo gracias por las enseñanzas brindadas durante este difícil recorrido.

También debo agradecer a **Timothy Thomson**, quien creyó en mí desde un primer momento, porque confió en mí para llevar a cabo varias colaboraciones de las cuales surgieron dos publicaciones durante pandemia. Gracias por el apoyo brindado.

Aunque he estado prácticamente sola en el laboratorio, siempre tuve una buena compañía, **Laila Asskour**, del grupo de Cefaleas, quien me brindó su compañía y muchas veces su ayuda durante el camino doctoral. Gracias por tu amistad.

Durante los 4 años de doctorado, tuve la oportunidad de tener dos estudiantes de máster, **Javier García** y **Anna Giné**, aunque por pandemia los tiempos fueron cortos, ambos han sido de gran apoyo en la ejecución de esta tesis.

Debo agradecer a **Patricia Bogdanov**, gracias por cada vez que pasabas por el lab y me dabas tu compañía, por tu apoyo e interés incluso hasta poco antes de marcharme. A **Marta Barber**, siempre con una sonrisa transparente, siempre dispuesta a ayudar, muchas gracias por tu compañía en aquellos días en la sala de cultivos. A **Marc Velilla**, gracias por tu amabilidad, compañerismo y buena onda, a **Xingpeng Xiao**, gracias por tu amistad y por las veces que me acompañaste a comer cuando estaba sola. ¡Te espera muchas cosas buenas! Al grupo de Investigación en Cáncer Stem Cells, liderado por **Matilde Leonart**, gracias por los consejos y el apoyo, también a **Marina y Yoelsis** por la buena onda y amabilidad para conmigo.

Por supuesto, a los compañeros del **laboratorio de Bioquímica Clínica**, liderado por **Roser Ferrer**, que, sin su apoyo durante pandemia, no hubiese sido posible realizar nuestro proyecto en COVID-19 y lograr la publicación. Asimismo, al grupo de **Inmunología traslacional**, con el apoyo de **Mónica Martínez, Iría Arrese. Manuel Hernández, Ricardo Pujol y el equipo técnico**, también lo hicieron posible. ¡Muchas gracias!

No puedo olvidarme de **Andrés, Tamara, Lourdes**, ¡guardianes del instituto! y por supuesto de **Eulalia** de coordinación, personas quienes formaron parte de mi día a día y noches también, quienes me brindaron su amistad y cariño. Un gran abrazo a todos.

Financiación

Parte de este proyecto ha sido posible gracias al financiamiento del Programa estatal de Investigación del Ministerio de Ciencia e Innovación (RTI2018-096055-B-100) de España.



Table of contents

Index of Figures.....	VII
Index of Tables.....	XI
Abbreviations.....	XIII
Abstract.....	XV
Resumen.....	XVII
Resum.....	XIX
GENERAL INTRODUCTION	1
1. Hormone Metabolism	3
1.1. Hypothalamic-pituitary-gonadal (HPG) axis	3
1.2. Steroid hormones synthesis:	6
1.3. Steroid hormone’s function	7
2. Hormone Metabolism and Diseases	9
2.1. Hormones and critical illness:	9
2.1.1. Steps in the Acute phase response:.....	10
2.1.2. Hypothalamus- Pituitary – Gonadal axis in critical illness.....	11
2.2. Sex steroid hormones and viral infectious diseases	11
2.2.1. Steroid hormones and innate immune cells:.....	12
2.2.2. Steroid hormones and regulation of cytokines and chemokines.....	13
2.2.3. Steroid hormones and T-cell response.....	14
2.3. Sex steroid hormones and cancer	15
2.4. Metabolic reprogramming in cancer	16
2.4.1. Lipidic metabolic reprogramming in cancer.....	17
CHAPTER I ANDROGEN METABOLISM AND PROSTATE CANCER	19
CHAPTER I - INTRODUCTION	21
1. The Prostate	23
1.1. Anatomy	23
1.2. Histology	25
1.3. Function	27
1.4. Mechanism of prostate function	27
2. Prostate cancer	28
2.1. Epidemiology of prostate cancer	28
2.2. Natural history of prostate cancer (course y evolution)	29

2.3.	Processes promoting prostate carcinogenesis	30
2.4.	Diagnosis of PCa.....	32
3.	Prostate cancer treatment	35
3.1.	Localized Prostate Cancer (Early Stage):	35
3.2.	Locally Advanced Prostate Cancer:	36
3.3.	Metastatic Prostate Cancer:	36
3.4.	Resistant Prostate Cancer:	36
4.	Mechanisms implicated in Castration Resistant Prostate cancer:.....	37
4.1.	Androgen Receptor (AR) Signaling Persistence	37
4.2.	Androgen-Independent Pathways	38
4.3.	Intratumoral <i>de novo</i> steroidogenesis:	39
5.	Models to study prostate cancer	40
5.1.	<i>In vivo</i> models:	40
5.2.	<i>In vitro</i> models:	40
6.	Senescence and Prostate cancer	41
6.1.	Senescence	41
6.2.	Senescence and cancer	41
6.3.	Senescence and prostate cancer	42
	CHAPTER I - PREMISE	43
	CHAPTER I - HYPOTHESIS AND OBJECTIVES.....	49
	CHAPTER I - MATERIALS AND METHODS	51
1.	Cellular cultures:.....	53
1.1.	Cell lines:.....	53
1.2.	Cell lines maintenance:	54
1.3.	Ex vivo Prostate primary cultures (hnPCs):.....	55
1.4.	hnPCs culture and maintenance:	55
2.	Tissue samples and biopsies	56
2.1.	Samples of benign prostatic hyperplasia (BPH) and Radical prostatectomies (RP)	56
2.2.	Samples of needle biopsy tissues	57
3.	Serum samples from PCa patients.....	57
3.1.	Patient recollection	57
3.2.	Serum sample collection	57
4.	DNA manipulation	57

4.1.	DNA extraction.....	57
4.2.	DNA genotyping for SNiPs.....	59
4.3.	DNA sequencing.....	59
5.	RNA manipulation.....	61
5.1.	RNA extraction from cell cultures.....	61
5.2.	RNA from OCT tissues.....	61
5.3.	RNA quality assessment.....	62
5.4.	Real time polymerase reaction (RT-PCR).....	62
5.5.	RNA transient interference (siRNA).....	67
6.	Protein manipulation.....	69
6.1.	Protein extraction.....	69
6.2.	Protein concentration.....	69
6.3.	SDS-PAGE.....	69
6.4.	Protein transference.....	70
6.5.	Western Blotting.....	71
7.	Functional analysis.....	72
7.1.	Immunofluorescence.....	72
7.2.	Cellular fractionation.....	73
7.3.	Cellular senescence analysis.....	74
8.	Bioinformatics analysis.....	76
9.	Statistical analysis.....	76
	CHAPTER I – RESULTS.....	77
1.	SNP P72R of TP53 gene in Prostate cancer.....	79
1.1.	The TP53 SNP P72R.....	79
1.2.	P72R and allele frequencies in primary cultures and tissues.....	80
1.3.	P72R is associated with prostate cancer occurrence.....	81
1.4.	P72R SNP may not be associated with PCa aggressiveness.....	83
2.	Steroidogenesis pathway in hormone-naïve primary cultures.....	85
2.1.	Identification of key steroidogenic genes in databases.....	85
2.2.	AI and AD hnPCs show similar steroidogenic gene expression profiles.....	86
2.3.	De novo steroid synthesis machinery is enhanced in hnPCs and tumorigenic tissue.....	87
2.4.	Changes in gene expression profiles in hormone naïve primary cultures show steroidogenic reprogramming.....	89
2.5.	De novo synthesis of Testosterone and estrogen in primary cultures.....	90

2.6.	Expression profiles in hnPC and PCa tissues:	92
2.7.	CDKN1A is strongly overexpressed in hnPCs.....	94
3.	p21^{WAF1} and its relationship with androgen metabolism	96
3.1.	CDKN1A (p21 ^{WAF1}) silencing significantly affected the expression of ARK1C3.....	96
3.2.	p21 ^{WAF1} subcellular localization in LNCaP AD cells and hnPCs	100
3.3.	p21 ^{WAF1} subcellular localization reveals senescent-like state in hnPCs	101
4.	Cancer stemness is promoted in all hnPCs compared to LNCaP cells.....	106
	CHAPTER I – DISCUSSION	109
1.	Primary cultures from hormone-naïve patients: a useful pre-clinical model.....	111
2.	Polymorphic variant rs1042522 (P72R) in prostate cancer.....	112
3.	Steroid hormone metabolism in hormone-naïve primary cultures models.....	114
4.	p21 ^{WAF1} – associated senescence and its role in androgen metabolism.....	117
	CHAPTER I – CONCLUSIONS	129
	CHAPTER II ANDROGEN METABOLISM AND COVID-19	133
	CHAPTER II - INTRODUCTION	135
1.	Coronavirus Disease-19 (COVID-19).....	137
1.1.	COVID-19 epidemiology.....	137
1.2.	SARS-COV-2.....	138
1.3.	SARS-CoV-2 mechanism of host entry	141
1.4.	Clades and variant D614G during the first wave of pandemic.....	142
2.	COVID-19 characteristics and symptoms.....	143
3.	Sex difference in immune response.....	144
4.	Androgen receptor mediated TMPRSS2 regulation in COVID-19	145
	CHAPTER II – PREMISE	147
	CHAPTER II – HYPOTHESIS AND OBJECTIVES	151
	CHAPTER II - MATERIAL AND METHODS	155
1.	Study design.....	157
2.	Patient selection.....	158
3.	Patient classification.....	158
4.	Data and sample collection	159
4.1.	Data collection	159
4.2.	Samples collection	159
4.3.	Principal biochemical and hematological parameters throughout hospitalization	160

4.4.	Serum sample processing and storage.....	161
5.	Serological determinations	161
5.1.	Hormones quantification by CLIA.....	161
5.2.	Total Serum Testosterone (TST) levels	161
5.3.	Luteinizing hormone (LH) levels	162
5.4.	Androstenedione hormone levels	162
5.5.	Interleukine-6 (IL-6) levels.....	162
5.6.	Hormone references.....	162
5.7.	Bioavailable-free testosterone calculation.....	163
6.	Immuno-phenotyping.....	163
7.	Statistical analysis	166
8.	Ethical considerations.....	166
	CHAPTER II - RESULTS.....	167
1.	Baseline characteristics of the male and female study populations	169
2.	Biochemical and hematological predictors of outcome in COVID-19 patients	173
2.1.	Severe outcomes correlate with high neutrophils counts, IL-6, D-dimer and LDH in both males and females but are m	173
2.2.	Serum testosterone at admission point is significantly lower in severe patients and significantly correlates with lymphocytes	176
2.3.	IL-6 is the best risk predictors for severe disease at admission point in both females and males, whereas Testosterone and % lymphocytes are the best predictors for mild-moderate outcomes.....	177
3.	Serum testosterone as predictor of outcome in the longitudinal analysis	179
3.1.	Evolutionary trajectories of biochemical parameters in males.....	179
3.2.	Recovery of serum testosterone accurately predicts survival in male patients	181
3.3.	TST trajectory slopes correlate with age in severe survivor patients.....	181
3.4.	The LH-androstenedione axis is not significantly perturbed in male COVID-19 patients	183
4.	Immunophenotyping in COVID-19 male outcomes.....	185
4.1.	Lethal male COVID-19 is associated with a depletion of circulating T helper	185
	CHAPTER II - DISCUSSION	189
	CHAPTER II – CONCLUSIONS.....	197
	REFERENCES.....	201
	ANNEX: PUBLICATIONS.....	227

Index of Figures

Figure 1 Hypothalamus-pituitary-gonadal axis ³	5
Figure 2 Synthesis of cholesterol from squalene.....	6
Figure 3 Map of the steroid hormone pathway.....	7
Figure 4. Mechanism of action of steroid hormones.....	8
Figure 5. Endocrine changes in critical illness.....	10
Figure 6. Sex hormones and modulation of immune response.....	15
Figure 7. Metabolic reprogramming in cancer cells.....	17
Figure 8. General anatomy of the prostate gland.....	23
Figure 9. Zonal anatomy of the prostate gland.....	24
Figure 10. Composition of the prostate epithelium.....	26
Figure 11. Hormonal physiology of prostate gland.....	28
Figure 12. Prostate cancer stages.....	30
Figure 13. Genetic alterations in prostate cancer.....	32
Figure 14. Gleason Pattern.....	34
Figure 15. Stages in Prostate cancer progression and associated therapies.....	37
Figure 16. Dual role of senescence in cancer.....	42
Figure 17. Electropherograms obtained with BioAnalyzer 2100.....	62
Figure 18. Schematic representation of siRNAs transfection workflow.....	68
Figure 19. Canonic transcript of TP53 gene and the SNP rs1042522.....	79
Figure 20. Representative melting curves from qPCR.....	80
Figure 21. P72R Allele frequencies in Prostate cancer.....	82
Figure 22. Distribution of P72R variants in 94 patients according to Gleason grade.....	84
Figure 23. Bar plot for differential gene expression between two groups of samples in prostate cancer datasets.....	85
Figure 24. Volcano plot of the most significant differentially expressed genes in the steroidogenic pathway across prostate cancer datasets.....	86
Figure 25 Exploratory characterization of primary cultures.....	87
Figure 26. Heatmap of steroidogenic gene expression.....	88
Figure 27. Changes in normal gene expression in steroid metabolism.....	89
Figure 28. Expression of steroidogenic genes involved in de novo hormone synthesis in primary cultures.....	90
Figure 29. Map of steroid synthesis pathway and the enzyme expression profiles in primary cultures.....	91

Figure 30. Analysis of similarity between cultures and tissues from prostatectomies.	92
Figure 31. Heatmap of the expression profiles of primary cultures in comparison with original biopsies.	93
Figure 32. Overexpressed CDKN1A correlates with several steroidogenic genes.	95
Figure 33. p21 ^{WAF1} is associated with AKR1C3 expression in LNCaP.	96
Figure 34. STAR and HSD3B1 expression are affected by p21 KD in LNCaP cells.	97
Figure 35. Bar plot of expression analysis of MDM2 and TP53 with p21-siRNAs in LNCaP cells.	97
Figure 36. p21 ^{CIP/WAF1} is associated with AKR1C3 expression in primary cultures.	99
Figure 37. CYP19A1 and MDM2 expression in p21-KD hnPCs.	99
Figure 38. Subcellular localization of p21 ^{WAF1} in LNCaP cells.	100
Figure 39. Subcellular localization of p21 ^{WAF1} in hnPCs.	101
Figure 40. Immunofluorescence confocal microscopy images of p21 in hnPCs.	102
Figure 41. Percentages of proliferation in LNCaP and primary cultures.	103
Figure 42. Expression of senescent markers in hnPCs.	104
Figure 43. Notch1 expression in hnPCs.	105
Figure 44. Notch1 signaling mediates secondary senescence.	106
Figure 45. Expression of three stem cell markers in hnPCs.	108
Figure 46. Global allele frequency of P72R SNP rs1042522.	113
Figure 47. CDKN1A expression in prostate cancer and normal tissue.	118
Figure 48. Negative correlation between CDKN1A and AKR1C3 observed in LNCaP AD and AI models.	120
Figure 49. Model for the preferential induction of apoptosis by RITA.	122
Figure 50. Proposed model for attenuation of canonical TGF- β SMAD and activation of non-canonical TGF- β -NF- κ B signaling pathways in HNSCC.	123
Figure 51. The oncogenic model of nuclear p21 proposed by Galanos et al.	125
Figure 52. Dual role of p21-associated senescence.	127
Figure 53. Senescence-associated reprogramming in prostate primary cultures.	128
Figure 54. New COVID-19 cases and deaths confirmed up to July 2023.	138
Figure 55. SARS-CoV-2 structure.	139
Figure 56. SARS-CoV-2 entry pathways.	142
Figure 57. Phylogenetic tree of SARS-CoV-2 in 2020.	143
Figure 58. Schematic representation of the study design.	157
Figure 59. The Vermeulen equation for calculated free testosterone.	163

Figure 60. Baseline characteristics of COVID-19 patients.	171
Figure 61. Distribution of COVID-19 patients.	172
Figure 62. Association analyses between biochemical parameters and outcomes.	174
Figure 63. Clinical biochemistry features of male and female COVID-19 patients, associated with outcomes.	175
Figure 64. Serum Testosterone at admission in male patients with COVID-19.	176
Figure 65 Assessment of clinical biochemistry parameters as predictors of risk of severe disease or death from COVID-19.	178
Figure 66. Longitudinal trajectories of biochemical parameters.	180
Figure 67. Recovery of serum testosterone levels and blood lymphocyte counts predict survival in male COVID-19 patients.	181
Figure 68. Correlations of age with testosterone trajectory slopes.	182
Figure 69. Bioavailable testosterone serum levels and correlation between Age and sex-hormone binding globulin (SHBG)	183
Figure 70. The luteinizing hormone (LH)-androstenedione axis is not significantly perturbed in male COVID-19 patients.	185
Figure 71. Immune switch during the course of disease in severe and deceased patients	187
Figure 72. Flow cytometry of representative cases of male patients with COVID-19.	188

Index of Tables

Table 1. Prostate cancer classification in groups according to Gleason pattern.	35
Table 2. Cycling conditions for Melting curve analysis	59
Table 3. Protocol y conditions to synthesize cDNA	60
Table 4. RT-qPCR reaction components and concentration with UPL	63
Table 5. RT-qPCR reaction components and concentrations with TaqMan	64
Table 6 Cycling conditions for RT-qPCR	64
Table 7. Primers for UPL assay	65
Table 8 TaqMan assays for RT-qPCR	66
Table 9. List of siRNAs for CDKN1A transient knockdown	67
Table 10. Details of siRNAs reaction preparation.	68
Table 11. Ingredients for polyacrylamide gels preparation.	70
Table 12. List of primary antibodies for western blot	72
Table 13. List of secondary antibodies for western blot	72
Table 14. List of reagents for immunofluorescence	73
Table 15. Treatment arrangement in 96-well plate	75
Table 16. P72R genotyping in primary cultures and radical prostatectomy tissues	81
Table 17. Association analysis between P72R SNP and prostate cancer	83
Table 18. Hormonal composition in Fetal Bovine Serum	94
Table 19. WHO classification of disease outcome (adapted from Grein et al.¹)	158
Table 20. Timetable of sample collection	159
Table 21. Biochemical parameters	160
Table 22. Panels and antibodies used for immunophenotyping	165
Table 23. Baseline clinical characteristics of the male study population	169
Table 24. Baseline clinical characteristics of the female study population	170
Table 25. Comparison between Mild-moderate and Severe outcomes in males	172
Table 26. Comparison between Mild-moderate and Severe outcomes in females	172

Abbreviations

ADT: Androgen deprivation therapy	IL: Interleukine
AKR1C3: Aldo-keto reductase family 1 member C3	LDH: Lactate dehydrogenase
AR: Androgen receptor	LH: Luteinizing Hormone
ATCC: American type culture collection	mCRPC: metastatic castration resistant prostate cancer
AUC: Area under the curve	NLS: Nuclear localization signal
BPH: Benign prostatic hyperplasia	OR: Odd ratios
BSA: Bovine serum albumin	PBS: Phosphate-buffered saline
CDKN1A: Cyclin dependent kinase inhibitor	PCa: Prostate cancer
CDKs: Cyclin-dependent kinase	PSA: Prostate-specific antigen
cDNA: Complementary DNA	PTOV1: Prostate Tumor Overexpressed 1
COVID-19: Coronavirus disease 2019	ROC: Receiver operating characteristic
CSCs: Cancer stem cells	RP: Radical prostatectomy
Ct: Threshold cycle	RT: Room temperature
DHT: Dihydrotestosterone	RT-qPCR: Quantitative real time polymerase chain reaction
DRE: Digital rectal examination	SNP: Single nucleotide polymorphism
EGF: Epidermal growth factor	siRNA: Small interference RNA
ERK1/2: Extracellular Signal-Regulated Kinase ½	T: Testosterone
FBS: Fetal bovine serum	TEMRA: Terminally differentiated effector memory
FC: Fold change	TMPRSS2: Transmembrane protease serine 2
hnPC: Hormone-naïve Primary culture	TST: Total Serum testosterone
IGF-1: Insulin growth factor	UPL: Universal probe library of Roche

Abstract

The proper functioning of the endocrine system plays a crucial role in maintaining human health, as hormones are vital for regulating bodily homeostasis. Disruptions in normal hormone signaling pathways can lead to various diseases, compromising the immune system's response to infections and contributing to cancer-related behaviors at the cellular level, including cell proliferation, migration, invasion, and metastasis formation. Initially, our thesis aimed to investigate the role of steroid hormones in prostate cancer. However, due to the pandemic, we expanded our focus to study male hormones in COVID-19.

Prostate cancer is hormone-dependent, and androgen deprivation therapy (ADT) is the standard treatment for inoperable tumors. Unfortunately, resistance to ADT remains a significant challenge, often attributed to intratumor hormone biosynthesis. To better understand these mechanisms, we utilized primary cultures from hormone-naïve patients (hnPCs) with aggressive tumors. Our analysis revealed substantial changes in these cultures, impacting androgen pathways (*AR*, *SRD5A1*, *AKRIC3*, *PAPSS2*), estrogen pathways (*ESRRA*, *CYP11B1*, *CYP19A1*), and the p53 pathway (*TP53*, *MDM2*, *CDKN1A*), demonstrating that these models are undergoing a metabolic reprogramming in order to enhance the production of steroid hormones. Notably, we observed a strong overexpression of *CDKN1A*(p21^{WAF1}), which was significantly associated with *AKRIC3* and other steroidogenic genes, hinting at a potential oncogenic role for p21^{WAF1}. Further analyses revealed nuclear localization of p21^{WAF1} and the expression of senescence markers, however, hnPCs show moderate but sustained proliferation, high intrinsic chemoresistance and expression of cancer stem markers. Current studies have revealed the paradoxical role of senescence, demonstrating that it can promote cancer progression and aggressiveness. Therefore, our results show evidence of a senescence-like state in these cultures, which may promote metabolic reprogramming and aggressiveness in prostate cancer.

Severe COVID-19 cases are associated with factors such as old age, male sex, socioeconomic status, and comorbidities. Our research delved into the link between serum testosterone levels, immune cell profiles, and disease severity in male COVID-19 patients. We identified significant differences in biochemical predictors of disease outcomes between male and female patients. Longitudinal analysis revealed that serum testosterone trajectories were the strongest predictors of survival among all biochemical parameters studied, even surpassing single-point admission serum testosterone values. In cases leading to fatalities, we observed irregular patterns in serum luteinizing hormone (LH) and androstenedione levels, suggesting a failure to restore normal testosterone levels. This phenomenon was associated with impaired T helper differentiation and increased circulating classical monocytes, indicating the substantial influence of testosterone status on immune responses to COVID-19.

Resumen

El adecuado funcionamiento del sistema endocrino desempeña un papel crucial en el mantenimiento de la salud humana, ya que las hormonas son esenciales para regular la homeostasis. Las interrupciones en las vías normales de señalización hormonal pueden llevar a diversas enfermedades, comprometiendo la respuesta inmune o contribuyendo a con el cáncer a nivel celular, como la proliferación celular, la migración, la invasión y la formación de metástasis. Inicialmente, nuestra tesis tenía como objetivo investigar el papel de las hormonas esteroides en el cáncer de próstata. Sin embargo, debido a la pandemia, ampliamos nuestro enfoque para estudiar las hormonas masculinas en la COVID-19.

El cáncer de próstata es dependiente de hormonas y la terapia de privación de andrógenos (ADT) es el tratamiento estándar para tumores no operables. Desafortunadamente, la resistencia al ADT sigue siendo un desafío, a menudo atribuido a la síntesis intratumoral de hormonas. Para comprender mejor estos mecanismos, utilizamos cultivos primarios de pacientes con tumores agresivos hormone-naive (hnPCs). Nuestro análisis reveló cambios sustanciales en los cultivos, que afectaron las vías de andrógenos (*AR*, *SRD5A1*, *AKR1C3*, *PAPSS2*), las vías de los estrógenos (*ESRRA*, *CYP11B1*, *CYP19A1*) y la vía p53 (*TP53*, *MDM2*, *CDKN1A*), demostrando que estos modelos experimentan una reprogramación metabólica para aumentar la producción de hormonas esteroides. Notablemente, observamos una fuerte sobreexpresión de *CDKN1A* (p21^{WAF1}), que estuvo significativamente asociada a *AKR1C3* y otros genes esteroidogénicos, insinuando un posible papel oncogénico para p21^{WAF1}. Análisis adicionales revelaron la localización nuclear de p21^{WAF1} y la expresión de marcadores de senescencia; sin embargo, los hnPCs muestran una proliferación moderada pero sostenida, alta quimiorresistencia y expresión de marcadores de stemness. Estudios actuales han revelado el papel paradójico de la senescencia, demostrando que puede promover la progresión y agresividad del cáncer. Por lo tanto, nuestros resultados muestran evidencia de un estado similar a la senescencia en estos cultivos, que puede promover la reprogramación metabólica y la agresividad en el cáncer de próstata.

Los casos graves de COVID-19 se asocian con factores como la edad, el sexo masculino y las comorbilidades. Nuestra investigación profundizó en la relación entre los niveles séricos de testosterona, los perfiles de células inmunológicas y la gravedad de la enfermedad en pacientes hombres con COVID-19. Identificamos diferencias significativas en los predictores bioquímicos de la enfermedad entre pacientes hombres y mujeres. El análisis longitudinal reveló que las trayectorias de los niveles séricos de testosterona fueron los predictores más sólidos de la supervivencia entre todos los parámetros bioquímicos estudiados, incluso superando los valores únicos de testosterona en la admisión. En los casos fatales, observamos patrones irregulares en los niveles séricos de hormona luteinizante (LH) y androstenediona, lo que sugiere una incapacidad para restablecer los niveles normales de testosterona. Este fenómeno se asoció con una diferenciación deficiente de las células T auxiliares y un aumento de los monocitos clásicos circulantes, lo que indica la influencia significativa del estado de testosterona en las respuestas inmunológicas a la COVID-19.

Resum

El funcionament adequat del sistema endocrí desempeña un paper crucial en el manteniment de la salut humana, ja que les hormones són essencials per regular la homeòstasi del cos. Les interrupcions en les vies normals de senyalització hormonal poden portar a diverses malalties, compromentent la resposta immunològica i contribuint a amb el càncer a nivell cel·lular, com la proliferació cel·lular, la migració, la invasió i la formació de metàstasis. Inicialment, la nostra tesi tenia com a objectiu investigar el paper de les hormones esteroides en el càncer de pròstata. No obstant això, a causa de la pandèmia, vam ampliar el nostre enfocament per estudiar les hormones masculines en la COVID-19.

El càncer de pròstata és dependent d'hormones i la teràpia de privació d'andrògens (ADT) és el tractament estàndard per a tumors no operables. Desafortunadament, la resistència a l'ADT continua sent un desafiament significatiu, sovint atribuït a la biosíntesi intratumoral d'hormones. Per comprendre millor aquests mecanismes, vam utilitzar cultius primaris de pacients sense exposició prèvia a hormones (hnPCs) amb tumors agressius. La nostra anàlisi va revelar canvis importants en aquests cultius, que van afectar les vies dels andrògens (*AR*, *SRD5A1*, *AKR1C3*, *PAPSS2*), les vies dels estrògens (*ESRRA*, *CYP11B1*, *CYP19A1*) i la via p53 (*TP53*, *MDM2*, *CDKN1A*), demostrant que aquests models experimenten una reprogramació metabòlica per augmentar la producció d'hormones esteroides. Destacablement, vam observar una forta sobreexpressió de *CDKN1A* p21^{WAF1}, que va estar significativament associada a *AKR1C3* i altres gens esteroidogènics, insinuant un possible paper oncogènic per a p21^{WAF1}. Anàlisis addicionals van revelar la localització nuclear de p21 i l'expressió de marcadors de senescència; no obstant això, les hnPCs mostren una proliferació moderada però sostinguda, alta quimiorresistència intrínseca i expressió de marcadors de cèl·lules mare canceroses. Estudis actuals han revelat el paper paradògic de la senescència, demostrant que pot promoure la progressió i l'agressivitat del càncer. Per tant, els nostres resultats mostren evidències d'un estat similar a la senescència en aquests cultius, que pot promoure la reprogramació metabòlica i l'agressivitat en el càncer de pròstata.

Els casos greus de la COVID-19 es relacionen amb factors com l'edat avançada, el sexe masculí, l'estatus socioeconòmic i les comorbiditats. La nostra recerca va aprofundir en la relació entre els nivells sèrics de testosterona, els perfils de cèl·lules immunològiques i la gravetat de la malaltia en pacients masculins amb la COVID-19. Vam identificar diferències significatives en els predictors bioquímics de la malaltia entre pacients masculins i femenins. L'anàlisi longitudinal va revelar que les trajectòries dels nivells sèrics de testosterona eren els predictors més forts de la supervivència entre tots els paràmetres bioquímics estudiats, fins i tot superant els valors únics de testosterona en l'admissió. En casos que van portar a la mort, vam observar patrons irregulars en els nivells sèrics de la hormona luteïnitzant (LH) i l'androstenediona, suggerint una incapacitat per restablir els nivells normals de testosterona. Aquest fenomen va estar associat amb una diferenciació deficient de les cèl·lules T auxiliars i un augment dels monocits clàssics circulants, indicant la influència significativa de l'estat de testosterona en les respostes immunitàries a la COVID-19.

GENERAL INTRODUCTION

GENERAL INTRODUCTION

1. Hormone Metabolism

The Endocrine system is one of the most important regulators of homeostasis within the human body. The active molecules responsible for the regulator effect on target organs or tissues are called hormones and they are the “chemical messengers” produced and released by specialized glands (endocrine glands) into bloodstream where are transported to exert a physiological action both proximal and distal areas of the body^{1,2}. Hormones signals to the organism through the binding to hormone receptors, which can be either membrane or cytoplasmic receptors, many of them are nuclear which upon ligand binding translocate into the nucleus.

Hormones can be grouped into three classes:

- a. Protein/peptide hormones:
 - Pancreas hormones: Insulin, Glucagon
 - Hypophysis hormones: Thyrotropin (TSH), Corticotropin (ACTH), Gonadotropins (GTH, FSH, LH), Somatotropin (SH).
 - Parathyroid hormone: Parathormone (PTH)
 - Gastrointestinal hormones: Gastrin, Secretin, Hepatocrinin, Parotin.
- b. Steroid hormones:
 - Ovarian hormones: β -estradiol, Estriol, Estrone (C₁₈), progesterone (C₂₁)
 - Testicular hormones: Testosterone, Androsterone, Dehydroepiandrosterone (C₁₉)
 - Adrenal cortical hormones: Androstenedione, Adrenosterone (C₁₉), Aldosterone, Cortisone, Cortisol, corticosterone (C₂₁)
- c. Amino acid derivatives
 - Thyroidal hormones: Triiodothyronine (T3), Tetraiodothyronine (T4)
 - Adrenal medullary hormones: Adrenalin, Noradrenalin.

1.1. Hypothalamic-pituitary-gonadal (HPG) axis

The hypothalamic-pituitary-gonadal axis (HPG axis) is a sophisticated hormone control system consisting of three distinct parts that work together in coordinated manner. This axis plays a vital role in overseeing various reproductive and developmental processes in humans and other animals³.

Hypothalamus: The process begins in the hypothalamus, a region of the brain. Specialized neurons within the hypothalamus produce the gonadotropin-releasing hormone (GnRH), a tropic peptide hormone that acts as a signal to stimulate the anterior pituitary gland.

Pituitary Gland: The anterior pituitary gland receives the GnRH signal and responds by releasing two important hormones:

Luteinizing Hormone (LH): a glycoprotein hormone that is co-secreted with follicle-stimulating hormone (FSH) by the gonadotrophin cells in the adenohypophysis (anterior pituitary). LH consists of two subunits: the α -unit with 92 amino acids is similar to FSH, whereas the β -units is specific and consists of 120 amino acids.

LH travels through the bloodstream to the gonads (testes in males, ovaries in females) and stimulates them to produce sex hormones (testosterone in males, estrogen and progesterone in females) by interaction of β -subunit with LH receptor.

Follicle-Stimulating Hormone (FSH): FSH, like LH, is released by the pituitary gland and travels to the gonads. FSH is a 35.5 kDa glycoprotein heterodimer, consisting of two polypeptide units: the α -subunit is similar to LH, but the β -subunit of 111 amino acids (FSH β) is specific and confers its specific biologic action interacting with its receptor. It plays a crucial role in the development of sperm in males and the maturation of ovarian follicles in females.

Gonads (Testes or Ovaries): In response to LH and FSH, the gonads produce sex hormones:

Testosterone (T): (4-androsten-17 β -ol-3-one) is a C19 steroid hormone with a molecular weight of 288.4 Dalton. In males, LH stimulates the Leydig cells in the testes to produce testosterone, which is responsible for male secondary sexual characteristics and sperm production. In addition, testosterone has anabolic effects that lead to increase linear growth, nitrogen retention, and muscle development.

Dihydrotestosterone (DHT): is an androgen derived from T, which is converted into DHT through the action of an enzyme called 5-alpha-reductase (SRD5A1/2). This conversion primarily takes place in target tissues like the liver, prostate gland, skin, and hair follicles. DHT is estimated to have a binding affinity for androgen receptors that is approximately 2.5 to 10 times higher than that of testosterone. This means that DHT forms a stronger and more stable complex with androgen receptors (ARs) compared to testosterone.

Estrogens (E): In females, FSH and LH stimulate the ovaries. FSH promotes the growth and maturation of ovarian follicles, while LH triggers ovulation and stimulates the corpus luteum to produce mainly three types of estrogens: Estrone (E1), Estradiol (E2) and Estriol (E3). Estrogens interact and activate estrogen receptors (ERs) which in turn modulate the expression of many genes⁴ Also, estrogens bind and activate rapid-signaling membrane estrogen receptors (mERs)^{5,6} such as GPER (GPR30)⁷

Estradiol (E2): 17 β -estradiol is about 10 times more potent than estrone and nearly 80 times more potent than estriol in its estrogenic effects. E2 is synthesized by conversion of T by the aromatase enzyme (CYP19A1). In an alternative androgen pathway, androstenedione can be aromatized to estrone, which is subsequently converted to estradiol.

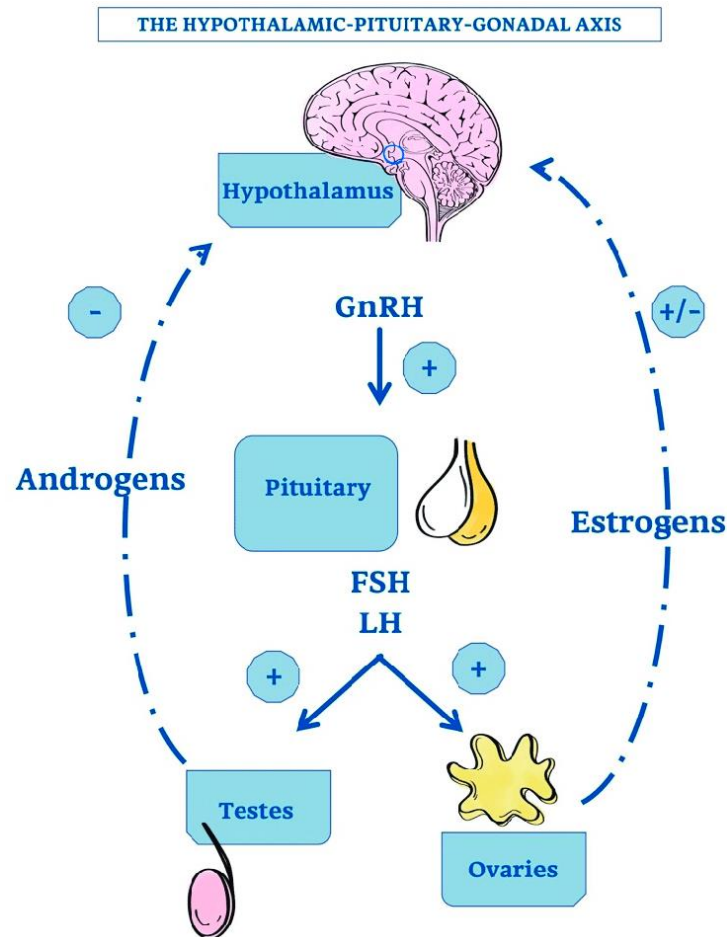


Figure 1 Hypothalamus-pituitary-gonadal axis. GnRH is released to pituitary, where FSH and LH are stimulated to be produced and release towards blood circulation. Both hormones, arrive to testes and ovary, where androgens and estrogens are synthesized to exert several functions. *Figure taken from Rezzani et al. 2020*³.

1.2. Steroid hormones synthesis:

The majority of sexual hormones are steroid molecules derived from Cholesterol, which is synthesized from Squalene. After epoxidation, squalene is rearranged by the oxidosqualene synthase to lanosterol, which now has the four cyclic rings characteristic for steroids. Lanosterol undergo several oxidation steps to cholesterol, the base of all steroids, or to another compound-like vitamin D₃⁸ (**Figure 2**)

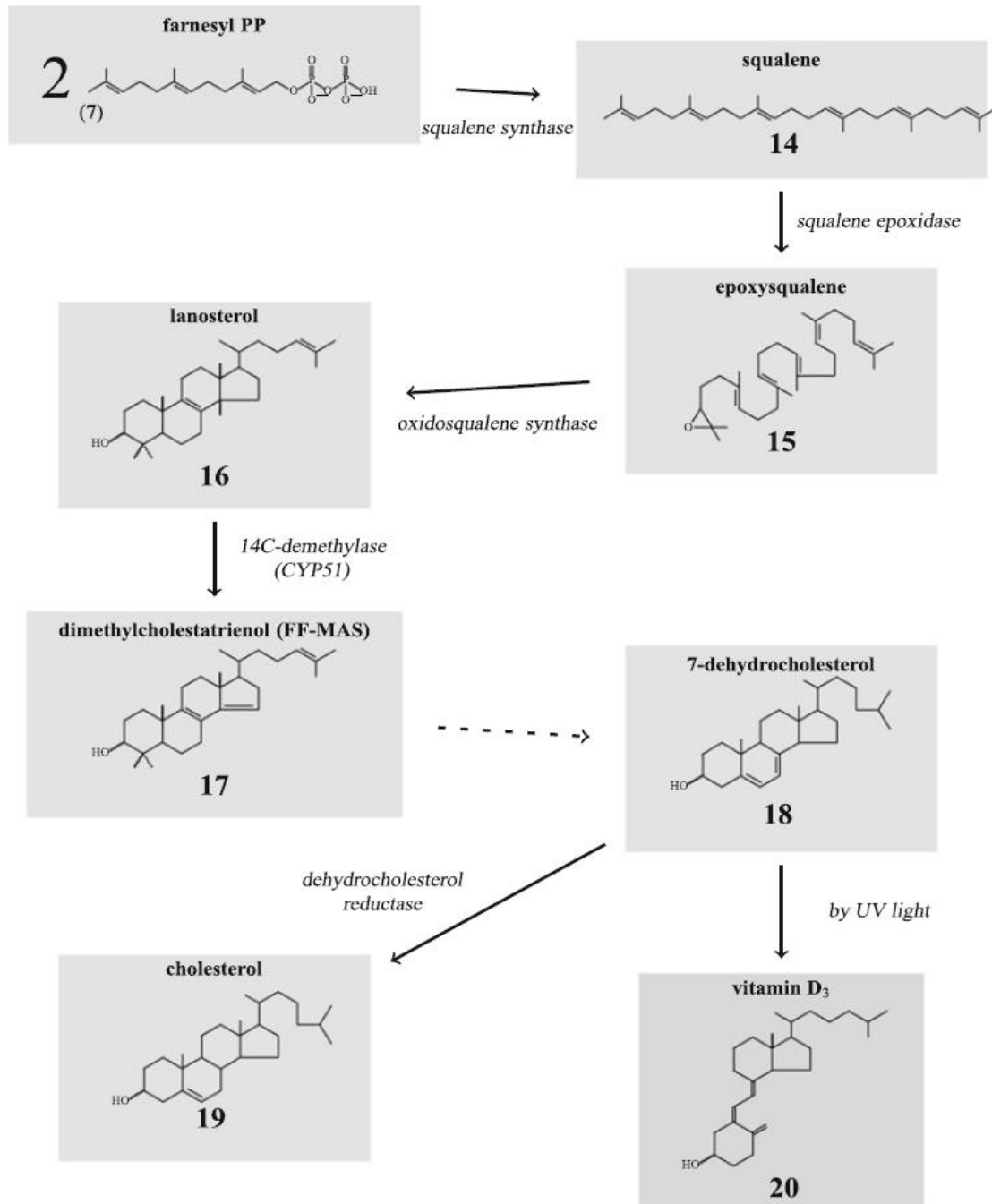


Figure 2 Synthesis of cholesterol from squalene. Six enzymatic steps are needed to form Cholesterol and Vitamin D₃. From, *Hormones and the endocrine system*, 2016⁸

Steroid hormones derive from pregnenolone which is generated by the cleavage of cholesterol processed by CYP11A1. From there, a series of concatenated reactions takes place until the synthesis of dihydrotestosterone (DHT) and 4OH-estradiol, the most potent hormones in this pathway (**Figure 3**).

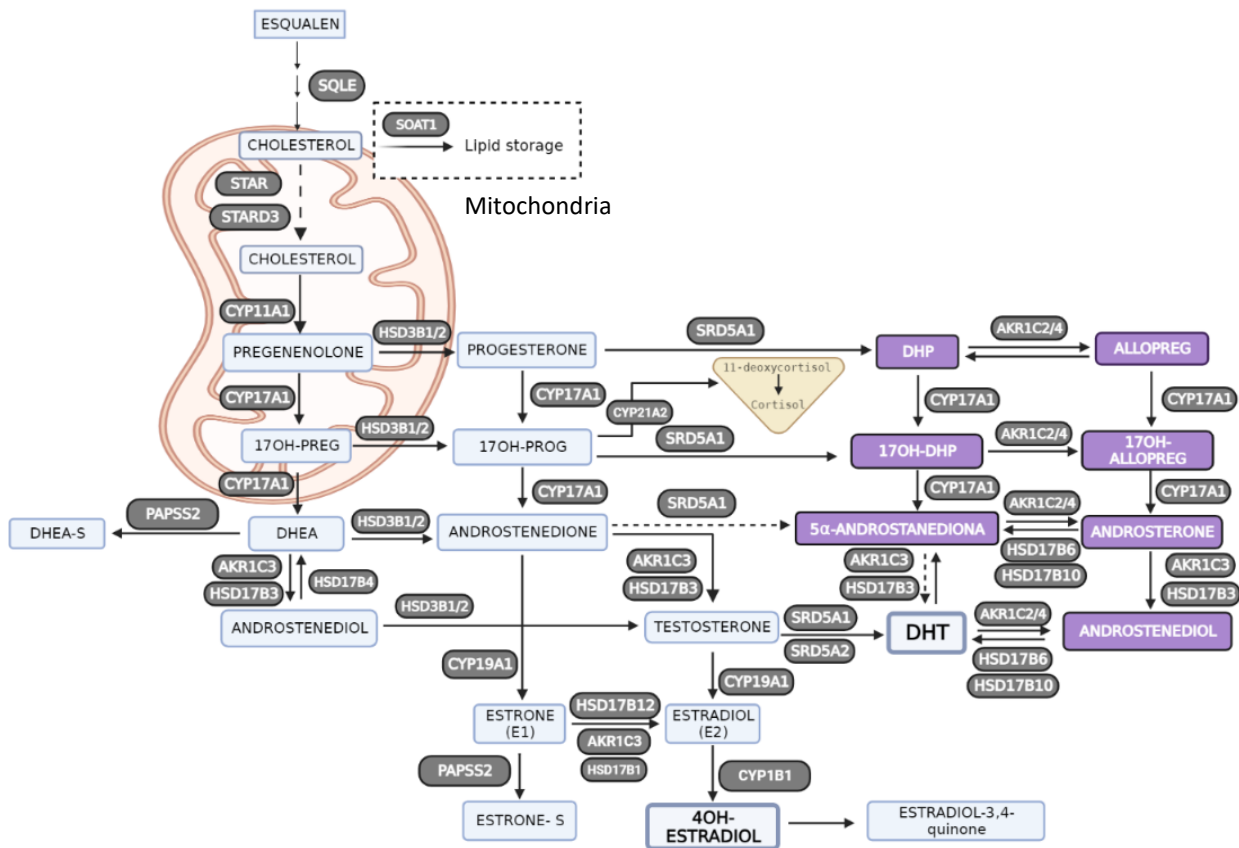


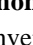


Figure 3 Map of the steroid hormone pathway. From squalene to active 4OH-estradiol. Enzymes are represented in black color , conventional pathway or front-door pathway is shown in light blue , whereas the alternative or back-door pathway is shown in purple . *Figures develop with Biorender.com*

1.3. Steroid hormone's function

Steroid hormones primarily exert their effects by interacting with specialized receptors located inside cells, known as intracellular nuclear receptors. These receptors are like switches that can be turned on when hormone molecules bind to them. They are part of a larger group of proteins called the nuclear receptor superfamily and are responsible for mediating various functions of sex steroids.

The principal mechanism by which steroid hormones act is to induce the synthesis of proteins in target cells. The steroid hormone enters the cytoplasm and binds with high affinity to its specific receptor protein. The hormone-receptor complex is activated and translocates to the nucleus, where it functions as a transcription factor interacting with the DNA. The mRNA produced is translated into the cytoplasm to synthesize particular proteins that promote a specific response² (**Figure 4**). Using this mechanism, hormones exert a wide range of functions in the body, including growth, development, energy metabolism and reproduction. The dysregulation in a number of points of these processes leads to the development of various diseases.

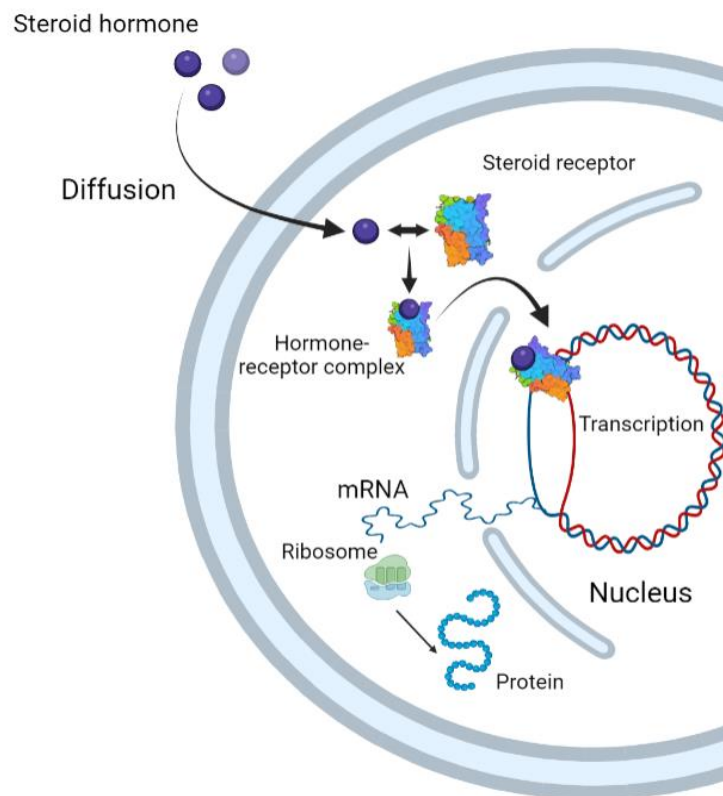


Figure 4. Mechanism of action of steroid hormones. Steroid hormones can enter the cell by simple diffusion, in the cytosolic compartment, hormones bind to and activate its respective steroid receptor, then this complex is translocated to the nucleus to interact with DNA and modulate gene transcription. *Figures develop with Biorender.com*

2. Hormone Metabolism and Diseases

The adequate function of the endocrine system is critical for the maintenance of human health. Classical endocrine diseases related to the overproduction of hormones are diabetes, hyperthyroidism, Cushing's disease, polycystic ovarian syndrome, and precocious puberty. Conversely, Addison's disease, hypothyroidism, and hypopituitarism are common diseases caused by insufficient hormone production⁸. Also, improper hyperplasia within endocrine glands can cause and be caused by dysregulation of hormone production or secretion.

However, not only a dysregulation of hormone production lead to diseases, but also diseases can induce hormonal imbalances. Therefore, hormonal dysregulation and diseases can influence each other bidirectionally.

2.1. Hormones and critical illness:

Critical illness is defined as the presence of acute, life-threatening organ dysfunction requiring vital organ support⁹. This process can be produced by major trauma, extensive surgery, mechanical ventilation or infections¹⁰. After initiation of organ dysfunction, multiple physiologic processes are initiated to recover the homeostasis, this process is also called as "stress response." The principal components of the stress response are the neuroendocrine and immune systems. These components include: the *central nervous system, paraventricular nucleus and locus coeruleus, Hypothalamus-Pituitary axis, and target organs*. In addition, the *immune inflammatory* component is included, comprising the innate and the specific immune response, via cytokines and inflammatory mediator^{10,11}. The first response to critical illness is typically the activation of the sympathetic nervous system, followed by the release of stress hormones from the hypothalamus-pituitary-adrenal (**HPA**) axis and the initiation of the inflammatory response. These responses occur almost simultaneously and are part of the body's immediate reaction to a critical medical condition known as Acute phase¹⁰⁻¹² (**Figure 5**).

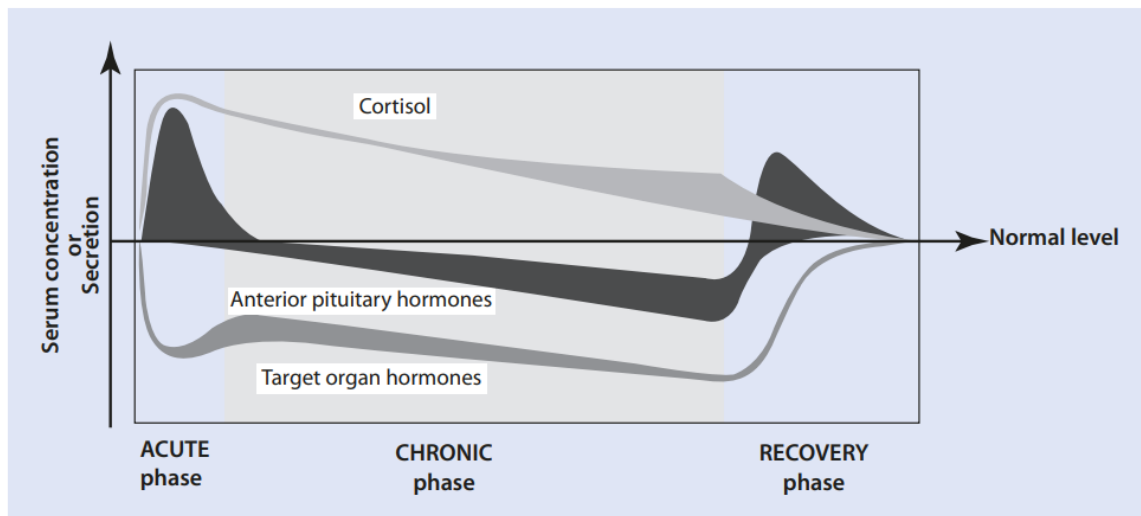


Figure 5. Endocrine changes in critical illness. At the onset of illness, anterior pituitary hormones surge with an associated peripheral inactivation of target organ hormones. Once the chronic response has been engaged, the sensitivity to pituitary hormones is restored, but both remain low due to failure of the pituitary to resume normal secretory activity. *From Van den Berghe et al.*¹²

2.1.1. Steps in the Acute phase response:

1. Sympathetic Nervous System (SNS) Activation:

- The sympathetic nervous system is a part of the autonomic nervous system responsible for the body's "fight-or-flight" response to stress or perceived threats.
- In the event of critical illness or injury, the SNS is rapidly activated to prepare the body for immediate action.
- Activation of the SNS leads to increased heart rate, increased blood pressure, dilation of the pupils, and shunting of blood away from non-essential organs (such as the digestive system) to prioritize blood flow to vital organs (such as the brain, heart, and muscles).
- The SNS response is essential for providing the body with the necessary energy and resources to respond to the critical situation.

2. Hypothalamus-Pituitary-Adrenal (HPA) Axis Activation:

- The HPA axis is a complex neuroendocrine system that regulates the body's response to stress and plays a crucial role in maintaining homeostasis during critical situations.
- When the body experiences stress due to critical illness, the hypothalamus releases corticotropin-releasing hormone (CRH).
- CRH then stimulates the pituitary gland to release adrenocorticotropic hormone (ACTH) into the bloodstream.

- ACTH, in turn, stimulates the adrenal glands to release stress hormones, primarily cortisol, into the bloodstream.

- Cortisol helps the regulation of various physiological processes, including glucose metabolism, immune response, and inflammation.

3. Inflammatory Response:

- The inflammatory response is another immediate reaction to critical illness or injury.

- Tissue damage, infection, or other forms of cellular stress trigger the release of inflammatory mediators, such as cytokines and chemokines.

- These inflammatory mediators help recruit immune cells to the site of injury or infection and activate the immune response to combat potential threats.

- Inflammation is a vital part of the body's defense mechanism to promote healing and repair damaged tissues.

All these responses, the activation of the sympathetic nervous system, the HPA axis, and the initiation of the inflammatory response, work together to prepare the body for the challenges presented by the critical illness. They help to mobilize resources, increase oxygen and nutrient supply, and activate the immune system for protection against further damage and promote healing. In addition to the HPA axis, a key role in critical illness is also played by the Hypothalamus - Pituitary – Gonadal axis (HPG).

2.1.2. Hypothalamus- Pituitary – Gonadal axis in critical illness

It has been described that the circulating levels of sex hormones decrease after the beginning of a critical disease. In men, Testosterone levels drop dramatically, despite normal or even higher levels of LH. Cytokines have been implicated in Leydig cell dysfunction and increasing of androgen aromatization, by which testosterone is converted into estrogen by aromatase enzyme⁹.

2.2. Sex steroid hormones and viral infectious diseases

Hormones are crucial in regulating the immune system's response to infection, by strengthening or weakening the body's immune system. For example, adrenal hormone cortisol is known to suppress immunity. People with chronic stress or high levels of cortisol in the blood are therefore more likely to be infected. On the contrary, estrogens have an immune enhancement effect^{13,14}.

Sex Hormones and immunity

Sex hormones estrogens and androgens are widely recognized as reproductive hormones due to the well-studied effects on reproductive tissues. However, extensive research has established their broad physiological effects in the central nervous, cardiovascular, skeletal system and the immune system.

2.2.1. Steroid hormones and innate immune cells:

The physical barriers such as skin, mucosal tissue or chemical barriers as saliva, mucus, and tears are a first line of defense against foreign antigens invasion. When antigens manage to bypass the first line, neutrophils, macrophages, natural killer cells (NK) and dendritic cells (DCs) appear as a second line of defense.

Neutrophils, the first responders to infections, combat pathogens through phagocytosis¹⁵ and the release of toxic oxygen radicals¹⁶. Estrogen affects neutrophils by suppressing their production¹⁷, reducing chemotaxis¹⁸, altering adhesive proteins, and decreasing neutrophil function. Estrogen has additional varying effects on inflammation depending on factors like estrogen type, dose, tissue, and injury type. On the other hand, Testosterone has been implicated in the increasing of circulating neutrophils¹⁹, and its receptor (AR) has been found important for the development of neutrophils in AR-deficient mice²⁰.

Unlike neutrophils, macrophages can phagocytose repeatedly and produce large amounts of inflammatory proteins. Estrogen enhances macrophage phagocytic activity, while androgens inhibit macrophage function *in vivo* and *in vitro* probably because ARs have been identified in this type of cells^{21,22}, reducing proinflammatory products and receptor expression. DCs are potent antigen-presenting cells that activate T lymphocytes and help regulate immune responses. 17 β -estradiol promotes the differentiation of functional DCs, increasing their activation markers as nitric oxide production. Estrogen also influences cytokine production, increasing IL-6 and IL-10 expression while Testosterone decreases inflammatory cytokines from DCs. Finally, NK cells are lymphocytes that can kill pathogen-infected and tumor cells. Estrogen decreases NK cell activity both *in vivo* and *in vitro*. Estrogen treatment increases the number of NK cells and certain receptor expression but reduces their cytotoxicity in a dose-dependent manner. Conversely, Testosterone administration reduces NK cell activity in mice, but dehydroepiandrosterone supplementation in postmenopausal women increases CD8⁺/CD56⁺ NK cells²³. Steroid hormones play a significant role in NK cell function.

2.2.2. Steroid hormones and regulation of cytokines and chemokines

Innate immune cells, particularly macrophages, express toll-like receptors (TLRs) that recognize specific patterns on antigens known as pathogen-associated molecular patterns (PAMPs), triggering an immune response. There are 13 TLRs identified in mammals, some located on cell membranes, like TLR4 and others in intracellular endosomes that are crucial for recognizing intracellular pathogens such as viruses²⁴. Activation of TLR4, can lead to induce various proinflammatory molecules.

In vitro, 17 β -estradiol augmented TLR4 expression in murine macrophages²⁵. Estrogens, enhance macrophages ability to produce inflammatory mediators and cytokines upon subsequent TLR activation mediated by ER alpha *in vivo*²⁶. Postmenopausal women, show lower expression of TLR4 and CD14, possibly explaining their reduced inflammatory responses. In contrast to estrogen, Testosterone typically has an immunosuppressive impact, primarily through mechanisms involving the androgen receptors (AR). When natural Testosterone is depleted through castration, it leads to increased production of IL-1b and IL-6 in response to LPS²⁷. Additionally, when exposed to Testosterone *in vitro*, both the time and dose play a role in reducing the levels of TLR4 on the cell surface of RAW 264.7 macrophage-like cells and primary murine peritoneal macrophages²⁸.

The innate immune system has profound effects on adaptive immunity, primarily through cytokine production. These cytokines include tumor necrosis factor- α (TNF- α), Interleukin-1 (IL-1), Interleukin-6 (IL-6), and Interleukin-12 (IL-12), among others. Estrogens have demonstrated to regulate TNF- α in a contradictory manner. For example, when murine bone marrow-derived macrophages (BMM) are exposed to estrogen before being stimulated with LPS *in vitro*, a reduction in TNF- α protein levels is observed²⁹, however, in the case of human monoblastic U937 cells stimulated with phorbol-myristate-acetate (PMA), the addition of 17 β -estradiol resulted in increased TNF-a production³⁰. Regarding IL-12, it has been observed that macrophages from female SJL mice produce more IL-12 protein compared with male SJL mice³¹. Regarding IL-6, Straub et al. demonstrated that IL-6 levels are decreased by estrogen replacement therapy in postmenopausal women³², restating the findings of previous studies that IL-6 production is negatively affected by estrogens³³

On the other hand, Testosterone enhanced LPS-induced IL-6 and macrophage chemotactic protein-1 expression by activating the ERK1/2/NF-kB signaling pathways in 3T3-L1 adipocytes³⁴.

2.2.3. Steroid hormones and T-cell response

T-bet, a specific transcription factor that induces IFN- γ production, is mainly found in immune cells, initially at low levels in resting CD4+ T cells but upregulated upon activation of T cells and splenic NK cells. In mice treated with 17 β -estradiol, T-bet expression in splenic lymphocytes and T cells increases, especially when IL-27 is present³⁵. This suggests that estrogen may prepare lymphocytes for Th1 differentiation by boosting T-bet expression and making them more responsive to immediate Th1-inducing cytokines like IL-27. Regarding androgens, it was found a direct suppressive effect of Testosterone on T cells confirmed by a decrease of IFN- γ and T-bet expression in splenic derived CD4+ T cells after treatment with synthetic Testosterone *in vitro*^{36,37}. Estrogen promoted Th2 cytokine production IL-5 and IL-13 and estrogen receptor α was expressed by CD4+ T cells from allergic mice³⁸. Also, 17- β estradiol significantly enhanced DC capacity to produce Th2 response *in vitro* (IL-4 and IL-13), on the contrary, when CD4+ T cells were co-cultured with DHT-treated antigen-pulsed DC there was a dramatic suppression of the Th2 priming ability with a complete ablation of IL-4, IL-10 and IL-13 production³⁹

Immune modulation by sex hormones has been demonstrated during years and can explain the variability of immune responses between males and females. Hormones can activate or inhibit several components of the immune system⁴⁰ (Figure 6). Thus, hormones may be used as target therapies in several diseases.

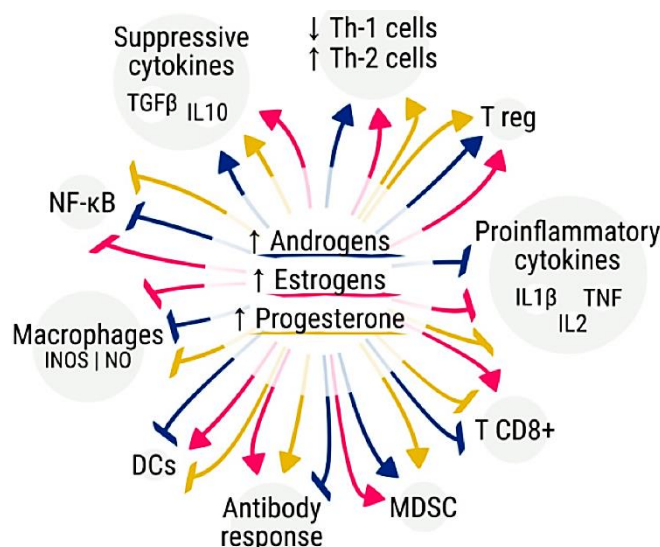


Figure 6. Description in the next page

Figure 6. Sex hormones and modulation of immune response. Androgens (blue), estrogens (pink), and progesterone (yellow) can activate and inhibit several components of the immune response. TGF β : transforming growth factor-beta; IL:interleukin; Th-1:T helper 1; Th-2:T helper 2; T reg: T regulatory cells; TNF:tumor necrosis factor; MDSC:myeloid-derived suppressor cells; DCs:dendritic cells; INOS:inducible nitric oxide synthase; NO:nitric oxide; NF- κ B:nuclear factor kappa-light-chain-enhancer of activated B cells. *From Cattrini et al 2020*⁴⁰

2.3. Sex steroid hormones and cancer

Cancer is a complex disease characterized by a series of genetic and metabolic changes that drive genome instability, allowing malignant cells to acquire various traits known as the hallmarks of cancer. These characteristic traits include: self-sufficiency in growth signals, insensitivity to anti-growth signals, resistance to apoptosis, sustained angiogenesis, limitless replicative potential, and the ability to evade tissues and metastasize^{41,42} However, hormones can also play a significant role in the development of certain cancers. Steroid hormones, which include corticosteroids and sex steroids, are vital for maintaining normal bodily functions. Disruptions of the normal hormone signaling pathways can lead to various diseases and contribute to cancer-related behaviors at the cellular level, such as cell proliferation, migration, invasion, and the formation of metastases^{43,44}.

Hormone-related cancer such as endometrium, adrenal, breast and prostate cancer, are treated with hormonal therapy, in which the production of hormones is either blocked by the inhibition of hormone receptors, or by inhibition of the enzymes in charge of their synthesis.

Hormone receptors are particularly recognized as key actors in cancer development. Steroid hormone receptor (SHRs) are ligand-activated transcription factors, and include Progesterone Receptor (PR), Estrogen Receptor (ER), Androgen Receptor (AR) and mineralocorticoid Receptor (MR)⁴⁵. Changes in the expression or structure of these receptors can make cells more sensitive to their respective hormone ligands. Approximately 30% of these changes involve activating mutations in the ligand binding domain (LBD) of ER in breast cancer⁴⁶. Polymorphisms in the ER gene can also impact the binding of ER to its response element in the DNA and other co-regulatory proteins, affecting the subsequent transcription of ER target genes, and have been linked to breast cancer risk and susceptibility to treatment^{47,48}. Also, it has been shown that 17 β -estradiol promoted proliferation, metastasis and angiogenesis by increasing levels of the chemokine CCL2⁴⁹

In the case of AR, various alterations have been observed, including amplifications, point mutations, and splice variants, which result in increased AR activity. For example, Exon 1 of the AR gene contains a polymorphic CAG repeat sequence that codes for a polyglutamine (polyQ) chain in the transcriptional activation region (AF1). The length of this polyQ chain is inversely correlated with AR's transcriptional activity. Since prostate cancer development depends on androgens, men with shorter polyQ repeat lengths, associated with higher AR transcriptional activity, are proposed to be at a greater risk of prostate cancer⁴⁵. Notwithstanding, the androgen receptor is directly involved in prostate cancer progression, and Testosterone alone appears to be associated to a higher risk of aggressive prostate cancer. Mendelian randomization analysis showed a significant association between free Testosterone and aggressive disease⁵⁰

Therefore, the steroid hormone metabolism plays an important role in regulating body homeostasis and disease progression such as cancer. In this regard, changes in the steroid metabolic pathways are essential to overcome the physiological barriers built in response to the progression of malignant cells. In fact in the last decade, metabolic reprogramming has been recognized as a new hallmark of cancer⁵¹

2.4. Metabolic reprogramming in cancer

To maintain the viability, uncontrolled growth and proliferation, the tumor needs metabolic adaptations to meet the demands of malignant cells^{52,53}. The tumor microenvironment is generally hypoxic and acidic and has distinct cell accompaniment compared to the healthy tissue^{54,55}. One of the main metabolic hallmarks is the alteration in energy metabolism, specifically in the glycolysis, this effect is known as Warburg effect. In normal cells under aerobic conditions, the pyruvate (product of glycolysis) continues to oxidative phosphorylation in mitochondria to produce energy (ATP). In cancer cells, despite the presence of oxygen, there is an increased amount of glucose uptake which is fermented to produce lactate. This process in normal cells is produced under anaerobic conditions, however, in cancer cells is conducted under aerobic conditions, i.e. aerobic glycolysis or Warburg effect (**Figure 7**).^{51,56,57} Cancer cells also rely on glutamine consumption, which provides carbon and amino-nitrogen needed for amino-acid, nucleotide and lipid biosynthesis⁵⁸. Beyond energy metabolism, alterations in lipid- and cholesterol-associated pathways in tumors are now well recognized and more frequently described.

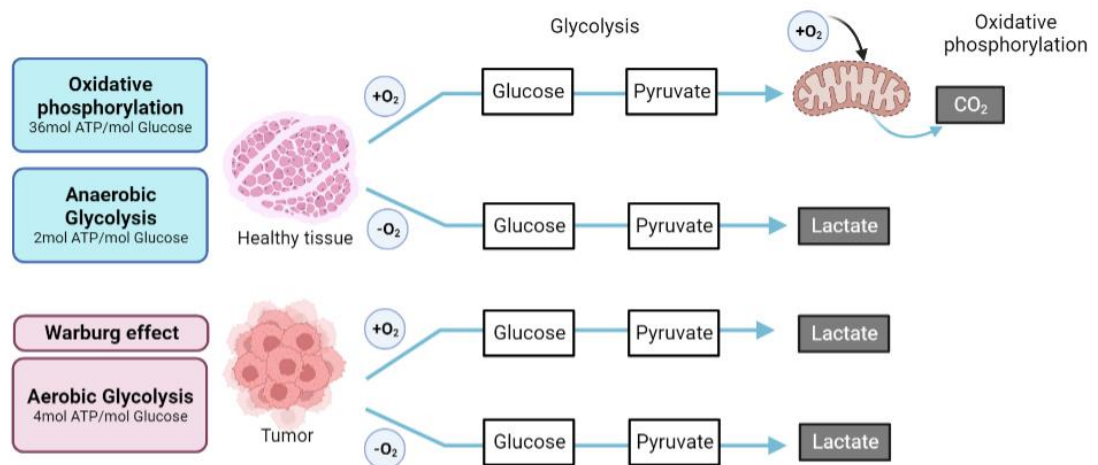


Figure 7. Metabolic reprogramming in cancer cells. Malignant cells adapted to a new tumor environment, conducted glycolysis even in aerobic conditions, in order to produce lactate and energy. Adapted from Yangjin Kim et al. ⁵⁸ and develop with Biorender.com

2.4.1. Lipidic metabolic reprogramming in cancer

Lipids are categorized into two main groups: simple lipids and complex lipids. Simple lipids encompass triglycerides (TAGs), which are commonly referred to as fats. Complex lipids consist of sterols and their esters, phospholipids (PL), and glycolipids⁵⁹. Lipids exert multiple biochemical functions in cells, including membrane synthesis, energy production, and the activation of intracellular signaling pathways. Numerous human diseases, including metabolic disorders, immune system disorders, central nervous system disorders, and cancer, often result from disruptions in lipid metabolic enzymes and their associated pathways. Highly proliferative cancer cells exhibit a significant demand for lipids and cholesterol, which they satisfy through increased uptake of external (dietary) lipids and lipoproteins or by ramping up their internal production, including lipogenesis and cholesterol synthesis. ⁵⁸. Comparisons of lipid profiles between malignant tumors and normal tissues have revealed variations. Hepatocellular carcinoma shows higher levels of saturated fatty acids (SFAs) and monounsaturated fatty acids (MUFAs), while colorectal cancer is characterized by an abundance of various lysophospholipids compared to its benign counterparts⁶⁰.

In most tumors, a nearly universal phenotypic alteration involves the upregulation of lipogenic enzymes such as acetyl-CoA carboxylase (ACC), fatty acid synthase (FASN), and ATP citrate lyase (ACLY), which also contribute to cholesterol synthesis^{61,62}.

Downstream enzymes involved in cholesterol biosynthesis could also be altered to adapt tissues and cells to new environments and to promote proliferation and malignancy. Thus, reprogramming in steroid hormone metabolism also play a key role in cancer.

CHAPTER I

ANDROGEN METABOLISM AND PROSTATE CANCER

**Study of the mechanisms of androgen
metabolism reprogramming in aggressive
prostate cancer models**

CHAPTER I: INTRODUCTION

CHAPTER I - INTRODUCTION

1. The Prostate

The prostate is a gland found in the male reproductive system. It's located just below the bladder and in front of the rectum. The prostate plays a crucial role in the production and transport of semen, which is the fluid that carries sperm during ejaculation⁶³.

1.1. Anatomy

The prostate gland appears round, elliptical, or triangular from an axial view. It weighs only a few grams at birth and about 20 grams by the age of 20. The prostate consists of several anatomical parts:

- a. Base: The top or base of the prostate is situated near the bladder.
- b. Apex: The bottom or apex of the prostate is located towards the urogenital diaphragm.
- c. Capsule: The prostate is surrounded by a fibrous capsule that helps maintain its shape.

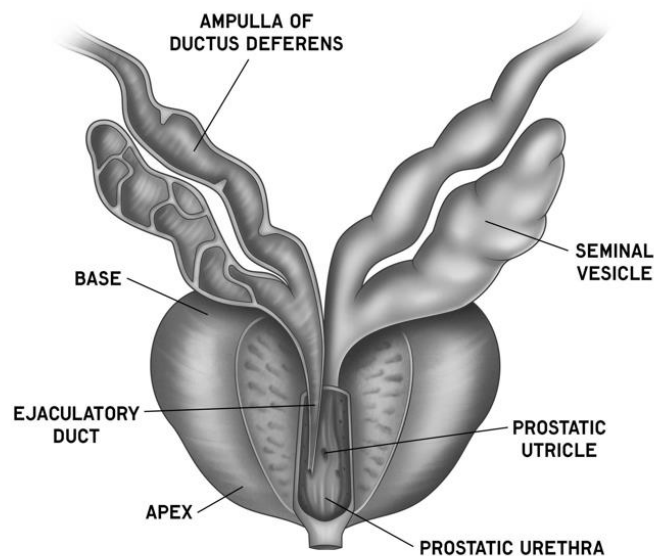


Figure 8. General anatomy of the prostate gland. Created by AnatomyStuff.co.uk

Histopathological analysis of the prostate reveals four different regions or zones. These include the peripheral zone (where most prostate cancers originate), central zone, and transition zone.⁶⁴

- 1.1.1. *Peripheral Zone*: The peripheral zone is the outermost region of the prostate gland. It surrounds the central zone and makes up the majority of the prostate's posterior and lateral surfaces. This zone contains a higher density of glandular tissue, including the acini that produce prostatic fluid, which contributes to semen. It is also the zone where most commonly develops prostate cancer.
- 1.1.2. *Central Zone*: The central zone lies in the inner part of the prostate, surrounding the ejaculatory ducts as they enter the prostate. This zone has fewer glandular structures compared to the peripheral zone. It is characterized by a higher proportion of fibromuscular stroma and fewer acini. Its primary function is to provide structural support. It plays a role in the contraction of smooth muscles during ejaculation.
- 1.1.3. *Transitional Zone*: The transitional zone surrounds the urethra as it passes through the prostate gland. It's located near the base of the prostate, close to the bladder. This zone is characterized by numerous glandular structures and a higher density of acini. The transitional zone contributes to prostatic fluid production and can impact urinary flow due to its location near the urethra. Enlargement of the transitional zone can lead to the development of benign prostatic hyperplasia (BPH).

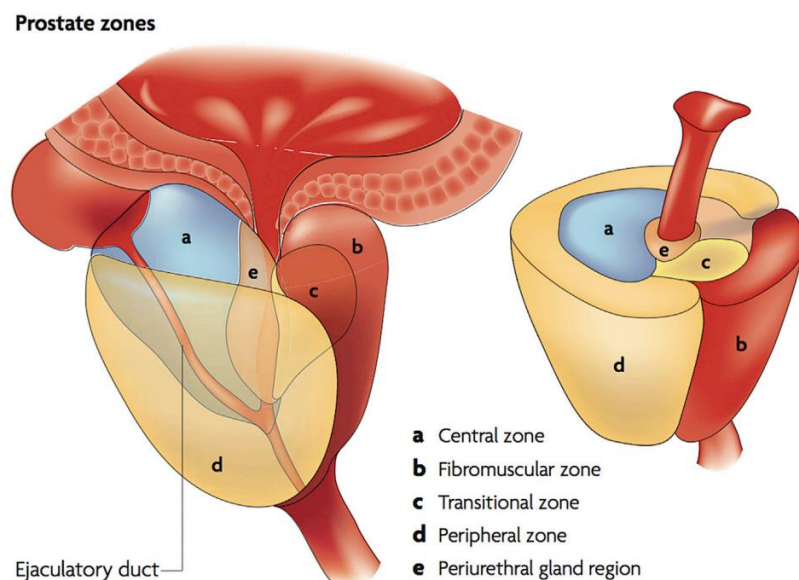


Figure 9. Zonal anatomy of the prostate gland. From Reeves et al.2016⁶⁴.

1.2. Histology

The prostate gland comprises both glandular and non-glandular tissues. A total of 30–50 glands are embedded in the prostate. The glandular tubes contain epithelial cells which coat the lumen and are responsible for the secretion during ejaculation. Prostatic glands are surrounded by interstitial tissue which accommodates smooth muscle cells, fibrocytes, elastic and collagen fibers, blood and lymph vessels, as well as nerves⁶⁵.

1.2.1. *Glandular Tissues*: This tissue is responsible for producing the prostatic fluid that makes up a significant portion of semen. The glandular tissue is organized into microscopic structures called acini and ducts, which are small sacs or clusters of cells that produce and store the prostatic fluid. There are four types of cells: luminal epithelial, intermediate epithelial, neuroendocrine, and basal cells.

1.2.2. *Stromal Tissues*: The stromal tissues of the prostate include the fibromuscular stroma, which provides support and structure to the gland. The stromal tissues contain smooth muscle cells that help with the contraction of the prostate during ejaculation, aiding in the expulsion of semen.

1.2.3. *Connective Tissues*: Connective tissues surround and support the various components of the prostate, helping to maintain its shape and integrity. It is composed of fibroblast cells.

1.2.4. *Blood Vessels and Nerves*: The prostate is well-supplied with blood vessels and nerves that play a role in regulating its function and responsiveness. Endothelial cells line the blood vessels within the prostate and play a role in blood supply. Nerves in the prostate are involved in sensations related to sexual arousal and orgasm.

Approximately 70-80% of prostate cancers originate in the peripheral zone of the prostate gland⁶⁶. The peripheral zone (**Figure 9**) contains a higher density of glandular tissue, including the acini that produce the prostatic fluid. The characterization of different cell populations in the prostate by analysis of gene signatures allowed the good management and treatment of prostate cancer⁶⁷. Several gene markers have been described associated with the different cell types in the prostatic epithelium. Basal cells express cytokeratins (CK), CK5, CK14 and p63 (a homologue of p53 tumor suppressor gene) and low levels of androgen receptor (AR). These cells are believed to act as stem cells for the regeneration of epithelial cells⁶⁸. Luminal cells mainly express PSA (*KLK3*), the cytokeratins CK8 and CK18 and to

a lesser extent Prostate-Specific Membrane Antigen (PSMA) often involved in folate metabolism and AR activity⁶⁹. It has been described a persisting luminal population in the mouse prostate that expresses also stemlike genes (Sca1⁺ and Psca⁺) which promoted the regeneration of the prostate after androgen deprivation. This suggests that the basal cells are not the only population with the potential for stemness⁷⁰. The neuroendocrine cell component is involved in regulating hormonal and paracrine signaling within the prostate gland. These cells are scattered among the secretory epithelial cells. They are smaller and rare, and commonly express neuronal markers like synaptophysin (SYP), the neural cell adhesion molecule (NCAM), neural specific enolase (NSE), chromogranin A, but no AR or PSA⁷¹. In addition, neuroendocrine cells also express very high levels of the prostate tumor overexpressed-1 (PTOV1) protein⁷². Neuroendocrine cells participate in the development of the most aggressive subtype of prostate cancer, the Neuroendocrine Prostate Cancer (NEPC), characterized by the absence of AR, PSA but the presence of neuronal markers⁷³. Finally, intermediate cells, that have been identified with a keratin phenotype intermediate between basal and luminal cells that co-express high levels of K5 and K18 (K5/18) as well as hepatocyte growth factor receptor c-MET⁷⁴. These cells have also been suggested to represent the prostatic progenitor stem cell population⁷⁵

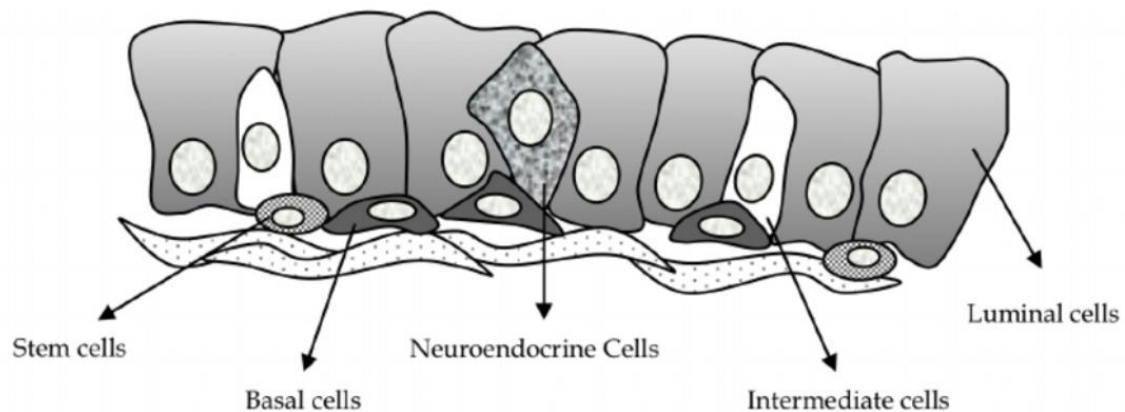


Figure 10. Composition of the prostate epithelium. From Espinoza et al.⁷⁵

1.3. Function

The prostate gland serves a vital role in the male reproductive system. Its primary functions include seminal fluid production, a milky alkaline fluid that makes up a significant portion of semen that helps to nourish and protect sperm as they travel through the reproductive tract⁷⁶. The prostate also produces PSA, an enzyme necessary to liquify semen and aids in sperm mobility. The prostate is also important for the contraction of the muscles that help to propel the semen into the urethra during ejaculation.

1.4. Mechanism of prostate function

The prostate requires hormones (Testosterone) to function properly. The Testosterone is mainly produced by the Leydig cells of the testes and to a lesser amount by the adrenal glands. Testicular androgens act in the development of the prostate during embryogenesis, in the prostate growth during puberty, and the enlargement in elderly men with BPH^{65,77}

In the prostate, Testosterone is metabolized into the active hormone dihydrotestosterone (DHT) inside the prostatic epithelial cells by the enzyme 5 α -reductase (SRD5A1/2). SRD5A1 is encoded on chromosome 5 and has minor expression and activity in the prostate but it has a predominant activity in extra prostatic tissues, such skin and liver. On the other hand, SRD5A2, encoded on chromosome 2 is predominantly expressed and active in the stromal and basal cells of the prostate⁶⁵. DHT binds to its receptor AR and the DHT-AR complex enters the nucleus where promotes specific gene transcription, protein translation, and growth hormone synthesis (*e.g.* PSA, epidermal growth factor [EGF] and vascular endothelial growth factor [VEGF]) that result in cell proliferation. AR is expressed in both epithelial and stromal tissues.

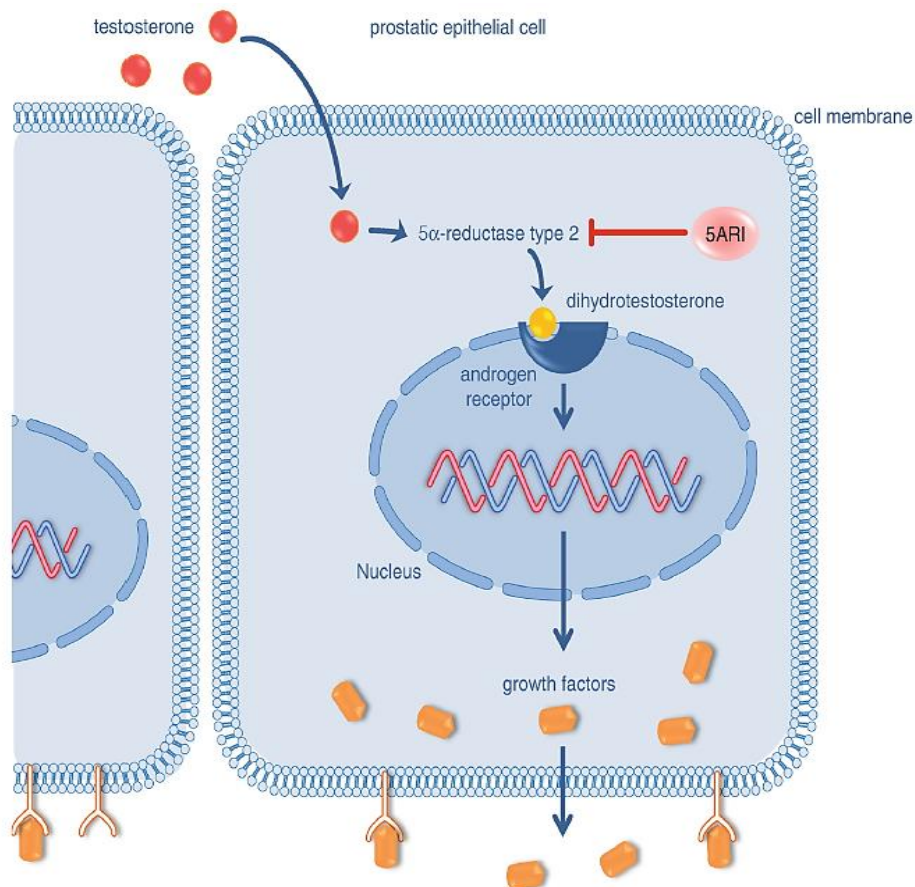


Figure 11. Hormonal physiology of prostate gland. Testosterone is converted into dihydrotestosterone inside the prostatic epithelial cell by SRD5A2. The DHT-receptor complex initiates gene transcription resulting in protein and growth hormone synthesis as well as cell proliferation. *From M. Oelke, 2020*⁶⁵

2. Prostate cancer

2.1. Epidemiology of prostate cancer

PCa is highly prevalent in industrialized countries, it is the most frequent cancer in men and the third cause of cancer death, after lung and colorectal, in Europe. PCa is also highly prevalent in Africa and Latin America^{78,79}. In most cases, it is efficiently eradicated by surgical prostatectomy but the late-diagnosed cancer or the aggressive phenotype have a five-year relative survival rates lower than 30%⁸⁰.

The incidence of PCa generally increases with age, approximately 60% of cases of PCa were diagnosed in men ≥ 65 years old⁸¹. Between the ages of 45 and 54 years, the percentage of diagnosed cases increased to 8.6% and 22% of all cases occurred in men 75-84 years old, and roughly 5% of cases were found in those ≥ 85 years old⁸².

2.2. Natural history of prostate cancer (course y evolution)

The natural history of prostate cancer is far from complete. This is partly because the disease is heterogeneous in both morphology and clinical behavior. The general prognosis varies widely with age, ethnicity, and genetic background⁸².

2.2.1. Initiation:

The tumor-initiating cells or the cells of origin of a prostatic adenocarcinoma are thought to originate from the basal or luminal prostate epithelial cells, and accumulation of genetic mutation is thought to be a primary driver of disease. The identity of a true cell of origin of all human prostatic adenocarcinomas remains controversial. The heterogeneous nature at both morphological and genetic level, impede the adequate knowledge of the real origin of this disease⁸³. However, it is generally accepted that during the tumorigenesis the transformation from benign to malignant disease occurs after a series of phenotypic changes, including cell signaling changes possibly as a consequence of genetic mutation.

2.2.2. Progression:

Tumor progression is accompanied by the rising of PSA levels, suggesting AR activity, a consequence of proliferation of luminal epithelial cells. However, some studies reported that PCa progression is possible despite minimal serum PSA elevation, in fact near to 22% of the patients in those studies developed metastasis with undetectable PSA levels⁸⁴. Disease progression is multifactorial and can arise from cells intrinsically resistant or that may acquire resistance induced by the treatment⁸³. The mechanisms of PCa progression are not well understood generally because of the lack of experimental models that reproduce the heterogenous characteristics of PCa. Tumors progress through distinct stages including non-malignant hyperplasia, carcinoma in situ, organ-confined localized tumors, indolent tumors with limited growth potential, and aggressive metastatic tumors⁸⁵. In the early stages, prostate cancer is confined to the prostate gland without spreading to nearby tissues or distant sites. Treatment options for localized prostate cancer may include active surveillance, surgery (radical prostatectomy), or radiation therapy. If the cancer grows or spreads beyond the prostate capsule, although it remains within the nearby tissues, lymph nodes, or seminal vesicles, it is considered locally advanced. Treatment options might include radiation therapy, androgen deprivation therapy (ADT), or a combination of therapies. Finally, if the cancer cells evade from the prostate gland and travel through the bloodstream or lymphatic

system to other parts of the body, it is considered metastatic hormone sensitive prostate cancer (mHSPC), or metastatic castration sensitive prostate cancer (mCSPC). At this stage, patients may eventually develop resistance to the ADT treatment and become castration-resistant prostate cancer (mCRPC), indicating that the cancer continues to grow despite low levels of Testosterone (if treated with ADT). This stage often requires more aggressive treatment approaches, such as newer targeted therapies, immunotherapies, chemotherapy, and other interventions **Figure 12)**

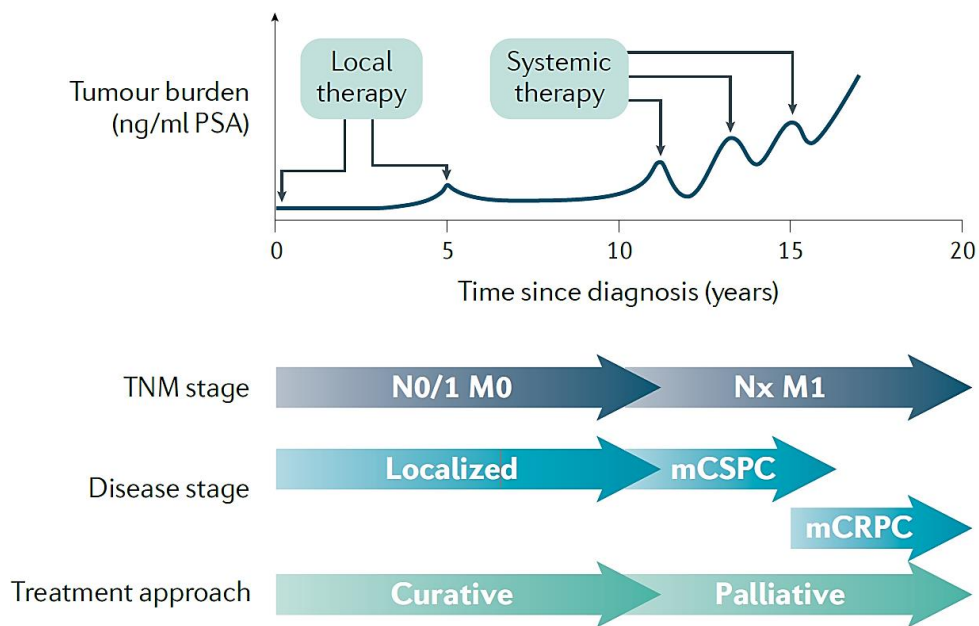


Figure 12. Prostate cancer stages. Tumor burden, estimated by PSA level over time since diagnosis, increases in patients whose cancer fails to respond to local and systemic therapies as the disease progresses to metastatic disease. These aggressive prostate cancers are associated with high tumor–node–metastasis (TNM) staging, progression from localized to metastatic castration-sensitive prostate cancer (mCSPC) and metastatic castration-resistant prostate cancer (mCRPC) and a change from curative to palliative care. *From Rebello et al.*⁸³

2.3. Processes promoting prostate carcinogenesis

2.3.1. Inflammation: chronic inflammation is usually linked to carcinogenesis. Inflammation might influence the pathogenesis of cancers by inflicting cell and genome damage, triggering restorative cell proliferation to replace damaged cells, and elaborating a portfolio of cytokines that promote cell replication, angiogenesis and tissue repair⁸⁶. Many epithelial lesions are associated with acute and chronic inflammation⁸⁷, indeed administration of the potent

heterocyclic amine PhIP (2-amino-1-methyl-6-phenyl-imidazo[4,5-b]pyridine), results in chronic inflammation and promotes prostatic hyperplasia and PIN in rodents⁸⁸. Interleukin-6 (IL-6), one of the most important markers of inflammations, is elevated in patients with untreated metastatic or CRPC, has been seen able to promote PCa cell proliferation and inhibit apoptosis *in vitro* and *in vivo*⁸⁹

2.3.2. Oxidative stress and DNA damage: it has been suggested that one of the major aging-associated effects on prostate carcinogenesis is oxidative stress and its cumulative impact on DNA damage⁸⁸. Oxidative stress occurs when the production of ROS exceeds antioxidant capacity, chronic increases in ROS over time are known to induce somatic mutations and neoplastic transformation⁹⁰. Interestingly, androgens may induce the production of spermidine⁹¹, which undergoes a polyamine catabolic pathway, increasing ROS levels. It has been described that the AR needs JunD protein as a coactivator to activate this oxidative pathway in LNCaP cells^{92,93}

2.3.3. Genetic alterations: Prostate cancer is believed to be strongly associated with the accumulation of somatic mutations in the prostate epithelial cell genome over a patient's lifetime. Frequent alterations in localized PCa are fusions of AR-regulated promoter regions with erythroblast transformation specific (*ETS*) genes family. Of these, *TMPRSS2-ERG* is the most frequent detected in around 50% of biopsies⁹⁴, followed by *TMPRSS2-ETV1*, in only 8%. Other alterations are found in the *SPOP* gene, which codes for the substrate-recognition component of the Cullin3-based E3-Ubiquitin ligase. The loss-of-function mutations in *SPOP* are less frequent (13%) and found in *TMPRSS2-ERG* negative tumors⁹⁵, similarly to the gain-of-function mutations in *FOXA1* (3%)⁹⁶. The progression from localized to metastatic disease, or mCSPC, to mCRPC involves deregulation of key genes of growth control, such as *PTEN*, encoded by a dual-specificity protein phosphatase. *PTEN* alterations are present in about 12-17% of localized and metastatic PCa^{97,98}. *MYC* has a wider role in prostate carcinogenesis, as *MYC* is almost ubiquitously expressed at every stage of tumor development. *MYC* overexpression was shown to diminish the AR

transcriptional program (genes directly targeted by AR) in luminal cells⁹⁹. In more advanced PCa, genes regulating cell cycle arrest, such as *TP53* and *RB1*, are frequently altered in approximately 27% of mCSPC and 50% of mCRPC^{100,101}. A gene involved in homologous DNA repair, the *ATM* (Ataxia Telangiectasia Mutated) is altered in 5% of mCSPC and 7% of mCRPC;^{100,101}

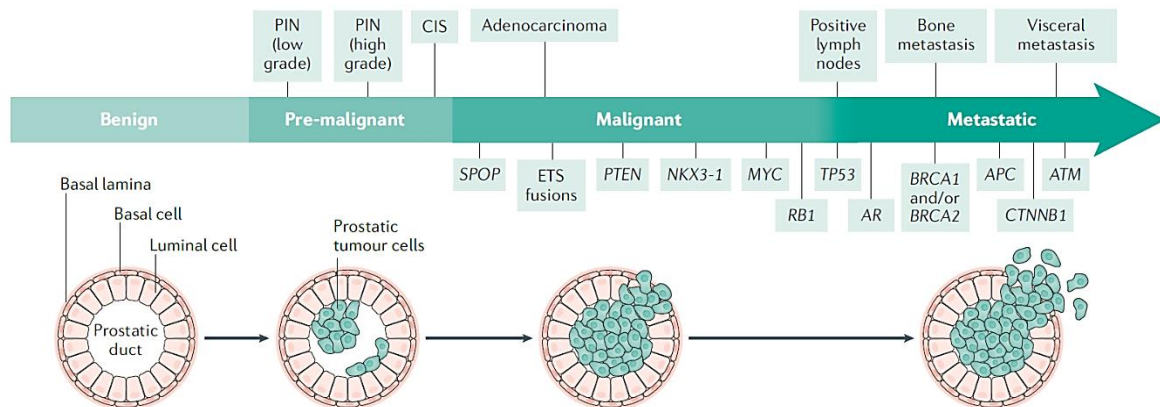


Figure 13. Genetic alterations in prostate cancer. Common mutations in prostate cancer are shown according to their enrichment at different disease stages. CIS, carcinoma in situ; PCF, Prostate Cancer Foundation; PIN, prostatic intraepithelial neoplasia. *From Rebello et al.*⁸³

2.3.4. Senescence: Cell senescence has been implicated in cancer progression. This topic will be discussed with more detail in senescence and prostate cancer section.

2.4. Diagnosis of PCa

Standard diagnostic tools for detecting prostate cancer include a digital rectal examination (DRE) to check for abnormalities, serum PSA levels, and prostate biopsy. Additionally, the Gleason score gives information about clinical stage and marker of prognosis.

2.4.1. *Digital rectal examination (DRE)*: DRE was the first diagnostic tool for PCa and the most common strategy for early detection¹⁰². This method consists in analyze the peripheral zone of the prostate gland by palpation through the low rectum. An abnormal DRE results include, a hard mass or nodule, induration or asymmetry¹⁰³.

- 2.4.2. *Serum PSA:* Prostate-Specific Antigen (PSA) a protein encoded by *KLK3* gene, belonging to the kallikrein family of serine proteases located in the chromosome 19, is commonly used as a screening tool for prostate cancer because is easily detected in the blood¹⁰⁴. PSA is present in circulation as a complex with α -antichymotrypsin and, in a minor fraction, as free PSA¹⁰⁵. Elevated PSA levels can be indicative of prostate-related conditions, generally, a PSA level of 4.0 ng/mL is considered the threshold for normal/abnormal, but this value can vary based on age and other factors. PSA levels between 4.0 and 10.0 ng/mL are often considered in a gray area, and further evaluation is needed¹⁰⁶.
- 2.4.3. *Prostate biopsy:* prostate biopsy is the standard and official method used to confirm the presence of prostate cancer. The needle biopsy procedure is typically guided by imaging techniques such as transrectal ultrasound (TRUS) or magnetic resonance imaging (MRI) fusion, which help target specific areas of concern within the prostate gland¹⁰⁷. TRUS-guided biopsy is recommended when DRE is suspicious and PSA levels are elevated.
- 2.4.4. *Clinical stage:* The staging system commonly used for most cancers is the TNM system, which stands for Tumor, Nodes, and Metastasis. It assesses three key factors to determine the stage of cancer: T, N, and M. Each factor provides specific information about the extent and spread of the cancer. T (Tumor) describes the size and extent of the primary tumor and ranges from 0 through 4. N (Nodes) assesses whether cancer has spread to nearby lymph nodes. Lymph nodes are small, bean-shaped structures that play a crucial role in the immune system and ranges from 0 to 3). Finally, M (Metastasis), indicates whether the cancer has metastasized, meaning it has spread to distant organs or tissues beyond the primary site and regional lymph nodes. The M category has two possible values: M0: No distant metastasis or M1: Distant metastasis is present.
- 2.4.5. *Gleason grade:* Gleason grade is a classification system used to grade the histological appearance of prostate cancer cells under a microscope. It provides valuable information about the aggressiveness and potential behavior of this cancer. The Gleason Grade System categorizes prostate cancer cells into five distinct patterns:

Pattern 1: well differentiated uniform single glands, closely packed in masses with relatively circumscribed boundaries.

Pattern 2: well differentiated but more variable single glands, slightly spaced apart, boundaries of tumor less well circumscribed.

Pattern 3: moderately differentiated glands that may range from small to large, growing in spaced-out infiltrative patterns, may be papillary or cribriform.

Pattern 4: cells raggedly infiltrating, fused-glandular tumor frequently with pale cells, may resemble hypernephroma of kidney.

Pattern 5: anaplastic carcinoma with minimal glandular differentiation, diffusely infiltrating prostatic stroma.

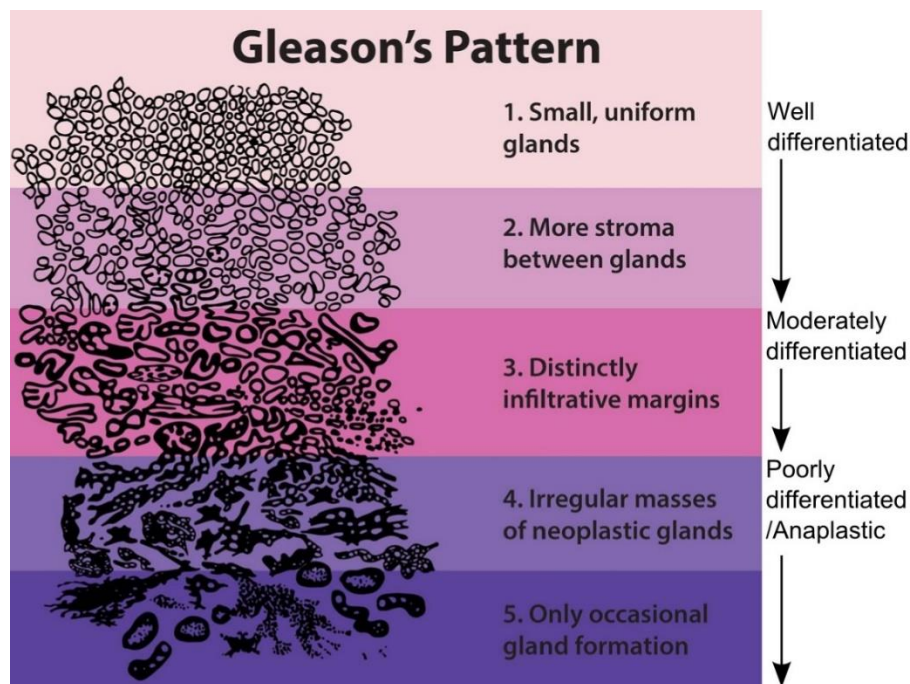


Figure 14. Gleason Pattern. Diagram of differentiation grades in prostate cancer from low aggressiveness (well differentiated) until high aggressive (poor differentiated). *adapted from the Gleason et al.¹⁰⁸ Image obtained from the National Cancer Institute.*

The Gleason grading attempts to represent the heterogeneity of the tumor. The pathologist informs the results as a **score** which is derived from the sum of the first most prevalent pattern observed in the tissue sample and the second more frequent: for example, 4+3=7. The new system revised in 2014 by the International Society of Urological Pathology

(ISUP), established five groups, adjusting PCa grading to other carcinomas grading systems¹⁰⁸. (**Table 1**)

Table 1. Prostate cancer classification in groups according to Gleason pattern.

Patterns	Score	Group	Risk factor
1+2, 3+2, 3+3	≤ 6	1	Very low/Low
3+4	7	2	Low/intermediate
4+3	7	3	Intermediate
3+5, 4+4, 5+3	8	4	High
4+5,5+4	9	5	Very high
5+5	10	5	Very high

As shown in table 1, in the new classification the score 7 is divided in two groups, depending on whether the most frequent pattern is 3 or 4. According to the original grading, cribriform glands were considered to be in pattern 3, however, it was demonstrated that this pattern is more related to the aggressive PCa in 84% of the cases. Therefore, nowadays, cribriform glands are included in pattern 4¹⁰⁸.

3. Prostate cancer treatment

The treatment options for prostate cancer vary based on the stage and extent of tumor development. Prostate cancer is often classified into different stages based on factors such as tumor size, spread to nearby lymph nodes, and whether it has metastasized (spread) to distant parts of the body. The treatment approach may change as the cancer progresses (**Figure 15**).

3.1. Localized Prostate Cancer (Early Stage):

Men with localized PCa have a low-risk or slow-growing prostate cancers (low risk of biochemical relapse, BCR), active surveillance may be recommended. Regular monitoring with PSA tests, digital rectal exams, and occasional biopsies are conducted to ensure the cancer is not growing or spreading rapidly. If the risk increases (PSA >10), surgery (Radical Prostatectomy) is recommended. This can be done through open surgery or minimally invasive techniques such as laparoscopic or robotic-assisted surgery. Also, radiation therapy can be recommended. Options include external beam radiation therapy and brachytherapy

(implantation of radioactive seeds directly into the prostate). These patients have a very good survival rate (>95%)

3.2. Locally Advanced Prostate Cancer:

Patients with PSA>20 and stages T 3-4 or lymph node invasion (N1), commonly are treated with a combination therapy: radiation therapy may be combined with hormone therapy (Androgen Deprivation Therapy - ADT), before radical prostatectomy. This group of patients present a BCR risk >50%¹⁰⁹.

3.3. Metastatic Prostate Cancer:

The median survival for patients who progress to a metastatic PCa (Overall Survival -OS) in low volume disease is 92.4 months and 55.2 months in high volume disease. However, when metastatic PCa is detected at diagnosis the OS is 51.6 months in low volume disease and 43.2 months for high volume disease¹¹⁰. In these patients ADT is the standard treatment approach and may consist of Luteinizing hormone-releasing hormone (LHRH) agonists, LHRH antagonists or bilateral orchiectomy. Also combination therapy with docetaxel is applied¹¹¹. This type of metastatic disease is also known as hormone sensitive PCa (mHSPC), however, after 1-5 years up to 40% of patients eventually develop a castration resistance PCa (mCRPC).

3.4. Resistant Prostate Cancer:

The treatment for resistant PCa could be a second-Line hormone therapy. Until 2004, cancer resistance to initial hormone therapy, was treated with the addition of secondary hormonal manipulations, including: antiandrogens as bicalutamide and nilutamide and corticoids. However, the use of docetaxel (a taxane, inhibitor of microtubule), was the first systemic therapy demonstrating survival benefit in mCRPC¹¹². In addition to docetaxel, most agents for the treatment of mCRPC were approved based on demonstrable survival benefit in randomized studies as cabazitaxel, abiraterone acetate and enzalutamide¹¹³. In the last decade the development of new cancer treatments has focused on immunotherapy¹¹⁴. One of the first treatments for mCRPC was Sipuleucel-T¹¹⁵, an autologous cellular immunotherapy, composed of autologous antigen-presenting cells cultured with a fusion protein, PA2024, a prostatic acid phosphatase linked to granulocyte-macrophage colony-stimulating factor¹¹².

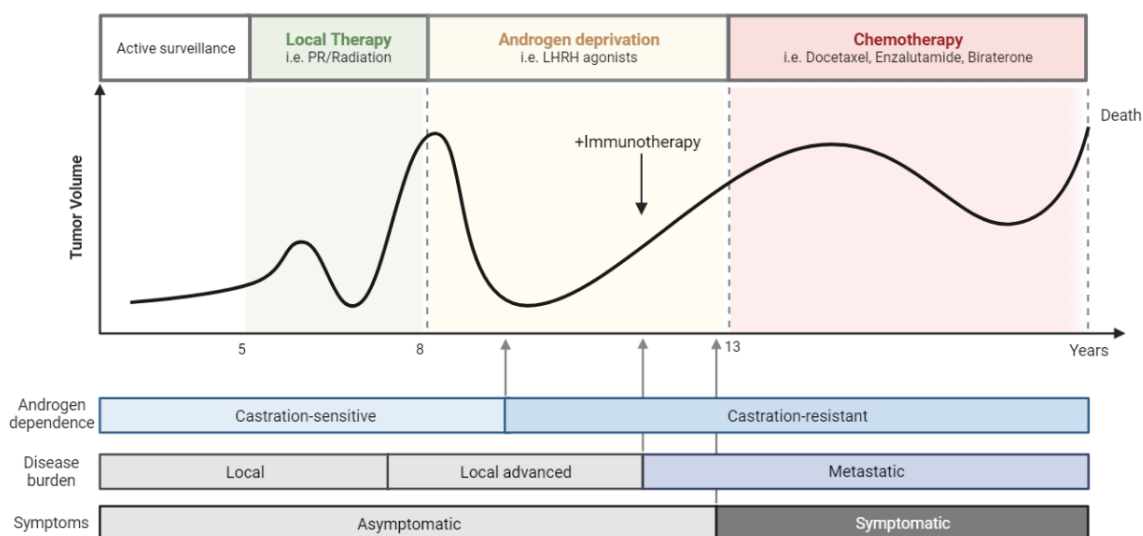


Figure 15. Stages in Prostate cancer progression and associated therapies.

4. Mechanisms implicated in Castration Resistant Prostate cancer:

Despite the initial high efficacy, the resistance to ADT invariably provokes the development of a castration-resistant prostate cancer (CRPC). This form of prostate cancer represents a significant challenge in the treatment of advanced PCa.

4.1. Androgen Receptor (AR) Signaling Persistence

Many prostate cancer cells continue to rely on the AR signaling for growth, even in the absence of high levels of circulating androgens, a subset of cells develop hypersensitivity to androgens either through amplification or mutations in the AR^{116,117}. Such mutations are absent in localized PCa but are frequent in advanced or metastatic PCa and in CRPC.

- 4.1.1. *AR Mutations*: Mutations in the *AR* gene can lead the receptor to enhance its sensitivity to the ligand in low androgen environments, acquire affinity for non-androgens ligands, and even to antagonist-to-agonist switching. There are >100-point mutations that appear in the *AR*, and the majority of them present in the NTD or LBD region, among them: L702H, H875Y, W742C, F877L and T878A, being the last two the most studied mutations. These LBD-mutations resulted in increased AR transactivation activity and decreased ligand

specificity, promoting activation not only by androgens but also other steroid hormones^{117,118}.

4.1.2. *AR Amplification*: Gene amplification is defined as an increase in gene copy number beyond the normal diploid copy number. In CRPC, cells can increase the number of androgen receptors on their surface, enhancing their sensitivity to low androgen levels. Over 80% of patients with CRPC had a significant increase of AR mRNA and protein levels. The comparison of AR protein levels in CRPC samples to multiple isogenic tumor xenograft models using microarray-based profiling, found increased AR expression in CRPC cells¹¹⁹

4.1.3. *AR Splice Variants*: The production of alternative forms of the androgen receptor, or splice variants, is an additional manner for cancer cells to achieve the capture of the necessary androgen hormones or increase the activity of the AR. AR splice variants are truncated AR proteins prone to persistent activation. They lack the LBD region, and just the NTD and DBD regions are transcriptionally activated, independent of the presence or absence of ligand-binding or antagonist effect. AR variants can be produced through genomic structural rearrangements (GSRs) during ADT, altered mRNA splicing, or high transcriptional rates of the full-length AR itself.

4.2. Androgen-Independent Pathways

PCa cells adapt to survive without high levels of androgens because they succeed to activate alternative growth pathways that are not reliant on AR signaling:

4.2.1. *PI3K/AKT/mTOR Pathway Activation*: This pathway plays a pivotal role in cell growth and survival. Activation of this pathway can lead to resistance by promoting cell growth independently of AR signaling.

4.2.2. *HER2/Neu Overexpression*: Overexpression of the *HER2* receptor gene can drive PCa cell growth, even when androgen levels are low.

4.2.3. *Neuroendocrine Differentiation*: Some PCa cells can undergo neuroendocrine differentiation, thus becoming less dependent on AR signaling for growth.

4.3. Intratumoral *de novo* steroidogenesis:

Androgen deprivation therapy entails the reduction of circulating androgens or their activity within the body, which typically inhibits the growth of PCa cells that depend on androgens for their survival and proliferation. Although the synthesis of Testosterone mostly occurs in Leydig cells in the testis, some prostate cancer cells can adapt to the low androgen environment by developing the ability to synthesize their own androgens. In models of castration-resistant prostate cancer (CRPC) with low circulating androgen levels, it has been established that intra-tumoral androgen levels mirror or even surpass those produced in eugonadal men, indicating an alternate source of androgen production in the tumor. The source of Testosterone in prostatic tissue after ADT implies intracrine production within the gland, converting adrenal androgens to dihydrotestosterone (DHT). Specifically, dehydroepiandrosterone (DHEA) and its sulfated form DHEA-S, unaffected by ADT, are reduced to form α -androstanedione which can be converted to DHT by HSD3B, AKR1C3 and SRD5A1 enzymes, through the “backdoor” pathway^{120,121}. In addition to the utilization of weak adrenal androgens, some studies indicated augmented expression of steroidogenic enzymes such HSD3B1, HSD3B2, HSD17B3, AKR1C3, and SRD5A1, suggestive of a *de novo* production of steroids and androgens^{122,123}. Studies on tissue samples from metastatic CRPC patients revealed a significant upregulation of the genes *FASN*, *CYP17A1*, *HSD3B1*, and *HSD3B2* compared to primary prostate cancer^{124–127}. Immunohistochemical staining of the enzymes CYP11A1, CYP17A1, and 17 β -hydroxysteroid dehydrogenase-3 (17 β HSD3) in lymph node metastasis also demonstrated higher staining intensity than primary PCa samples. Multiple investigations have confirmed the active intratumoral steroidogenesis in CRPC cells¹²⁸. Both cholesterol and adrenal androgens (DHEA) emerge as plausible sources for intratumoral DHT synthesis. The key steroidogenic enzymes that are upregulated in CRPC emerge as attractive targets for a therapeutic intervention aimed at reducing intraprostatic androgen levels. However, given the absence of a single enzyme target, a combination of drugs becomes necessary to inhibit diverse enzymes. This approach, at times, yields less than favorable outcomes or incurs in notable side effects. Thus, exploring into the mechanisms implicated in steroidogenic reprogramming it is imperative to identify new biomarkers and enhance the therapeutic paradigm.

5. Models to study prostate cancer

5.1. In vivo models:

Among the animals models available, mouse models for cancer studies are relatively quick and easy for breeding schemes, ease of manipulation of embryonic cells *in vitro*, stability of genotype(s), and availability of multiple mouse strains with specific gene alterations¹²⁹, however, mice prostate substantially differs from human prostate at anatomical and physiological level^{130,131}. The prostate in the mouse is composed of distinct lobes, whereas human only possesses a single and compact structure. However, the most important histological differences are the lower content of basal cells and stroma, and the low amount of smooth muscle cells present in the stroma¹³².

New techniques have allowed the development of genetically manipulated mice to study the natural history of prostate cancer. Current mouse models for prostate cancer can be divided into 2 broad categories: genetically engineered mouse (GEM) models and xenograft (PDXs) models^{133,129}. The convenience of xenograft investigations is their rapid progression from the tumor implantation to its development, which renders xenograft models an appealing and pivotal component within numerous contemporary preclinical drug assessments¹³⁴. Nonetheless, the disadvantages associated with xenograft models encompass the restricted availability of tumor cell lines harboring specific genetic modifications, dissimilar tumor growth kinetics in comparison to human tumors, lack of proper stromal-tumor interactions, and the inadequate elicitation of appropriate immunological responses¹²⁹. GEM models overcome most of the xenograft shortcomings, however, several drawbacks of these models include: the necessity of long-term studies, long tumor latency, time and high cost associated with breeding, skills and genotyping. In addition, many common genotypes are not represented, patented strains are unavailable, and spontaneous strain-dependent tumorigenesis independent from genetic engineering has been¹²⁹

5.2. In vitro models:

In vitro cells cultures models, mainly from human origin, are among the most useful tools due to the high availability, easy to use, and low cost. Ideally, a tumor models should reflect inter-patient and intra-patient heterogeneity, resistance, interaction with their

microenvironment, and have similar effects of the tissue architecture on drug penetration, bioavailability and efficacy¹³⁵. However, *in vitro* PCa cell cultures, have proven to be particularly difficult to obtain in comparison with other types of cancers, and the few available cell lines lack many of the characteristic genetic lesions commonly associated with prostate cancer and do not represent the tumor heterogeneity^{136,137}.

The most widely used cell lines are LNCaP, Du145 and PC3, all of which are derived from metastatic nodules of different organs and therefore, they poorly represent the primary tumor heterogeneity. To overcome some of these problems, three-dimensional (3D) patient derived organoids (PDOs) are perhaps a more efficient alternative, as they still maintain tumor heterogeneity and appropriate disease modeling. Organoids, or “mini organs”, are clusters of cells grown *in vitro* that self-organize and differentiate into functional cell types¹³⁸. These models, however, also show some disadvantages, such as longer timescale than cell cultures, requires more extensive analyses, data obtained are highly dependent on the environment, causing high variability¹²⁹.

6. Senescence and Prostate cancer

6.1. Senescence

Replicative senescence, originally described by Hayflick and Moorhead¹³⁹, is defined as an irreversible proliferative arrest after a limited number of divisions¹⁴⁰. Cellular senescence has been considered essentially a stress response that protect the adult organism against insults that damaged cells may cause and therefore senescence was described as a critical tumor suppressor mechanism acting as a barrier preventing the proliferation of tumor cells^{141,142}.

6.2. Senescence and cancer

Current findings have convincingly demonstrated a paradoxical role of senescence¹⁴³. For example, cellular senescence response in embryo development has been demonstrated to provide not only cellular proliferative control but also signals for tissue remodeling activity¹⁴⁴, being a developmental force that can promote plasticity, improvement of regeneration and proliferation¹⁴⁵. Similarly, recent studies have shown that senescence can promote cancer stemness and aggressiveness. Gene expression analysis showed that senescent B- cell lymphomas upregulated stem cell markers and WNT signaling comparing versus non-senescent cells¹⁴⁶.

6.3. Senescence and prostate cancer

Interestingly, almost 20 years ago, Chen and collaborators showed that a complete conditional inactivation of the tumor suppressor *PTEN* in genetically engineering mice, resulted in PIN lesions that displayed a senescence phenotype¹⁴⁷, Shen and Abate⁸⁸ interpreted these results as a temporarily activated senescence during which additional oncogenic events are completed to bypass senescence and promote cancer progression. More recently, the metalloproteinase inhibitor TIMP1 has been identified as a crucial determinant in the effects of senescence within prostate cancer. In mouse models, senescence induced by *PTEN* deficiency or chemotherapy, effectively limits prostate cancer progression. However, when TIMP1 is absent, senescence promotes metastasis¹⁴⁸.

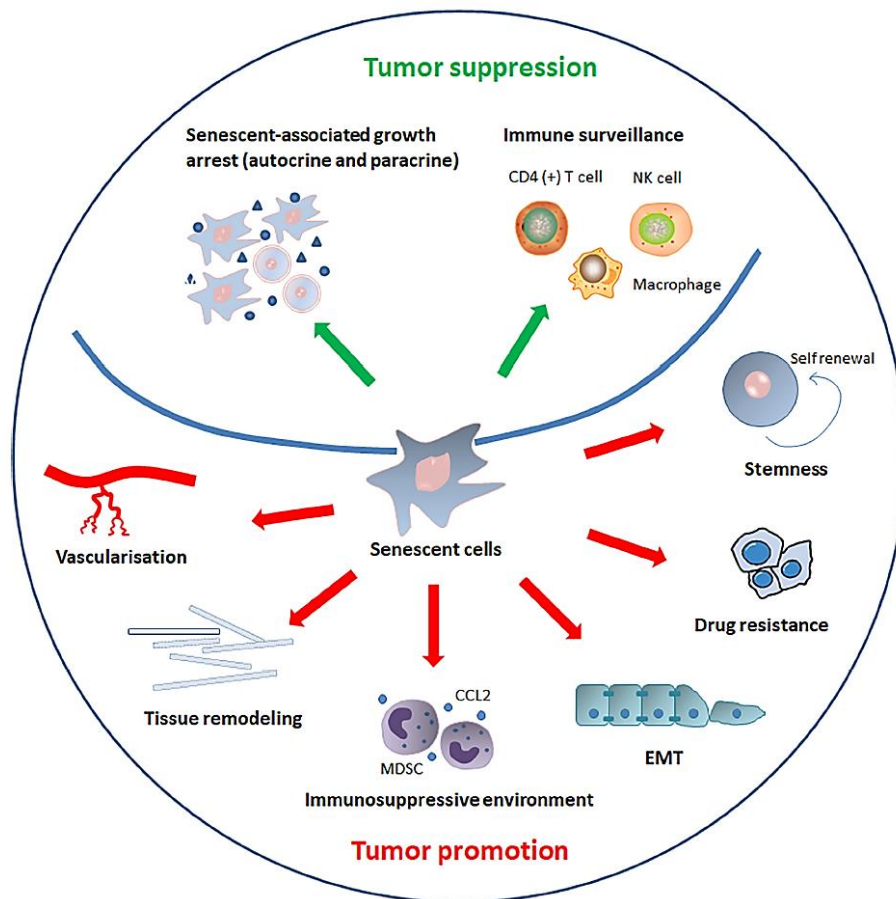


Figure 16. Dual role of senescence in cancer. SASP components can induce or enhance growth arrest, immune surveillance inhibiting cancer progression, however, SASP can also activate vascularization, tumor remodeling, drug resistance, immunosuppression and stemness to promote cancer progression. From Yang et al 2021¹⁴³

CHAPTER I: PREMISE

CHAPTER I - PREMISE

PCa is a hormone-dependent tumor^{149,150} and so the gold standard treatment for patients with inoperable tumors is the androgen deprivation therapy (ADT), which is effective to reduce the tumor volume¹⁵¹. However, the progress to a resistant cancer in the great majority of cases treated with ADT remains the biggest problem^{152–155}. One of the mechanisms proposed to explain the development of resistance is intratumor hormone biosynthesis. Tumors develop capacities to synthesize their own androgen hormones after a deprivation therapy. Studies that revealed the presence of steroids in tumor tissues and the expression of key steroidogenic enzymes, indicate the tumors' potential for a *de novo* steroids synthesis^{122,156–158}. However, the study of the mechanisms that lead to cancer resistance has been challenging, mostly due to the limited number of cell lines and xenograft models and the lack of tumor representativeness^{159,160}. PCa has been characterized by a great level of intra- and inter-tumor heterogeneity, which makes it difficult to accurately model PCa *in vitro*¹⁶¹. In fact, the presently available seven PCa cell lines cannot represent the heterogeneity of these tumors and, for example, only VCaP cells have shown abilities for *de novo* steroids synthesis¹⁶². Currently, novel tools to study PCa, as well as patient-derived models have shown better correlations with clinical stages of the disease^{163–165}. Among them, cultures derived from primary prostate tumors have shown to represent good *in vitro* models to study the disease mechanisms and predict the patient's response to ADT.^{166–168}

Recently, in our laboratory we have developed *ex vivo* cell cultures derived from hormone-naïve aggressive inoperable primary prostate tumors. Preliminary genetic characterization of these cultures showed good representation of the heterogeneity of prostate tumors. Interestingly, more than 70% of cultures contained a genetic alteration in the *TP53* gene, P72R (rs1042522). This SNP remains controversial as a prostate cancer biomarker or predictor for the disease.

An early intervention, preventive for the development of resistance, would require the improvement of tools to study new biomarkers able to predict the patient response to ADT, and possibly the discovery of new target genes that contribute to androgen production in prostate cancer. To know the mechanisms implicated in the rewiring of the steroidogenic metabolism in aggressive PCa could be a promising route for improving the diagnosis, prognosis, and management of these patients.

CHAPTER I: HYPOTHESIS AND OBJECTIVES

CHAPTER I - HYPOTHESIS AND OBJECTIVES

1. Hypothesis

Recently, our laboratory has developed *ex vivo* cell cultures from hormone-naïve primary prostate tumors, to better represent the heterogeneity of prostate tumors, and be used as models to study the mechanism of resistance that originate in the primary tumor. In agreement with the current problems above exposed, we hypothesized that:

- i.** Primary cultures derived from prostate tumors of naïve patients could be a useful and representative model to study the mechanisms of resistance. The characterization of this model in reference to the original tissue by detecting major mutated genes, indicate the *TP53* SNP is associated with prostate cancer in the European population.
- ii.** Focusing in the intratumor steroidogenesis to discover new markers for future therapies, hormone-naïve Primary Cultures (hnPCs) might be showing changes in gene expression of steroidogenic enzymes (reprogramming) necessary to maintain proliferation and survival.
- iii.** The reprogramming of the steroidogenic metabolism would be promoted by the senescence-associated cancer stemness signature observed *in vitro*.

2. General objective

Study the steroidogenic pathway and mechanisms involved in hormone metabolism reprogramming in hormone- naïve primary cultures to search for new biomarkers.

3. Specific objectives

- i.** Examine the association between P72R SNP in *TP53* gene and prostate cancer.
- ii.** Analyze the expression of steroidogenic enzymes in hnPCs along the hormone steroid synthesis pathway.
- iii.** Compare the gene expression profiles between primary PCa cultures and tumor tissues.
- iv.** Determine the role of cellular senescence in the hormone metabolism reprogramming.

CHAPTER I: MATERIALS AND METHODS

CHAPTER I - MATERIALS AND METHODS

1. Cellular cultures:

1.1. Cell lines:

LNCaP: is a human prostate epithelial cell line that was obtained in 1977 from a needle aspiration biopsy of a lymph node in the left supraclavicular region of a 50-year-old Caucasian man who had metastatic prostate carcinoma¹⁶⁹. These cells exhibit the presence of androgen receptor (AR), estrogen receptor (ER), and prostate-specific antigen (PSA), and they respond to androgen stimulation¹⁷⁰. Additionally, the cells express cytokeratins 8, 18, and 20, along with wild type (WT) p53 and PTEN inactivation. Notably, this cell line carries a T877A mutation in the AR gene sequence, which leads to a strong binding affinity to various steroid compounds. LNCaP cells have a slow growth rate, taking around 60-72 hours for their population to double, and their karyotype typically ranges from 33 to 91 chromosomes. When transplanted into mice (xenografts), LNCaP cells show a moderate success rate of 50% in developing tumors, and these tumors have a doubling time of approximately 86 hours¹⁷¹.

Du145: is a human prostate cancer cell line that originated from a metastatic site in the brain¹⁷². These cells do not produce prostate-specific antigen (PSA) and do not respond to androgens. Their population doubling time (PDT) is approximately 29 hours. The cell line has undergone extensive chromosomal rearrangements, showing a range of 58 to 63 chromosomes in each metaphase spread, with a predominant count of 64 chromosomes. Notably, these rearrangements affect around 70% of the 22 different autosomal chromosomes, including modifications such as t(11q12q), del(11)(q23), 16q+, del(9)(p11), and del(1)(p32). In terms of cancer grade, Du145 cells give rise to grade II adenocarcinoma and have the capability to spread to various organs, including the spleen, lungs, and liver¹⁷¹. While the Du145 cell line were initially characterized as lacking the androgen receptor (AR), recent research has shown the presence of AR protein in these cell lines and its induction following treatment with dihydrotestosterone (DHT). However, this upregulation of AR protein did not lead to the activation of AR-responsive reporter genes. As a result, the authors proposed that Du145 cell line should be described as "androgen non-responsive" rather than "AR-negative"¹⁷³.

Sublines:

The docetaxel-resistant cellular models Du145 were provided by Dr. Begoña Mellado from the Laboratory and Medical Oncology Department at Hospital Clínic in Barcelona. The development of (docetaxel resistant) DR-Du145 cells occurred through a process of selection by exposing cells to escalating doses of docetaxel over extended periods of 1 year from Du145. The initial concentration of docetaxel used for the culture was 5 nM, and surviving cells were cultured while gradually increasing the docetaxel concentration to 10, 25, 50, 100, and 250 nM. In a parallel manner, the parental Du145 cells were subjected to the same dose-escalation protocol, with exposure to DMSO (vehicle solution).

The androgen-independent (AI) and androgen-dependent (AD) models LNCaP cells were obtained from the laboratory of Dr. Anna C. Ferrari at the Division of Neoplastic Diseases in the Department of Medicine at Mount Sinai School of Medicine in New York. In brief, the LNCaP AI subline was established by continuously culturing LNCaP cells in RPMI medium deprived of androgens, with 10% charcoal-stripped, heat-inactivated FBS for a period of 6 months.

1.2. Cell lines maintenance:

Cells were maintained at a temperature of 37°C in an environment containing 5% CO₂. Du145 cells and LNCaP cells were grown in RPMI-1640 medium from BioWest. All media were supplemented with 10% heat inactivated fetal bovine serum (FBS), 2 mM L-glutamine, 100 U/mL penicillin, 100 µg/mL streptomycin, and 0.1 mM non-essential amino acids, all provided by BioWest. The LNCaP AI subline was cultivated in RPMI-1640 medium with charcoal-treated and heat inactivated 10% FBS. Docetaxel resistant Du145 cells were maintained in RPMI-1640 supplemented with 2.5 nM docetaxel (Sigma-Aldrich, St. Louis, MO).

For cryopreservation, two million cells were slowly frozen in 1 mL of ice cold FBS containing 10% DMSO. Cells were kept at -20°C for one day, then transferred to -80°C for 3-5 days. For extended storage, vials were stored in a liquid-nitrogen freezer to maintain temperatures below -160°C. To recover cryopreserved cells, frozen vials were rapidly thawed in a 37°C water bath, diluted in pre-warmed complete culture medium, centrifuged

at 1200 rpm for 5 minutes, resuspended in complete culture medium, and seeded into appropriate flasks.

1.3. Ex vivo Prostate primary cultures (hnPCs):

Primary cultures were previously established in our laboratory from prostate tumor needle biopsies of hormone-naïve patients (i.e., without previous treatments, hnPCs). In brief, all patients were selected for (i) high levels of serum PSA (>50 ng/mL), (ii) positive digital rectal examination. DRE and PZA >50 ng/mL. Five needle biopsies were used for culture. Biopsies were cut into small pieces (< 1mm³) using a razor blade, then centrifuged for 10 min at 250 xG and seeded on plates (collagen, or Poly-D-lysine treated) with complete DMEM-F12 medium to promote attachment. Cells were allowed to migrate from tissue pieces and fill the plate. After the first passage, epithelial cells were purified from fibroblasts using a two-step trypsinization method: the initial step with TRYPLE at 0.5X in PBS for 5 min at room temperature. After removal of fibroblasts, a subsequent trypsinization step with concentrated TRYPLE 1X at 37°C for 5 min. was used to collect epithelial cells. TRYPLE was eliminated by centrifugation and addition of fresh complete DMEM-F12 medium. In the following experiments of this study, after thawing, each cell culture was treated with trypsin (0.05%) in the initial passages to remove fibroblasts and ensure that the cultures were free from contamination. Subsequent passages were performed with Trypsin 0.25%.

1.4. hnPCs culture and maintenance:

Hormone-naïve primary cultures were cultured at 37°C in at atmosphere of 5% CO₂, with complete DMEM-F12 medium. The complete medium contained: 2mM of L-Glutamine, 100U of penicillin/mL, 100 µg streptomycin/mL, 0.1mM of non-essential amino acids, 1mM of sodium pyruvate and 7% fetal bovine serum, with supplement 1X and human FGF-10 (10ng/µL), human EGF (20ng/µL), Vitamin A and E (200ng/µL). Growth factors and vitamins were added freshly whereas supplements were prepared and stored at -20°C until its used. Supplement (100X) was prepared in DMEM-F12 containing glucose (6 mg/mL), transferrin (1000µg/mL), human insulin (2.500µg/mL), putrescine (97µg/mL), sodium selenite (30 µM) and hydrocortisone (100µM).

1.4.1. Plates pre-treatment

Plates were treated with collagen I or poly-D-lysine 1X. Briefly, 50 µL/mL of collagen I (Merck) were added into the plate/wells and incubated for 1 hour at 37°C. Remaining

solution volume was aspirated, and plates were allowed to dry overnight in the incubator. Coated dried plates were sterilized by exposure to UV light in a sterile culture hood for 15 minutes, sealed and store at 4°C until ready to use.

Poly-D-Lysine (0.1mg/mL) 100X was used for coverslips coating in immunofluorescence. In brief, coverslips were washed with ethanol and rinsed with sterile water. Once coverslips were dry, Poly-D-Lysine at 1X was added to the well containing the coverslip and was incubated for 1 hour at room temperature on cabinet. Finally, excess of volume was removed, and coverslips were washed with water and allowed to dry in the incubator. Also, plates were sterilized previously to use.

1.4.2. Androgen deprivation model

In order to mimic androgen deprivation therapy *in vivo*, hormone-naïve primary cultures were previously treated in our laboratory to establish two models: Androgen Independent (AI) model and Androgen Dependent (AD) model.

AI model for each culture, were treated with medium lacking steroid hormones (Charcoal treatment), cells able to grow in those conditions for at least seven days were selected and surviving cells were trypsinized and replated at same conditions. AD models, were the counterpart cultures, growing in medium with hormones.

2. Tissue samples and biopsies

2.1. Samples of benign prostatic hyperplasia (BPH) and Radical prostatectomies (RP)

Three tissues samples from benign prostatic hyperplasia (BPH) donors were used as controls samples and eleven radical prostatectomies (RP) samples from patients with low-grade tumor status (Gleason < 8) were used to compare with hnPCs and tissues biopsies. Samples from BPH and RP were collected by the Unit of Urology of Vall d'Hebron Hospital (Barcelona, Spain) and preserved in Optimal Cutting Temperature compound (OCT) and store at – 80 °C until frozen sectioning.

Frozen tissue were transported on dry ice for precise sectioning with a cryostat and cut in sections 10µm thick at -20°C. Collected section were transferred to cryotubes on dry ice for RNA extraction. For each sample, a section at maximum diameter location at thickness of 5 µm both immediately before and immediately after the tissue sections was collected for

Hematoxylin and eosin staining.

2.2. Samples of needle biopsy tissues

From each patient, two additional sample of needle biopsy were collected for further analysis with RNA extraction. These samples were previously collected in RNA later (Qiagen) stored for one day at 4°C. After that, RNA later was removed, and tissue were then stored at -80°C until RNA extraction.

3. Serum samples from PCa patients

3.1. Patient recollection

Patients with prostate cancer diagnosis admitted to Vall d'Hebron Hospital (HVH) were selected from the hospital database. Criteria for selection were patients with PSA \geq 50ng/mL white, southern European. In total we were able to collect 94 patients (protocol approved by the Hospital's CEIC (PR (AG) 96/2015, CEIC Hospital Vall d'Hebron).

3.2. Serum sample collection

Serum samples were collected from surplus samples routinely checked at the Biochemistry Dept. of the Hospital Vall d'Hebron. Briefly, samples blood collected in SST yellow tubes containing separator gels, were centrifugated at 3,500 rpm for 15 minutes at 4°C. The resulting serum was collected in 2 mL tubes, properly labeled and codified in the biobank system, were then stored at -80°C. Sample processing was performed according to the scientific and ethical guidelines approved by biomedical research law (Decret 1716/2011) at the Vall d'Hebron Hospital Biobank.

4. DNA manipulation

4.1. DNA extraction

4.1.1. DNA from cell cultures

Genomic DNA was isolated utilizing the DNeasy mini kit from Qiagen, following the manufacturer's guidelines. This kit employs chaotropic salts to bind nucleic acids to the spin minicolumn membrane for DNA purification. For cell cultures, the medium was aspirated, and cells were washed with cold PBS. Subsequently, cells were centrifugated at 1200 rpm

and resuspended in 200 μ L of PBS containing Proteinase K (20 μ L) and 4 μ l RNase A (100 mg/ml), mixed by vortexing, and incubated 2 min at room temperature. Then, 200 μ L of AL (lysis) buffer was added and mixed thoroughly by vortex before incubation at 56°C for 10 min. After this, ethanol was added (200 μ L) and the mixture was again mixed and transferred to the DNeasy Mini spin columns. These were centrifugated at 8,000 rpm for 1 minute and the flow-through was discarded. The spin columns were subsequently washed and centrifugated with AW1 and AW2 wash buffer (500 μ L). Finally, the purified DNA was eluted using a buffer of low ionic strength, rendering the DNA suitable for single-nucleotide polymorphism analysis.

4.1.2. DNA from tissue samples

The same procedure for DNA isolation from cell culture was performed with some modifications, following manufacturer instructions. Frozen tissue sections, placed in criotubes were mixed with 180 μ L of ATL buffer and homogenized by passing it through a 20-gauge needle attached to an RNase-free syringe about 5-10 times, then 20 μ L Proteinase K was added and incubated at 56°C until the tissue was completely lysed (approximately 1 hour) by vortexing every 20 minutes during the incubation period. The following steps were processed as with cell cultures.

4.1.3. DNA from serum samples

For the genomic DNA extraction from serum samples of prostate cancer patients, the MagNA Pure 24 Instrument, and total Isolation Kite (Roche) was used. This fully automated system is based on the use of magnetic glass particle technology (MGP), that allows the processing of up to 24 samples in about 70 minutes. Briefly, the sample material is lysed, nucleic acid is released, and nucleases are denatured. After that, DNA binds to the silica surface of the MGPs by action of chaotropic salts and the high ionic strength of the lysis/binding buffer. MGP with bound nucleic acids are magnetically separated from the residual lysed sample and unbound substances, such as proteins, cell debris, and PCR inhibitors are removed by several washing steps. Purified DNA is eluted from the MGP in elution buffer.

4.2. DNA genotyping for SNIps

To analyze the Pro72Arg SNP of *TP53*, genotyping was conducted for all samples using the Melting Curve analysis with a customized Light SNIp assay (TIB MOLBIOL) on a LightCycler 480 II instrument (Roche). The reactions were carried out in a final volume of 20 μ L, comprising 2.0 μ L of LightCycler FastStart DNA Master HybProbe mix (Roche), 1.0 μ L of LightSNIp mix, 3 mM MgCl₂, and 50 ng of DNA. The ThermoCycler was set up under the conditions outlined in **Table 2**. Subsequently, the melting curves were assessed using the Melt Curve Genotyping software on the LightCycler 480 II instrument (Roche).

Table 2. Cycling conditions for Melting curve analysis

Phase	Cycles	Temperature	Hold	Ramp rate ($^{\circ}$ C/s)
Denaturation	1	95	10 min	4.6
Cycling	45	95	10 sec	4.6
		60	10 sec	2.4
		72	15 sec	4.6
Melting	1	95	30 sec	4.6
		40	2 min	2.0
		75	0 sec	-
Cooling	1	40	30 sec	2.0

4.3. DNA sequencing

DNA sequencing using the Sanger method, also known as chain termination sequencing, enables the determination of the exact order of nucleotide bases in a DNA molecule. This method, developed by Frederick Sanger et al. in 1977, played a pivotal role in deciphering genetic information. This technique involves synthesizing DNA fragments using normal nucleotides and chain-terminating dideoxynucleotides (ddNTPs) by the DNA polymerase in *in vitro* replication. Each ddNTP is labeled with a fluorescent marker, by convention arginine (A) is marked with green, fluorescent dye, thymine (T) with red dye, guanine (G) with black and cytosine (C) with blue. The resulting fragment will extend until the available ddNTP and will show the respective color at different positions. Then, fragments are separated by size electrophoretically in a single glass capillary filled with a polymer. Visualization of these fragments reveals their sequence pattern, and can be interpreted by the color that corresponds to a particular nucleotide¹⁷⁴.

DNA sanger sequencing can be performed using as a template, genomic DNA, plasmids, or complementary DNA (cDNA) synthesized from mRNAs. To analyze the presence of

variants in the *TP53* gene, specifically to confirm the presence of the polymorphic variant Pro72Arg (rs1042522) in the expressed gene and compared with genotyping analysis in genomic DNA, we performed a reverse transcription of RNA to DNA (cDNA). Then the cDNA was sequenced by the Sanger's method.

4.3.1. cDNA synthesis

The reverse transcription (RT) *in vitro* was performed with NZY M-MuLV first strand cDNA synthesis kit (NZY Tech) and the 2720 Thermocycler from Applied Biosystems. The kit includes a combination of random hexamers and oligo(dT)₁₈ primers in order to increase sensitivity. The primers are included in the NZYRT 2X Master Mix, which also contains dNTPs, MgCl₂ and an optimized RT buffer. NZYM-MuLV RT Enzyme Mix includes both NZY M-MuLV Reverse Transcriptase (RNase H minus) and NZY Ribonuclease Inhibitor in order to protect RNA against degradation due to ribonuclease contamination. An RNA H from *E. coli* is added at the final step to remove any cDNA-RNA hybrid in the product. The starting amount of total RNA was 1.0 µg, previously extracted and verified for good quality (RNA manipulation methods section). General protocol is shown in **Table 3**.

Table 3. Protocol y conditions to synthesize cDNA

Reactive	Quantity	Procedure
NZYRT 2X master mix	10 µL	Mix and incubation at 25°C for 10 minutes.
NZYM-MLuV RT enzyme	2 µL	
RNA (1µg)	Up to 20 µL	Then rise temperature at 37°C, incubation for 50 minutes,
DEPC- treated H ₂ O	To complete 20 µL	
Reaction Volume	20 µL	Inactivation by heating at 85°C for 5 minutes, and chill on ice
NZY RNase H	1 µL	Incubation for 20 minutes at 37°C
Final product	21 µL	Store at -20°C

5. RNA manipulation

5.1. RNA extraction from cell cultures

Total RNA was isolated using the RNeasy mini kit (QIAGEN) as per the manufacturer's protocol. This method was designed to extract total RNA (with lengths greater than 200 bases) from small quantities of animal cells or tissues. It relies on a silica-gel-based membrane that selectively binds RNA due to its specialized high-salt buffer system, allowing up to 100 µg of RNA longer than 200 bases to bind. The procedure involves lysing and homogenizing biological samples in a denaturing guanidine isothiocyanate-containing buffer to promptly deactivate RNases and ensure intact RNA isolation. Ethanol is added to facilitate proper binding conditions, followed by applying the sample to a mini spin column where total RNA binds to the membrane and impurities are effectively removed. High-quality RNA is subsequently recovered in 50 µL of water.

5.2. RNA from OCT tissues

TRIzol-based RNA isolation has some advantages in comparison to the silica column-based extraction method for isolating RNA from small amounts of tissue because it can produce a higher RNA concentration¹⁷⁵, however residual contamination with phenol traces or the tissue fixation reagents (OCT, FFPE) can impair RNA purity and integrity¹⁷⁶. The use of silica-based methods improves the acid nucleic purification, providing efficient separation of RNA from contaminants such as proteins, DNA, and impurities.

Consequently, a combination between both techniques were used to improve RNA quality from OCT tissues. In brief, frozen tissue sections placed into cryotubes, were embedded with 1.0 mL of Qiazol lysis reagent (Qiagen), followed by a homogenization step with a gentle vortex at low speed. Then, samples were incubated for 5 minutes at room temperature and 200 µL of chloroform was added. The mixture was shake by tube inversion 10 times, and centrifugated at 12000 rpm at 4°C for 20 minutes. The upper aqueous phase (~300 µL) was transferred to another tube (Eppendorf 1.5 mL), then the same volume (300 µL) of RLT buffer (RNeasy mini kit) was added, mixed, and incubated at room temperature for 3 minutes. After that, 300 µL of ethanol was added, mixed, and samples incubated for 2 additional minutes. The mixture was transferred to a silica column from RNeasy mini kit and centrifuged at 8000 rpm for 1 minute at 4°C, followed by two washes steps with RPE buffer according to the manufacturer. RNA was eluted in 50 µl of nuclease-free water.

5.3. RNA quality assessment

Good quality RNA is essential for further applications as RT-PCR, microarrays, or RNA sequencing. To determine the integrity and the concentration of total RNAs from cell cultures and tissues, we used the 2100 Bioanalyzer from Agilent, a chip-based system that utilizes microfluidic technology to perform electrophoresis and fluorescence detection, enabling the precise quantification and analysis of biological samples¹⁷⁷. Only 1µl of sample is required, 11–12 samples can be run on the same chip, and analysis is complete in 30–40 minutes. The RNA integrity is measured as a number (RIN), considering the entire electrophoretic trace of the RNA including the ratio of 28S and 18S rRNAs. The RIN scale ranges from 0 to 10, with 10 indicating maximum RNA integrity. The ratio of 28S and 18S rRNA peaks also is given. As RNA degradation becomes more apparent, peak heights for the 28S and 18S rRNA decrease, while smaller or degraded RNA peaks become more prominent (**Figure 17**).

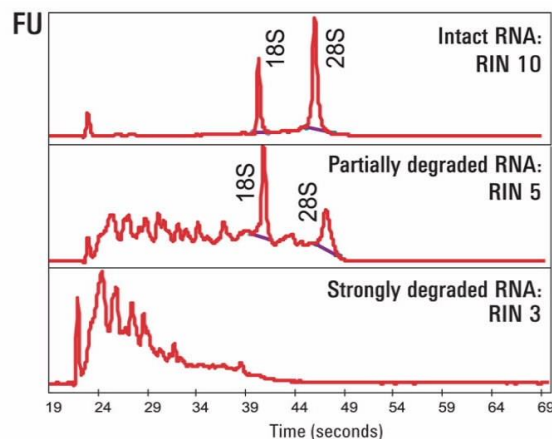


Figure 17. Schematic representation of electropherograms obtained with BioAnalyzer 2100. Top panel: represent excellent quality of RNA showing fragments distribution in two peaks. Center panel: medium quality, showing RNA degradation. Bottom panel: low quality RNA, showing total degradation of sample. *From Agilent.com*

5.4. Real time polymerase reaction (RT-PCR)

Reverse Transcription-Polymerase Chain Reaction (RT-PCR) is a sensitive method frequently used to detect mRNA and quantify gene expression changes. This technique involves two successive reactions: first, RNA is converted into complementary DNA (cDNA) via reverse transcription, and subsequently, the cDNA serves as the template for PCR amplification. For the RNA retrotranscription step, the NZY M-MuLV First-Strand

cDNA Synthesis Kit (NZY Tech) was employed, following the manufacturer's instructions, with a final volume of 20 μL . This kit employs both random hexamers and oligo(dT)18 primers, ensuring high cDNA yields and excellent sensitivity in subsequent RT-PCR. The samples were incubated in a 2720 Thermal Cycler (Applied Biosystems, USA) for 10 minutes at 25°C, followed by 1 hour at 37°C and 5 minutes at 85°C. The resultant cDNA was then diluted 1:20 in RNase-free water and stored at -20°C.

The cDNAs were employed in RT-PCR using the NZYSpeedy qPCR Probe Master Mix protocol (NZY Tech). Gene expression quantification was achieved using two types of probes. The first preliminary assays were performed using the Universal Probe Library (UPL) Set, Human (Roche) method. However, the manufacturer discontinued the UPL product line in 2020, thus the TaqMan probe assay (ThermoFisher Scientific) was used in its place. All reactions were carried out on a LightCycler 480 instrument (Roche).

5.4.1. UPL probe protocol:

Each 5 μL RT-PCR reaction contained 2.5 μL of NZYSpeedy qPCR Probe Master Mix, 0.05 μL of UPL-probe, 0.2 μL of forward primer (10 μM), 0.2 μL of reverse primer (10 μM) (ThermoFisher), 0.8 μL of RNase-free water, and 1.25 μL of cDNA. Final concentrations of each component are found in **Table 4**.

Table 4. RT-qPCR reaction components and concentration with UPL

Component	Volume	Initial Concentration	Final concentration
Master mix qPCR 2X	2.5 μL	2X	1X
UPL probe	0.05 μL	10 μM	100 nM
Forward primers	0.2 μL	10 μM	400 nM
Reverse primers	0.2 μL	10 μM	400 nM
H ₂ O	0.8 μL	-	-
cDNA 1:20	1.25	2.5 ng/ μL	0.625 ng/ μL

5.4.2. TaqMan probe protocol:

Each 5 μL RT-PCR reaction contained 2.5 μL of NZYSpeedy qPCR Probe Master Mix, 0.125 μL of TaqMan-probe (with primers incorporated), 1.125 μL of RNase-free water, and 1.25 μL of cDNA. Final concentrations of each component are found in **Table 5**.

Table 5. RT-qPCR reaction components and concentrations with TaqMan

Component	Volume	Initial Concentration	Final concentration
Master mix qPCR 2X	2.5 μL	2X	1X
TaqMan probe	0.125 μL	18 μM (20X)	450 Nm (0.5X)
H ₂ O	1.125 μL	-	-
cDNA 1:20	1.25	2.5 ng/ μL	0.625 ng/ μL

The ThermoCycler settings can be found in **Table 6**.

Table 6 Cycling conditions for RT-qPCR

Stage	Cycles	Temperature	Hold	
			UPL assay	TaqMan assay
Preincubation	1	95°C	5 min	10 min
Amplification	45	95°C	10 sec	15 sec
		60°C	30 sec	60 sec
		72°C	1 sec	-
Cooling	1	40°C	10 sec	10 sec

5.4.3. Primers for UPL and TaqMan probes

Primers (**Table 7**) were designed using the Universal ProbeLibrary Assay design center (Discontinued) (<https://qpcr.probefinder.com/organism.jsp>).

Table 7. Primers for UPL assay

GENE	UPL probe	Forward	Reverse
AR	#14	GCCTTGCTCTCTAGCCTCAA	GGTCGTCCACGTGTAAGTTG
CREB1	50	CAGTGACGGAGGAGCTTGTA	GCATCTCCACTCTGCTGGTT
CREBBP	78	ACAAGCGAAACCAACAAACC	AAAGAAGTGGCATTCTGTTGC
SQLE	#22	TCATCAGTGAAGAAACGAGGTG	GATACCCTTTAGCAGTTTTCTCCA
STAR	#44	TACGTGGCTACTCAGCATCG	GGACAGGACCTGGTTGATGA
STARD3	#79	GGCAAGACGTTTATCCTGAAGA	GTTCCACAGCACCATCCTC
SOAT1	#31	TTGGTGACAGGATGTTCTATAAGG	CCACATTCCAGGTTCTATAATAGTTG
AKR1C3	#41	TTGAATCATCAGAATCATCTCTTTT	CAAAGCTTTACTTCTCGGAACC
CYP1B1	#61	GGCATTAGAGTCAACTACACAAAGC	GAATGGCAAGTGCCAAAAA
CYP11A1	#59	AGGAGGGGTGGACACGAC	TTGCGTGCCATCTCATACA
SRD5A2	#22	AATGATGAGGTTACATGCTGCTT	TTGGGGCTTCTGCTGTACTION
SRD5A1	#79	CAGTACGCCAGCGAGTCC	CGCATCAGAAATGGGTAAATTAAG
HSD3B1	#80	TCCAGCTTTTAAACAATCTAACTAATGC	AAGATGCTGGGGAGCAGAT
HSD17B3	#66	CGTCCTGGAACAGTTCTTCAT	GGAGAATCTCACGCACTTCCG
HSD17B6	#67	GCACGGGGAAGAATTGTC	CCCAAAATGTTGAATCTCACG
HSD11B2	#64	GGGGGTCAAGGTCAGCAT	CACTGACCCACGTTTCTCAC
HSD17B10	#36	GCCTTCGAGGGTCAGGTT	GGTCATCACCCGGATACCTA
HSD17B12	#31	TGTAAGATGACACAATTGGTACTGC	TTCAGAATAGCCCCTTTGGAT
RDH5	#03	ACTTGGGCTCCAGCTATGTG	CACAGCACTGCCCAGAGTAA
RDH16	#24	CCCATTTTCTGCATCAGTCA	GGGAGAGGATGGGCAAATAG
CD44	41	CAAGCAGGAAGAAGGATGGAT	AACCTGTGTTTGGATTTGCAG
CD133	86	GGAAACTAAGAAGTATGGGAGAACA	CGATGCCACTTTCTCACTGAT
TBP	#87	GAACATCATGGATCAGAACAACA	ATAGGGATTCCGGGAGTCAT
IP08	#18	CAAATGTGGCAGCTTCTTAGGT	ATGCAGGAGAGGCATCATGT

Table 8 TaqMan assays for RT-qPCR

GENE	Catalog number	TaqMan assay	Amplicon (bp)
AR	4453320	Hs00171172_m1	72
ESR1	4453320	Hs01046816_m1	65
ESR2	4453320	Hs01100353_m1	73
ESRRA	4453320	Hs01067166_g1	146
GPER1	4453320	Hs01922715_s1	136
SIRT1	4453320	Hs01009006_m1	91
STAR	4448892	Hs00986559_g1	78
STARD3	4448892	Hs00199052_m1	90
AKR1C3	4453320	Hs00366267_m1	112
CYP1B1	4453320	Hs00164383_m1	118
CYP19A1	4453320	Hs00903411_m1	72
HSD3B1	4448892	Hs04194787_g1	112
HSD17B3	4448892	Hs00970004_m1	125
HSD17B10	4448892	Hs00189576_m1	76
HSD17B12	4448892	Hs00275054_m1	65
SRD5A1	4448892	Hs00971645_g1	100
SRD5A2	4448892	Hs00936406_m1	105
PAPSS2	4331182	Hs00989928_m1	69
ENO2	4453320	Hs00157360_m1	77
SYP	4453320	Hs00300531_m1	63
CHGA	4453320	Hs00900370_m1	67
CHGB	4453320	Hs01084631_m1	112
TP53	4453320	Hs01034249_m1	108
MDM2	4453320	Hs00540450_s1	104
CDKN1A	4453320	Hs00355782_m1	66
CDKN2A	4453320	Hs00923894_m1	115
TBP	4453320	Hs00427620_m1	91
IPO8	4453320	Hs00914057_m1	88

5.5. RNA transient interference (siRNA)

RNA interference (RNAi) is a powerful cellular mechanism that regulates gene expression by silencing specific genes using small interfering RNA (siRNA) molecules. The mechanism is based on the sequence-specific degradation of host mRNA through the cytoplasmic delivery of a long double-stranded RNA (dsRNA) complementary to the target sequence, which is processed to form the effector molecule called siRNA by action of Dicer enzyme¹⁷⁸. The siRNA nascent, and the endogenous Dicer, TRBP and Argonaut (Ago2) proteins form the RNA-induced silencing complex (RISC) complex, which mediated the gene target degradation or silencing¹⁷⁹.

Pre-designed and specific dsRNA against CDKN1A (p21^{WAF1}) was obtained from Integrated DNA Technologies (IDT) (**Table 9**). Dicer-Substrate short interference RNAs (DsiRNAs) are dsRNAs 27mer RNA duplexes, chemically synthesized, optimized for Dicer processing showing increased potency compared with 21mer siRNAs. DsiRNAs were acquired in TriFECTa RNAi Kit, containing, three pre-designed DsiRNAs target-specific with different sequences (2 nmol), three control DsiRNAs: TYE563 transfection control (1nmol), HPRT-S1 positive control (1 nmol), Negative control or scramble (1nmol); and nuclease-free duplex buffer for resuspending DsiRNAs.

Table 9. List of siRNAs for CDKN1A transient knockdown

Gene	siRNA	Sequence 5'-3'	Reference
-	siRNA positive control	TYE 563 Transfection Control	51-01-20-19
CDKN1A	siRNA.1	GCCUCUGGCAUUAGAAUUAUUUAAA GUCGGAGACCGUAAUCUAAUAAAUUU	232777410
	siRNA.2	GUAAACAGAUGGCACUUUGAAGGGG UUCAUUUGUCUACCGUGAAACUUC CCC	232777413
	siRNA.3	AGCGAUGGAACUUCGACUUUGUCAC ACUCGCUACCUUGAAGCUGAAACAGUG	232777416
-	siRNA negative control	Scramble negative control	51-01-19-08

5.5.1. Transfection protocol:

LNCAp cells were seeded in 12-well plates and incubated for 24 hours at 37°C (5% CO₂), the were transfected with *CDKN1A* DsiRNAs, transfection control (CTRF) and negative control (CNT) DsiRNAs, at 10nM for 48 hours (**Figure 18**). Mixes for transfection were

prepared according to Table. Primary cultures were transfected using the same protocol but in petri dishes 60mm (p60), scaling up the volume of the transfection mixes.

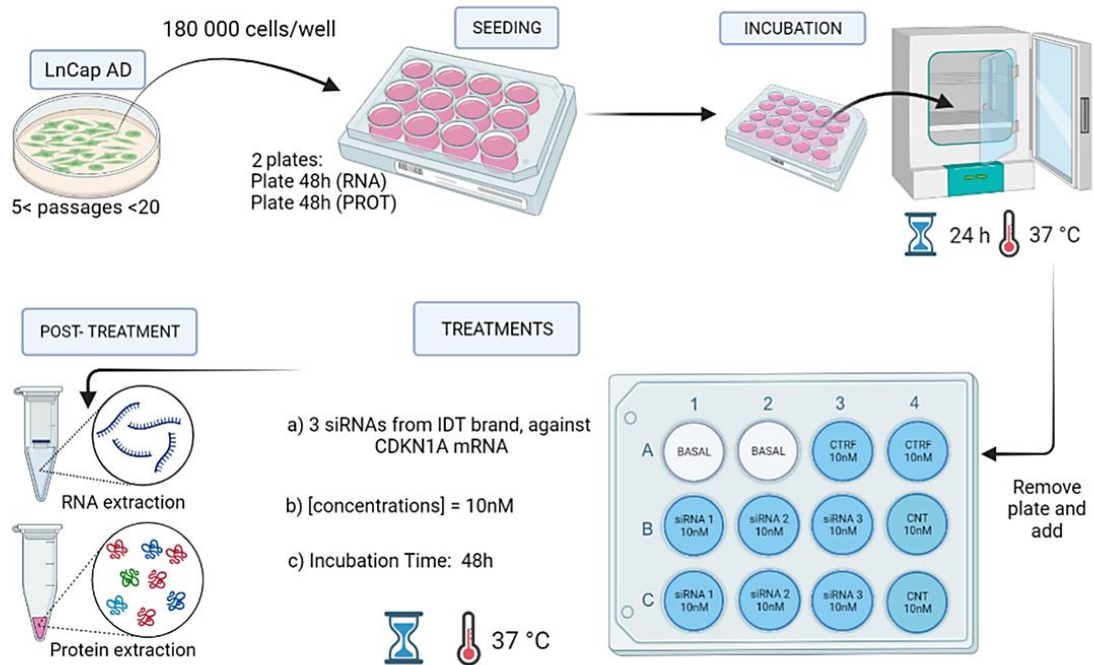


Figure 18. Schematic representation of siRNAs transfection workflow. Cells were seeded and incubated for 24 hours before transfection. Then, siRNAs and controls are added and incubated for additional 48 hours. Finally, cells are harvested to extract RNA and protein. *Figures develop in Biorender.com*

Two siRNAs transfection mixes were prepared as in **Table 10** with Limpofectamine RNAiMax reagent (Thermofisher) in different tubes and incubated for 5 minutes at room temperature, then both tubes were combined and incubated for additional 20 minutes. 200 μL / well of the mix were added to each well. Transfected cells were incubated for 48 hours before harvested to analyze gene expression.

Table 10. Details of siRNAs reaction preparation.

		24-well		12-well		60mm-plate
Plate/well	Growth medium	0.5 mL		1.0 mL		5.0 mL
Tube 1	DsiRNA	0.6 μL		1.2 μL		6.0 μL
	OptiMEM	50 μL	6	100 μL	12	500 μL
Tube 2	Lipofectamine	1.0 μL	picomoles (10nM)	2.0 μL	picomoles (10nM)	10 μL
	OptiMEM	50 μL		100 μL		500 μL
Tube 3	Mix 1-2	100 μL		200 μL		1.0 mL
Final volume		600 μL		1.2 mL		6.0 mL

6. Protein manipulation

6.1. Protein extraction

Cultured cells were subjected to lysis using a lysis buffer consisting of 50 mM Tris pH 7.5, 200 mM NaCl, 5 mM EDTA, 0.1% Triton X-100, along with protease inhibitors (Protease Inhibitor Cocktail from Sigma-Aldrich, diluted 1:200) and phosphatase inhibitors (1 mM Sodium Fluoride). The detailed procedure is as follows:

Cells were washed twice with cold PBS. Following this, ice-cold lysis buffer was added to the cells (approximately 100 μ L per 1×10^6 cells in a 10 cm dish). Adherent cells were detached using a cell scraper, transferred into a pre-cooled microfuge tube, vortexed, and maintained on ice for a duration of 30 minutes. Afterward, the lysates underwent centrifugation at 13000 rpm for 15 minutes at 4°C. The resulting supernatant was collected into a new tube, kept on ice, and subsequently stored at -20°C for future utilization.

6.2. Protein concentration

The Bradford method was employed to determine protein concentrations, utilizing bovine serum albumin (BSA) as a reference standard. This technique relies on quantifying changes in absorbance caused by the interaction between the dye Coomassie Blue G-250 and proteins, thus enabling the assessment of total protein levels within solutions. A series of bovine serum albumin (BSA) standards was prepared from a stock solution of 2 mg/mL, the concentrations used were: 0, 0.25, 0.5, 0.75, 1, 1.5, 1.75, and 2 mg/mL. Subsequently, five μ L of standards or the sample under investigation were added to individual wells of a 96-well plate. Following this, 200 μ L of Bradford solution (PanReac AppliChem) was introduced, and the plate was incubated at room temperature for 15 minutes. Absorbance was quantified at a wavelength of 595 nm using an Epoch™ Microplate Spectrophotometer (BioTek). The values derived from the BSA standards were used to construct a standard curve, facilitating the comparison of sample absorbance readings to discern their respective protein concentrations.

6.3. SDS-PAGE

SDS-PAGE, or Sodium Dodecyl Sulfate Polyacrylamide Gel Electrophoresis, is a widely used laboratory technique for separating proteins based on their size. In SDS-PAGE, proteins are mixed with a detergent called sodium dodecyl sulfate (SDS), which denatures the proteins and coats them with a negative charge proportional to their length. This makes the

proteins uniformly negatively charged, allowing them to be separated primarily based on their molecular weight during electrophoresis.

Briefly, proteins just extracted and quantified were denatured in loading buffer (Laemmli buffer: 250 mM Tris pH 6.8; 10% SDS; 0.5% Bromophenol blue; 50% Glycerol; 500 nM DTT) and boiled at 95°C for 5 min. In general, 30 µg of the protein sample in LB is loaded per lane onto a polyacrylamide gel, the ingredients for preparation of polyacrylamide gels are shown in **Table 11**.

Table 11. Ingredients for polyacrylamide gels preparation.

Component	Stacking gel 5% (10mL)	Resolving gel 8% (10mL)	Resolving gel 10% (10mL)	Resolving gel 12% (10m)
H ₂ O	6.8 mL	4.6 mL	4.0 mL	3.3 mL
Acrylamide/Bisacrylamide 29:1	1.7 mL	2.7 mL	3.3 mL	4.0 mL
TRIS-HCl 1.0 M (pH 6.8)	1.25 mL	-	-	-
TRIS-HCl 1.5 M (pH 8.8)	-	2.5 mL	2.5 mL	2.5 mL
SDS 10%	100 µL	100 µL	100 µL	100 µL
APS 10%	100 µL	100 µL	100 µL	100 µL
TEMED	10 µL	6.0 µL	4.0 µL	4.0 µL

The electrophoresis was run in the running buffer (25 mM Tris base; 190 mM glycine; 0.1% SDS; pH: 8.3) for approximately 1.5 h or until the migration front reached the bottom of the gel.

6.4. Protein transference

Following the completion of electrophoresis, the isolated proteins were transferred onto a stable support framework, a polyvinylidene difluoride (PVDF) membranes, to immobilize the proteins using the wet transfer method. For the preparatory stage, the PVDF membranes were pre-soaked with methanol and then submerged into transfer buffer (consisting of 25 mM Tris-HCl pH 8.3, 192 mM glycine, and 20% v:v methanol). The gel and PVDF

membrane were immersed beneath the transfer buffer within tanks, positioned in such a way that they were enveloped between buffer-moistened filter papers (sandwich) in direct contact with flat-plate electrodes. Through the application of an electric field, negatively charged proteins were prompted to move towards the positively charged electrode until they are captured and arrested by the membrane itself.

The conditions for electrophoretic transference encompassed the following:

For larger proteins (>100 kD), the transference was executed at a gradual pace throughout the night, set at 60 mA/hour.

For smaller proteins (<100 kD), the transference was conducted over a span of 2 hours, utilizing a current of 400 mA/hour.

To visualize the proteins that had been transferred, the membranes underwent staining with Ponceau S for a duration of 5 minutes. Subsequently, the identification of specific proteins on the membranes was achieved by subjecting them to incubation with antibodies.

6.5. Western Blotting

Firstly, the membranes were blocked to prevent non-specific antibodies from binding. The blockage solution was a 5% non-fat milk solution or a BSA solution formulated in the Tris buffer solution buffer (TBST) (50 mM Tris-Cl pH 7.5, 150 mM NaCl, 0.1% Tween) for 30 minutes incubation. Primary antibodies prepared in the same solution were diluted according to the data sheet (**Table 12**) and incubated overnight at 4oC. Membrane was washed several times with TBST and incubated for 1 h with secondary antibodies in RT. Secondary antibodies associated with horseradish peroxidase (HRP) were diluted in blocking buffer of 1:2000 (**Table 13**). Finally, ECL Western Blotting Detection (Amersham, GE Healthcare) was used to detect specific proteins in membranes. This is a light emitting nonradioactive method for detection of immobilized specific antigens with HRP-labelled antibodies.

Table 12. List of primary antibodies for western blot

Primary antibodies	Host	Concentration	Dilution	Supplier	Reference
p21 ^{WAF1}	Mouse	200 µ/mL	1:200	Santa Cruz biotechnology	sc-6241
MDM2	Mouse	200 µ/mL	1:200	Santa Cruz biotechnology	sc-56154
AKR1C3	Rabbit	710 µ/mL	1:500	Invitrogen	PA5-97446
Notch1	Goat	200 µ/mL	1:200	Santa Cruz biotechnology	sc-6014
Actin	Goat	200 µ/mL	1:200	Santa Cruz biotechnology	sc-1616
β-Tubulin	Mouse	200 µ/mL	1:200	Santa Cruz biotechnology	sc-5274
Laminin A/C	Rabbit	200 µ/mL	1:200	Santa Cruz biotechnology	sc-20681

Table 13. List of secondary antibodies for western blot

Secondary Aantibodies	Origen	Dilution	Reference
Anti-goat immunoglobulins/HRP	Goat	1/2000	Dako
Anti-rabbit immunoglobulins/HRP	Rabbit	1/2000	Dako
Anti-mouse immunoglobulins/HRP	Mouse	1/2000	Dako

7. Functional analysis

7.1. Immunofluorescence

Cells were seeded on 15mm sterilized pre-treated coverslips (cell culture section 1.4.1) in 6 well- plates and incubated for 24 hours. Then, Cells were rinsed twice with phosphate-buffered saline (PBS) and then fixed with paraformaldehyde (PFA) at 4% for 15 minutes in room temperature. After that, fixed cells were washed with PBS 3 times. Afterward, the cells were subjected to a 30-minute incubation with a blocking/permeabilization (BP) buffer consisting of 3% BSA-PBS and 0.25% Triton-X at room temperature to enable cell permeabilization. After this, coverslips, with fixed cells, were washed twice with PBS and placed in a humid and dark environment (humidity chamber) for 3 hours, incubating with p21^{WAF1} antibody at a concentration of 2.0 µg/mL, diluted in BP buffer. Following this incubation, the cells were again washed three times with PBS and subsequently incubated for 1 hour in the humidity chamber with a secondary antibody, Alexa Fluor 594 (Invitrogen), which was conjugated with a fluorophore and used at a concentration of 4 µg/mL. Cells were washed and stained with phalloidin FITC-conjugated (Sigma-Aldrich) at a final concentration of 50 µg/mL diluted in BP buffer and incubated for 40 minutes in the chamber, finally were washed three times with PBS and mounted using the ProLong Diamond

Antifade Mountant with DAPI (Thermo-Fisher), with the cell-side placed facing downwards. A negative control was concurrently prepared in which the primary antibody was omitted.

Table 14. List of reagents for immunofluorescence

Target	Reagent	Concentration	Dilution	Supplier	Reference
p21 ^{WAF1}	Mouse Anti-p21	200 µg/mL	1:100	Santa Cruz	Sc-6246
	Anti-mouse IgG Alexa 594	2000 µg/mL	1:500	Thermo-Fisher	A-11005
Actin	Phalloidin-FITC	5.0 mg/mL	1:100	Sigma-Aldrich	P5282
Chromatin	DAPI	1-2 µg/mL	1:1	Thermo-Fisher	P36962

7.2. Cellular fractionation

Cellular fractionation methods have been developed to segregate different cellular elements while maintaining their distinct functionalities. To evaluate the subcellular localization of p21^{WAF1}, we separated the nucleus and cytoplasmic fractions by differential weight of the nucleus and the cytoplasmic components and by using different salts concentrations. In brief, cells were seeded in 60mm plates and incubated until 70-80% confluency, then were washed with cold PBS and maintained on ice. PBS was aspirated and 100 µL of hypotonic buffer (20 mM Tris-HCl (pH 7.4), 10 mM KCl, 2 mM MgCl₂, 1 mM EGTA, 0.5 mM DTT) was added to harvest cells by scraping. For each 1mL, 5uL of PMSF 100 µM final, 5uL of Protease inhibitor cocktail (Merck) and 5uL of phosphatase inhibitor cocktail 2 (Merck) were added. Harvested cells were transferred to an Eppendorf tube and incubated on ice for 5 minutes, then 1 µL of Triton-X (10%) was added and the mixture was homogenized by pipetting gently, mix was incubated for 3 additional minutes. Subsequently, tubes were centrifugated at 3000 rpm for 5 minutes at 4 °C. Nucleus will be present in the pellet, while the cytoplasmic fraction in the supernatant. The supernatant was transferred to another tube and centrifugated at 13000 rpm for 1 minute to eliminate remain debris and the supernatant is the final cytoplasmic fraction. Nucleus pellet was resuspended and washed in 200 µL of isotonic buffer (20 mM Tris-HCl (pH 7.4), 150 mM KCl, 2 mM MgCl₂, 1 mM EGTA, 0.5 mM DTT). For each 1mL, 5uL of PMSF 100 µM final, 5uL of Protease inhibitor cocktail, 5uL of phosphatase inhibitor cocktail 2 and 10 µL of Triton-X (10%) were added. Nucleus

were centrifugated at 3000 rpm for 5 minutes, 4 °C. Pellet with nucleus were resuspended in 50 µL lysis buffer (from protein extraction section) and incubated on ice for 30 minutes to allow proteins release and finally centrifugated for 1 minute at 13000 rpm to recover the supernatant with the nuclear fraction.

The presence of p21^{WAF1} in cytoplasm or nucleus was corroborated by western blot analysis using protein markers for nucleus (laminin A/C) and cytoplasm (β-tubulin).

7.3. Cellular senescence analysis

7.3.1. β-Galactosidase expression

β-galactosidase (β-gal) is a lysosomal enzyme that catalyzes the hydrolysis of terminal β-galactose residues from various substrates¹⁸⁰. Is used as a cellular senescence marker due to its ability to reflect changes in cellular metabolism and lysosomal activity that occur during the senescence process. In senescent cells, there is an increase in lysosomal content, which leads to the accumulation of β-gal activity at a pH normally present in lysosomes (pH 6). This accumulation is known as senescence-associated β-galactosidase (SA-β-gal)¹⁸¹. SA-β-gal staining has become a widely accepted method for detecting cellular senescence, as it provides a relatively simple and reliable way to identify senescent cells in cultures and tissues.

To determine senescence in primary cultures, the CellEvent senescence green detection kit (Thermo-Fisher) was used. Seven treatments were considered for this experiment (**Table 15**): Basal, without any treatment; positive control, cells with etoposide at 10µM; transfection control, cells with dsRNA TYE563; negative control, with siRNAs scramble, and the treatment with three siRNAs against p21^{WAF1}. Briefly, cells were seeded on 96-well plate and incubated for 1 day before adding treatments. Next day, etoposide and siRNAs were added, and cells were incubated for another 48 hours. After this, plates are retired from incubation, the growth medium is aspirated, and cells are washed twice with PBS. Then, cells are fixed with 100 µL PFA 4% during 10 minutes at room temperature and protected from light. Subsequently, fixed cells are washed with PBS + BSA 1%. Then a Fluoro-X-Gal working solution, consisting of senescence green probe (1000X) diluted into pre-warmed senescence buffer (37 °C), was added to each well (100 µL/well). The plate was covered with plastic film to prevent moisture loss, then incubate for 2 hours at 37°C without CO₂ protected from light. After incubation, working solution was removed, then washed 3 times

with 100 μ L of PBS per well. And finally, 100 μ L of PBS per well was added, to take images using an Alexa Fluor™ 488/FITC filter set.

Table 15. Treatment arrangement in 96-well plate

Treatment	hnPC04			hnPC05			hnPC06		
Basal									
Positive CNT									
Transfection CNT									
Negative CNT									
siRNA #1									
siRNA #2									
siRNA #3									

Protein p16, the cyclin dependent kinase inhibitor 2a, encoded by the *CDKN2A* gene, was originally identified as a tumor suppressor acting as a specific inhibitor of the cyclin-dependent kinases CDK4 and CDK6. p16 is mainly active at the G1 phase of the cell cycle to prevent the cell transition from the G1 to S phase, causing a subsequent proliferation arrest. The p16 inhibitor is currently considered one of the hallmarks of senescence: in the majority of mammalian cells, senescence occurs with the inactivation of suppressor elements that lead to the enhanced expression of p16^{182,183}.

The expression of *CDKN2A* was measured in basal and p21-knockdown primary cultures by RT-PCR using TaqMan probe (assay ID: Hs00923894_m1, N°4453320).

8. Bioinformatics analysis

Exploration of differential gene expression was performed with R2: Genomics Analysis and Visualization Platform (<http://r2.amc.nl>). We searched 6 Prostate cancer datasets: GSE50936 (Phur n=30), TCGA 2022 (n=553), GSE70768 (Dunning n=199), GSE21034 (Sawyers n=370), GSE46691 (Jenkins n=545), GSE29079 (Suelman n=95) and were analyzed comparing two groups: low-grade Gleason vs High-grade Gleason, benign tissue vs tumor tissue or primary tumor vs metastasis, according to the availability in the dataset. The analysis was restricted to metabolism genes set (steroid synthesis and steroid hormone synthesis) corresponding to KEGG pathway annotation.

For visualization data and image analysis Circos (<http://circos.ca/>) and ImageJ (<https://imagej.net/software/fiji/>) tools were employed. For visualization and DNA/Protein sequence analysis, Benchling platform (<https://benchling.com/editor>) was used.

9. Statistical analysis

For the analysis of associations involving frequencies and proportions, contingency tables and Fisher's test were employed. Similarity and correlation analyses between two or more qualitative variables were computed using the Spearman coefficient. Gene expression data were presented as medians (+IQR) of fold changes relative to the control and as Log₂ of the fold changes. Differential expression analysis was conducted with a minimum of two independent experiments and three replicates. P-values were calculated using non-parametric tests: Wilcoxon (for two paired samples) or Kruskal-Wallis (for more than two independent samples), followed by the Dunn test. Proliferation and drug toxicity analyses were presented as the mean plus the standard deviation and p-values calculated by ANOVA followed by the Dunnett method. A significance level of $p < 0.05$ was considered. These analyses were conducted using GraphPad Prism 9 software.

CHAPTER I: RESULTS

CHAPTER I – RESULTS

1. SNP P72R of TP53 gene in Prostate cancer

1.1. The TP53 SNP P72R

TP53 is a tumor suppressor gene with essential functions for the prevention of tumor development. Thus, it is not a surprise that it has been described as the most mutated gene in different human cancer types, including Prostate cancer (PCa)¹⁸⁴. In PCa, *TP53* mutations appear more frequently as a later event, being a driver of aggressive and metastatic PCa¹⁸⁵, however, there are several types of variations that could be inheritable through the germline, approximately 5-20% of the cases are associated with inherited pathogenic variants in genes such *BRCA2* and *ATM*, whereas in PCa has been found to carry a *TP53* germline variant with a relative risk of 4.7-8.6, comparable with those genes¹⁸⁶. Germline variants known as a single-nucleotide polymorphisms (SNPs) are present in >1% of the population and occur naturally, although is considered not to have a severe impact on people health, much of these variants can affect the structure or function of the protein in some ways. In *TP53* gene there are more than 20 different SNPs¹⁸⁷, one of them, the variation rs1042522 affects the position 72 of the protein in exon 4 (Figure 19a) changing a proline (CCC) by an arginine (CGC) encoded by an cytosine or guanin at 357 position of the cDNA (Figure 19b). As can be seen in Figure 19c, the change implies a decrease in hydrophobicity (turquoise bars) which could modify the interaction with other ligand (CCAR2 or HRMT1L2) in this region.

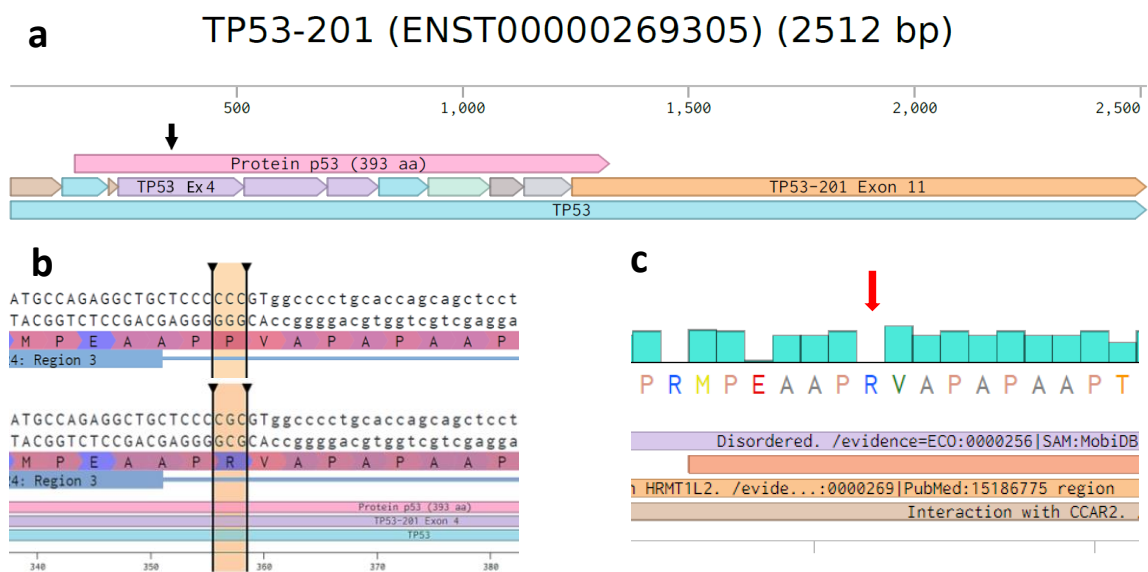


Figure 19. Canonic transcript of TP53 gene and the SNP rs1042522. a) TP53 Transcript 201, which consists of 11 exons and encodes a protein with 393 amino acids, is comprised of exons 2 through the beginning of exon 11. The SNP P72R (black arrow). b) Polymorphic variants, Proline (P)-CCC, and Arginine (R)-CGC, at position 357. c) The P72R change (red arrow), Hydrophobic amino acid P is changed by R, polar-positive amino acid. *Figures from Benchling.com*

1.2. P72R and allele frequencies in primary cultures and tissues

Previously in our laboratory, primary tumor cultures were found to carry the P72R SNP in 7 out of 10 established hnPCs by using cDNA Sanger sequencing. To validate these results in genomic DNA, we decided to carry out melting curve analysis in gDNA (**Figure 20**) to determine the specific genotype of each primary cultures and radical prostatectomies.

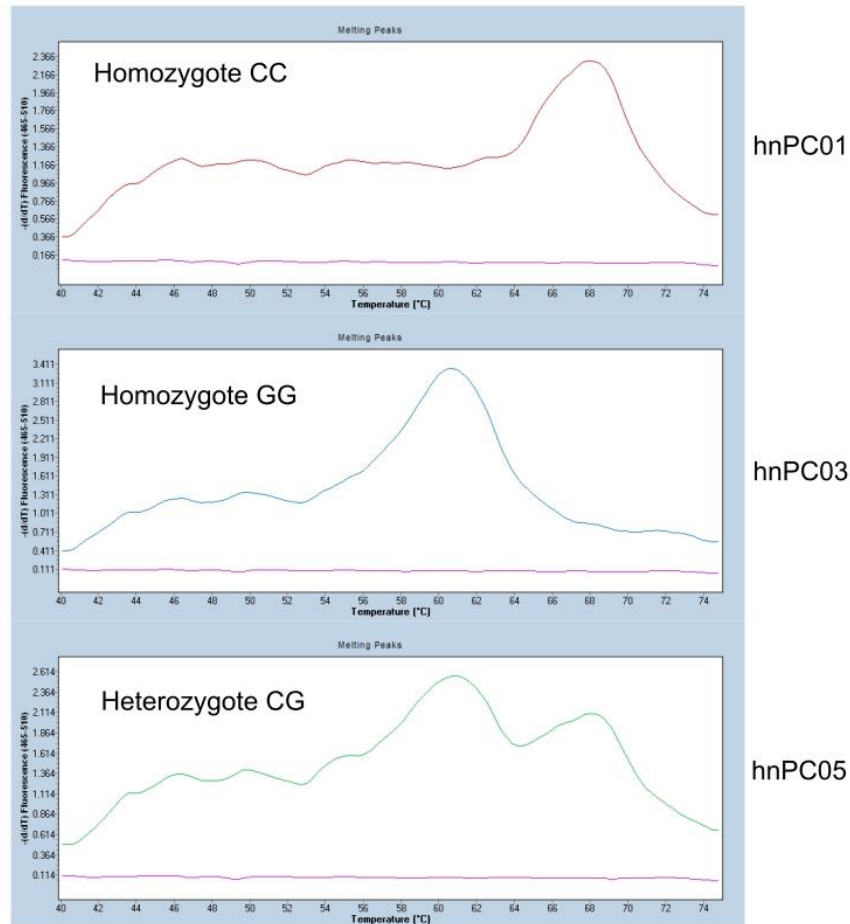

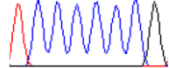

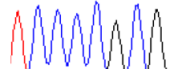


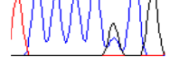
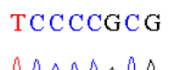


Figure 20. Representative melting curves from qPCR. Peaks of absorbance at different dissociation temperatures. Top panel: Homozygous samples with cytosine in both strands show a dissociation peak at 68°C. Center panel: Homozygous samples with guanine in both strands show a dissociation peak at 60°C. Bottom panel: Samples with each base on each strand show both peaks at two temperatures.

The results of cDNA sequencing and genotyping for both samples are shown in **Table 16**. In total we obtained 2 homozygotes for cytosine that expressed proline, 6 homozygotes for guanine that expressed arginine and 4 heterozygotes that predominantly expressed arginine aminoacid, in primary cultures. Regarding to tissues, we found 4 homozygotes for cytosine (C) expressing proline, 5 homozygotes for guanine (G) that expressed arginine and 4 heterozygotes that predominantly expressed arginine. The total frequency of C and G were 0.33 and 0.67 in primary cultures, while in RP tissues, frequency of C was 0.45 and G 0.55.

Table 16. P72R genotyping in primary cultures and radical prostatectomy tissues

SAMPLE	Sanger sequencing		LightSNiP assay	
	cDNA	Dominant Aminoacid	gDNA	
hnPC01	CCC 	Proline	CC	Homozygote Proline
hnPC06	CCC 	Proline	CC	
hnPC02	CGC	Arginine	GG	Homozygote Arginine
hnPC03	CGC 	Arginine	GG	
hnPC08	CGC 	Arginine	GG	
hnPC09	CGC 	Arginine	GG	
hnPC10	CGC	Arginine	GG	
hnPC12	CGC	Arginine	GG	
hnPC04	CGC 	Arginine	CG	Heterozygotes
hnPC05	CGC 	Arginine	CG	
hnPC11	CGC 	Arginine	CG	
hnPC07	N.D	N.D	CG	
RP11D	CGC	Arginine	CG	Heterozygote
RP14D	CGC	Arginine	GG	Homozygote
RP17B	CGC	Arginine	GG	Homozygote
RP18F	CGC	Arginine	GG	Homozygote
RP21D	CGC	Arginine	GG	Homozygote
RP23D	CCC	Proline	CC	Homozygote
RP36E	CCC	Proline	CC	Homozygote
RP37A	CGC	Arginine	CG	Heterozygote
RP40B	CCC	Proline	CC	Homozygote
RP63A	CGC	Arginine	GG	Homozygote
RP68C	CCC	Proline	CC	Homozygote

1.3. P72R is associated with prostate cancer occurrence

Thus, after these findings, we aimed to examine the potential association between the P72R and PCa. Therefore, we corroborate the presence of the SNP in 94 patients, using melting curve analysis (LightSNiP assay). Data of allele frequency is shown in **Figure 21a**.

P72R is a controversial SNP, it was found to be in different frequencies according to the sub-continental population in the world. Thus, we selected the European (non-Finnish)

population to analyze the common frequencies in healthy (non-cancer) population from GnomAD v2.1.1 with 134 187 samples (**Figure 21b**). We found 26.3% of the population presented arginine (G) allele, whereas 74.0%, proline (C) allele. We used this proportion as a control population to compare with the proportion found in primary cultures, tissue samples and a small cohort of PCa patients from HVH (**Figure 21c**).

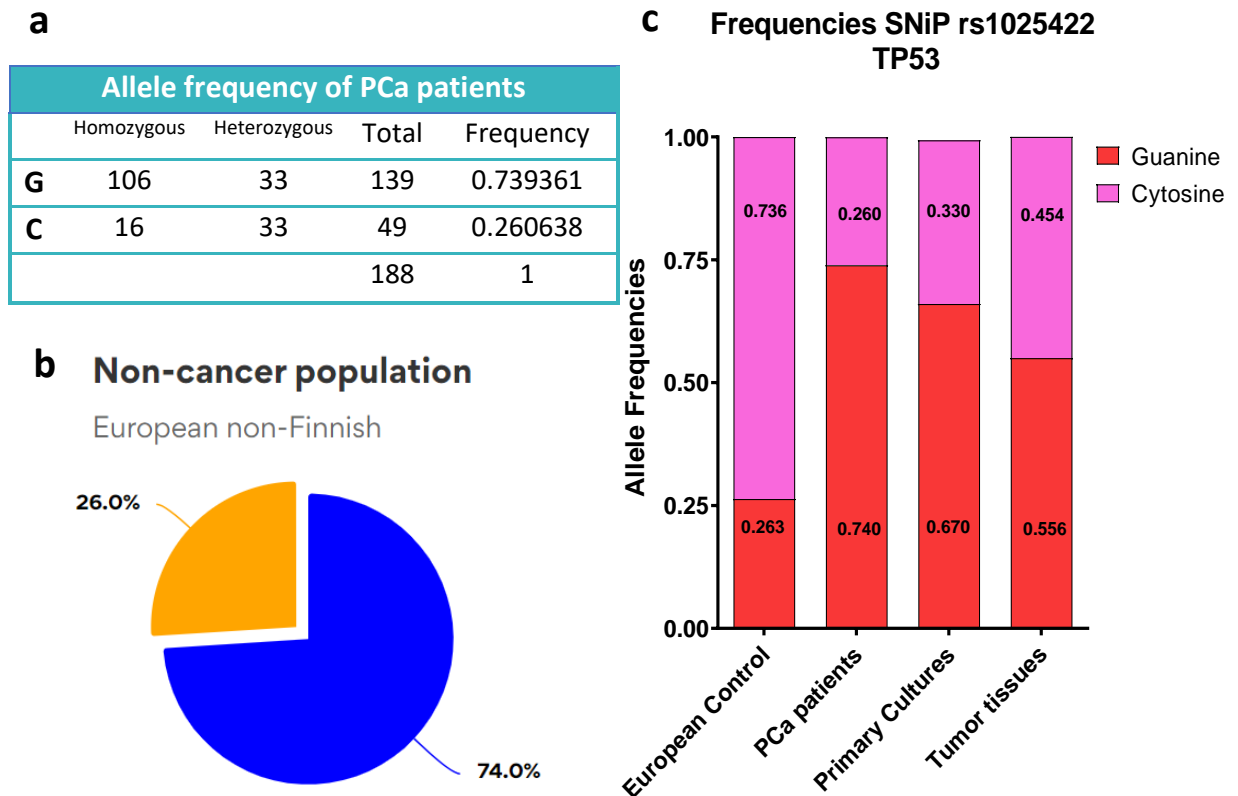


Figure 21. P72R Allele frequencies in Prostate cancer. a) A table displaying allele frequencies in 94 patients with PCa. b) Allele frequencies from the control European (non-Finnish) population. Yellow fractions correspond to the G allele (arginine), while blue fractions represent the C allele (proline). c) P72R allele frequencies in all samples. cDNA was sequenced by Sanger assay, and FASTA sequences were aligned against the reference canonical transcript of TP53 (ENST00000269305). Genomic DNA was genotyped with LightSNiP.

To evaluate the possible association between the presence of P72R and prostate cancer we performed a contingency analysis with Fisher's Test to obtain a significance value of the association and the odds ratio for prostate cancer population, primary cultures, and tissues (**Table 17**) we found a very significant association between the SNP and prostate cancer ($p < 0.0001$) y odds ratio of 7.937 (IC 95% 5.37-11.00), similar results were found for hnPCs and tissues from RP.

Table 17. Association analysis between P72R SNP and prostate cancer

TP53 P72R (cDNA seq and LightSnip)	Prostate Cancer, n (%)	GnomAD Non-cancer, n (%)	Odds Ratio (95% CI)	P- value
Arginin (G allele)	139 (0.74)	31021 (0.26)	7.937 (5.73– 11.00)	<0.0001
Proline (C allele)	49 (0.26)	86797 (0.74)		
Total	188	117818		
TP53 P72R (LightSnip)	Primary Tumor Cultures, n (%)	General Population, n (%)	Odds Ratio (95% CI)	P- value
Arginin (G allele)	16 (0.67)	31021 (0.26)	5.596 (2.395– 13.080)	<0.0001
Proline (C allele)	8 (0.33)	86797 (0.74)		
Total	24	117818		
TP53 P72R (cDNA seq)	Tumor Tissues n(%)	General Population, n (%)	Odds Ratio (95% CI)	P- value
Arginin (G allele)	12(0.55)	31021 (0.26)	3.358(1.451-7.772)	0.0058
Proline (C allele)	10(0.45)	86797 (0.74)		
Total	22	117818		

Contingency table to analyze the association between P72R SNP and Prostate cancer. As control, a **selected European (non-Finnish)** non-cancer population from GnomAD, was used . Odds ratio and p-values of the association were calculated with Fisher's Test.

1.4. P72R SNP may not be associated with PCa aggressiveness

R72 variant showed to be able to inactivate PGC-1 α ¹⁸⁴, which is related with apoptosis, by binding more efficiently to it¹⁸⁸, or to stabilize SREBP1/2, promoting cell invasion and metastasis. This led us to think of a higher R72 allele frequency would be present in aggressive PCa tumors. Hence, we consulted the medical record to extract the Gleason score of all the genotyped patients and we readjusted to Gleason grading (1 to 5 instead of 6 to 10) and divided them in two different groups: Low to medium aggressive tumor (GS 1 - 3) and to high aggressive tumor (GS 4 or 5). The data of the patients' genotypes named as hARG, hPRO (homozygotes) and heterozygotes (AR-PRO) was plotted in a Circos Plot (<http://circos.ca/>) according to the Gleason score is shown in **Figure 22a**. The figure indicates the distribution of patient's proportion in each feature. Although a higher R72 allele frequency was found in more aggressive tumors, this difference was not statistically significant (p-value = 0.2772), as shown in **Figure 22 a and b**.

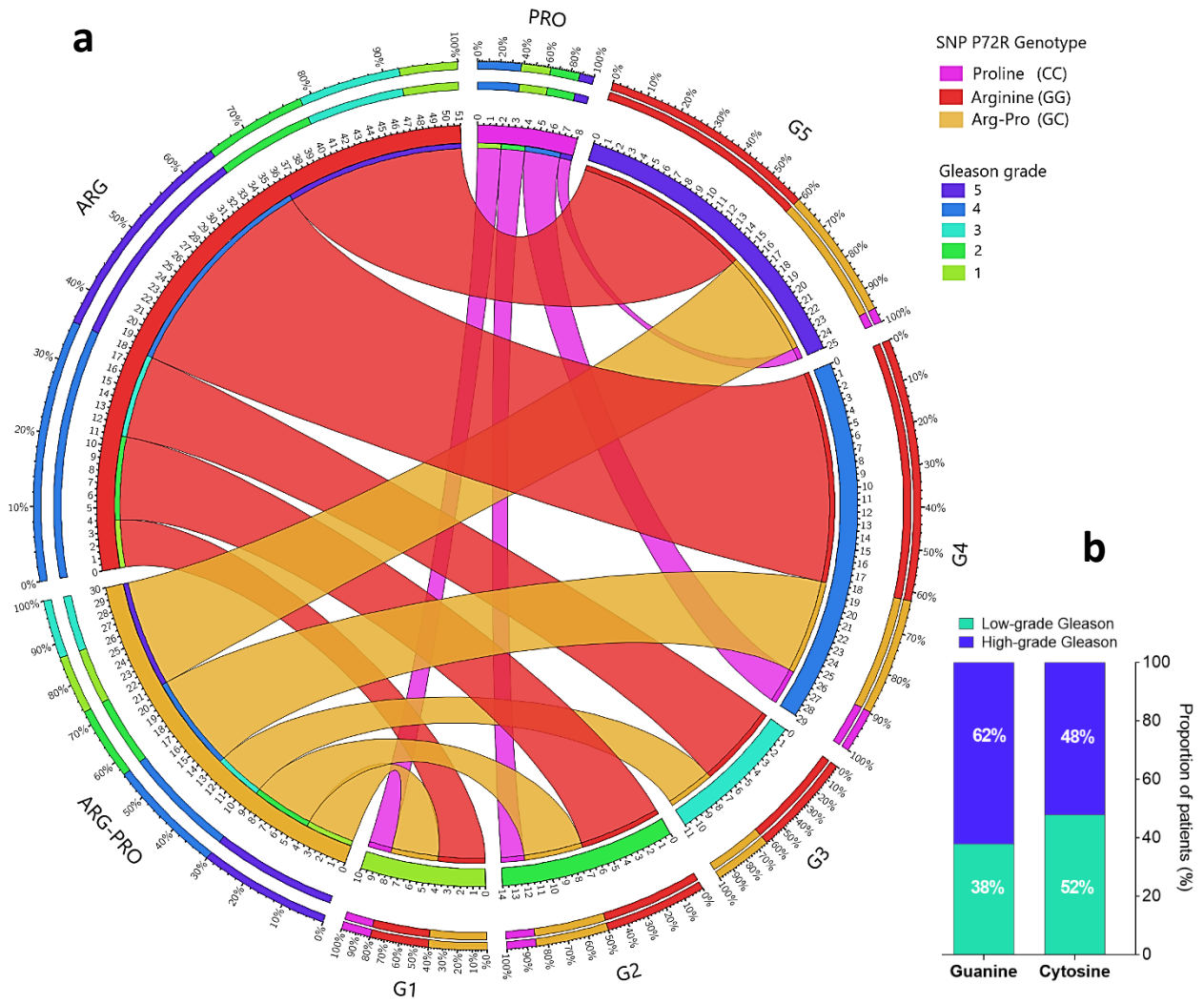


Figure 22. Distribution of P72R variants in 94 patients according to Gleason grade. a) Circos plot displaying the distribution of P72R genotypes for each Gleason score. b) Distribution of P72R SNPs in low (Gleason scores 1-3) and high (Gleason scores 4-5) Gleason grades; the contingency analysis of these proportions did not yield significant results.

2. Steroidogenesis pathway in hormone-naïve primary cultures

2.1. Identification of key steroidogenic genes in databases

In order to identify key enzymes in the steroidogenic pathway, we mined gene expression data from publicly available prostate cancer datasets. In total, 6 datasets were consulted for differential expression between two types of samples (**Figure 23**).

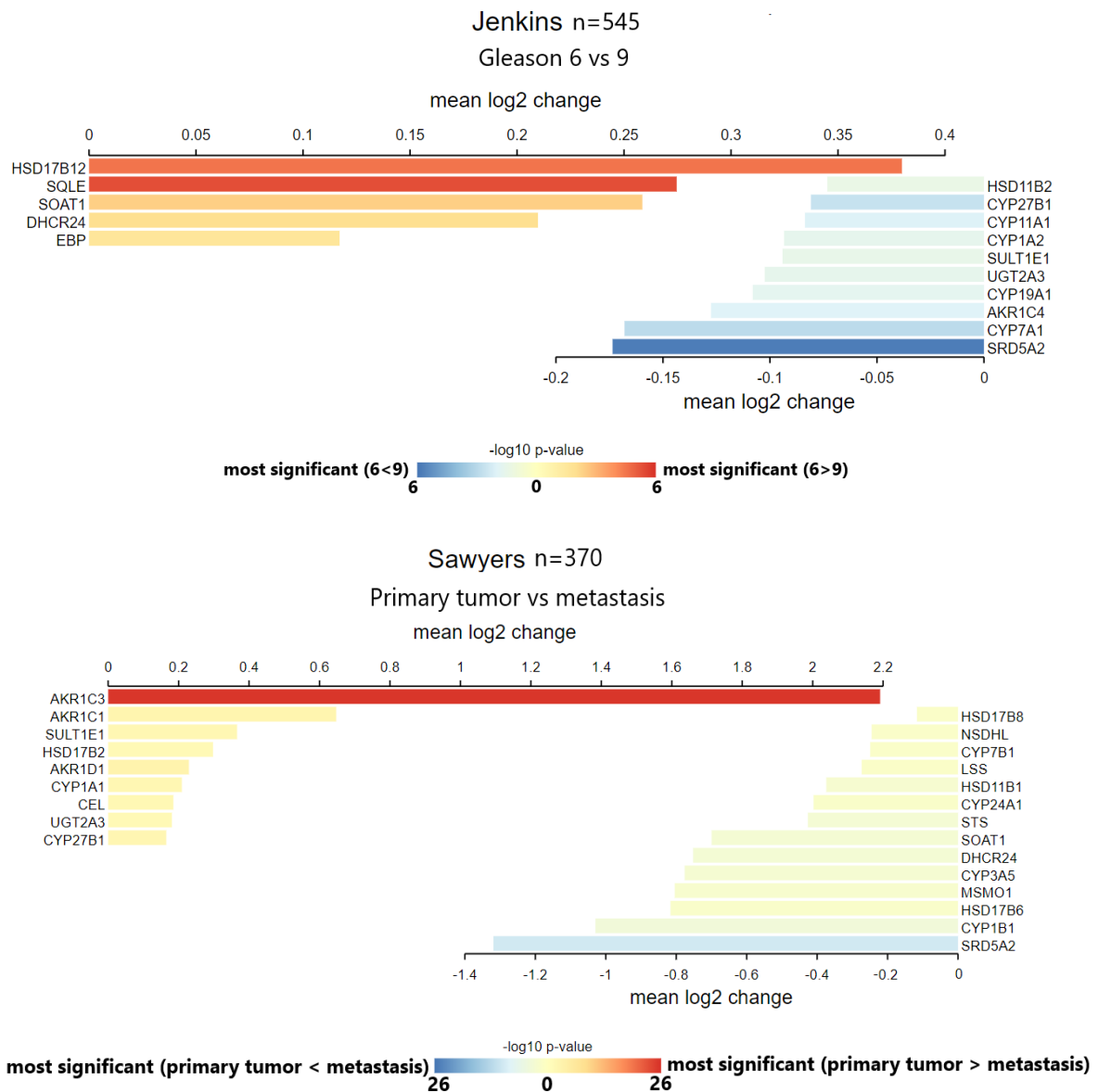


Figure 23. Bar plot for differential gene expression between two groups of samples in prostate cancer datasets. Top panel: differential gene expression between low-Gleason samples (G=6) and high-Gleason samples (G=9) in Jenkins dataset. Bottom panel: differential gene expression between primary tumor samples and metastatic samples in Sawyers dataset. Genes significantly different in expression are represented by a range of color from yellow to red (up regulated), and from yellow to blue (down regulated).

Fold changes (Log2) of each gene and its p-value (-Log10) obtained across datasets were compiled and plotted into a volcano analysis. Genes with a fold change ≥ 1.5 and p-value ≤ 0.05 were selected as shown in **Figure 24**, a total of 46 genes were found significantly up/down regulated in prostate cancer, of which 11 genes were available to study. Also, other genes were selected from literature. In total 21 genes involved in steroidogenesis, 7 genes coding for transcription factors including AR, 4 neuroendocrine genes and 3 genes in p53 pathway were studied.

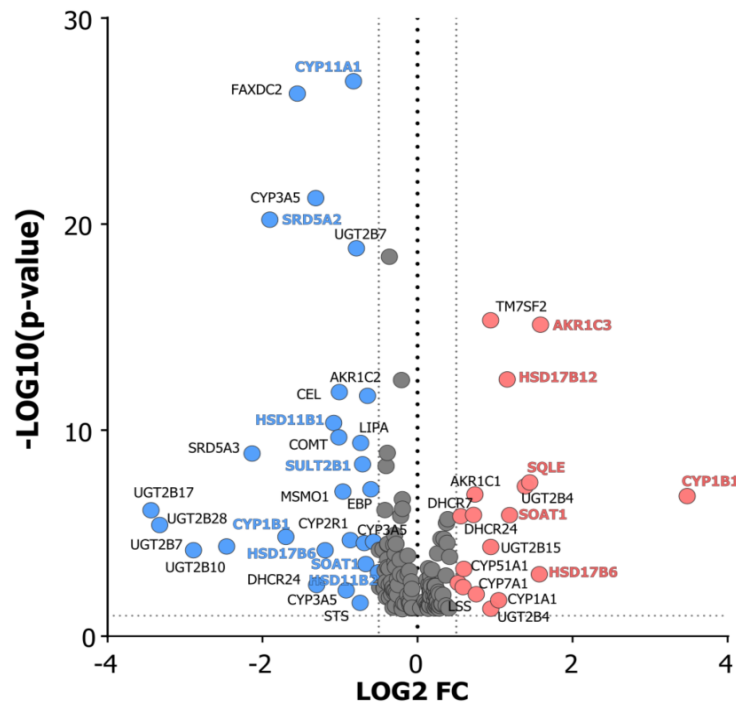


Figure 24. Volcano plot of the most significant differentially expressed genes in the steroidogenic pathway across prostate cancer datasets. The expression difference was considered significant for a p-value of 0.05 (-Log10P-value= 1.3) and a fold change ≥ 1.5 (Log2 FC=0.6), dashed lines.

2.2. AI and AD hnPCs show similar steroidogenic gene expression profiles and intrinsic AR insensitivity

Androgen dependent and independent models from LNCaP and hnPCs were previously evaluated to compare proliferation, motility capacity, drug resistance among other characteristics. We realized that there were no substantial differences between hnPC models with the exception of LNCaP, known to be androgen dependent. Therefore, we decided to preliminary compare the expression of some steroidogenic genes and AR. Surprisingly, it was found that both AD and AI models showed downregulation of AR and similar expression profiles of steroidogenic genes (**Figure 25a**). This result would explain why these primary cultures from aggressive tumors did not show significant differences in functional

characteristics, For example, all cultures were found to have a certain intrinsic docetaxel resistance capacity (**Figure 25b**)

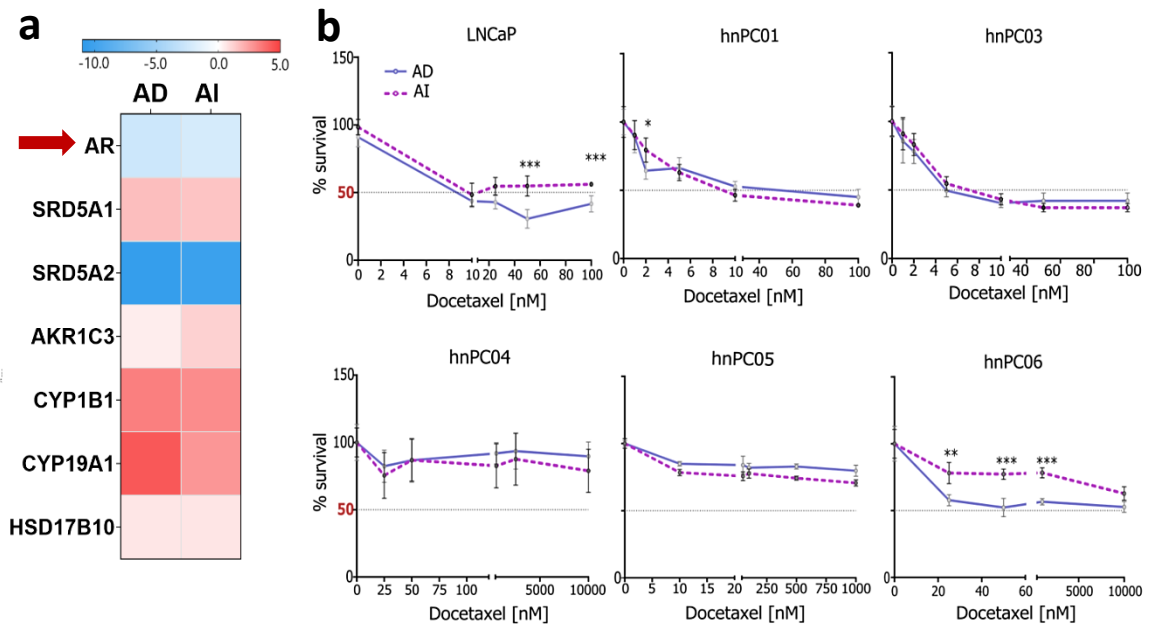


Figure 25) Exploratory characterization of primary cultures. a) Heatmap of gene expression in three representative primary cultures. Data are the mean fold changes of control (BPH) of the three hnPCs in triplicates. **b)** Previous results of initial characterization. Docetaxel resistance curves in AD and AI models of LNCaP and representative hnPCs, cells were treated with docetaxel for 72 hours. Data are the mean \pm S.D of three independent experiments in triplicates. * $P < 0.05$, ** $P < 0.01$, *** $P < 0.001$, **** $P < 0.0001$

Because both hnPC models were similar in behavior and expression profiles, we decided to continue the study with AD models.

2.3. De novo steroid synthesis machinery is enhanced in hnPCs and tumorigenic tissue

In order to characterize hormone metabolism in different types of samples, we evaluated the expression of steroidogenic genes in: (i) the cells lines Du145-DR, Du145-DS, LNCaP-AD and LNCaP-AI; (ii) the primary hnPC cultures, and (iii) the radical prostatectomies samples. As expected, the expression profiles from the cell cultures were different from those from the tissues. In addition, profiles from the established cell lines differed from those from hnPCs. However, a number of genes in the steroidogenic pathway were enhanced or overexpressed in the three types of samples. *AR* was only expressed in LNCaP, both AD and AI. Whereas *ESRRA* (estrogen-related receptor alpha) was enhanced in all cell cultures (**Figure 26**). *SQLE*, a key gene in cholesterol synthesis, was also enhanced in most samples, indicating that this cells cultures promoted aberrant cholesterol synthesis to survive and

proliferate. Interestingly, enzymes as *CYP19A1*, *CYP11B1*, *HSD17B10/12* were only overexpressed in hnPCs and RP tissues. *CYP19A1* and *CYP11B1* are key genes in estrogen metabolism, whereas *HSD17B10* is implicated in the androgen backdoor pathway. *AKR1C3* and *SRD5A1*, enzymes that metabolized the production on Testosterone and DHT, respectively, are also enhanced and overexpressed in primary cultures. (**Figure 26**)

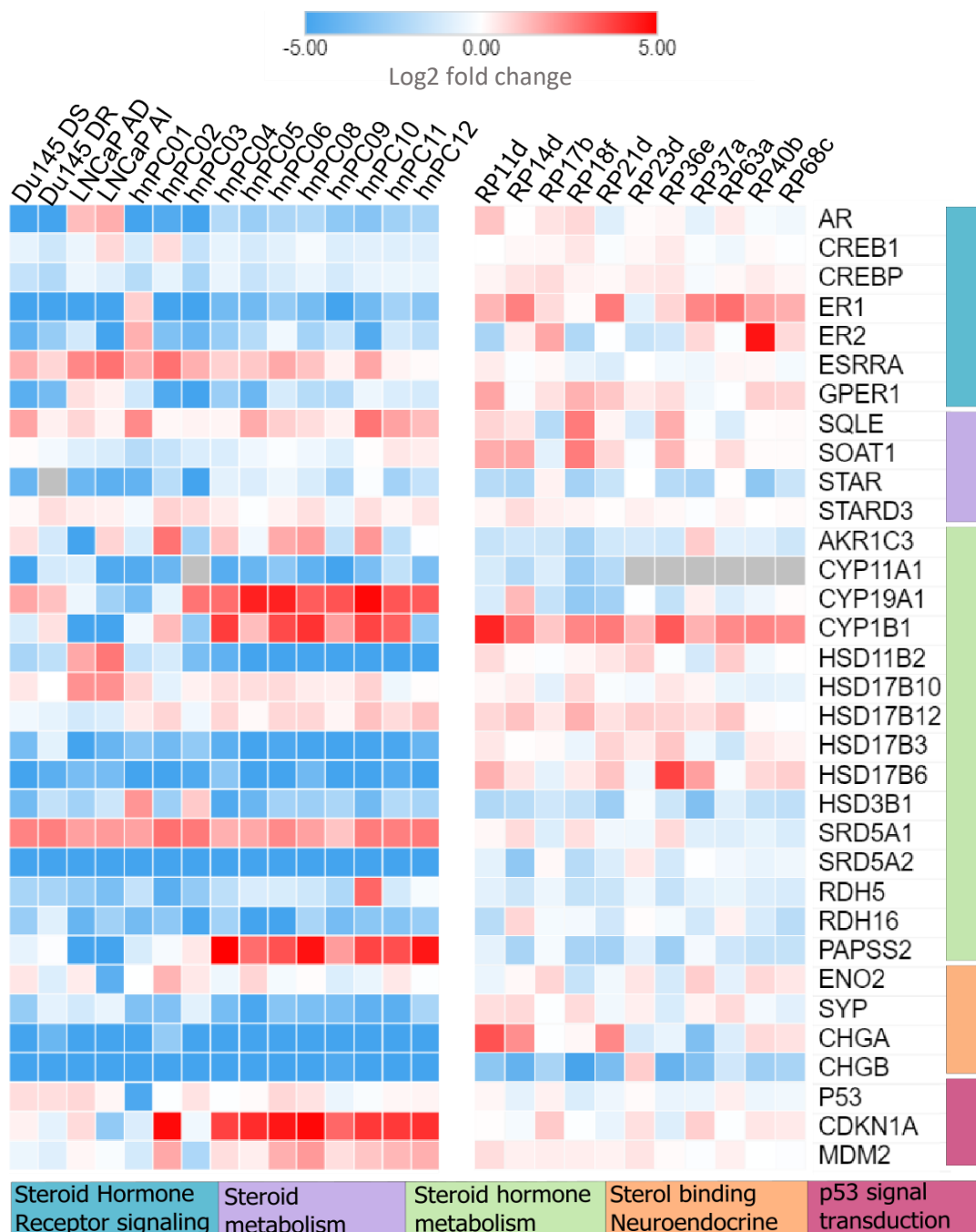


Figure 26. Heatmap of steroidogenic gene expression in hnPCs and radical prostatectomies. Expression profiles of 35 genes in three types of samples. Data are expressed as Log2 of Fold change (BPH control) in triplicates. *TBP* and *IPO8* were used as housekeeping genes. Upregulated genes are shown in red and downregulated genes in blue. Molecular pathways are indicated for each group of genes

2.4. Changes in gene expression profiles in hormone naïve primary cultures show steroidogenic reprogramming

Hormone naïve primary cultures (hnPCs) present a shift in gene expression compared to non-cancer tissues. The cholesterol overproduction might be related to an unbalanced enzyme expression (*SQLE* overexpression), and to a downregulation of *SOAT1* in these cultures, the enzyme in charge of cholesterol storage in the form of fatty acids. These changes suggest the need for these cells to accumulate cholesterol for posterior catabolic steps (**Figure 27a**). In addition, primary cultured cells and cancer tissues show a shift in the expression of *STAR* to *STAR3*, both implicated in cholesterol transport inside cells (**Figure 27a**). Finally, the shift from *SRD5A2* expression, ubiquitously expressed in the prostate and other healthy tissues, to *SRD5A1*, suggest cancer cells preference for the latter. **Figures 27b-c** show a similarity of 50% between these isoforms, pointing to differences in properties and structure possibly related to changes in ligand affinity.

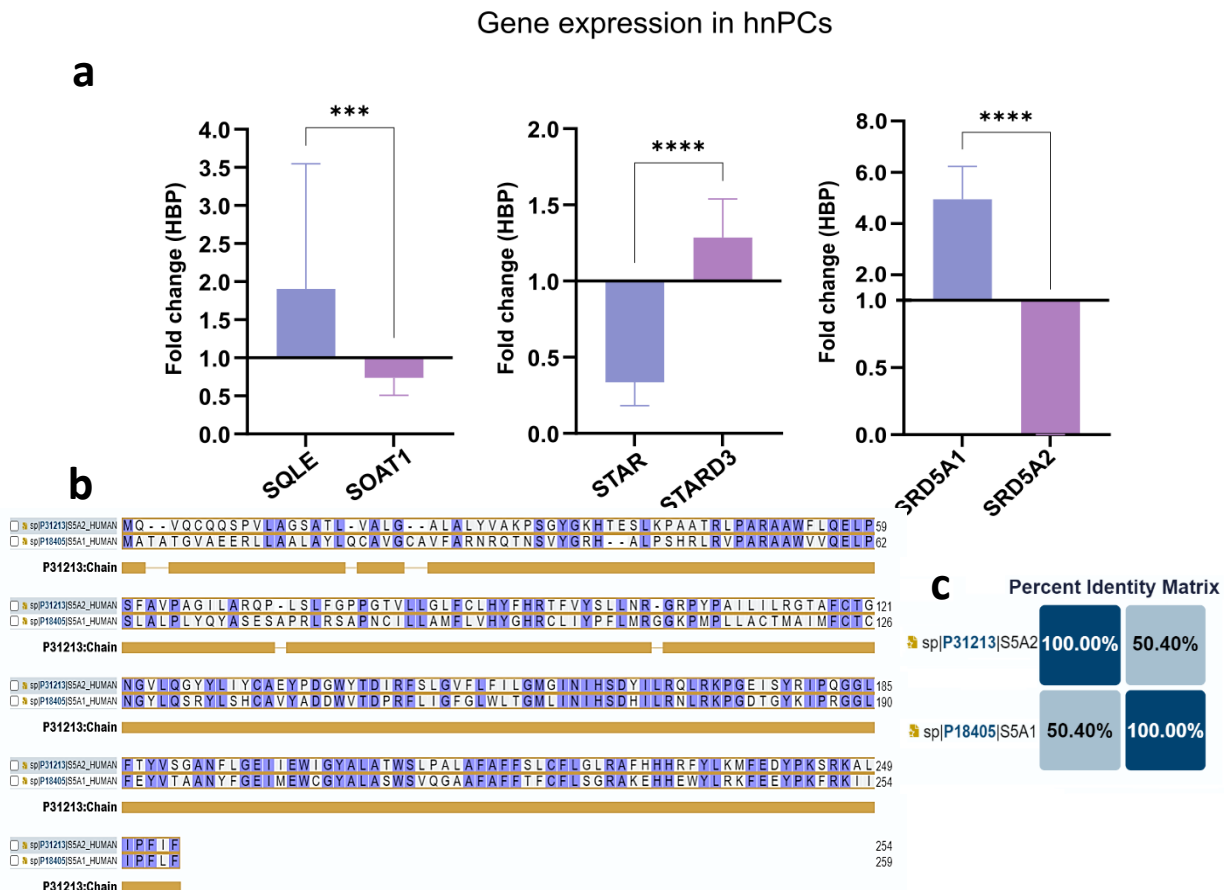


Figure 27. Changes in normal gene expression in steroid metabolism. a) Bars plot of expression of 6 steroidogenic genes in 11 primary cultures. Data are expressed as median (+ IQR) of fold change of 11 samples in triplicates. *TBP* and *IPO8* as housekeeping genes. p-values are result of Wilcoxon matched pair test * $P < 0.05$, ** $P < 0.01$, *** $P < 0.001$, **** $P < 0.0001$. **b)** Protein-protein alignment of *SRD5A1* (Uniprot ID P18405) and *SRD5A2* (Uniprot ID 31213) and **c)** percentage of identity. *UniProt alignment tool*³⁰⁸

2.5. De novo synthesis of Testosterone and estrogen in primary cultures

A significant reduction in AR expression is detected in hnPCs (n=11) and Du145 cell lines in contrast to LNCaP cells (**Figure 28a**). However, a significant increase in the expression of various steroidogenic genes (*AKRIC3*, *CYP19A1*, *CYP1B1*, *PAPSS2*) is observed, probably as a respond to it . *AKRIC3*, key enzyme for Testosterone synthesis, is detected in hnPCs and LNCaP resistant cells (**Figure 28b**). Generally, Testosterone is produced in the Leydig cells of the testis and a small fraction in the suprarenal glands. However, in hnPCs (of epithelial origin) the overexpression of *AKRIC3* is connected to their malignant transformation and suggests that endogen production of Testosterone is needed as a source of DHT, the most potent form. Moreover, the upregulation of *CYP19A1*, leading to the production of estrone, and of *CYP1B1*, that generates the active estrogen 4OH-stradiol, suggest that hnPCs are employing alternative sources as a strategy to support their survival and proliferation. Interestingly, hnPCs show upregulation of *PAPSS2*, a key enzyme for sulfonation of compounds implicated in diverse signaling pathways that regulate cell growth, survival, and proliferation¹⁸⁹ (**Figure 28c**.)

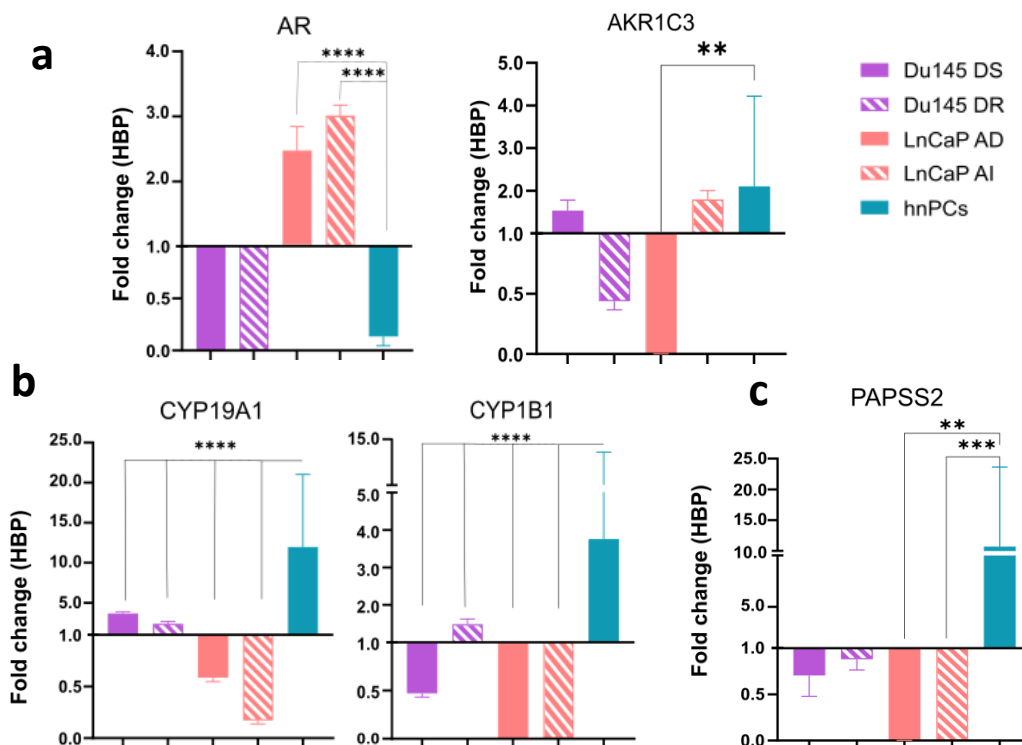


Figure 28. Expression of steroidogenic genes involved in de novo hormone synthesis in primary cultures. a) Despite AR downregulation, *AKRIC3* enzyme, is upregulated to synthesize de novo testosterone. b) *CYP19A1* and *CYP1B1*, estrogenic enzymes are upregulated. c) *PAPSS2* upregulation. *TBP* and *IPO8* as housekeeping genes. Cells lines data are expressed as median (+ IQR) of fold change in triplicates. hnPCs are shown as median +IQR of 11 samples in triplicates. p-values are result of Kruskal-Walli's test with Dunn's Test comparisons * P<0.05, **P<0.01, ***P<0.001, ****P<0.0001

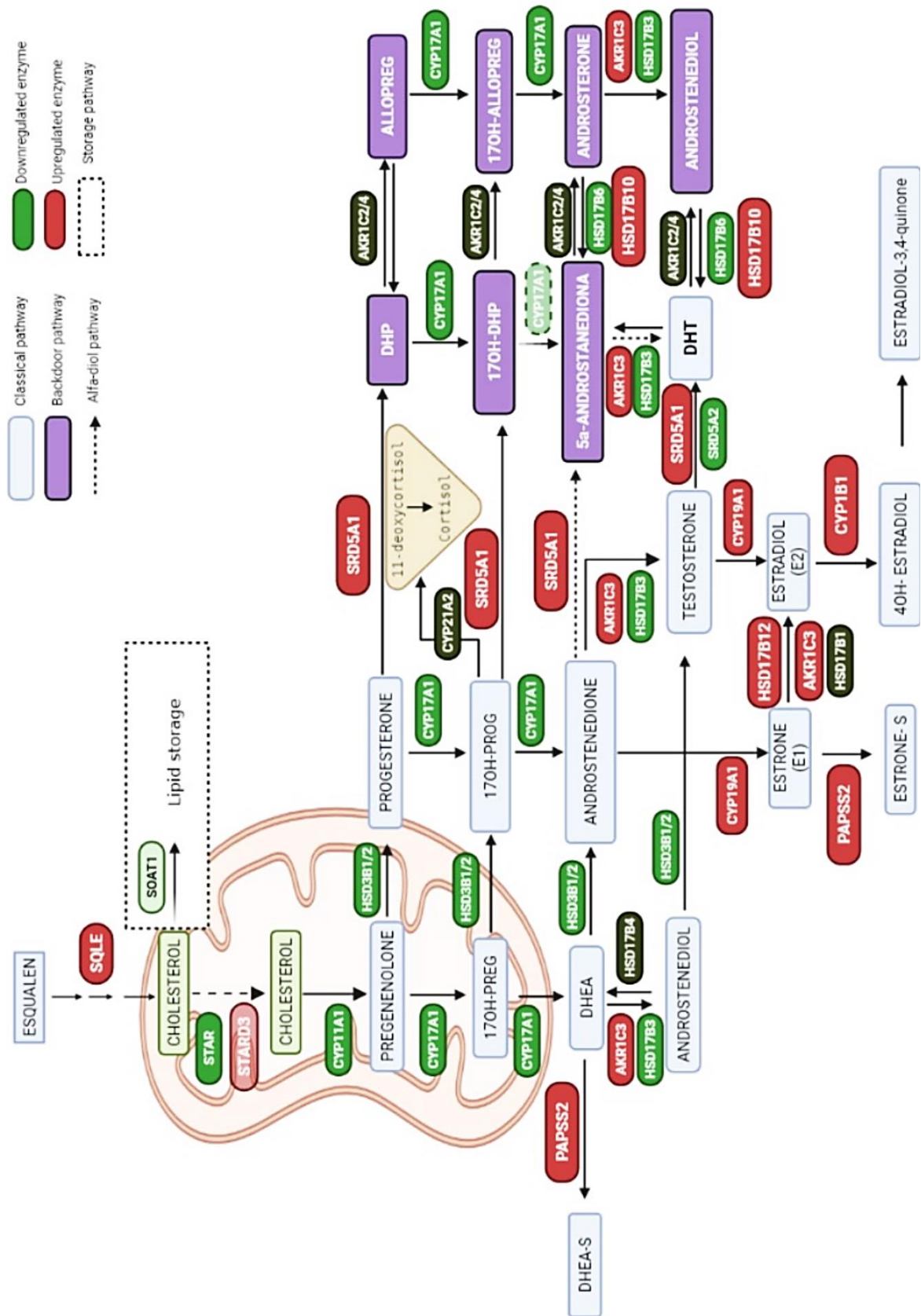


Figure 29. Map of steroid synthesis pathway and the enzyme expression profiles in primary cultures. Map shows the steroid biosynthesis pathway, from Esqualen to Estradiol. Key enzymes are represented in red (overexpressed) or green (underexpressed) according to expression level in primary cultures from prostate cancer. *Figures made with Biorender.com*

2.6. Expression profiles in hnPC and PCa tissues: comparison to original hnPC biopsies.

A Spearman similarity matrix was constructed based on gene expression data. This analysis revealed cell lines, hnPC, and tissues formed three different clusters (**Figure 30a**). To validate and visualize the relationships among sample groups, we conducted a principal component analysis (PCA). The PCA highlighted the presence of four distinct sample clusters (**Figure 30b**). In the PCA plot, RP tissue samples were notably separated from cell cultures, forming their own distinctive cluster, marked in blue. In contrast, cell cultures, exhibited close similarities to one another (pink) are subdivided into three smaller subclusters. Notably, hnPC01 demonstrated a strong affinity with LNCaP cells (green), while hnPC03 displayed a close similarity to Du145 cells (purple). However, it's worth noting that the remaining hnPCs appeared to be distinct and independent from the established cell lines. This finding aligns with prior characterizations of these primary cultures, which had already indicated that hnPC01 and hnPC03 exhibit unique behaviors distinct from the other hnPCs.

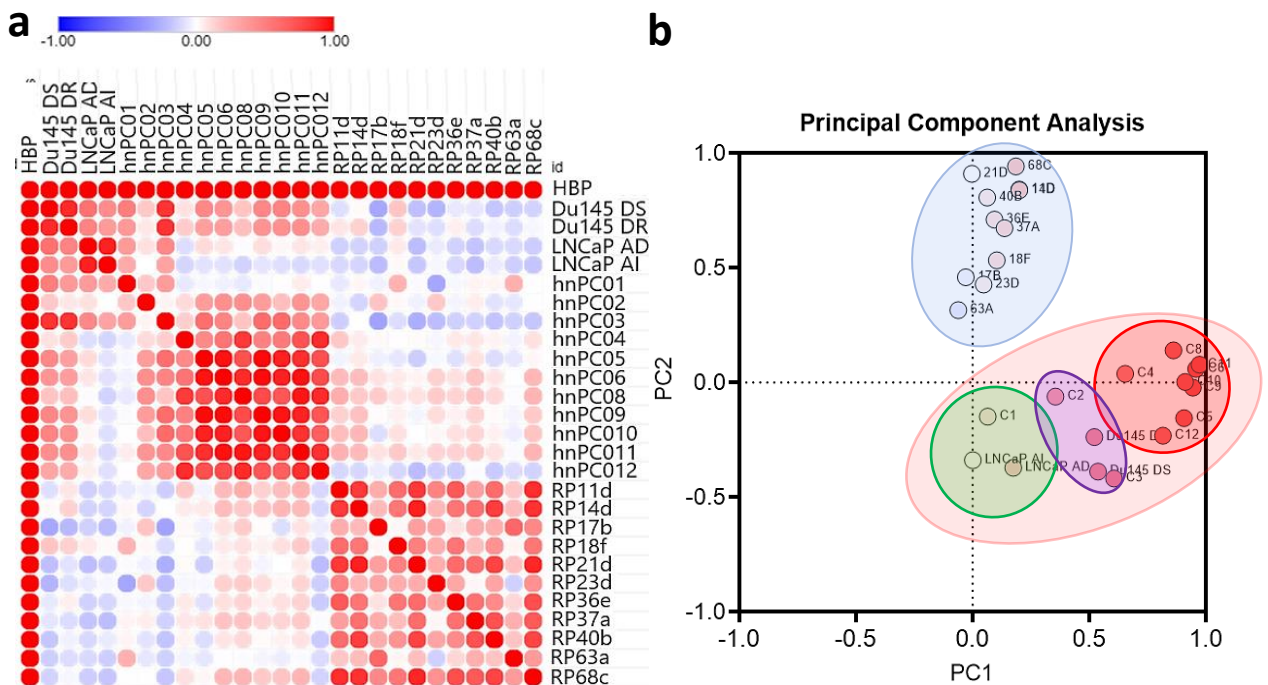


Figure 30. Analysis of similarity between cultures and tissues from prostatectomies. **a)** A similarity matrix was created using Spearman's rank correlation for cell lines (n=4), primary cultures (n=11), and RP tissues (n=11). The correlation coefficients (R) range between -1 (indicating a strong negative correlation) and 1 (indicating a strong positive correlation). **b)** Principal Component Analysis was conducted on the 26 samples based on gene expression. The results revealed the formation of two primary clusters: Blue (RP tissues) and Pink (cell cultures). Within the pink cluster, three subclusters were observed.

In this regard, we were interested in verifying if the established primary cultures were also different from its original biopsy tissues (TB) from which they were derived. We performed RNA extraction from each needle biopsy. However, from this experiment only 6 RNA samples were suitable for qPCR, and we added two samples more (hnTB13 and hnTB14). The expression profile obtained for some steroidogenic genes is shown in **Figure 31**. Both types of samples, primary cultures and corresponding biopsies, display similar gene expressions, although *ARK1C3* was not overexpressed in the original biopsy. An explanation might be the changes on the androgen availability, tissue receives the correct amount of androgen, while primary cultures have experienced a dramatic change in the environmental conditions, with limited sources of Testosterone.

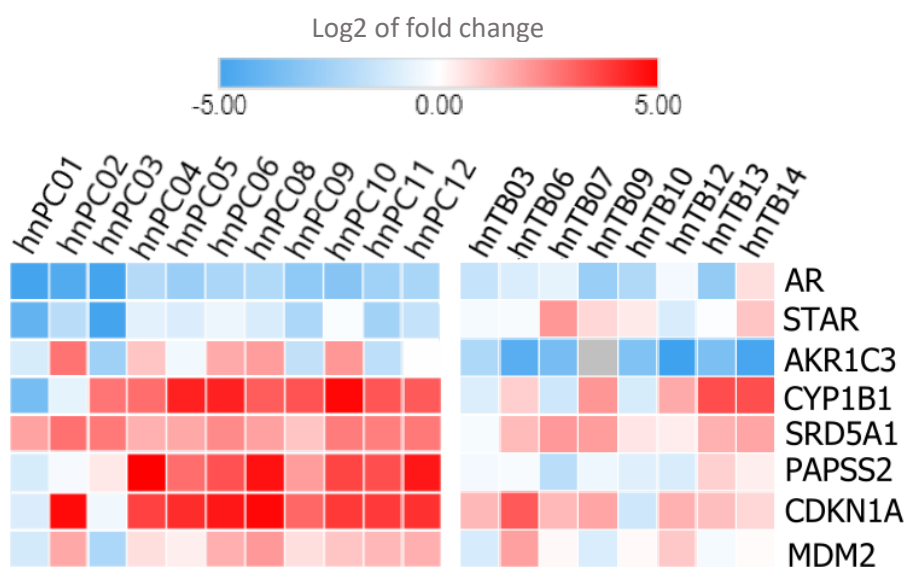


Figure 31. Heatmap of the expression profiles of primary cultures in comparison with original biopsies. Relative expressions are shown in Log2 of fold change (BPH) and analyzed in triplicates. TBP and IPO8 were used as housekeeping genes.

To further investigate if fetal bovine serum (FBS) might be an external source of Testosterone and other hormones, we analyzed the FBS hormonal composition by Chemiluminescent competitive immunoassays (CLIA) in automated analyzers (section of M&M in CHAPTER II). The results show that the addition of 7% FBS to the culture media used for the hnPC, did not represent a source of hormones (of the first steps on the pathway) comparable to the *in vivo* concentration (reference values in general population), instead we observed the presence of estrone, one of the final metabolites of the hormone pathway (**Figure 29**). Hormones, such as Testosterone and Androstenedione, were identified at

concentrations that closely resembled those typically encountered in androgen deprivation therapy (**Table 18**).

Table 18. Hormonal composition in Fetal Bovine Serum

Analyte	Concentration in FBS	Concentration in medium	Reference values in blood*
Cholesterol (mg/dL)	34.0	2.38 ↓	50-200
Triglycerides (mg/dL)	65.0	4.55 ↓	35-150
Estradiol (pg/mL)	11.0	0.77 ↓	20-350
SHBG (nmol/L)	1.5	0.11 ↓	23-160
Testosterone total (ng/dL)	5.0	0.35 ↓	300-1000
Cortisol (µg/dL)	0.64	0.045 ↓	5.27-22.5
DHEA-S (µg/dL)	2.0	0.14 ↓	100-375
DHEA (ng/dL)	0.4	0.028 <	0.06-0.7
17OH-Progesterone (ng/dL)	0.14	0.0098 ↓	0.35-3.0
Androstenedione (ng/dL)	0.2	0.014 ↓	0.5-3.5
IGF-1 (ng/dL)	113	7.91 ↓	180-500
17OH-Pregnenolone (ng/dL)	2.97	0.21 <	0.55-5.0
Estrone (pg/mL)	270	18.9 =	15-77

*Normal values in males from kit manufactures and Mayo Clinic (<https://endocrinology.testcatalog.org/>)
Concentration respect to normal values: ↓ very low, < low, = Equal

2.7. CDKN1A is strongly overexpressed in hnPCs and correlates with other steroidogenic genes

Notably, in hnPCs, with the exception of hnP01 and hnPC03, *CDKN1A* (p21^{WAF1}) were found significantly upregulated (**Figure 32a**) in comparison with cell lines (Kruskal-Wallis's test $p=0.011$). In neoplastic cells, several genes involved in DNA repair and cell cycle progression such cyclin-dependent kinase inhibitor p21 (*CDKN1A*) are activated. Cancer cells are able to escape senescence through the downregulation or loss of p21^{WAF1}. However, p21^{WAF1} overexpression has been shown to also promote aggressive phenotypes¹⁹⁰⁻¹⁹². Thus, to understand the functional significance of the overexpression of *CDKN1A* in the aggressive hnPCs, we studied its potential association with other known genes. For these studies multiple correlation matrix (Spearman analysis) was performed considering the levels of expression of all genes studied in the steroidogenic pathway (**Figure 32b**). The overexpression of *CDKN1A* was positively associated with several genes, including *STAR*, *HSD17B12*, *STAR*, *SOAT*, *SRD5A1* and *AKR1C3*. A simple Spearman correlation was then

used to evaluate the degree of correlations (**Figure 32c**). Interestingly, several genes showed significant correlation with *CDKN1A* ($R>0.5$), p -value < 0.05 .

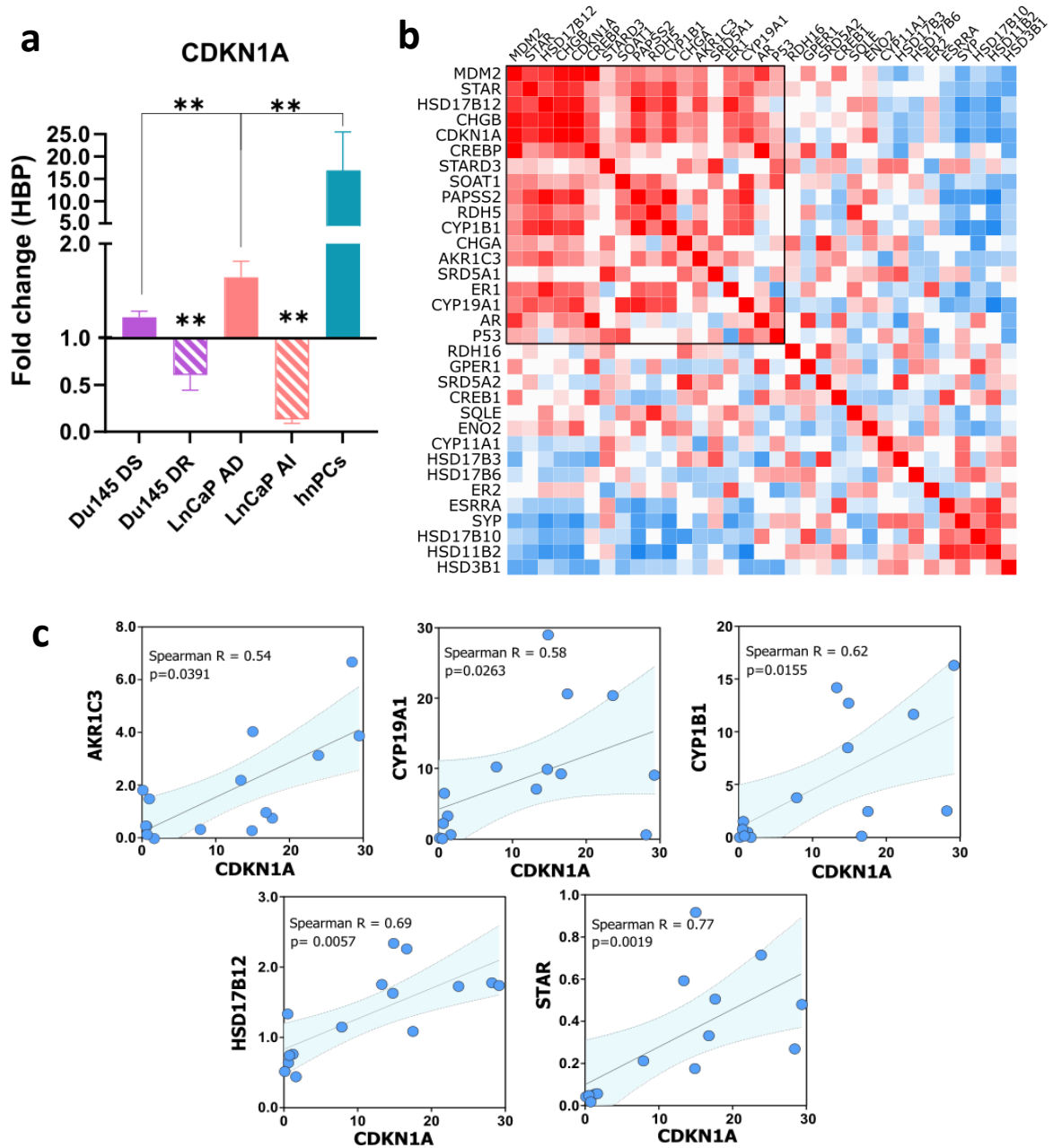


Figure 32. Overexpressed CDKN1A correlates with several steroidogenic genes. a) CDKN1A expression in cell lines (triplicates) and primary cultures ($n=11$, in triplicates), expressed as median +IQR. **b)** Multiple Spearman correlation matrix, showing the association between steroidogenic genes. **c)** Simple Spearman correlation analysis between CDKN1A and steroid genes. Expression gene p -values are result of Kruskal-Wallis's test with Dunn's Test comparisons * $P<0.05$, ** $P<0.01$, *** $P<0.001$, **** $P<0.0001$

The high degree of correlation observed of *CDKN1A* with *AKR1C3*, *CYP19A*, *CYP11B1*, *HSD17B12*, and *STAR* suggest a potentially close functional relationship among these genes and their products. To explore this connection, we studied the effects of the down regulation of *CDKN1A*.

3. p21^{WAF1} and its relationship with androgen metabolism in prostate cancer primary cultures

3.1. CDKN1A (p21^{WAF1}) silencing significantly affected the expression of ARK1C3

To further explore if the p21^{WAF1} overexpression was associated with the steroidogenic reprogramming in PCa cells, LNCaP AD and hnPCs were treated with 3 siRNAs against *CDKN1A* mRNAs. The transfection and knockdown efficiency obtained were >80% in LNCaP cells (**Figure 33a - 33b**). Upon p21^{WAF1} knockdown, a significant decrease in *AKR1C3* transcript (**Figure 33c**) and protein expression (**Figure 33d**) were observed, suggesting an association between AKR1C3 expression and p21^{WAF1}.

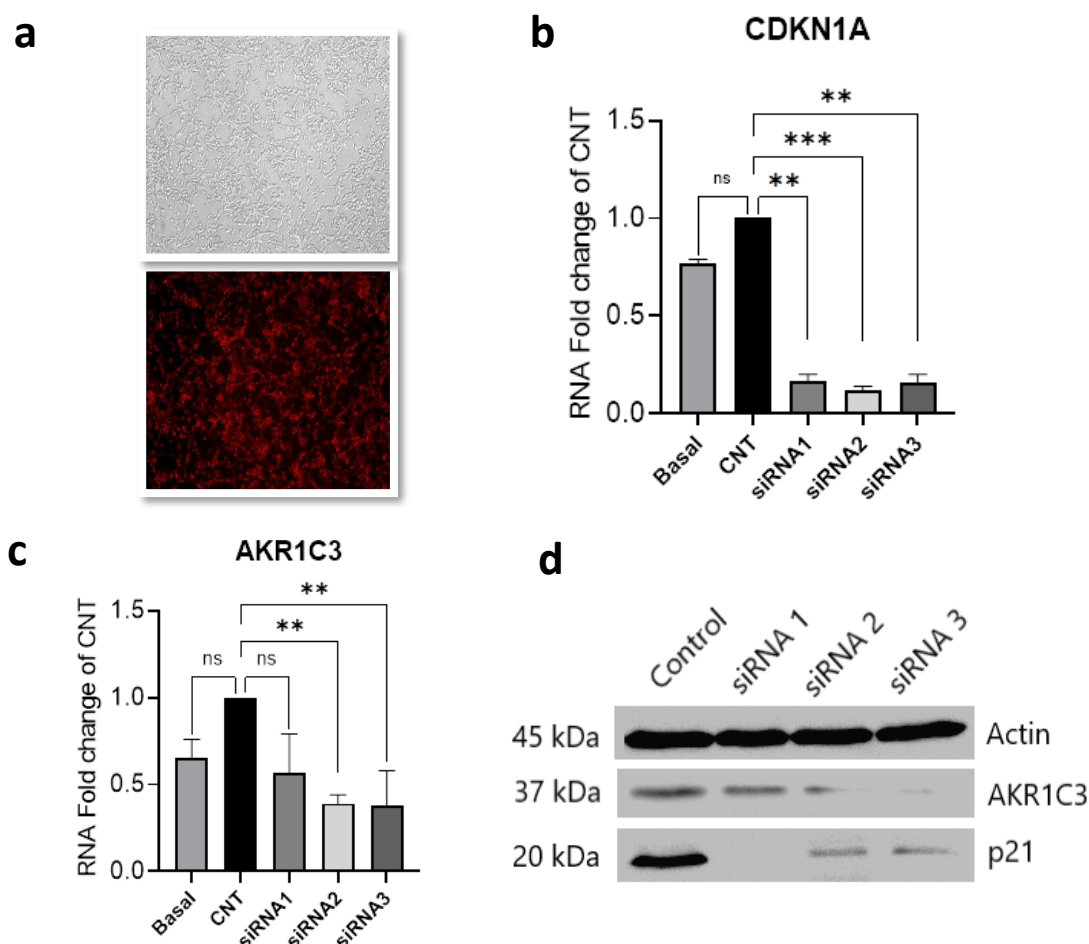


Figure 33. p21^{WAF1} is associated with AKR1C3 expression in LNCaP. a) Transfection efficiency in LNCaP cells knocked down for p21^{WAF1} by siRNAs. b) *CDKN1A* mRNA levels were depleted with high efficiency. c) *AKR1C3* mRNA levels were also significantly decrease and were corroborated by Western blotting (d). Control transfection was analyzed by fluorescence at 563nm of wavelength. All experiments were performed in triplicate. Data are medians + IQR. p-values are result of Kruskal-Wallis test with Dunn's Test comparisons. ns: no significant, * P<0.05, **P<0.01, ***P<0.001, ****P<0.0001

The knockdown of p21^{WAF1} also affected the expression of *STAR* and *HSD3B1*, although results were not consistent using three siRNAs (**Figure 34**).

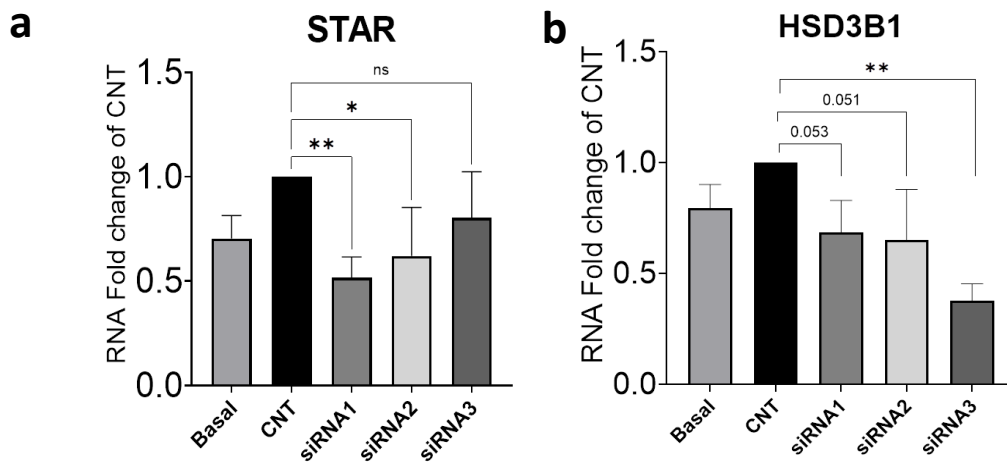


Figure 34. *STAR* and *HSD3B1* expression are affected by p21 KD in LNCaP cells. a) Knocked down cells for p21 by siRNA showed significant decrease in *STAR* expression with two siRNAs. b) *HSD3B1* mRNA levels were also significantly decreased with 1 siRNA, and nearly significant with 2 siRNAs. Experiments were performed in triplicates and three independent assays. Data are medians + IQR. p-values are result of Kruskal-Wallis test with Dunn's Test comparisons. ns: no significant, * P<0.05, **P<0.01, ***P<0.001, ****P<0.0001

MDM2 and *TP53* were also evaluated. Although no consistent results were observed in the expression of *MDM2* and *TP53* among the three siRNAs used (**Figure 35**).

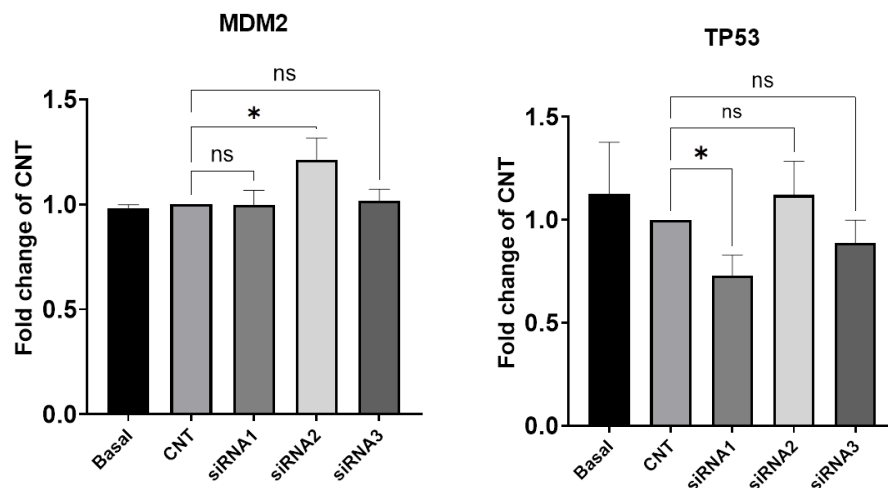


Figure 35. Bar plot of expression analysis of *MDM2* and *TP53* with p21-siRNAs in LNCaP cells. Experiments were performed in triplicates and three independent assays. Data are medians + IQR. p-values are result of Kruskal-Wallis test with Dunn's Test comparisons. ns: no significant, * P<0.05, **P<0.01, ***P<0.001, ****P<0.0001

Then, we explored the effects of *CDKN1A* silencing in primary cultures, using the same conditions as with LNCaP AD (**Figure 36a**). *AKR1C3* was significantly downregulated with p21 knockdown (Kruskal-Wallis, p-value=0.0003), with all three siRNAs (**Figure 36b, 36c**). Results were corroborated by western blot (**Figure 36d**). A significant decrease in *AKR1C3* was observed with all three siRNAs in hnPC04 and hnPC08, whereas in hnPC05 and hnPC06, a decrease in protein synthesis was observed with two siRNAs. Overall analysis of *AKR1C3* protein expression was performed quantifying bands.

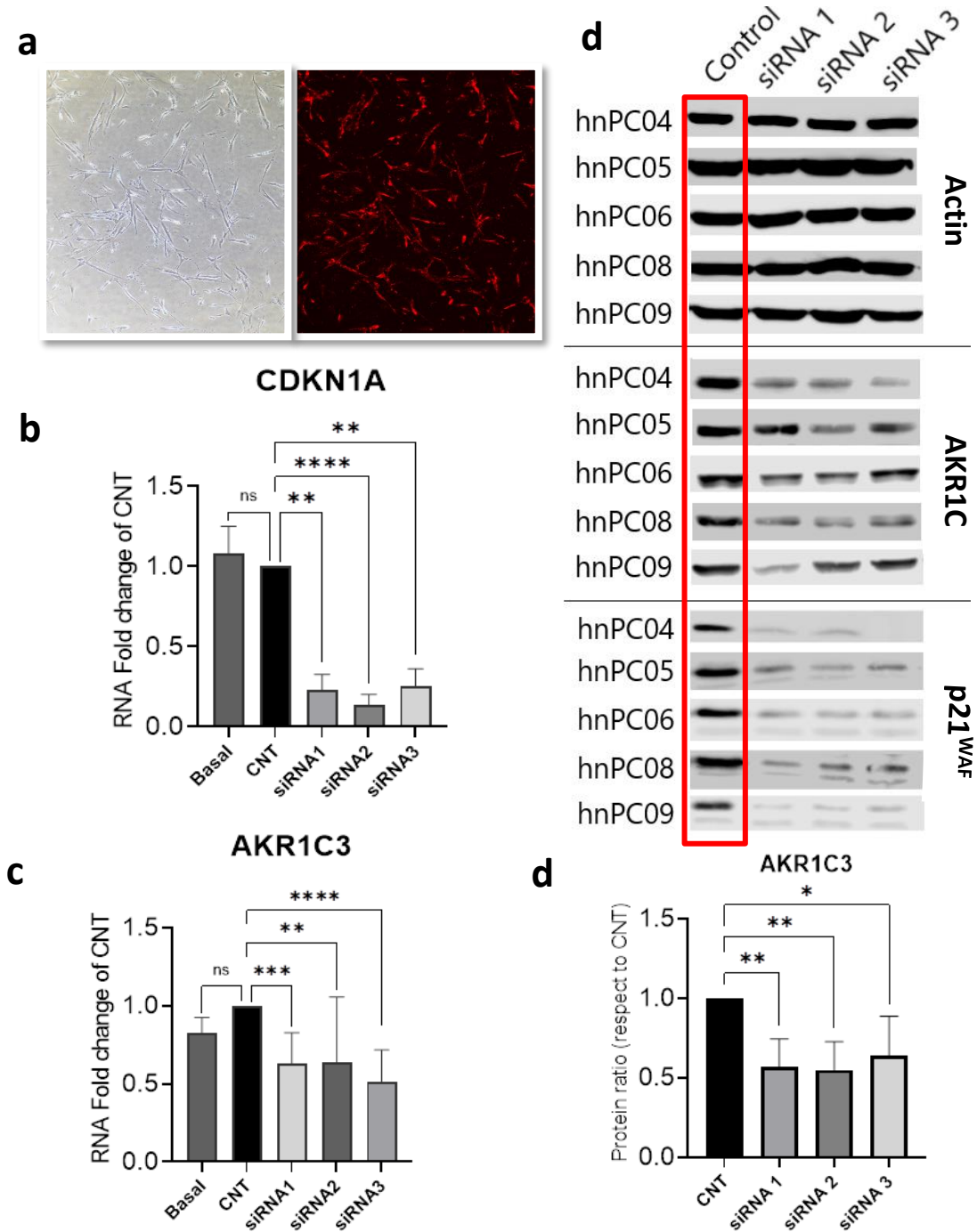


Figure 36. Description in the next page.

Figure 36. p21^{CIP/WAF1} is associated with AKR1C3 expression in primary cultures. a) Transfection efficiency in hnPCs knocked down for p21 by siRNAs. b) CDKN1A mRNA levels were depleted with high efficiency. c) AKR1C3 mRNA levels were also significantly decrease and were corroborated by Western blotting d) Control transfection was analyzed by fluorescence at 563nm of wavelength. Experiments were performed in triplicate in two independent assays. e) Protein levels quantification on western blots. Data of RNA expression are medians + IQR. p-values are result of Kruskal-Wallis test with Dunn's Test comparisons. Data of protein quantification are the median of the bands area from each primary culture. Protein levels were normalized to β -actin band and then compared respect to control. ns: no significant, * P<0.05, **P<0.01, ***P<0.001,****P<0.0001

CYP19A1 was also significantly downregulated in p21-knocked down hnPCs, although only with one siRNA. *MDM2* was significantly upregulated (Kruskal-Wallis's test p<0.001) with two siRNAs (Dunn's post-test). *TP53* was not affected by p21^{WAF1} downregulation (Figure 37).

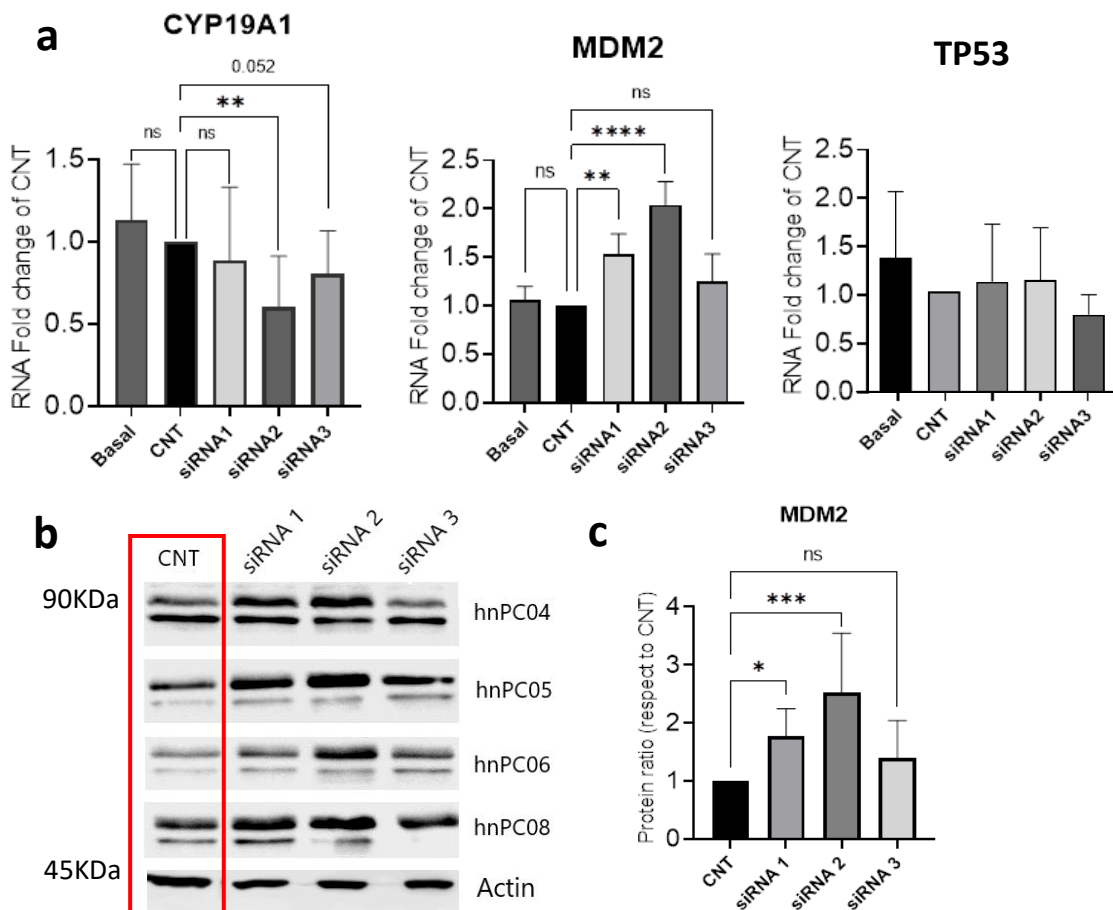


Figure 37. CYP19A1 and MDM2 expression in p21-KD hnPCs. a) Cells with p21 knockdown using siRNA exhibited a significant decrease in *CYP19A1* expression with one siRNA, *MDM2* mRNA levels significantly increased with two siRNAs but *TP53* not show significant differences. b) Western blots displaying MDM2 expression in four hnPCs after p21 knockdown. Representative β -Actin bands are shown for each sample. The experiments were performed in triplicates and across two independent assays. RNA expression data are presented as medians with interquartile ranges (IQR). p-values were obtained using the Kruskal-Wallis test with Dunn's Test comparisons. c) Protein quantification data represent the median of the band areas from each primary culture. Protein levels were normalized to the β -actin band and then compared to the control. ns: no significant, * P<0.05, **P<0.01, ***P<0.001,****P<0.0001

3.2. p21^{WAF1} subcellular localization in LNCaP AD cells and hnPCs

Because the p21^{WAF1} subcellular localization was suggested to be linked to its function as tumor suppressor (nuclear) or pro-oncogenic (cytoplasmic), a fractionation analysis was performed in LNCaP AD cells. As it is shown by western blotting, p21^{WAF1} was detected in the cytoplasmic fraction (**Figure 38a**), Laminin A/C (70-62 kDa) and the cytoplasmic β -tubulin (55KDa) correctly localized as nuclear and cytoplasmic proteins, respectively. Surprisingly, p21^{WAF1} was only observed in cytoplasm. To confirm these findings, an immunofluorescence assay was conducted. In this experiment, we observed that LNCaP AD cells (used only at passages < 20) primarily exhibited p21 expression in the cytoplasm, with lower nuclear expression. Only a minority of cells displayed exclusive nuclear expression (white arrow). This outcome implies that the slight overexpression observed in **Figure 32a** is attributed to cytoplasmic p21^{WAF1} rather than nuclear expression.

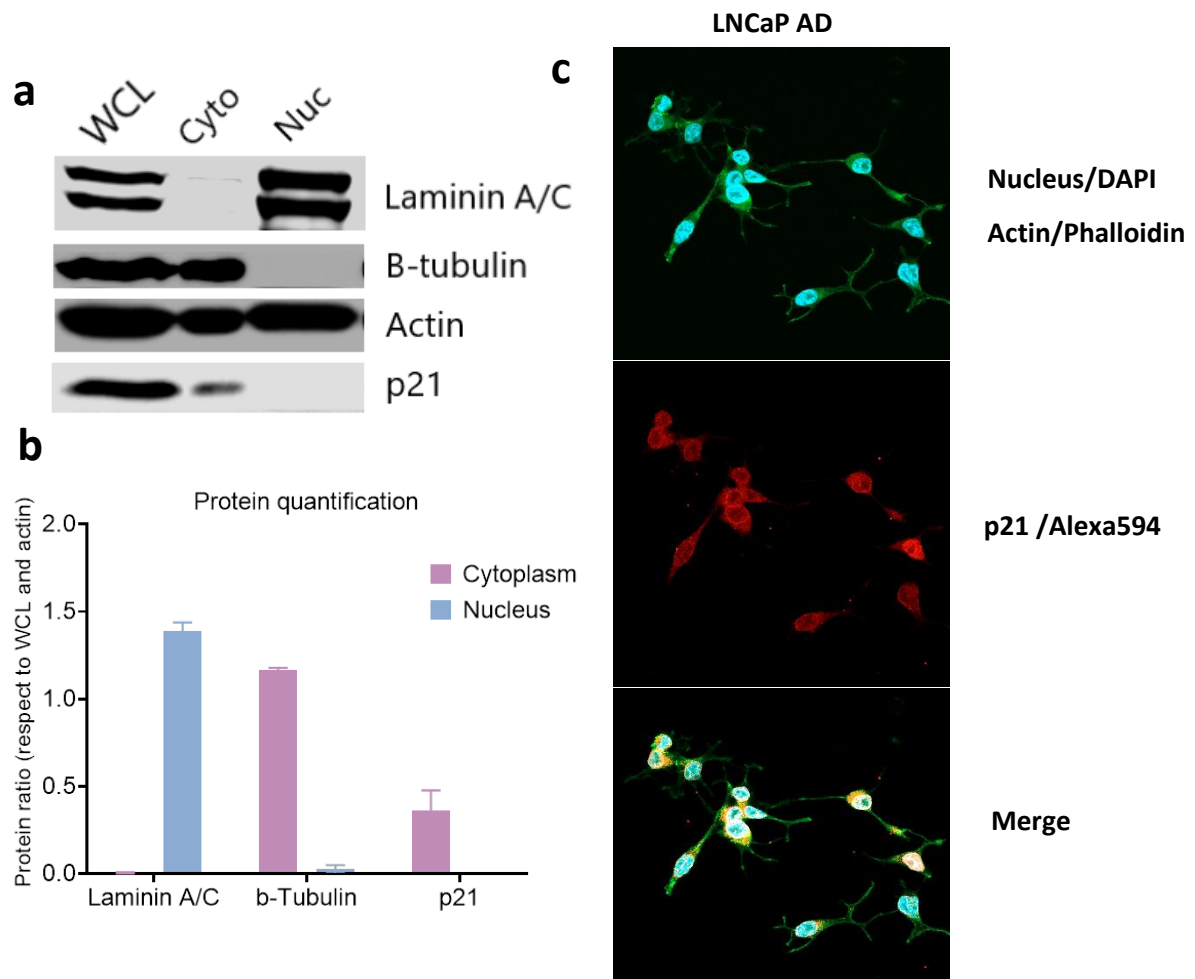


Figure 38. Subcellular localization of p21^{WAF1} in LNCaP cells. **a**) Representative western blot of LNCaP cell fractions. Protein p21 is observed in cytoplasm. WCL: whole cell lysis, Cyto: cytoplasm, Nuc: nucleus. **b**) Protein quantification in cytoplasm and nucleus. Protein band areas (in triplicates) were normalized respect to β -actin and then compared to WCL (ratio= 1). **c**) Immunofluorescence confocal microscopy images of LNCaP cells stained for markers of p21 (Red), Nucleus (DAPI-Blue) and Actin (Phalloidin-Green). It is observed that p21 localization (Alexa-594 red) is detected in cytoplasm in merge image.

3.3. p21^{WAF1} subcellular localization and senescent markers reveal senescent-like state in hnPCs

3.3.1. Subcellular localization analysis

In parallel assessments, we conducted fractionation analysis using 5 different hnPCs, with results closely resembling those obtained with LNCaP cells, showing the presence of p21^{WAF1} only in cytoplasmic fractions (**Figure 39**). Surprisingly, using immunofluorescence assays the hnPCs tested exhibited a higher frequency of p21^{WAF1} expression in the nucleus compared to the cytoplasm (**Figure 40**). In these images, a few cells display positive p21 staining in both compartments (**white arrow in Figure 40**).

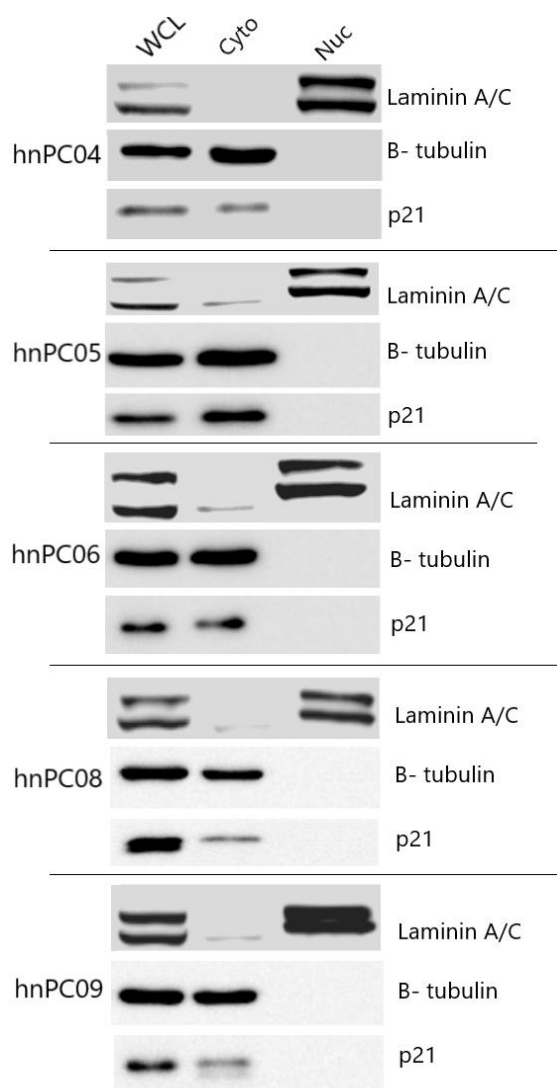


Figure 39. Subcellular localization of p21^{WAF1} in hnPCs. Representative western blot of hnPC cell fractions. Protein p21 is observed in cytoplasm. WCL: whole cell lysis, Cyto: cytoplasm, Nuc: nucleus.

These contrasting findings could potentially be attributed to the inherent characteristics of nuclear p21^{WAF1} protein. It is well-established that under normal growth conditions, this protein is inherently unstable and has a relatively short half-life^{193,194}. In contrast, cytoplasmic p21^{WAF1} appears to exhibit enhanced stability, primarily due to its interaction with Akt1/PKB¹⁹⁵. This stability would allow cytoplasmic protein to persist during the fractionation technique and be visualized in the Western blot analysis.

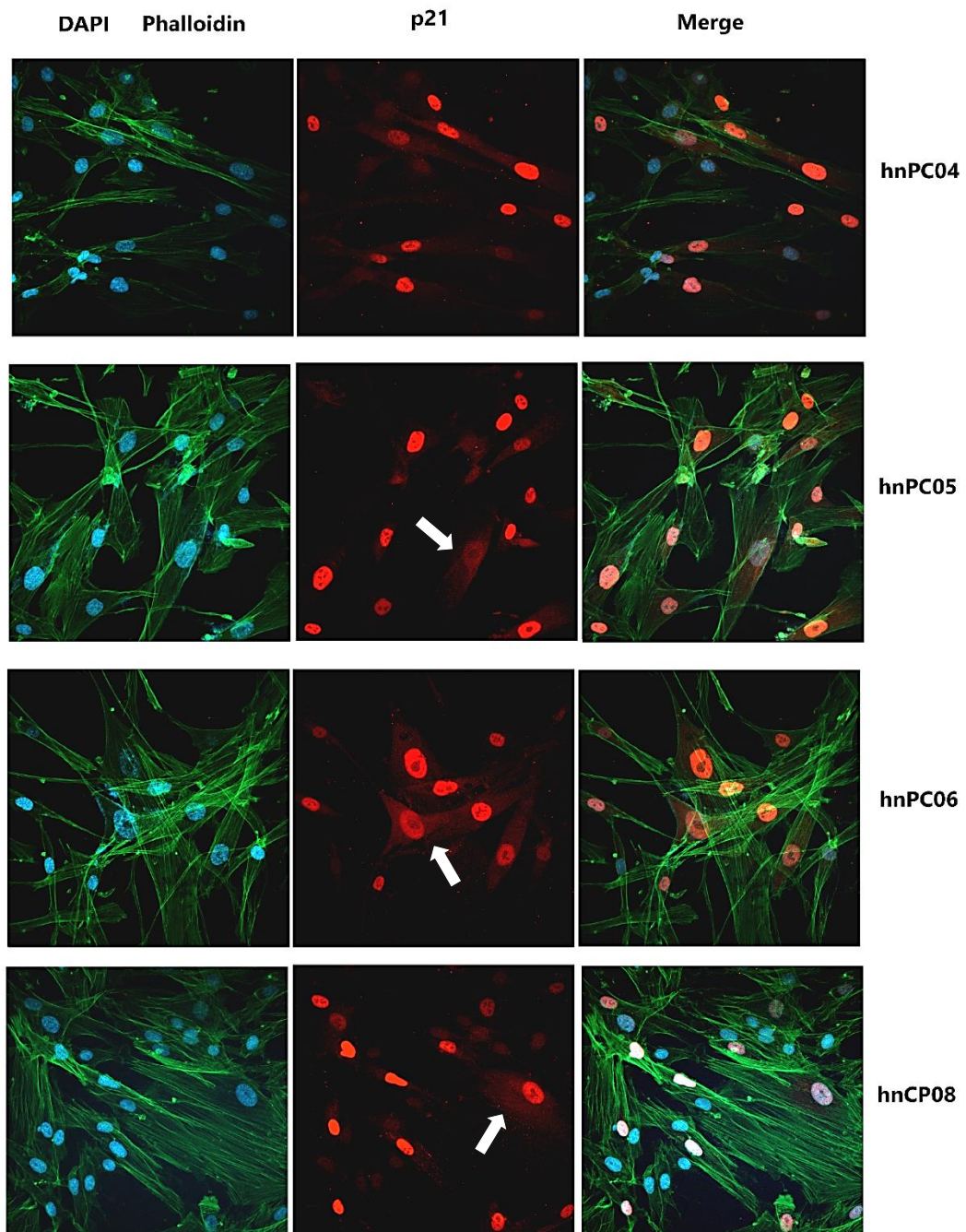


Figure 40. Immunofluorescence confocal microscopy images of p21 in hnPCs. Primary cultures were stained for markers of p21 (Red), Nucleus (DAPI-Blue) and Actin (Phalloidin-Green). It is observed that p21 localization (red) is detected more frequently in nucleus. Some cells showed p21 in both cytoplasm and nucleus (white arrows).

3.3.2. Nuclear p21^{WAF1} reveals senescence-like state in primary cultures

The pronounced overexpression of p21^{WAF1} in the nucleus led us to speculate that primary cultures might be entering a state of senescence. However, it's important to note that in previous characterizations, these cells exhibited a pattern of moderate yet sustained proliferation (**Figure 41**), which appears contradictory to the notion of senescence. Notably, hnPC01 displayed proliferation rates comparable to those of LNCaP cells, and both exhibited relatively low levels of p21^{WAF1} expression.

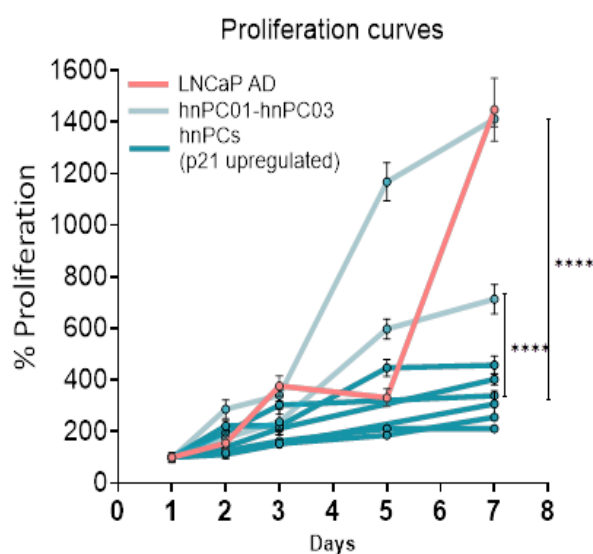


Figure 41. Percentages of proliferation in LNCaP and primary cultures. Primary culture hnPC01 shows similar growth rate to LNCaP cells at day 7. hnPC03 shows significant higher growth rate than p21-overexpressing primary cultures, although lower than LNCaP and hnPC01. Primary cultures with aberrant expression of p21^{WAF1} show significant low ratios of proliferation, although sustained along time. Data are the mean \pm S.D of three independent experiments, each performed in octuplicate- P-values * P<0.05, **P<0.01, ***P<0.001, ****P<0.0001

Therefore, additional markers were used to determine the senescence state of these cultures. The expression levels of *CDKN2A* (p16), one known hallmark of senescence, was analyzed by real-time PCR and found upregulated in all hnPCs that overexpressed p21 (**Figure 42a**). In addition, the detection of β -galactosidase activity was measured in hnPCs overexpressing p21^{WAF1} and in p21^{WAF1} knocked down cells. Interestingly, β -galactosidase activity was detected in basal and control cells but not in cells transfected with p21-siRNAs (**Figure 42b-d**). The expression of *CDKN2A* was not affected by the p21-knockdown (**Figure 42a**), suggesting that the β -galactosidase activity is associated to p21^{WAF1} overexpression rather than p16.

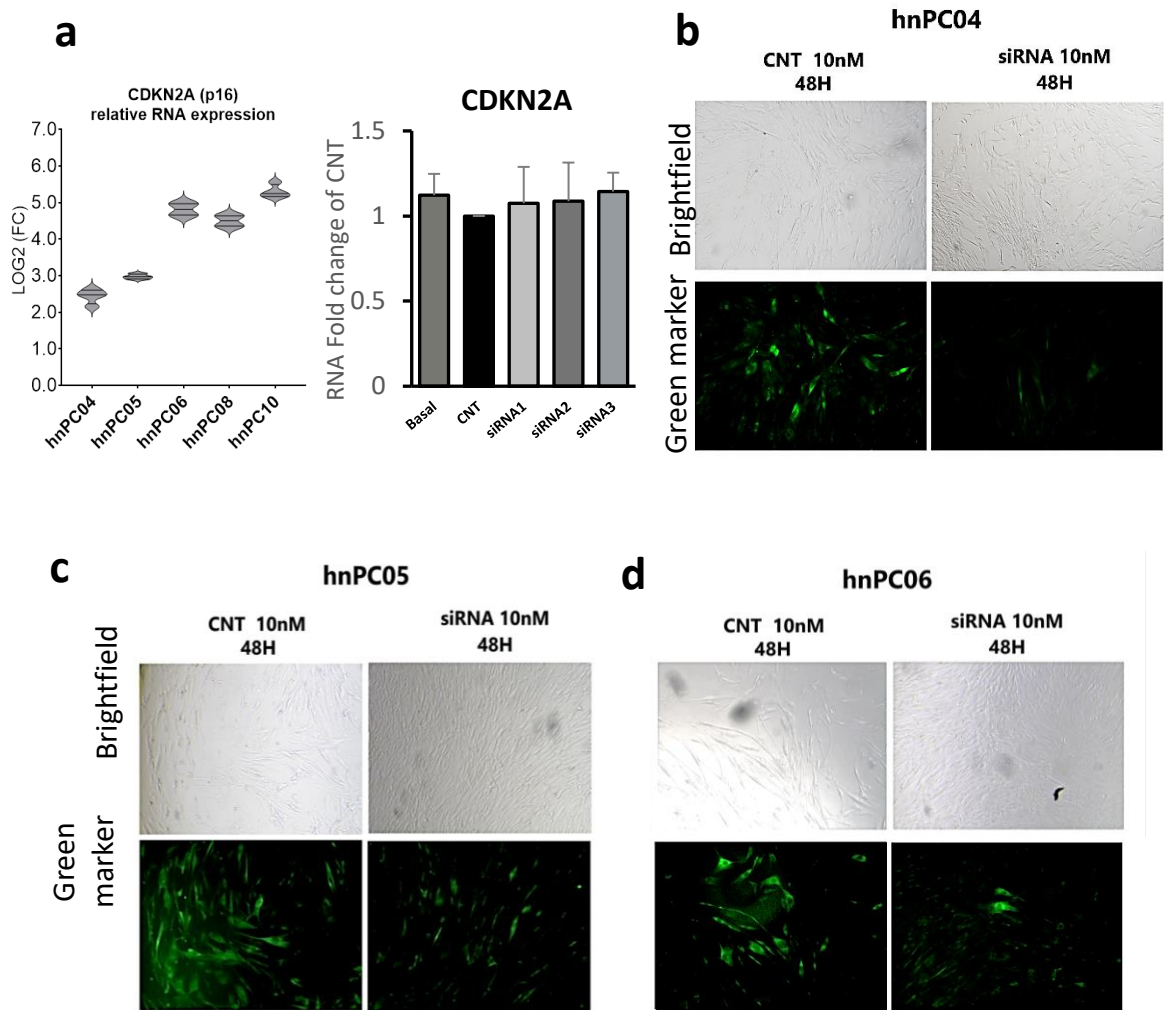


Figure 42. Expression of senescent markers in hnPCs. a) CDKN2A mRNA overexpression in 5 primary cultures and expression after p21-KD with siRNAs. Data are the Log2 of Fold change (BPH). **b,c,d**) β -Galactosidase (β -Gal) activity detected with green fluorescence in three primary cultures. Cells treated with siRNA control, show positive β -Gal activity, however, this activity is significantly reduced in cells treated with p21-siRNAs at 48 hours.

In summary, these findings collectively imply that hormone-naïve primary cultures are undergoing a state that resembles senescence, given their expression of senescence markers, while simultaneously displaying sustained proliferation over time.

Current studies on cellular senescence have implied the paradoxical role of cellular senescence in tumorigenesis, an altered senescence-associated secretory phenotype (SASP) in cells, can contribute to the microenvironment that promotes tumor development^{196,197}. One gene, linked to senescence and tumor suppression is the well-known protein Notch1.

Notch1 is known as a tumor suppressor, but several studies have shown conflicting results, regarding its oncogenic^{198,199} or suppressor role^{200,201} in cancer, depending on the cell context and tumor type. In a recent study of our laboratory, it was found that a significant overexpression of PTOV1 (an oncogenic protein) repressed the transcription of Notch1 targets, suggesting that PTOV1 is repressor of the antitumoral activity of Notch1 in prostate cancer²⁰². Thus, the effects of transient p21-downregulation in the expression of Notch1 (~120 kDa), were analyzed by means of siRNAs transfection and western blot in four hnPCs (**Figure 43**). The results show that, compared to control cells, p21-knocked down cells upregulated Notch1, and this upregulation was significant in hnPC04 and hnPC06.

NOTCH1 expression in hnPCs

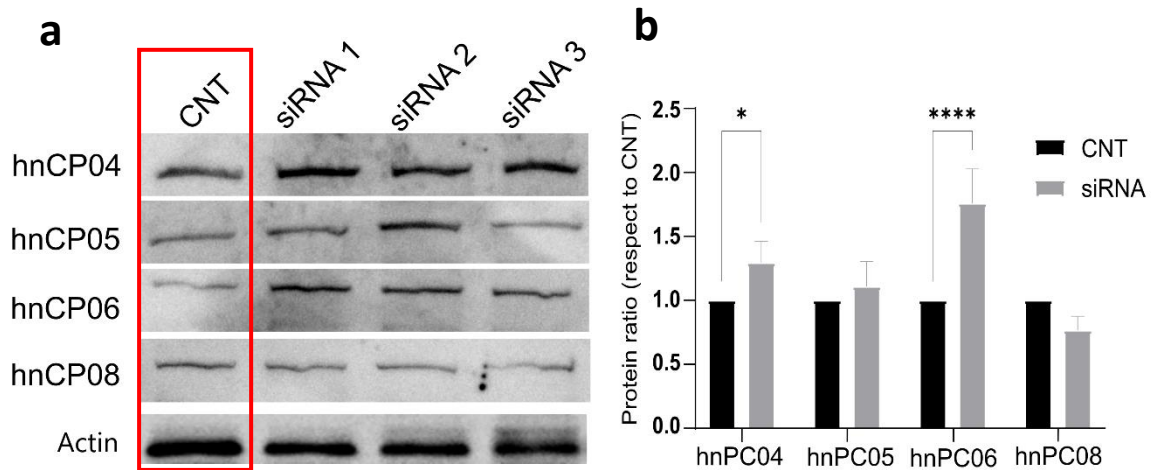


Figure 43. Notch1 expression in hnPCs. a) Western blots of Notch1 expression in four hnPCs after p21-KD. β -Actin bands are representative of each sample. Experiments were performed in triplicates. b) Data of protein quantification are the median +IQR of the bands area from each siRNA. Protein levels were normalized to β -actin band and then compared respect to control. p-values are result of Kruskal-Wallis test with Dunn's Test comparisons. ns: no significant, * $P < 0.05$, ** $P < 0.01$, *** $P < 0.001$, **** $P < 0.0001$

Notch1 is a transmembrane receptor. When activated by ligands, its cleaved intracellular domain (NICD) participates in nuclear activation of different transcriptional programs, such as embryonic development, cell fate decision, senescence^{203,204} and cancer^{200,205,206}. Some studies have highlighted the importance of Notch1 expression to promote tumor suppression, as such in cells expressing p73 α 1-mediated tumor suppressor²⁰⁶, and its implications in secondary senescence, where Notch1 is necessary to induce early-state senescence in neighboring cells in a juxtacrine manner, provoking aberrant expression of *CDKN1A* and

SASP in adjacent cells^{203,204}, which are showing Notch1 upregulation. Notably, in later established senescent cells, Notch1 is downregulated, allowing pro-inflammatory SASP (Figure 44). Consequently, our results are suggesting that primary culture cancer cells, undergoing fully secondary senescence-like state, expressed low levels of Notch1 to allow the expression of pro-inflammatory SASP. In contrast, in p21^{WAF1} downregulated cells, Notch1 is induced to promote tumor suppression and cell-to-cell interaction for a potential reactivation of SASP signaling

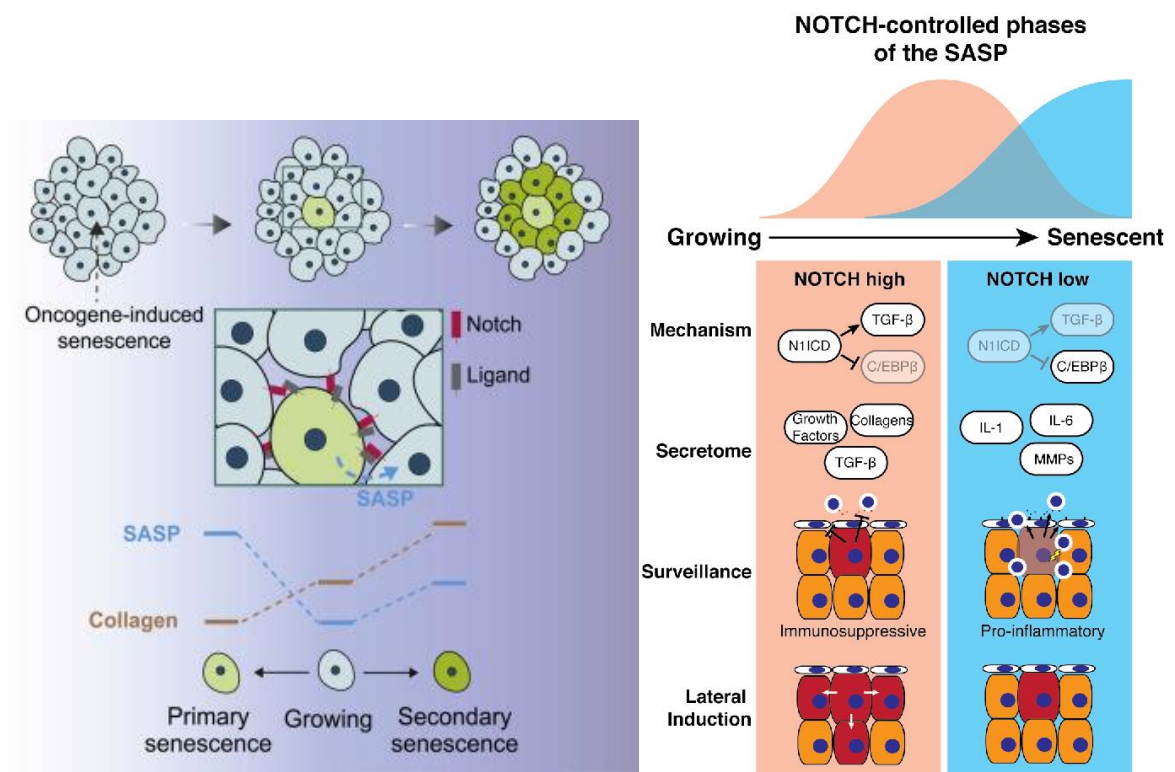


Figure 44. Notch1 signaling mediates secondary senescence. Notch1 is necessary to promote secondary senescence by juxtacrine interaction. In early steps of secondary senescence, Notch1 is highly activated to promote non-inflammatory SASP and maintain growing (Pink), whereas in later established senescence, with CDKN1A high expression, Notch1 is downregulated to allow pro-inflammatory SASP (Blue) and cell arrest. *Figures taken from Teo et al. 2019 and Hoare & Narita, 2017^{203,204}.*

4. Cancer stemness is promoted in all hnPCs compared to LNCaP cells

The above results have shown that the presence of elevated p21^{WAF1} levels is linked to a senescence-like condition in hnPCs. These cells also showed increased expression of *ARKIC3* and other steroidogenic genes. Studies investigating the complex role of cellular senescence have also revealed its involvement in processes like cellular reprogramming and the acquisition of stem cell-like properties. Surprisingly, senescence can also drive the development of more aggressive tumors and cancer stemness¹⁴⁶.

To evaluate the stemness capacity of hnPCs, the expression analysis of two pluripotency genes and one main cancer stemness markers, the *CD44* gene, was performed. Results show that *SOX2* was upregulated in LNCaP AI cells, indicating a more aggressive behavior in comparison with AD cells. However, in hnPCs only hnPC05 AI showed significant overexpression of *SOX2*. In addition, hnPC03 AD, but not the AI counterpart, showed significant upregulation of *SOX2*. Regarding the *OCT3/4* gene, only hnPC03 (AD and AI) showed significant overexpression in comparison with LNCaP cells (>100-fold change). Surprisingly, all hnPCs AD and AI, displayed an exaggerated overexpression of CD44 with respect to LNCaP AD. Notably, hnPC03 showing *OCT3/4* overexpression, was the only primary culture that express less than < 50-fold changes respect to control cells (**Figure 45**).

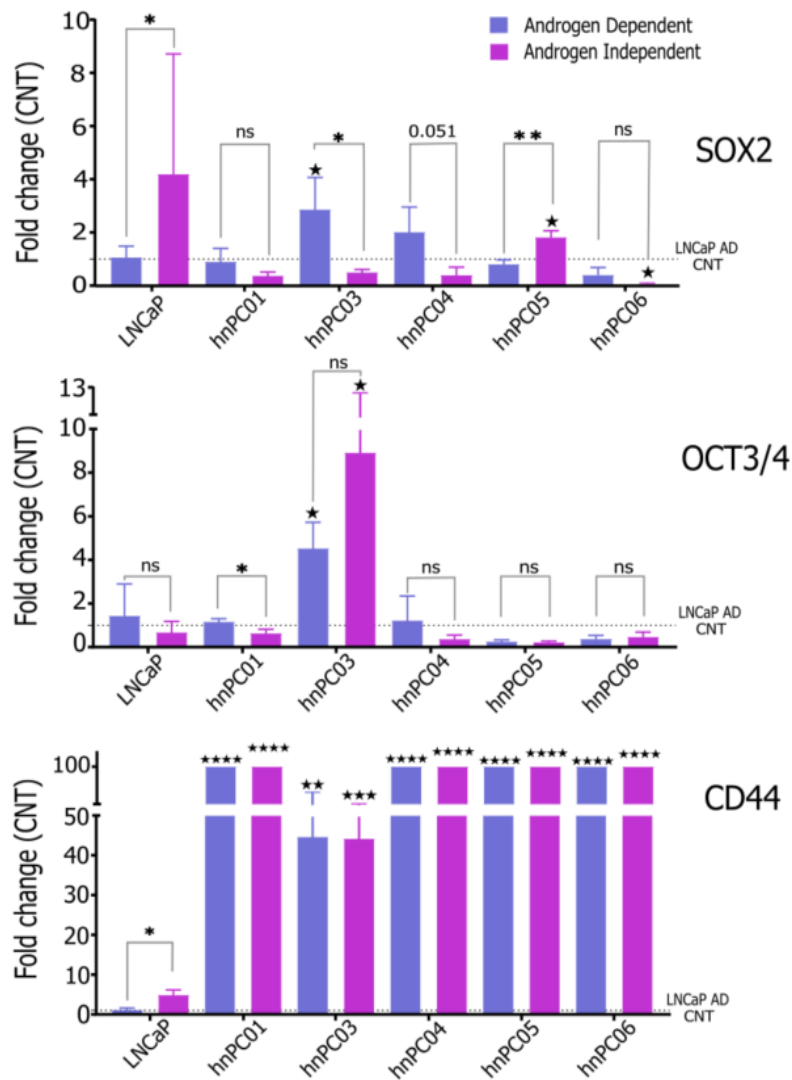


Figure 45. Description in next page.

Figure 45. Expression of three stem cell markers in hnPCs. Top panel: mRNA expression of SOX2 in LNCaP and primary cultures, AD and AI models. **Center panel:** OCT3/4 expression, only hnPC03 showed significant overexpression in comparison with LNCaP AD cells. **Bottom panel:** CD44 overexpression was observed in all primary cultures, with fold changes exceeding 100. However, the graphs only display values up to 100. Data are the fold change respect to LNCaP AD control. TBP and IPO8 were used as housekeeping genes. **ns:** no significant, * P<0.05, **P<0.01, ***P<0.001, ****P<0.0001. ★ p-value respect to LNCaP AD. * p-value AI vs AD models.

Stem cell properties in our primary cultures would be enhancing tumor progression and chemoresistance, also CD44 overexpression would be indicating that primary cells are undergoing cell reprogramming which may be implicated in the potential reprogramming of the hormonal metabolism that primary culture cells are showing *in vitro*.

CHAPTER I: DISCUSSION

CHAPTER I – DISCUSSION

1. Primary cultures from hormone-naïve patients: a useful pre-clinical model

Prostate cancer exhibits significant heterogeneity across clinical, spatial, and morphological dimensions, accompanied by a diverse genetic landscape²⁰⁷. This complexity poses challenges for PCa research for the creation of meaningful pre-clinical models useful to identify new targets, biomarkers, and novel drugs²⁰⁸.

Research efforts have been extensively focused on understanding the hormonal mechanisms driving PCa. Immortalized cell lines have been highly useful tools during the second half of the 20th century. Studies on the AR and hormone mechanism in the 80s²⁰⁹ led to significant advancements in cancer treatment. However, the unavoidable emergence of resistance to those treatments poses increased challenges to the findings of new targets and biomarkers able to improve patient response. Current challenges entail the develop of new pre-clinical models that can reflect disease progression, subtypes, and molecular mechanism of resistance. Recent advances in the field, have allowed to establish of 3D organoid cultures from cell lines, partially resembling the tumor complexity and patient derived xenografts (PDX) that resemble the original tumor, including its heterogeneity and microenvironment. Our group established 16 primary *ex vivo* cultures from hormone-naïve patients (hnPCs). Ten of such primary tumor cultures were partially characterized for common gene alteration, proliferation rates, and resistance capacity to chemotherapy²¹⁰.

Although 2D primary cultures present some disadvantages with respect to the tumor in site, e.g. different microenvironment and lack of immune modulation, these hnPCs are a unique collection of established cultures obtained from prostate needle biopsies of primary tumors from patients with inoperable, high Gleason grade (> 8) tumors. They represent a very useful alternative to study the aggressive metastatic prostate tumors that are not operable, therefore they fill a gap of basic necessity for research aimed to study the mechanisms of progression in these tumors.

In this thesis, we used the hnPCs to study the changes in the steroidogenic pathway established in aggressive PCa to identify potential biomarkers of aggressiveness and targets for more specific therapies. We compared the gene signatures from hnPCs, LNCaP and Du145 cell lines with those from tissues (radical prostatectomies, RP) and the original PCa biopsies. The primary hnPCs and cell lines showed similar expression profiles that were closer to each other than to prostate tumor tissues (RP) (Figure 30). Adaptation of cells from *in vivo* to the culture conditions implies drastic changes in their microenvironment, which

generate significant alterations in the expression of the genes functioning in those processes²¹¹⁻²¹⁵. Reports in this field found that gene expression patterns in different established cell lines and primary tumor cultures, were more similar to each other than to their respective tissues, suggesting an increased similarity in cell features related to the culture conditions, and decreasing the inherent differences originally present in each tumor in its natural state²¹². *In vitro* environments play a significant role in modulating gene expression. For example, it was described that the expression profiles from glioma tissues and from the corresponding *in vitro* cultures were clustered separately in a microarray analysis²¹⁶. The latter showed a marked enrichment of genes of the nucleic acid metabolism and cell proliferation, and loss of gene expression associated to development, transporter activity and brain specific-genes, indicating a more undifferentiated phenotype, compared with primary tumors²¹⁶. Despite the large evidence pointing to significant changes in gene expression patterns associated to culture conditions, the comparison between hnPCs and their original tissues did not reveal substantial differences in the expression of steroidogenic genes (**Figure 31**). In line with other studies²¹⁷⁻²¹⁹, our observations suggest that hnPCs may still reflect the clue gene patterns shown *in vivo*. Thus, although hnPCs and cell lines grouped into one cluster, most hnPCs were separated from LNCaP and Du145 cell lines, suggesting that primary cultures have sufficiently different gene expression patterns still retained from their original tissues.

2. Polymorphic variant rs1042522 (P72R) in prostate cancer

TP53, tumor suppressor gene, is the most mutated gene in different human cancer types, including PCa¹⁶⁶ and it was one of the focal points of our investigation. The finding that 7 out of 10 primary cultures contained arginine (CGC), while 2 cultures displayed proline (CCC) is particularly intriguing due to the unusually high frequency of this variant (**Table 16**). One possible explanation could be the Loss of Heterozygosity (LOH) phenomena, particularly studied in exon 4, where P72R variant is present. In fact, the loss of Proline (C) allele and the preferential retention of the Arginine (G) allele was described in primary tumors and metastatic tissues of squamous cell carcinoma of vulva²²⁰, head and neck²²¹, colorectal tumors²²², and lung cancer²²³. A recent metanalysis study using the TCGA pan-cancer database and patients selected for the P72R heterozygosity, 31% (127/409) of heterozygotes had lost the P72 allele in the corresponding tumor tissue²²⁴ indicating that the G allele is preferentially selected for tumor development, possibly due to enhanced p73-

induced apoptosis¹⁸⁸ and the modulation of tumor metabolism by regulating PGC-1 α ²²⁵. Given that the 10 hnPCs analyzed came from patients predominantly European Caucasian in which, according to 1000 Genomes Project, the G allele has a global prevalence below 50%, in most ethnic populations (**Figure 46**), we began to explore a potential association between the presence of this allele and the risk of developing prostate cancer.

1000 Genomes Project Phase 3 allele frequencies

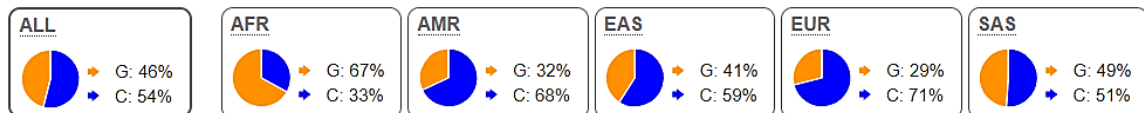


Figure 46. Global allele frequency of P72R SNP rs1042522. Allele G is present in minor frequency in all sub populations except for African population. *Picture from Ensemble.org*

The prevalence of the R72 variant in the 10 hnPCs, the PCa tissues and the 94 serum samples from prostate cancer patients was compared to a wider collection of genotypes: the European (non-Finnish) non-cancer population selected from the GnomAD v2.1.1, containing 134,187 genomes (**Figure 21b**). As shown in the contingency, the P72R SNP appears significantly associated to prostate cancer (**Table 17**). confirmed our findings, showing a higher occurrence of the 72R allele compared to 72P allele significantly associated with prostate cancer risk^{226–229}. However, it is worth noting that most studies showed controversial results^{230–232} or failed to demonstrate significant association between polymorphism and risk of any type of cancer^{233–237}. Probably due to limited sample sizes or selection bias. For example, in a colorectal cancer study in the North-European population, a significant association between presence of Pro allele and risk of cancer was reported²³⁸, but the control samples selected had a high frequency of Arg72 allele (61%) when its estimated frequency in European population (non-cancer) from GnomAD v2.1.1 is 26% (Figure 21). Appropriate representativeness in control samples is necessary for accurate results. In prostate cancer, studies are more limited and several have shown conflicting results^{239–241,236,242–244}.

Beyond these conflicting findings about the Arg frequency at codon 72 of p53, it is crucial to consider the potential impact of the Arg variant on cancer development, although is not fully understood. Studies in mice revealed that Homozygosity for the R72 variant show higher incidence of mammary tumors²⁴⁵. In addition, the R72 variant associated to increased phosphorylation of p53 and enhanced the transactivation of *CDKN1A* (p21^{WAF1}) in response

to starving, with consequent augmented growth arrest but reduced apoptosis, a situation that favors survival²⁴⁶. Additionally, *TP53* mutations tend to preferentially occur in the R72 allele. In cases of *TP53* with mutations (e.g. R175H, R273H, and A138V) and harboring the SNP (R72 allele), an enhanced capacity for migration, invasion, and metastasis in various cancer cell lines, including PCa, was reported²²⁵. These observations put into evidence that Arg at codon 72 impacts on the tumor suppression activity of p53.

Although no significant association of P72R with tumor grade (Gleason score) was found in our study, the G allele (R72) was more frequent in patients with high Gleason scores (≥ 8) suggesting an association to more undifferentiated-malignant PCa lesions (**Figure 22**). A few studies evaluated the association between this polymorphism and tumor grades and found no significant association with clinical stage or Gleason grade in PCa^{242,243,247,248}. One study identified a link with modest influence of the P72R SNP and shortened biochemical recurrence (BCR) after radical prostatectomy²⁴⁴. Another study in Japanese population²⁴⁰, observed a notably high frequency of Arg allele in patients with metastases and those with high-Gleason score (≥ 8). However, they analyzed the association using the arginine allele as a reference, meaning they calculated the significance level between the Pro/Pro and Pro/Arg genotype compared to arginine. As expected, they found no significant difference, as proline did not differ significantly from control group.

To validate and enhance our findings, further investigation with a larger sample size is necessary, taking into account the family history of prostate cancer, which may also influence our results.

3. Steroid hormone metabolism in hormone-naive primary cultures models

Steroid hormone metabolism plays a key role not only in regulation of homeostasis but also in disease development⁸. PCa is notably a hormonal disease that require androgens to proliferate and survive^{43,44}. To characterize the cellular model of hnPCs established in our laboratory and in order and find potential biomarkers for this aggressive cancer we studied the expression of several genes included in the steroidogenic pathway. An increase in the expression of several genes of the steroid hormone production compared to benign prostatic hyperplasia (BPH) was observed (**Figure 26**). Specifically, enzymes located earlier in the steroidogenic pathway, such as *SQLE*, *SOAT1*, *STAR*, and *STARD3*, showed altered expression levels (**Figure 27a**). The upregulation of *SQLE*, is in line with previous research

indicating its role as an oncogenic factor associated with poor survival outcomes in various types of tumors^{249–255} including prostate cancer²⁵⁶. Interestingly, *SOAT1* which catalyzes the formation of fatty acid-cholesterol esters stored in cellular droplets, was found downregulated in most primary cultures, which contradicts findings from other studies. Squalene epoxidase (*SQLE*) is the second rate-limiting enzyme involved in cholesterol synthesis, an essential component of cell membrane and vital for proliferation²⁵⁷. The concurrent upregulation of *SQLE* and downregulation of *SOAT1* suggest an increase of free cholesterol levels and a reduction in lipid droplet formation. This finding is particularly significant in prostate cancer, as excess of free cholesterol serves as the primary source for steroid hormone synthesis²⁵⁸. In addition, free cholesterol maintains lipid raft stability, activating the Src/PI3K/Akt signaling pathway²⁵⁵, and negatively regulates the infiltration levels of CD8+ T cells, follicular helper T cells, regulatory T cells, and activated mast cells, key components of the anti-tumor immunity²⁵³.

The steroid hormone synthesis pathway begins with the transport of cholesterol from the cytoplasmic compartment into mitochondria. One master protein transporter is the Steroidogenic acute regulatory (StAR) related lipid transfer protein domain 1 (*STARD1*) better known as *STAR*. A significant downregulation of *STAR* in hnPCs and RP tissues was observed concomitantly to overexpressed *STARD3*. This cholesterol transporter has been reported to be upregulated in several cancer, including prostate cancer^{259–262}. Notably, *STARD3* is localized in a chromosomal region (17q12-21) which is frequently amplified in cancer, as breast and colorectal cancer. *STARD3* is mainly found in endosomal vesicles and endoplasmic reticulum (ER)^{263,264}. When overexpressed, *STARD3* increases cholesterol accumulation in those compartments and contribute to the mobilization of endosomal cholesterol to mitochondria for the steroidogenic process^{265,266}.

In agreement with the above findings, several enzymes of the steroid synthesis pathway are upregulated (*AKRIC3*, *SRD5A1*, *CYP11B1*, *CYP19A1*, *HSD17B6*, *HSD17B10* and *HSD17B12*) in the majority of hnPCs indicating a change in the metabolic profile of cancerous prostate tissue (**Figure 28**). Thus, these cultures would be directing hormonal synthesis towards the production of Testosterone → Estradiol → **4OH-Estradiol** and Testosterone → **DHT** ← Androstenediol. The hormones, dihydrotestosterone (DHT) and 4OH-Estradiol, are considered as the most potent sex steroid hormones.

4OH-Estradiol exhibits a higher binding affinity for the estrogen receptor alpha (ER1) when compared to estradiol itself. Estrogens, similar to androgens, are known to play a significant

role in prostate cancer²⁶⁷. The enzyme CYP1B1 responsible for converting estradiol into 4OH-estradiol, is upregulated in the primary cultures. This is particularly relevant in prostate cancer because 4-hydroxyestradiol can undergo conversion into semiquinones and quinones, compounds associated with the formation of depurination adducts, that are able to induce mutations²⁶⁸. Additionally, semiquinones and quinones are linked to docetaxel resistance due to their binding affinity for tubulin^{269,270}.

DHT, compared to Testosterone, also shows greater binding affinity (2-folds) and lower dissociation rate (5-fold slower) for binding to the AR^{271,272}. In the normal prostate, the primary pathway for steroid hormone synthesis is known as the "classical" pathway. A crucial step in this pathway is the conversion of Testosterone (T) to DHT, typically catalyzed by the enzyme SRD5A2¹²⁰. However, when T levels drop significantly, reaching castration levels, two alternative pathways, namely the "backdoor" and the "5 α -dione" pathways, gain prominence in androgen synthesis. These pathways offer a workaround to the problem by producing DHT without relying on T by using other enzymes for this purpose²⁷³. Notably, we observed a significantly downregulation of *SRD5A2* in the primary cultures, and an upregulation of *SRD5A1*, typically overexpressed in PCa, especially in CRPC. The upregulation of several genes involved in the "backdoor" pathway of androgen synthesis, including *SRD5A1*, *HSD17B6*, and *HSD17B10*^{121,274,275} also was observed. These results support the hypothesis that hnPC cells exhibit a preference for androstenedione and 17-OH progesterone over testosterone as sources for DHT production¹²⁰. Notably, we also observed an upregulation of *AKR1C3* an enzyme that in healthy conditions is mainly expressed in the adrenal gland and the testis, where it plays a role in catalyzing the synthesis of testosterone, but is not detected in the normal prostate gland^{276,277}. The increased levels of *AKR1C3* in hnPCs would direct testosterone production through the "classical" pathway, indicating that, DHT may be synthesized through both the classical and backdoor pathways in aggressive PCa cells.

Very interestingly, we found the upregulation of the Estrogen-related receptor alpha (ERR α), better known as ESRR α (**Figure 26**), a ligand-independent orphan member of the nuclear receptor superfamily shown to be associated with development and poor prognosis of various hormone-dependent tumors as endometrial, ovarian, breast and prostate cancer²⁷⁸⁻²⁸¹. In a recent study, ESRR α was shown to play pro-steroidogenic role in CRPC, transactivating steroidogenic enzyme genes *AKR1C3* and *CYP11A1*²⁸². It was found that ESRR α can

exclusively stimulate DHT biosynthesis via the secondary backdoor pathway by directly targeting the steroidogenic enzyme AKR1C3.

These findings support the possibility that hnPCs may direct the steroidogenic pathway towards the production of more potent hormones, as DHT using the backdoor pathway to promote survival and proliferation.

Surprisingly, *AR*, was found significantly downregulated in our models (**Figure 28a**), similarly to the androgen-independent Du145 cell lines^{283,173,284}. The AR is a transcription factor that holds significant relevance in the Castration Resistance, where is frequently overexpressed or amplified. This phenomenon enables the tumor to adapt and survive in conditions of androgen deprivation, contributing to the development of resistance to anti-androgen therapies²⁸⁵. However, in patients undergoing long-term androgen deprivation therapy (ADT), AR tends to diminish. This reduced expression is associated with poor prognosis to which also contribute several factors, including the decreased sensitivity of the tumor to AR inhibitors. In addition, the decrease in AR is linked to cellular de-differentiation, that further complicates the management of the disease²⁸⁶. In cell lines, such as LNCaP, a prolonged androgen deprivation in culture led to downregulation of AR²⁸⁷. Interestingly, AD hnPC models, downregulate AR without undergoing androgen deprivation: although the growth media used, containing 7%FBS exhibited low concentrations of androgens, similar to ADT conditions *in vivo*, is it noteworthy that tissue biopsies also showed low levels of AR. The downregulation of AR has been attributed to a strong DNA methylation in *AR* promoter in Du145 cells²⁸⁸. In the context of very low levels of AR, DHT may still interact and activate AR responses. However, another possibility by which steroid hormones bypass the low levels of AR is by activating alternative pathways. In fact, androgen can activate non-genomic pathways, through the interaction with membrane ARs (mARs), such ZIP9²⁸⁹ and PI3K/Akt/Erk pathways^{290,291}. ZIP9 receptors and PI3K/Akt signaling activation can be localized in intracellular compartments^{292,293} which could facilitate the interaction with the *de novo*-synthesized hormones in the primary cultures.

4. p21^{WAF1} – associated senescence and its role in androgen metabolism

The *CDKN1A* gene, encodes the cyclin-dependent kinase inhibitor 1 (p21^{WAF1}) protein was the first discovered transcriptional target of p53^{294,295}. p21^{WAF1} originally has been described as tumor suppressor, that induce cell cycle arrest by blocking DNA replication through the binding to proliferating cell nuclear antigen (PCNA) and inhibits the activity of cyclin-CDKs

complexes^{295–297}. As a result, the cell cycle is arrested in the G1/S or G2/M checkpoints. Interestingly, several studies have reported a paradoxical role of p21^{WAF1} in promoting tumor growth and proliferation^{298–301}. In line with those results, *CDKN1A* was overexpressed ~15-folds in hnPCs with respect to BHP and showed significantly higher levels in comparison with LNCaP and Du145 cells (**Figure 32**). The strong expression of *CDKN1A* has been reported in cancerous cells showing proliferation features, independently of p53. These cells showed genomic alterations, aggressiveness and chemoresistance¹⁹¹. In prostate tumors, *CDKN1A* upregulation has been observed in comparison with normal adjacent tissues (Anova, p-value=0.016) (**Figure 47**)

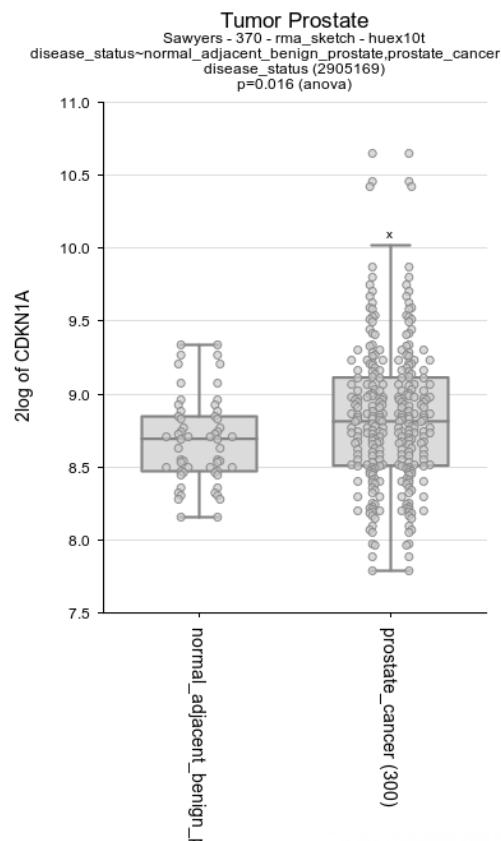


Figure 47. CDKN1A expression in prostate cancer and normal tissue. Box plot representing *CDKN1A* mRNA expression in prostate cancer tissues (n=300) in comparison with normal adjacent tissue (n=70). Anova comparison show significant difference (p<0.016). Data was obtained from Sawyers dataset published and GenomicR2.

The strong overexpression of *CDKN1A* in hnPCs cells, which display sustained proliferation and chemoresistance (Figure 25b), led us to hypothesize that *CDKN1A* might be associated to the steroidogenic reprogramming observed in these cells. After analysis of the correlation between *CDKN1A* and steroidogenic gene expression, a significant strong association was

found with *AKR1C3* (R=0.54), *CYP19A1* (R=0.58), *CYP11B1* (R=0.62), *HSD17B12* (R=0.69) and *STAR* (R=0.77). Using siRNA-mediated knockdown of *CDKN1A* in primary cultures and LNCaP AD, as expected *AKR1C3* mRNA and protein expression, were significantly reduced in both LNCaP and primary cultures. This result aligns with the positive correlation between *AKR1C3* and *CDKN1A* expression observed in untreated hnPC01 and hnPC03 cells, that showed no overexpression of *CDKN1A* and downregulation of *AKR1C3* (**Figure 26**). A similar positive correlation was observed in Du145 DS and DR cells,

Conversely, LNCaP AD and AI displayed a negative correlation between *CDKN1A* and *AKR1C3* expression levels, possibly associated to the presence of the AR in these cells. In these cells, *AKR1C3* appears to be regulated by other mechanisms. LNCaP AD and AI are AR⁺ and sensitive to androgen stimulation, independently of androgens in the medium³⁰². AR has been shown to be activated by IGF-1 to potentiate androgen signaling³⁰³.

Thus, LNCaP AD, might be expressing some steroidogenic genes stimulated by IGF-1 present in the culture media (**Table 18**), On the other hand, *CDKN1A* was shown to be upregulated by IGF-1 in MCF-7 cells through ERK1/2 pathway²⁹⁹ (**Figure 48a**). However, not substantial *CDKN1A* overexpression was shown in LNCaP AD (~1.6 folds), possibly because AR negatively regulates *CDKN1A*^{304,305} (**Figure 48a**). Probably, those levels of *CDKN1A* might be not sufficient to cause upregulation of *AKR1C3* (**Figure 48a**).

In LNCaP AI cells, the AR is expressed but IGF-1 has been removed from the serum (FBS-charcoal treated). This condition causes a significant upregulation of AR in comparison to AD²¹⁰ to overcome the lack of some steroidogenic genes. It potentially overcomes the lack of certain steroidogenic genes. Furthermore, *ESRRA* is highly overexpressed (6.8 folds) which might result in the transactivation of *AKR1C3* expression²⁸². Likewise, the lack of IGF-1 plus inhibitory action of AR^{304,305}, could be the reason of *CDKN1A* downregulation in these cells.

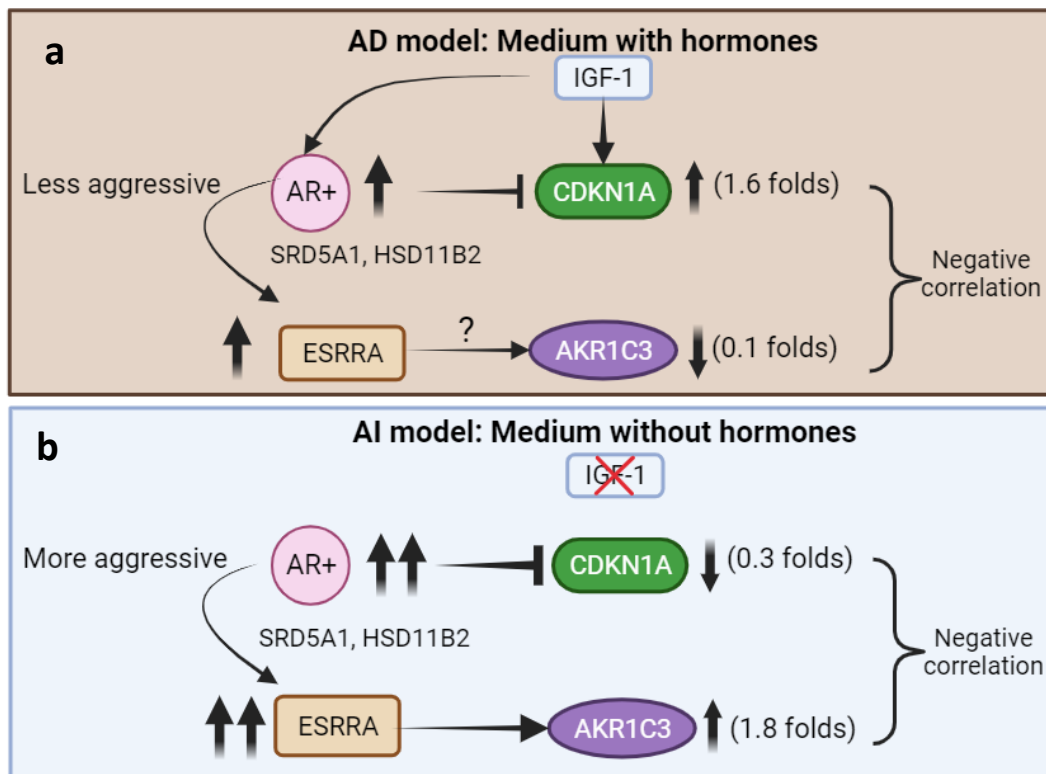


Figure 48. Negative correlation between CDKN1A and AKR1C3 observed in LNCaP AD and AI models. Up/downregulation of *CDKN1A* and *AKR1C3* depends on the LNCaP model. **a)** In AD model, LNCaP cells are growing in conventional media containing hormones, i.e., IGF-1. In presence of IGF-1 *CDKN1A* is upregulated but downregulated in presence of elevated AR levels. In presence of hormones and low expression of *CDKN1A*, probably *AKR1C3* is not upregulated. **b)** In AI model, LNCaP cells are growing in hormone-depleted media. In absence of IGF-1 *CDKN1A* is not activated and also is downregulated by AR, leading to strong downregulation. Stressing conditions leads to aggressive phenotype that promote *AKR1C3* upregulation induced by *ESRRRA*.

Other genes significantly altered by the knockdown of p21^{WAF1}, were *CYP19A1* and *MDM2* (Figure 37). *CYP19A1*, coding for the aromatase enzyme that catabolizes the synthesis of Estradiol (E2)³⁰⁶, was shown to be significantly downregulated with p21-siRNA#2, although we were not able to corroborate this result by western blot due to the impossibility to detect this protein. However, *CYP19A1* showed a significant positive correlation with the expression of *CDKN1A*, in (i) hnPCs that co-overexpress p21^{WAF1} and *CYP19A1*; and in (ii) hnPC01 and hnPC03, which under express both *CDKN1A* and *CYP19A1*.

MDM2 was significantly upregulated in hnPCs after knockdown of p21^{WAF1}. *MDM2* encodes an E3 Ubiquitin Ligase, which mediates the ubiquitination and subsequent degradation of several proteins, including p53, ARB1, DAXX, and others^{307,308}. *MDM2* and *CDKN1A* are regulated under p53-dependent manner^{295,307,309,310}. In one study was demonstrated that p21^{WAF1} acts as negative regulator of p53³¹¹, also *MDM2*, can also

downregulate p53 through proteasomal degradation in a ubiquitination dependent and independent manners³¹². Thus, the inhibition of MDM2, typically increases p53 protein levels. Following *CDKN1A* inhibition by siRNAs, *TP53* did not display changes in mRNA expression as a response (**Figure 37a**). Our findings suggest that *CDKN1A* and *MDM2* are mutually regulated in p53-independent manner.

Extensive studies have demonstrated that MDM2 represses p21^{WAF1} independently of p53 action³¹³. MDM2 regulates proteasomal degradation of several target proteins, both via ubiquitination dependent and independent pathways³¹². However, the degradation of p21^{WAF1} usually occurs in a ubiquitin-independent manner: MDM2 regulates the interaction between the protein 14-3-3 τ and proteasome 20S that degrade p21 at the G1 phase of the cell cycle³¹⁴ and inducing conformational change in p21^{WAF1} to make it accessible to C8 subunit of the proteasome³¹⁵. Furthermore, free MDM2 interacts with hnRNP K and promotes its degradation. When hnRNP K is degraded, a reduction of *CDKN1A* transcription, and expression of apoptotic genes are observed. However, when MDM2 is inhibited by nutlin3a, hnRNP K is activated and p21^{WAF1} expression is promoted, resulting in inhibition of apoptotic genes and upregulation of growth arrest and survival³¹⁶ (**Figure 49**). These observations suggest that free MDM2, favors p53 action on apoptosis induction, by the inactivation of p21^{WAF1} and hnRNP K. However, the report provides no information about the action of p21^{WAF1} on MDM2. In our study, the inhibition of *CDKN1A* by knockdown, caused a significant upregulation of *MDM2* both at transcript and protein levels. Similarly, one study reported that in p21^{-/-} HCT116 fibrosarcoma cells MDM2 was upregulated in comparison with parental p21^{WT} cells, although they attributed this upregulation to high levels of p53 present in those cells³¹¹. These findings provide evidence of a mutual regulation between MDM2 and p21 proteins.

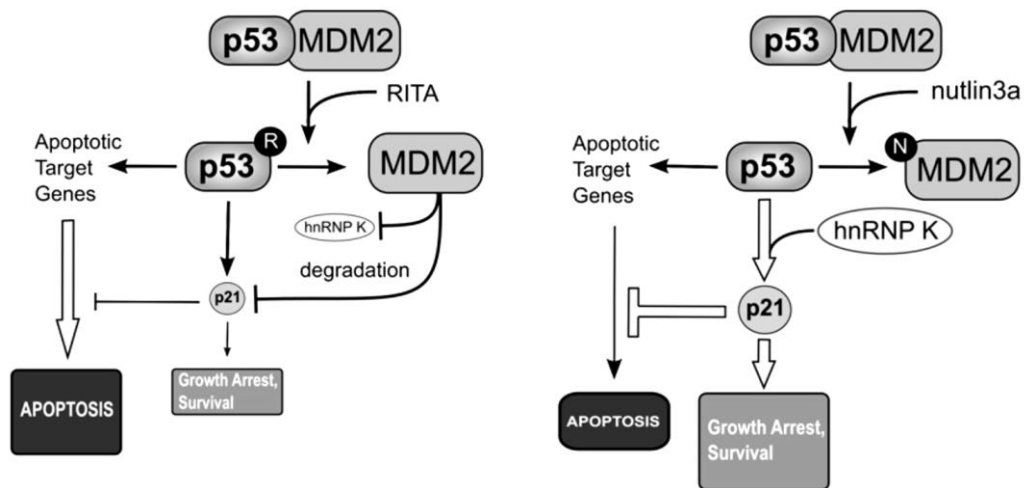


Figure 49. Model for the preferential induction of apoptosis by RITA. Left panel: RITA induces dissociation of active MDM2 from p53. Released MDM2 is free to promote degradation of its other targets such as p21 and hnRNP K. p53 transactivates expression of proapoptotic target genes, but transactivation of p21 is deficient because of hnRNP K deficiency. p21 protein levels are thus kept low by both direct degradation by MDM2 and inefficient transcriptional induction. Therefore, p21 can exercise neither its growth-suppressing activity nor its antiapoptotic activity, and the cell undergoes programmed cell death. Right panel: nutlin3a binds MDM2 and inhibits the p53/MDM2 interaction. Nutlin3a does not facilitate the binding of MDM2 to other substrates, including p21 and hnRNP K. hnRNP K facilitates transactivation of cell-cycle arrest genes by p53, including p21. High levels of p21 promote a potent cell-cycle arrest response as well as antagonizing apoptosis induction. *Figure from Enge et al. 2009*

Although there's limited information available on the mechanisms regulating the interplay between p21^{WAF1} and MDM2, the cross talk between the TGF- β and NF-kB signaling pathways, may play a crucial role. Several studies have shown the pro-oncogenic role of the NF-kB pathway in the regulation of cell proliferation, survival and malignant progression^{317,318}. Activin, member of the superfamily of TGF- β , was shown to induced the activation of NF-kB and increase MDM2 expression in colorectal cancer³¹⁹. In fact, NF-kB subunits were found to interact with the P1 promoter of *MDM2*, and induce its expression in activated T cells^{320,321}. On the other hand, the expression of *CDKN1A* has been shown to be induced by TGF- β canonical pathway, in a p53-independent way^{322–324}. Interestingly, the TGF- β and NF-kB pathways can cross-interact each other³²⁵. In head and neck squamous cell carcinoma (HNSCC), the interaction between TGF- β and the NF-kB pathways was described to occur through the activation of TAK1 (TGF- β -activated kinase 1) protein. In the scenario where the canonical TGF- β SMAD2/3 pathway is inhibited (i.e., *CDKN1A* downregulation) TAK1 becomes activated (non-canonical TGF- β) leading to nuclear

translocation of NF- κ B subunits, promoting the overexpression of genes such *MDM2* and *SMAD7*, which preferentially suppress canonic pathway (**Figure 50**)

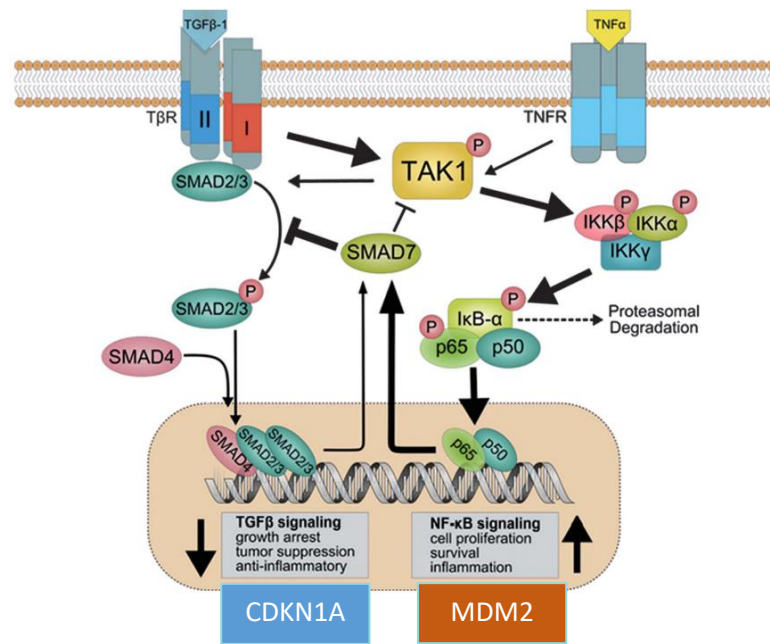


Figure 50. Proposed model for attenuation of canonical TGF- β SMAD and activation of non-canonical TGF- β -NF- κ B signaling pathways in HNSCC. TGF- β activates NF- κ B signaling through a sequential regulation of TAK1 and IKK kinases leading to phosphorylation of I κ B α , nuclear translocation and phosphorylation of NF- κ B subunit p65 and activation of NF- κ B downstream targets (MDM2). Both TGF- β and NF- κ B signaling induce expression of SMAD7, which in turn preferentially suppresses TGF- β -induced canonical and NF- κ B signaling (CDKN1A), relative to TNF- α -induced NF- κ B signaling. Figure modified from *Freudlsperger et al, 2013*.

Although we have not evaluated the NF κ B pathway in our primary cultures, it is important to note that IGF-1, present in the FBS-supplemented media, can activate and regulate this pathway^{326,327}. Interestingly, one study demonstrated the induction of *AKR1C3* expression in LNCaP cells by stimulation with activin A (member of the TGF- β superfamily)³²⁸. More studies are necessary to elucidate the mechanism by which the *CDKN1A* downregulation promoted *MDM2* upregulation in hnPCs cells, and whether the TGF- β pathway is implicated in the *CDKN1A* high expression observed in these cultures.

To investigate whether the oncogenic effect of p21^{WAF1} is primarily influenced by its overexpression, or it is driven by its subcellular localization, the experiments in LNCaP AD cells showed that cells predominantly expressed in the cytoplasm with few cells showing p21^{WAF1} exclusively in nucleus (**Figure 38b**). Our results are in line with other studies where, after drug treatment, p21^{WAF1} was observed in both cytoplasm and nucleus, or

exclusively in the cytoplasm, in drug-resistant LNCaP or other cancer cells^{329–332}. AKT-mediated NLS phosphorylation is essential for the cytoplasmic localization of p21, its stability and inhibition of degradation^{333–335}. Although we have not evaluated the phosphorylation state of LNCaP-p21, we observed that only the cytoplasmic fraction preserved the detection of p21 after the fractionation analysis, suggesting that nuclear p21^{WAF1} might have undergone a degradation processes. The results regarding hnPCs, were unexpected. In the immunofluorescence assay, most cells expressed p21^{WAF1} exclusively in the nucleus, with only a small fraction expressed in both compartments (**Figure 40**). It is widely accepted that p21 acts as tumor suppressor or oncogene depending on the subcellular localization^{336,337}. Its cytoplasmic localization was associated to chemoresistance induction^{329,331,334} and prevention of apoptosis^{316,335,338}. In turn, the nuclear p21^{WAF1} inhibit cell proliferation, by arresting cell cycle^{339–341} and it is associated to induction of apoptosis^{342–344}. Because primary cultures exhibited an intrinsic chemoresistance, sustained proliferation and *de novo* activation of steroid hormone synthesis, compatible with a hormone metabolism reprogramming, we expected to be detected in the cytoplasm fraction, not in the nucleus. In LNCaP AD cells, the cytoplasmic localization of p21^{WAF1} is not inhibiting cell proliferation, supported by the high proliferation ratio observed in these cells (**Figure 41**). However, LNCaP AD cells do not display a high chemoresistance capacity in comparison with LNCaP AI, or hnPCs. Considering that p21^{WAF1} in LNCaP AD cells is only slightly upregulated, those results suggest that the p21-associated oncogenic properties may be context-dependent, not only on its subcellular localization but also on the degree of overexpression¹⁹¹. Interestingly, similar behavior is observed in for TGF- β signaling, that can display a tumor suppressor phenotype at early stages of tumorigenesis, but it is pro-oncogenic at later stages of cancer progression³⁴⁵.

Contrariwise, hnPCs markedly overexpress p21^{WAF1} and show a higher frequency of p21^{WAF1} in the nucleus. Although nuclear p21^{WAF1} is associated to cell arrest, DNA synthesis inhibition, and apoptosis activation³³⁶, we observed that hnPCs displayed sustained proliferation and chemoresistance. The exaggerated expression of nuclear p21^{WAF1} would be in line with previous reports describing its nuclear localization acting deregulating the replication licensing machinery, inducing replication stress and DNA damage in a p53-independent manner^{191,346}, events that promoted chemoresistance and cancer progression. Galanos *et al.* proposed a model for the nuclear-p21 oncogenic effect observed in cancer

cells: these cells initially displayed senescence traits, and then escaped senescence re-enter to cell cycle but overexpressing p21^{WAF1} (**Figure 51**).

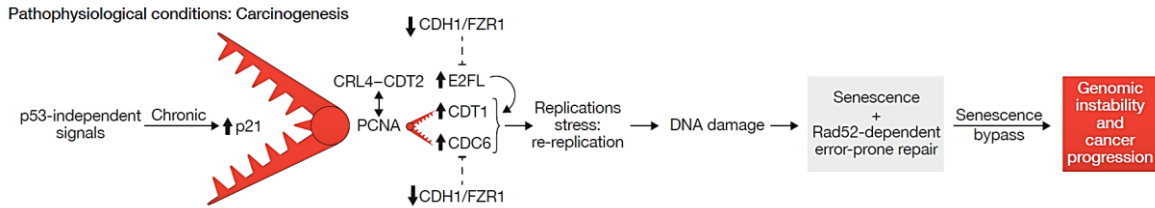


Figure 51. The oncogenic model of nuclear p21 proposed by Galanos et al. Chronic p53-independent expression of p21 leads to re-replication, DNA damage, error-prone repair, genomic alterations and eventually cancerous evolution. *Figure from Romanov and Rudolph, 2016*

To evaluate this scenario in hnPCs, the senescence status was verified by analysis of p16^{Ink4a} (*CDKN2A*) and β -Galactosidase (β -Gal) activity. In the common accepted model, p21^{WAF1} is transiently activated to initiate the proliferation suppression process which later result in G1 arrest, however, when the cell cycle arrest is established, p21^{WAF1} is downregulated and protein levels decrease^{347–349}. Conversely, p16^{nk4a} is upregulated and maintains the cell cycle arrest in senescent cells^{350–352}. It is currently accepted that senescence is primarily activated by *TP53* and *CDKN2A/p16* whereas *CDKN1A/p21* and *Rb1* acts as downstream effectors³⁵³. In addition, the β -Gal activity, is a known indicator of perturbation of the autophagy-lysosomal system, that results in the pathogenic production of senescence-associated secretory phenotype (SASP)^{353,354}. SASP is known as a hallmark of senescence mediating many of its patho-physiological effects³⁵³.

Our results in hnPCs showed a high overexpression of mRNA *CDKN2A* (similar to *CDKN1A* levels), and β -Gal activity, indicating that these cells are undergoing a cellular senescence-like state: they show (i) expression of senescence markers, together with (ii) sustained proliferation and (iii) chemoresistance. To confirm the activation of proliferation and consequent escape from senescence in these cells, it would be interesting to assess the expression of Ki67, a proliferation marker that has been observed to be co-expressed with p21 in certain aggressive cancer cells^{191,355,356}, although both are generally found mutually exclusive^{357,358}.

Interestingly, the downregulation of p21^{WAF1} in hnPCs had no effect on p16 overexpression, supporting that p21 is a downstream effector of p16^{Ink4a}³⁵⁴. On the other hand, β -Gal activity

was significantly suppressed in p21-knocked down hnPCs, indicating that the SASP phenotype is mainly associated to overexpression of *CDKN1A*.

SASP, also known as senescence messaging secretome, can mediate several effects. For example, it can reinforce senescence in autocrine and paracrine manners^{196,197}, but it is also implicated in secondary senescence induction by juxtacrine communication^{203,204}. These contribute not only to healthy physiological responses, but also to the pathogenesis of various diseases, including cancer³⁵⁹. Juxtacrine induction of secondary senescence is mainly mediated by Notch1. In early steps of secondary senescence, Notch1 is highly activated in cells adjacent to senescent cells, to receive SASP signals and provoke aberrant expression of *CDKN1A* and SASP in adjacent cells^{203,204}. Notably, in later senescent cells, Notch1 is downregulated, allowing pro-inflammatory SASP (**Figure 44**). In addition, Notch1 is recognized by its anti-tumoral function²⁰⁶. In two p21 knockdown hnPCs we observed significant upregulation of Notch1 in comparison with the control siRNA. That means that in p21-knocked down cells with β -galactosidase inactivation, Notch1 is upregulated to promote tumor suppression and cell-to-cell interaction for a potential reactivation of SASP signaling. Therefore, this suggests that these cells (no treated) are undergoing fully secondary senescence-like state, expressing low levels of Notch1 to allow the expression of pro-inflammatory SASP and suppress its anti-tumoral function. Although primary and secondary senescence display distinct gene expression profiles²⁰⁴, currently it remains challenging to completely understand the extent of the differences between secondary and primary senescent cells³⁶⁰.

Currently, increasing evidences support the paradoxical role of senescence that promotes tumor suppression but also contributes to oncogenesis may be due, at least in part, to the effects of SASP¹⁴³. Vascularization, tissue remodeling, immunosuppression or drug resistance are some of the effect induced by altered SASP in cancer cells¹⁴³. In addition, the induction of cancer stemness properties and reprogramming are a very promising fields of study.

In our study we have observed that primary cells show significant changes in the expression of several steroids hormones enzymes, display p21-associated senescence, and aggressive phenotypes, such as chemoresistance. Because the presence of CSCs could potentially be induced by senescence, we evaluated two pluripotency genes and CD44, a critical regulator of cancer stemness, including self-renewal, tumor initiation, and metastasis³⁶¹. All primary cultures overexpressed CD44 in an aberrant manner. It has been shown that CD44 can

promote reprogramming in colon cancer towards stem cell properties, and CD44 together with CD24 can coordinate cellular reprogramming in nasopharyngeal carcinoma cells³⁶². Interaction between CD44 variants (CD44v) and its ligand, hyaluronan, can fuel tumor growth, enhance the ability of cancer cells to move out of blood vessels, and contribute to metastasis. The alternative splicing process (AS) is found under the regulation of TAR DNA-binding protein-43 (TDP43) and Epithelial splicing regulatory protein 1 (ESRP1), and it has been shown that the loss of any of these splicing factors lead to inhibition of stemness by reducing the abundance of CD44v in breast cancer stem cells³⁶³, inhibition of pluripotency and efficient reprogramming of human somatic cells towards iPSCs³⁶⁴.

In summary, our results suggest that the prostate cancer primary cultures derived from hormone-naïve patients with aggressive tumors (hnPCs) are an excellent model to study the steroid metabolism reprogramming and the specific characteristics of the original tumors. Here we have shown that these cultures have overcome the senescence through “bypassing” the barriers but no “escaping” from senescence (**Figure 52**), since they still proliferate in presence of senescence markers³⁶⁵, here denoted as senescence-like state. In this context, hnPCs are exploiting the role oncogenic of senescence, promoting cell and metabolic reprogramming^{366,367} which in turn lead to increase of aggressiveness chemoresistance and survival (**Figure 53**).

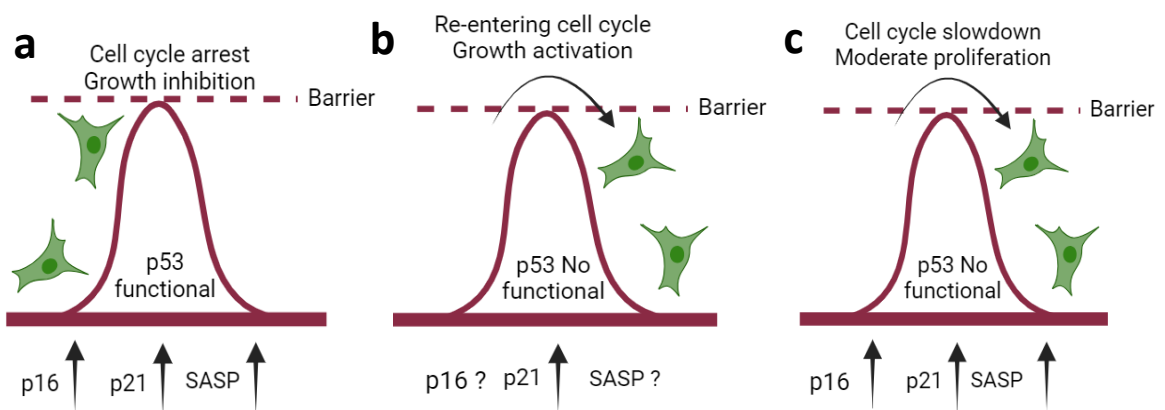


Figure 52. Dual role of p21-associated senescence. a) p21 transient overexpression in p-53 dependent manner. Cancer cells cannot overcome senescence barrier and display growth inhibition. b) Cancer cells escape from senescence but overexpressing p21, no display senescence features. c) Cancer cells bypass senescence, they display senescence features but not its consequences (i.e., cell arrest). Instead, maintain moderate growth. *Based on: p21: A two-faced genome guardian from Georgakilas et al. 2017*

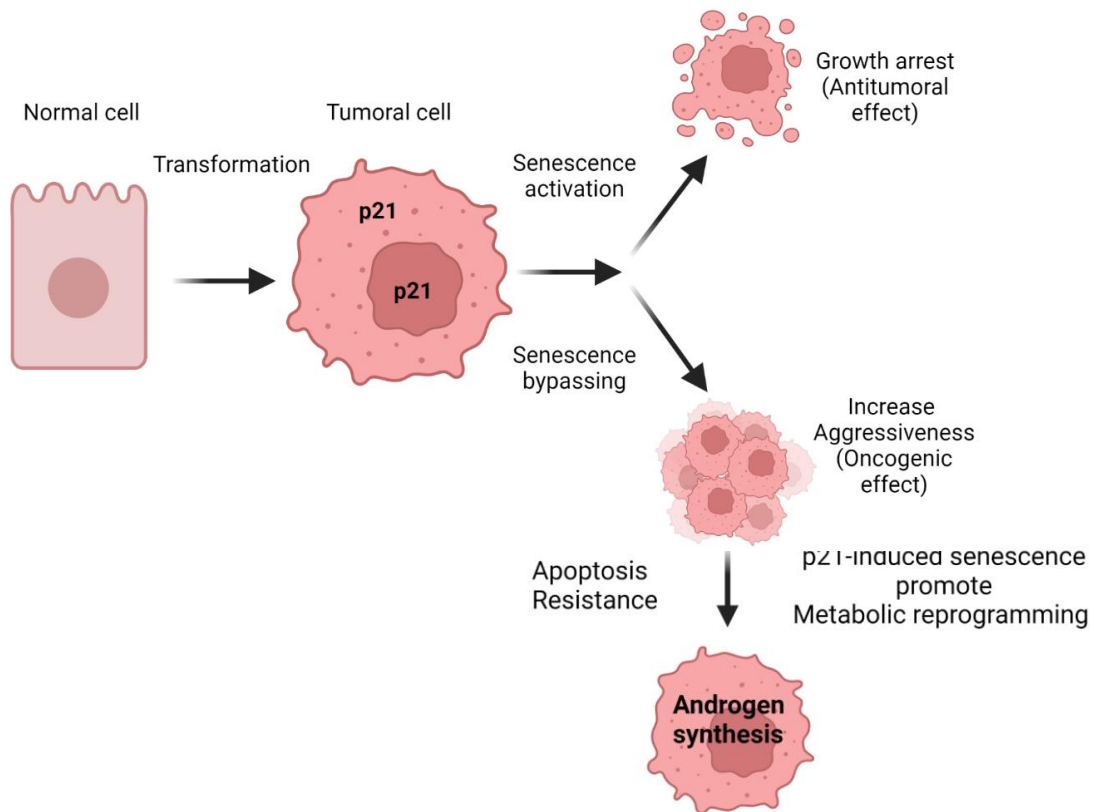


Figure 53. Senescence-associated reprogramming in prostate primary cultures. Normal epithelial cell undergoes oncogenic transformation, which leads to stress response: p16^{INK4a}, p21^{WAF1/CIP1}, among others. This results in cellular senescence, which in turn, is bypassed for a subset of cells exhibiting more aggressive phenotype, apoptosis and drug resistance which finally promote metabolic reprogramming.

CHAPTER I: CONCLUSIONS

CHAPTER I – CONCLUSIONS

1. Primary cultures derived from hormone-naïve tumors (hnPCs) retained gene expression patterns from their original tissues and represent a useful alternative to study resistance mechanisms in prostate cancer.
2. The P72R polymorphism studied in hnPCs and a cohort of prostate cancer patients, show significant association with the risk for prostate cancer development in European Caucasian population.
3. hnPCs exhibit metabolic reprogramming within the steroidogenic pathway, demonstrating changes in the expression pattern and *de novo* activation of hormone synthesis enzymes.
4. hnPCs demonstrate a senescence-like state characterized by p21^{WAF1} overexpression, which is strongly associated with steroidogenic reprogramming, chemoresistance, and enhanced survival in these cells.

CHAPTER II

ANDROGEN METABOLISM AND COVID-19 Study of the association between Testosterone and COVID-19

Publications

- 1) Recovery of serum testosterone levels is an accurate predictor of survival from COVID-19 in male patients. **Toscano-Guerra E**; Martínez-Gallo M; Arrese-Muñoz I; Giné A; *et al.* BMC Medicine, 2022.
- 2) C1 esterase inhibitor and the contact system in COVID-19. Thomson T; **Toscano-Guerra E**; Casis E and Paciucci R. British Journal of Haematology, 2020

CHAPTER II: INTRODUCTION

CHAPTER II - INTRODUCTION

1. Coronavirus Disease-19 (COVID-19)

1.1. COVID-19 epidemiology

The COVID-19 emerged at the end of 2019, as a result of infections by the new coronavirus 2019 named as Severe Acute Respiratory Syndrome Coronavirus 2 (SARS-COV-2). This disease is characterized by different clinical outcomes from asymptomatic infections to severe pneumonia and death. COVID-19 has affected millions of people and has been estimated over 767 million cases and 6.9 million of death around the world according to the World Health Organization³⁶⁸ (**Figure 54**)

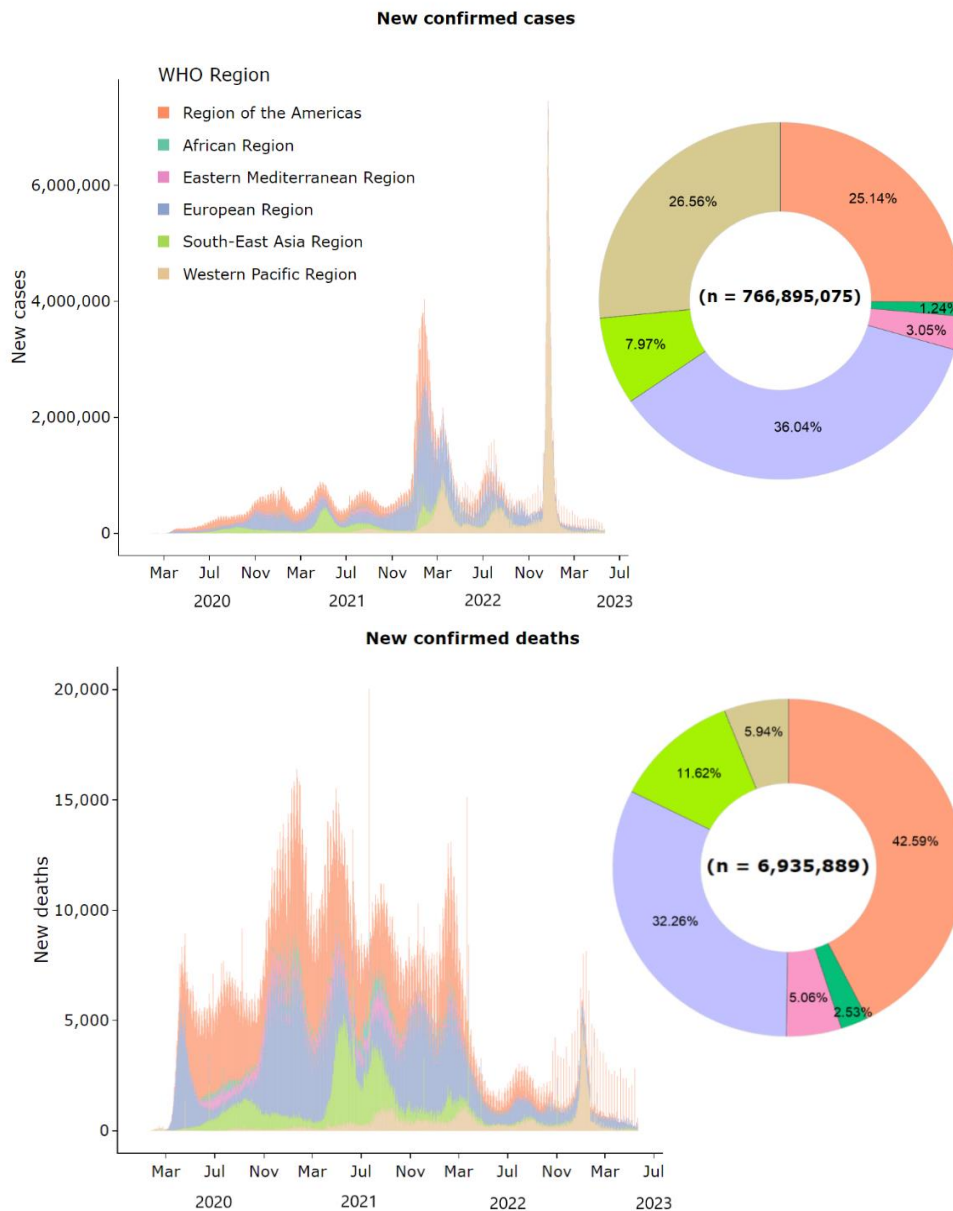


Figure 54. Description in the next page.

Figure 54. New COVID-19 cases and deaths confirmed up to July 2023. Stock graphs display daily confirmed cases or deaths, with WHO regions represented in different colors. Donut charts illustrate the percentages of the total cases or deaths in each region. Source: *WHO COVID-19 Dashboard*

1.2. SARS-COV-2

The Severe acute respiratory syndrome coronavirus 2 (SARS-COV-2) was discovered for first time in December 2019, in Wuhan, China, after a few firsts cases were reported symptoms of severe pneumonia^{369,370}. SARS-CoV-2 belongs to the Coronaviridae family, which encompasses a diverse group of enveloped viruses containing a positive, single-stranded RNA genome. The genome of SARS-CoV-2 consists of approximately 30,000 nucleotides and is composed of 13–15 open reading frames (ORFs), 12 of which are functional. It contains 11 protein-coding genes, resulting in the expression of 12 proteins (**Figure 55a**). This nucleic acid is enclosed within a capsid, formed by the nucleocapsid protein N, and surrounded by a lipid membrane. Embedded within the membrane are three proteins: the membrane protein (M), the envelope protein (E), and the glycoprotein Spike (S). Spike is essential for binding to host receptors and facilitating virus entry into host cells.^{371,372} (**Figure 55b**).

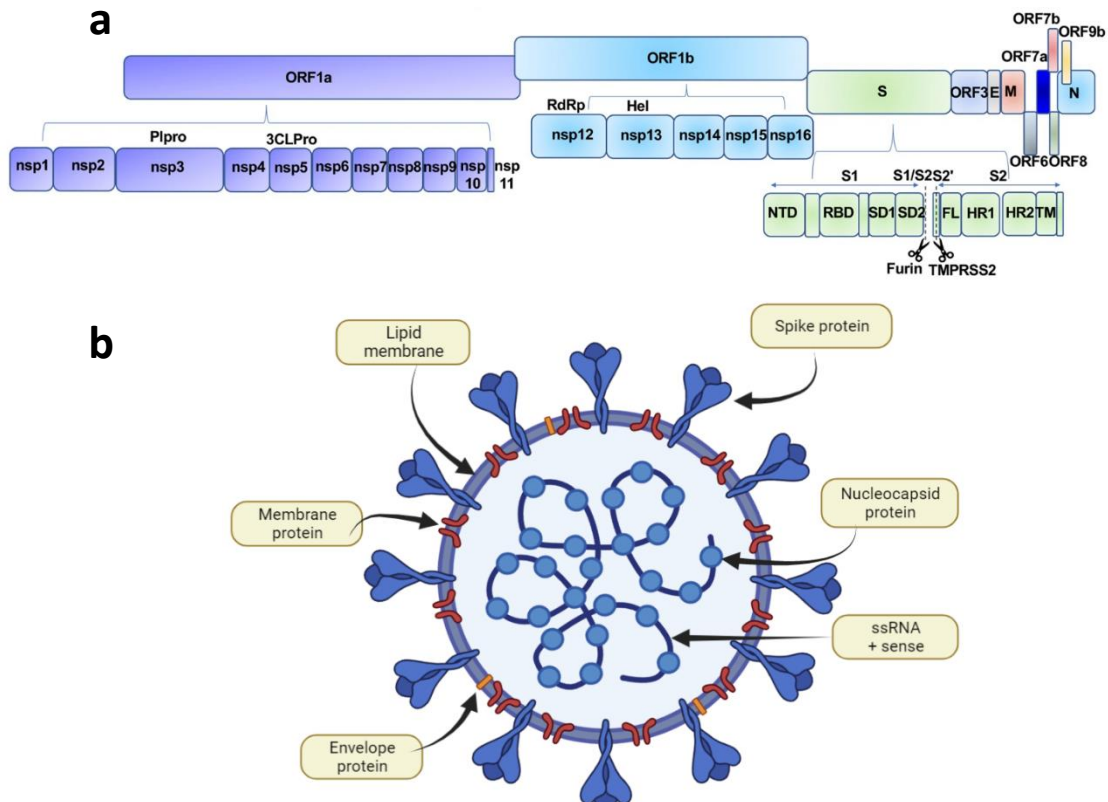


Figure 55. SARS-CoV-2 structure. **a)** Genomic organization of SARS-CoV-2, the genome encodes two large genes ORF1a (purple), ORF1b (blue) (which encode 16 non-structural proteins) and for structural genes encoding spike (S), envelope (E), membrane (M), and nucleocapsid (N). **b)** Schematic diagram of the structural features of SARS-CoV-2 and its primary structural proteins. Figure a) from Zhang *et al.* 2021. Figure b) developed with Biorender.com

1.2.1. Structural proteins

The structural proteins are particularly important as they form the virus's outer shell and facilitate its entry into host cells. The four main structural proteins of SARS-CoV-2 are:

- A. Spike (S) Protein:** The spike protein is perhaps the most well-known protein of SARS-CoV-2 because it plays a key role in viral entry into host cells. It is anchored in the virus's surface in a characteristic "corona" shape, which is why the virus is named "coronavirus." The spike protein binds to the ACE2 receptor on the surface of human cells, initiating the process of viral attachment and fusion. This protein is a target for many vaccines and therapeutic interventions.
- B. Envelope (E) Protein:** The envelope protein is a small protein that is involved in the assembly and release of new virus particles. It plays a role in the virus's ability to infect host cells and contributes to the formation of the viral envelope.
- C. Membrane (M) Protein:** The membrane protein is another integral component of the viral envelope. It plays a critical role in maintaining the virus's structure and shape. It interacts with other viral proteins, including the nucleocapsid protein, and helps shape the viral membrane.
- D. Nucleocapsid (N) Protein:** The nucleocapsid protein encapsulates the viral RNA genome, forming a complex known as the nucleocapsid. This protein is essential for maintaining the RNA genome's stability and plays a role in the virus's replication and packaging.

1.2.2. Non-structural proteins

SARS-CoV-2 also encodes a set of non-structural proteins (NSPs) that play role in the virus's replication, transcription, translation, and evasion of the host immune response.

- A.** NSP1: This protein inhibits host gene expression and interferes with the host cell's antiviral defenses, inhibiting host translation by blocking the mRNA entry tunnel on the ribosome; this interferes with the binding of cellular mRNAs to the ribosome.
- B.** NSP2: NSP2 is believed to interact with other host proteins as Prohibitins (PHBs) 1 and 2, which potentially impact the host cell environment to facilitate its replication and survival.
- C.** NSP3: PLpro, Responsible for cleaving of NSP1, NSP2, and NSP3 from the N-terminal region of pp1a and 1ab.
- D.** NSP4: is thought to Potential transmembrane scaffold protein which helps modify ER membranes.
- E.** NSP5 (Main Protease, Mpro): Also known as the 3C-like protease (3CLpro), this enzyme is essential for cleaving the viral polyprotein into individual functional proteins. It is a target for some antiviral drug development efforts.
- F.** NSP6: is implicated in the formation of DMVs (double-membrane vesicles) and is involved in the induction of autophagosomes from host ER.
- G.** NSP7 and NSP8: These proteins form a complex that acts as a cofactor for the viral RNA-dependent RNA polymerase (RdRp), enhancing its activity in viral genome replication.
- H.** NSP9: is a single-stranded RNA-binding protein that likely plays a role in viral RNA synthesis and genome replication.
- I.** NSP10: is a cofactor that enhances the enzymatic activities of NSP14 (exonuclease) and NSP16 (2'-O-methyltransferase), both of which are involved in viral RNA modification.
- J.** NSP12 (RdRp): The RNA-dependent RNA polymerase is a crucial enzyme responsible for copying the viral RNA genome and synthesizing new RNA strands. It is a prime target for antiviral drug development.
- K.** NSP13: is a helicase that unwinds viral RNA during replication, facilitating RNA synthesis and genome replication.

- L.** NSP14: NSP14 is a multifunctional protein with exonuclease activity that assists in proofreading and editing the viral RNA genome.
- M.** NSP15: NSP15 is an endoribonuclease that likely plays a role in viral RNA processing and evasion of the host immune response.
- N.** NSP16 and NSP10 (2'-O-Methyltransferase Complex): This complex is responsible for adding a methyl group to the 2'-O position of viral RNA, which helps the virus evade host immune detection.

1.3. SARS-CoV-2 mechanism of host entry

The entry of SARS-CoV-2 into host cells involves a multi-step process that allows the virus to attach to the cell surface, fuse with the host cell membrane, and release its genetic material into the cell (**Figure 56**).

Process: Attachment: The virus attaches to host cells using the Spike (S) protein. The S protein is composed of two subunits: S1 and S2. The receptor-binding domain (RBD) within the S1 subunit specifically interacts with the ACE2 (Angiotensin-converting enzyme 2) receptor on the surface of the host cell. **Conformational Changes:** Virus binding to ACE2 induces conformational changes in the S1 subunit and exposes the S2' cleavage site in the S2 subunit. Depending on the entry route taken by SARS-CoV-2, the S2' site is cleaved by different proteases, TMPRSS2 or Cathepsin. **S1-S2 junction cleavage:** before acting fusion proteases, a prerequisite is the previous cleavage of the S1-S2 boundary by Furin protein. **TMPRSS2-mediated entry:** In the presence of TMPRSS2, S2' cleavage occurs at the cell surface. **Internalization-mediated entry:** process via clathrin-endocytosis, where S2' cleavage is performed by cathepsins, inside of the lysosome because require an acidic environment for their activity. **Membrane Fusion:** In both entry pathways, cleavage of the S2' site exposes the fusion peptide (FP). This fusion allows the virus to release its genetic material, including RNA, into the host cell.

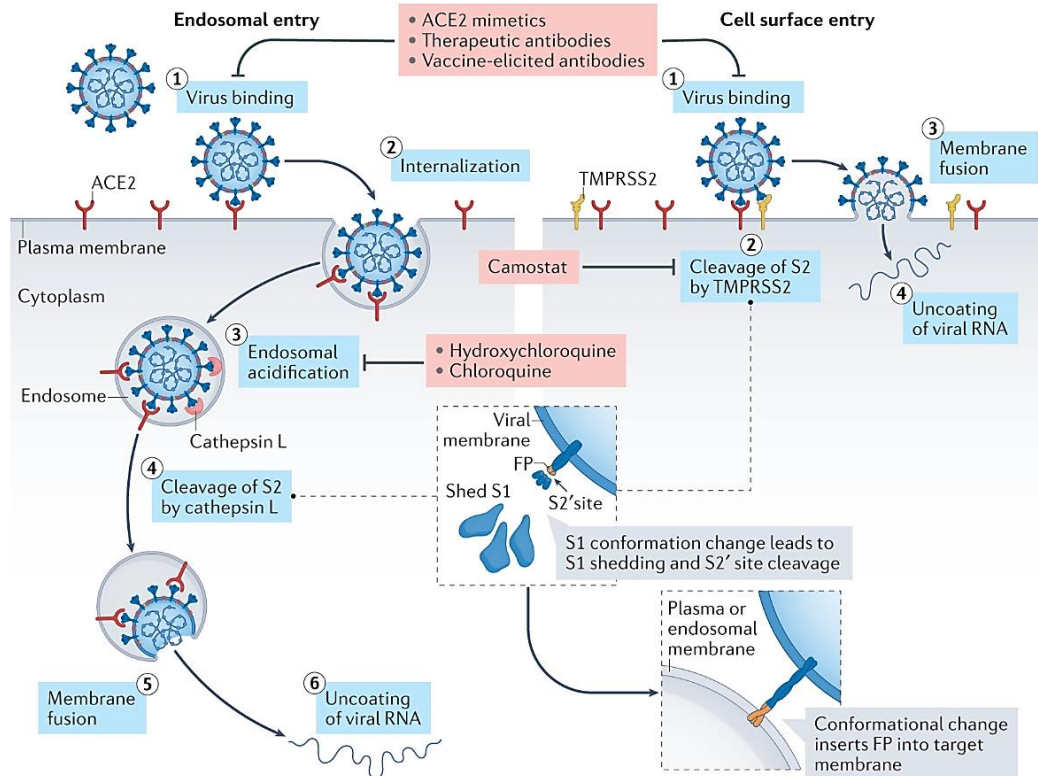


Figure 56. SARS-CoV-2 entry pathways. SARS-CoV-2 can use two entry mechanism to infect cells. *Endosomal entry:* The virus-ACE2 complex is internalized by endocytosis into endolysosomes. *Cell surface entry:* Fusion between viral and cellular membranes forms a fusion pore through which viral RNA is released into the host cell cytoplasm for uncoating and replication

1.4. Clades and variant D614G during the first wave of pandemic

Coronaviruses are RNA-viruses with a high-rate mutation capacity, adapting to new environments through mutation and recombination with relative ease^{373,374}. Due to the genetic variations of the virus, it has been developed classification methods to group and study similarities and differences between SARS-CoV-2 viruses and improve the management. According to NextClade classification (<https://nextstrain.org>), SARS-CoV-2 is divided in clades, being the first emerging clades: 19A, 19B, 20A, 20B, followed by the new variants known as Alpha (20 I), Beta (20H), Delta (21A), among others. During the first wave of the pandemic, the most spread and frequent variants were 20A and 20B, also called D614G variant, because this variation in the RBD, was the first identified mutation^{375,376}.

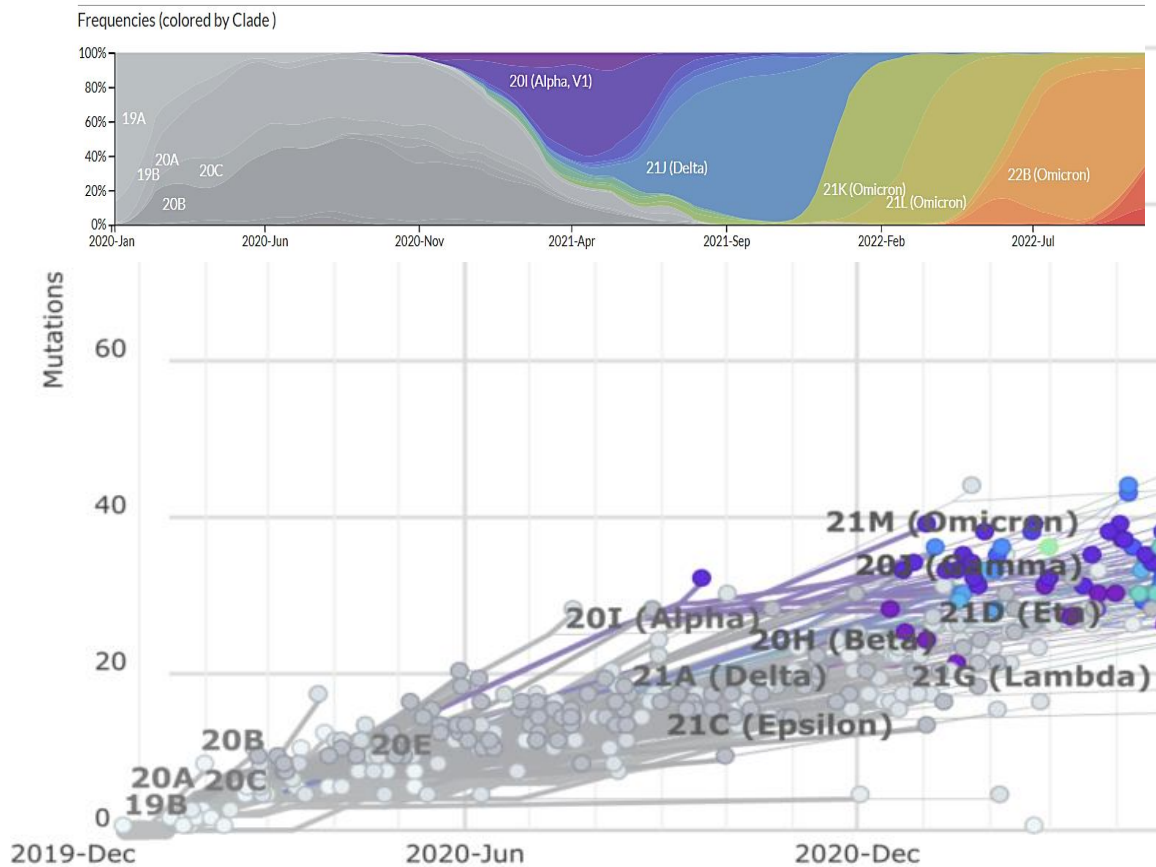


Figure 57. Phylogenetic tree of SARS-CoV-2 in 2020. The phylogeny is represented as a root-to-tip plot. X axis represents the dates of detection, and the Y axis represents the number of genomewide mutations. Top panel represents the predominant variant by period of time.

2. COVID-19 characteristics and symptoms

COVID-19 is characterized for being principally a respiratory illness. The disease primarily spreads through respiratory droplets from coughs, sneezes, or close contact with infected individuals. The incubation period for COVID-19, which is the time from exposure to the virus to the onset of symptoms, ranges from 2 to 14 days, with an average of around 5-6 days. Similarly to patients with SARS and MERS, these patients showed symptoms of viral pneumonia, including fever, cough and chest discomfort, and in severe cases dyspnea and bilateral lung infiltration³⁷⁷.

2.1. Clinical features of a mild disease: COVID-19 symptoms vary widely. Some individuals may be asymptomatic (showing no symptoms). However, the most common symptom is cough, followed by hyposmia and sputum, nasal congestion, fever ($>37.5^{\circ}\text{C}$). In general, these patients do not need hospitalization and are discharged from hospital in a few days³⁷⁸. Regarding to immune markers, they present mild lymphocytopenia, does not experience a noticeable decrease in total number of T cells or B cells, although they show high plasma concentrations of cytokines/chemokines, this increase is of rapid resolution³⁷⁹.

2.2. Clinical features of severe disease:

COVID-19 primarily affects the respiratory system, causing symptoms such as fever, cough, and shortness of breath. It can progress to severe pneumonia, acute respiratory distress syndrome (ARDS), and respiratory failure, especially in vulnerable populations.

Systemic Effects: In addition to respiratory symptoms, COVID-19 can affect multiple organ systems, including the cardiovascular system (causing heart inflammation), gastrointestinal system (leading to nausea, diarrhea), and neurological system (loss of taste and smell, headaches).

Cytokine Storm: Severe cases of COVID-19 can lead to an excessive immune response known as a cytokine storm. This hyperinflammatory state can damage organs and contribute to severe complications.

3. Sex difference in immune response

In hospitalized COVID-19 patients, the mortality rate for males was 75% higher than that for females³⁸⁰. In Europe, data showed that the ratio of male to female COVID-19 hospitalizations was 1.5, and the case fatality rates for males were 1.7 to 1.8 times higher than for females³⁸¹. Among individuals with severe disease, males exhibited significantly higher levels of pro-inflammatory cytokines like IL-6, IL-8, and MCP-1 compared to females. Conversely, females had notably higher levels of the anti-inflammatory cytokine IL-10 at 14 days compared to males³⁸². Male patients also had elevated plasma levels of innate immune cytokines such as IL-8 and IL-18 and showed a more robust induction of non-classical monocytes. In contrast, female patients displayed more robust T cell activation during SARS-CoV-2 infection. Importantly, a weaker T cell response was associated with older age and worse disease outcomes in male patients but not in female patients³⁸³.

4. Androgen receptor mediated TMPRSS2 regulation in COVID-19

Androgens regulate downstream genes by binding to the androgen receptor (AR), which acts as a hormonal transcription factor. Once liganded, AR-androgen complex translocates into the nucleus. Within the nucleus, AR forms homodimers and directly attaches to specific DNA sequences called Androgen Response Elements (AREs). The consensus AR-binding motif (i.e., canonical AREs, AGAACAnnnTGTTCT) consists of two hexameric half-sites (5'-AGAACA-3') often arranged as inverted repeats with 3bp of separating nucleotide. AR recognizes and interacts with AREs through its DNA-binding domain (DBD)³⁸⁴. One gene of interest that is regulated by AR and has been studied in the context of COVID-19 is the TMPRSS2 (Transmembrane Serine Protease 2), involved in the entry of SARS-CoV-2 into host cells. The expression of TMPRSS2 in respiratory cells is a factor that can influence susceptibility to COVID-19 and the severity of the disease.

TMPRSS2 (transmembrane protease, serine 2) is a member of the type II transmembrane serine proteases, a family of 17 serine proteases that are characterized by a short cytoplasmic N-terminal domain, a single transmembrane domain, and an extracellular C-terminal domain containing the serine protease domain. TMPRSS2 is predominantly expressed in the luminal cells of the prostate epithelium, where its expression is positively regulated by androgens (4–7). However, It is widely expressed across several human tissues: stomach, pancreas, lungs, kidney, liver, breast, testis among others³⁸⁵. TMPRSS2 gene possess two AR-binding sites at -13kb and -60b upstream of the gene, and its predicted sequences are AGAGTGcacTGCCT and GGAACGttgTGAAAC , respectively^{386,387}. Due to a genomic translocation present in at least 50% of prostate cancers (CaP), the androgen-regulated promoter of TMPRSS2 is fused to the coding sequences of ERG (*v*-ets erythroblastosis virus E26 oncogene-related gene). This results in androgen-regulated overexpression of ERG and explains why this oncogene is the most frequently overexpressed oncogene in CaP (8–13). TMPRSS2 was identified for the first time in 2010 to be essential for Spike protein priming facilitating SARS-CoV entry into host cell^{388,389}. During pandemic for SARS-CoV2, the role of TMPRSS2 in virus cell entry was more elucidated³⁹⁰ and several studies have pointed out the essential role of TMPRSS2 in infection. However, despite the fact that TMPRSS2 is regulated by Testosterone, men and women show comparable risks of infection^{391,392}

CHAPTER II: PREMISE

CHAPTER II – PREMISE

The COVID-19 pandemic, caused by SARS-CoV-2, is characterized by a diversity of clinical manifestations, including exacerbated inflammatory states³⁹³ accompanied with tissue and organ destruction beyond direct viral cytopathic effects³⁹⁴. From the outset of the pandemic, it was observed that men presented a higher risk of severe disease and death^{395,396}. The association between risk of severe disease and male sex was also observed in other coronavirus infections, such SARS-CoV and MERS-CoV³⁹⁷. In addition to male sex, other risk factors have been considered to explain gender differences in the development of severe COVID-19, including different impacts of age, comorbidities such as cardiovascular diseases, high blood pressure, diabetes, or cancer and the ethnicity³⁹⁸. However, the mechanisms that may account for the differences between men and women in the development of severe COVID-19 are not completely understood.

Previously, it has been described that hormones are crucial in regulating the immune system's response to infection^{13,14} contributing to the differential immune response between sexes³⁹⁹, pointing to women having stronger antiviral mechanisms, stronger T regulatory cells, higher numbers of group 2 innate lymphoid cells (ILC2), and superior immune-mediated tissue repair capacities as compared to men^{400,401}. Nonetheless, hormones also regulate other hundreds of genes involving a diverse cellular functions across human tissues⁴⁰². In this regard, during pandemic, androgens as testosterone, were described to transcriptionally regulate ACE2, the main cellular receptor for SARS-CoV-2 and TMPRSS2, the major viral fusogenic membrane-associated protease⁴⁰³, indicating that men would present a higher propensity of infection by SARS-CoV-2 and to develop more severe disease due to high concentration of testosterone, however, men and women show comparable risks of infection³⁹¹ and early pandemic studies showed that COVID-19 in male patients was accompanied with diminished levels of circulating testosterone at hospital admission^{404,405}.

Taken together these findings and evidence, suggest that androgens would be having a critical role in immune response leading to development of a severe disease, but it is still not clear the relationship between testosterone status (low or high), COVID-19 progress and immune response.

CHAPTER II: HYPOTHESIS AND OBJECTIVES

CHAPTER II – HYPOTHESIS AND OBJECTIVES

1. Hypothesis

Serum levels of Testosterone could be associated with severity in COVID-19 in male patients and could be represent a powerful biomarker of survival.

2. General objective

Study the relationship between serum testosterone concentration and COVI-19 severity in male patients.

3. Specific objectives

- i.** Compare clinical parameter between male and female patients to determine the worse response to SARAS-COV2
- ii.** Determine serum testosterone levels in male patients upon admission at hospital (admission-point)
- iii.** Determine serum testosterone in male patients throughout hospitalization (longitudinal points)
- iv.** Analyze the power of serum testosterone levels as a biomarker of severity in male patients with COVID-19
- v.** Evaluate the association between serum testosterone levels and the immune response to SARS-COV-2 infection in male patients.

CHAPTER II: MATERIALS AND METHODS

CHAPTER II - MATERIAL AND METHODS

1. Study design

This study was retrospective, longitudinal observational study, with the aim of exploring factors that may underlie worse progression of COVID-19 in men. The number of recruited patients was 497, where 249 were males and 248 females. All patients were admitted to the Vall d'Hebron Hospital (HVH) between May 1st and June 30th, 2020, and were positive to SARS-CoV-2 infection, diagnosed with RT-PCR method.

Patients were first studied for serum biochemical and hematological variables in all samples collected at or near admission (Entry point or Sample 1), for baseline assessment. Subsequently, a subcohort of 115 male patients was studied for the progression of the disease by analyzing the same variables longitudinally, and samples from this subcohort were further analyzed for serum luteinizing hormone (LH) and androstenedione levels, as well as an extensive phenotyping of circulating immune cells (**Figure 58**).

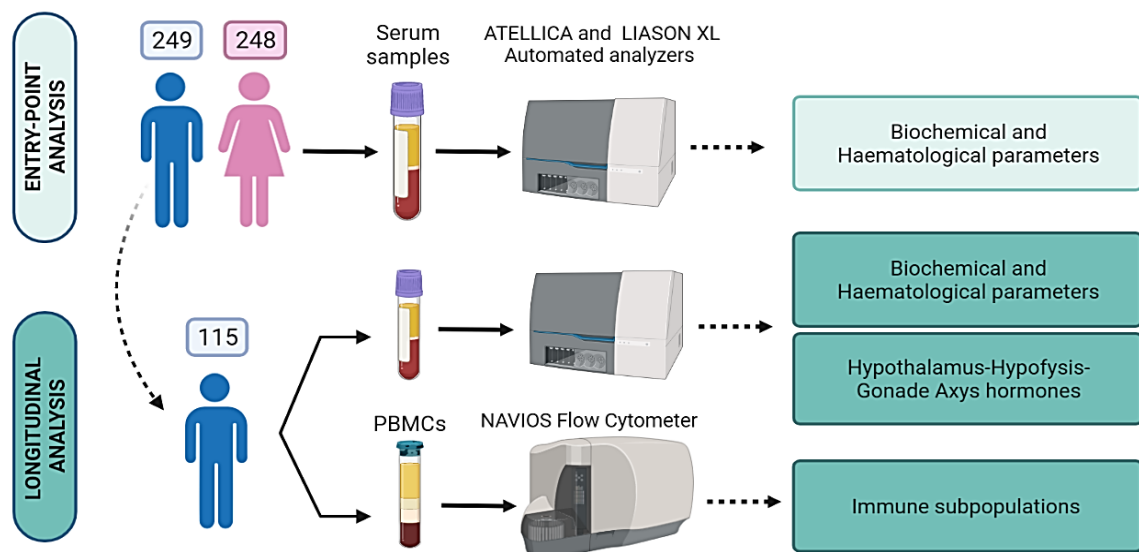


Figure 58. Schematic representation of the study design.

2. Patient selection

Patients included in the study were consecutive patients admitted to the HVH, with the following exclusion criteria: previously hospitalized, recently transplanted, immunosuppressed, and hormonally depleted. The subcohort, one hundred fifteen male patients for study longitudinal analyses were chosen based on serum sample availability. Within this subcohort, a group of 24 patients, for whom matched serum and peripheral blood mononuclear cells were available, was studied for immune phenotyping.

3. Patient classification

Patients were classified in 4-point scale adapted from the 6-point ordinary scale used by Grein et al.⁴⁰⁶, as follows: mild, moderate, severe-survivor, and severe-deceased, (**Table 19**): Mild: symptomatic patients with PCR-diagnosed SARS-CoV-2 infection that were in emergency unit or required hospitalization for less than 2 weeks; Moderate: hospitalized patients requiring low flow oxygen (mask or nasal prongs) or high-flow oxygen, not requiring ICU admission; Severe-survivor: patients admitted to the ICU requiring non-invasive or invasive mechanical ventilation, then discharged; and Severe deceased: ICU patients with a fatal outcome.

Table 19. WHO classification of disease outcome (adapted from Grein et al.¹)

Group	Outcome	Definition	Stay Type
1	Mild	Not hospitalized or hospitalized without oxygen	Discharge from emergency to home or Ward
2	Moderate	Hospitalized with low flow oxygen by mask or nasal prongs or with high flow oxygen	Ward
3	Severe-Survivor	Hospitalized with non-invasive ventilation or with invasive mechanical ventilation	ICU
4	Severe-Deceased	Death	Exitus

4. Data and sample collection

4.1. Data collection

The final dataset for this study was compiled using as a resource the Vall d’Hebron prospective COVID-19 cohort database, which was collected prospectively from medical doctors during the first and second wave of the pandemic using a case report form (CRF) designed by the Infection Disease Department in RedCAP web-based platform. The data collected from this resource, included Clinical data, demographics, co-morbidities, hospital admission, discharge, death dates, time from symptoms onset to hospitalization, length of hospital stay, treatments, requirement for oxygen support, and ICU requirement.

Comorbidities considered were chronic lung disease, cardiovascular disease, diabetes, chronic kidney disease, liver disease, HIV infection with good adherence, obesity (BMI \geq 30), and cancer.

For the **entry-point analyses**: data were obtained on (or near) hospital admission date. For **longitudinal analyses**: data were collected throughout hospitalization with serial time-point sample collection every 7 days in average (**Table 20**).

4.2. Samples collection

For patients in the severe outcome groups, up to five time-point samples were analyzed. Patients in the combined mild-moderate outcome groups were discharged in average, after 2 weeks of admission, and a maximum of three time-point samples were procured from them. For immune phenotyping analyses, at least two independent samples (Sample 1 and Sample 2) were collected, separated by 5 to 20 days.

Table 20. Timetable of sample collection

	Entry point	Longitudinal analysis			
Mild					
Moderate					
Severe survivor					
Severe deceased					
Immune phenotyping					

During first wave of the pandemic, blood samples were collected by medical staff to evaluate the principal biochemical and hematological parameters, Two or three Vacutainer tubes containing ethylene-diamine-tetra-acetic acid (EDTA) as anticoagulant (BD Plymouth), or Serum separator gel (SST) were obtained and were processed within 4h after collection to evaluate patient status. One SST tube was processed to obtain serum and were stored in the biobank or the serum library of HVH.

4.3. Principal biochemical and hematological parameters measured throughout hospitalization

Table 21. Biochemical parameters

Parameter	Units	Normal range
Red blood cells	x10E12/L	4.00-5.20
Hemoglobin	g/dL	12-15
Erythroblasts	%	0.0-2.0
Leucocytes	x10E9/L	4.00-11.00
Lymphocytes	%	20-50
Neutrophils	%	40-80
Monocytes	%	2.0-11.0
Eosinofils	%	0.0-5.0
Basofils	%	0.0-2.0
Platelets	x10E9/L	140-400
Prothrombin time	%	65-120
Derived Fibrinogen	g/L	2.39-6.1
D-Dimer	ng/mL	0-243
Ferritin	ng/mL	25-250
Glucose	mg/dL	74-110
Urea	mg/dL	17-43
Creatinine	mg/dL	0.51-0.95
Bilirubin	mg/dL	0.30-1.20
Ions Sodium/potassium	mmol/L	136-146/3.5-5.10
Aspartate aminotransferase (AST)	UI/L	10-35
Alanine aminotransferase (ALT)	UI/L	7-35
Lactate Dehydrogenase (LDH)	UI/L	0-248
Triglycerides	mg/dL	43-200
Proteins	g/dL	6.6-8.3
C reactive protein (PCR)	mg/dL	0.03-0.50

4.4. Serum sample processing and storage

SST tubes containing blood samples, were processing according to the scientific and ethical guidelines approved by biomedical research law (Decret 1716/2011) at the Vall d'Hebron Hospital Biobank. Briefly, samples collected in yellow tubes containing the separator gels, were centrifugated 3500rpm for 15 minutes at 4°C. The resulting serum was collected in 2mL serum tubes, properly labeled, and codified in the biobank system, then were storage at -80°C for further studies.

5. Serological determinations

Serum biochemical variables were measured by automated analyzers at the Biochemistry Service Core Laboratory Facility at HVH. All determinations were compared to internal controls used for reference ranges at the Core Facility.

5.1. Hormones quantification by Chemiluminescent competitive immunoassays (CLIA)

Hormones were quantified with CLIA method which is the combination between Chemiluminescence and immunoassay with antibodies. Chemiluminescence (CL) is defined as the emission of electromagnetic radiation caused by a chemical reaction to produce light. Similar with other labeled immunoassays (RIA, FIA, ELISA), CLIA utilize antibodies bound to a solid phase (nanoparticles coated with streptavidin or similar). The analyte (hormone) competes with a conjugate labeled with a luminescent probe for binding with anti-hormone antibody. The conjugate could be an hapten labeled with acridinium ester or a polymer linked to an isoluminol derivative. After the incubation between analyte and conjugate competitor, a reaction initiator reactive or trigger solution activator is added to start the chemiluminescent reaction. The intensity of the emitting light is inversely proportional to the hormone concentration in the sample.

5.2. Total Serum Testosterone (TST) levels

Total Serum Testosterone was measured by chemiluminiscent competitive immunoassays (CLIA) on an Atellica™ IM Analyzer (Siemens Inc., NY), using testosterone TSTII Kit (Siemens ref. 10995707). This assay measures the total (bound and unbound) testosterone in human serum. Briefly, the Atellica system automatically perform the following steps: 20

μL of sample and $90\mu\text{L}$ of **releasing agent** (reactive to unbound testosterone from proteins) are dispensed in a tube, the mixture is incubated about 9 minutes at 37°C . After that, $50\mu\text{L}$ of **Lite reactive** (Hapten labeled and antibodies with biotin) and $150\mu\text{L}$ of **solid phase** (particles with streptavidine) are added into the sample mixture, and are incubated during 3minutes at 37°C . After this, the mixture is separated and washed and added $300\mu\text{L}$ of both **Atellica Acid and Base** to start the chemiluminescent reaction. Finally, the system reports the results.

5.3. Luteinizing hormone (LH) levels

Luteinizing hormone was also measured by CLIA on an AtellicaTM IM Analyzer (Siemens Inc., NY), (Siemens ref. 10995634) kits. The same steps performed for Testosterone were followed for LH level determination.

5.4. Androstenedione hormone levels

Androstenedione was measured on a LIASON XL Analyzer (DiaSorin, Saluggia, Italy), using the LiasonR androstenedione (ref. 318870) CLIA assay. In brief, LIASON system, transfer the sample (or control) into reaction module, then add the magnetic nanoparticles and the assay buffer. Then incubate for 10 minutes and add the conjugate (polymer bound to androstenedione derivate and isoluminol) incubate again 10 minutes. Finally, the sample is washed and added the trigger solution.

5.5. Interleukine-6 (IL-6) levels

Measurements of IL-6 levels in plasma were performed using a fluorescence immunoassay with microfluidic technology (ELLA Proteinsimple, Bio Techne). Samples were 1:2 diluted with sample diluent provided by the manufacturer and loaded onto multiplex cartridges according to manufacturer's instructions prior to their analysis. Results were expressed as pg/mL .

5.6. Hormone references

As references for healthy men, we used median TST levels of 409.72 ng/dL (90% CI $197.44\text{--}669.58$) for $< 50\text{-year-old}$ individuals and 377.46 ng/dL (90% CI $187.72\text{--}684.19$) for $\geq 50\text{-year-old}$ individuals (FDA-approved protocol, [https:// www. acces sdata. fda. gov/ cdrh_ docs/ pdf19/ K1915 33. pdf](https://www.accessdata.fda.gov/cdrh_docs/pdf19/K191533.pdf)). For luteinizing hormone (LH), the reference median values

were 2.8 mIU/mL (90% CI 1.5–9.3) for < 70-year-old individuals and 8.0 mIU/mL (90% CI 3.1–34.6) for ≥ 70-year-old individuals. For androstenedione, the reference median value was 1.80 ng/mL (90% CI 0.5–3.5).

5.7. Bioavailable-free testosterone calculation

Bioavailable-free testosterone was determined using the formula developed by Vermeulen et al.⁴⁰⁷. This calculation estimates how testosterone is distributed among the SHBG-bound, albumin-bound, and free components based on association constants governing the interactions between testosterone and these compartments. The equation, illustrated in **Figure 59**, relies on values for total testosterone, SHBG concentration, and albumin concentration. For this study we used the online calculator developed at the Hormonology department, University Hospital of Ghent, Belgium (<https://www.issam.ch/freetesto.htm>)

$$FT \left(\frac{\text{mol}}{\text{L}} \right) = \frac{-b + \sqrt{b^2 + 4a[T]}}{2a}$$

Where

$$a = k_{at} + k_t + (k_{at} \times k_t)([SHBG] + [albumin] - [T])$$

$$b = 1 + k_t[SHBG] + k_{at}[albumin] - (k_{at} + k_t)[T]$$

Figure 59. The Vermeulen equation for calculated free testosterone.

6. Immuno-phenotyping

Blood samples were collected in Vacutainer tubes containing ethylene-diamine-tetra-acetic acid (EDTA) as anticoagulant (BD-Plymouth, PL6 7BP, UK) and processed within 4 h after collection. Absolute counts and relative numbers of peripheral blood lymphocytes were determined for all study participants using tetra CHROME Tube 1 (CD45-FITC/CD4-PE/CD8-ECD/

CD3-PC5) and tetra CHROME Tube 2 (CD45-FITC/ CD56-PE/CD19-ECD/CD3-PC5) panels (Beckman Coulter). Samples were fixed in 1X lysing solution (BC) and acquired on a BC Navios EX instrument. For multicolor staining and analysis, extended lymphocyte subpopulations were assessed with 5 different flow cytometry panels designed according to the HIPC protocol⁴⁰⁸. Two additional panels were added to analyze basic lymphocyte populations and RTE. Compensation controls were used in each panel to avoid overlapping

of the different fluorochromes. Gating strategies were as described⁴⁰⁹, and the antibody panels were summarized as follows and in **Table 22**.

- **Panel 1:** Panel 1: General immune phenotype for T, B, and natural killer (NK) lymphocyte subpopulations, gating by CD45 versus SSC.
- **Panel 2:** Gating strategy for differentiated CD4+ and CD8+ T cell subsets, based on CD45RA and CCR7 expression defining: CD45RA+/CCR7+ (naïve), CD45RA-/CCR7+ (central memory [TCM]), CD45RA-/CCR7- (effector memory [TEM]), and CD45RA+/CCR7- (terminal effector memory [TEMRA]). CD4+ T helper (Th) populations (Th1, Th2, Th17, Th1-17), based on CCR6 and CXCR3 expression, were analyzed by gating on CD45RA-TCM and TEM cells.
- **Panel 3:** T regulatory (Treg) cell populations: CD3+CD4+CD25+, CD127-, CCR4+, and CD45RO+.
- **Panel 4:** B cell populations (naïve, pre-switched, switched memory, and exhausted) depending on expression of IgD and CD27. The differing pattern of CD24+ and CD38+ expression identified transitional cells and plasmablasts. CD27 and CD21 enabled study of the CD21low population.
- **Panel 5:** Dendritic cells (DC), natural killer (NK) cells, and monocyte populations were analyzed in the CD3-CD19-gate. NK subpopulations (NKdim and NKbright) were studied using CD56 and CD16 expression. CD16 and CD14 were used to identify classical monocytes (CD14+CD16-) and non-classical monocytes (CD16+CD14-). DCs were studied selecting for populations negative for the following markers: CD3, CD14, CD16, CD19, CD20, and CD56. High expression of HLA-DR and CD11c and CD123 was used to identify plasmacytoid DCs (HLA-DR+CD123+) and myeloid DCs (HLA-DR+CD11c+).
- **Panel 6:** Recent thymic emigrant cells (RTEs) were studied using CD3, CD4, CD27, CD31, CD45RA, and CD62L expression.

Data were acquired on a NAVIOS EX (BC) flow cytometer. At least 100,000 events were acquired for each sample. Flow cytometry data were analyzed with Kaluza Software. Absolute values were calculated from the absolute number of leucocytes and lymphocytes as determined on a hematological analyzer (XN-2000; Sysmex, Japan).

Lymphocyte populations	Fluorophore	Isotype	Clone
CD45/CD8/CD4/CD3	FITC/PE/ECD/PC5	IgG2b/IgG1/IgG1/IgG1	B3821F4A/SFCI12T4D11/SFCI21Thy2D3/UCHT1
CD45/CD56/CD19/CD3	FITC/PE/EDC/PC5	IgG2b/IgG1/IgG1/IgG1	B3821F4A/SFCI12T4D11/SFCI21Thy2D3/UCHT1
T-cell populations			
CXCR3/CD183	AF488	IgG1	G025H7
CCR7/CD197	PE	IgG2a	G043H7
CD45RA	ECD	IgG1	ALB11
CCR6/CD196	PC7	IgG2a	B-R35
CD4	APC	IgG1	13B8.2
CD8	APC700	IgG1	SFCI21Thy2D3 (T8)
CD3	APC750	IgG1	UCHT1
HLA-DR	PB	IgG1	Immu-357
CD45	KRO	IgG1	J.33
Recent Thymic Emigrant			
CD31	FITC	IgG1	5.6E
CD62L	PE	IgG1	DREG56
CD3	ECD	IgG1	UCHT1
CD27	PC7	IgG1	1A4CD27
CD4	APC	IgG1	13B8.2
CD45RA	PB	IgG1	2H4LDH11LDB9 (2H4)
CD45	KRO	IgG1	J.33
T regulatory cell population			
CD45RO	FITC	IgG2a	UCHL1
CD25	PE	IgG2a	B1.49.9
CD3	ECD	IgG1	UCHT1
CCR4/ CD194	PC7	IgG1	1G1
CD4	APC	IgG1	13B8.2
CD127	APC700	IgG1	R34.34
HLA-DR	PB	IgG1	Immu-357
CD45	KRO	IgG1	J.33
DC/Monocytes/NK			
CD16	FITC	IgG1	3G8
CD11c	PE	IgG1	BU15
CD3	ECD	IgG1	UCHT1
CD19	ECD	IgG1	J3-119
CD20	ECD	IgG2a	B9E9(HRC20)
CD56	PC7	IgG1	N901 (NKH-1)
CD123	APC	IgG1	SSDCLY107D2
CD14	APC750	IgG1	RMO52
HLA-DR	PB	IgG1	Immu-357
B-cell populations			
IgD	FITC	IgG2a	IA6-2
CD21	PE	IgG1	BL13
CD19	ECD	IgG1	J3.119
CD27	PC7	IgG1	1A4CD27
CD24	APC	IgG1	ALB9
CD38	APC750	IgG1	LS198-4-3
IgM	PB	IgG1	SA-DA4
CD45	KRO	IgG1	J.33

Table 22. Panels and antibodies used for immunophenotyping

7. Statistical analysis

Continuous variables were expressed as mean \pm SD or median and interquartile range (IQR). Simple and multiple comparisons were performed using parametric (two sided Student's t test or ANOVA) and non-parametric (Mann-Whitney U test or Kruskal–Wallis) statistical tests with Dunn's and Tukey's post hoc tests. Categorical variables were presented as numbers and percentages and compared using the 2-sided Fisher's exact test as appropriate. Correlation between variables were assessed using simple linear regression. ROC curves were calculated with the univariate logistic regression model implemented in GraphPad and the EasyROC web tool ([http:// www. bioso ft. hacet tepe. edu. tr/ easyROC/](http://www.biosoft.hacettepe.edu.tr/easyROC/)). The groups classified by the model were used in 2×2 contingency analyses to calculate odds ratios (OR) and significance determined by Fisher's exact test. For longitudinal analyses, trajectories were plotted for each patient and average values for each parameter calculated for each time-point, followed by linear regression. The resulting linear regression slope values were used in univariate logistic regression analysis to assess the outcome predictive power of the trajectories. P values ≤ 0.05 were considered significant. For principal component analysis (PCA), the variables analyzed included all the biochemical parameters and immune subpopulations, including numerical assignments for outcome (1, mild–moderate; 2, severe; 3, deceased) and selecting for ≥ 3 components, of which the 2 summarizing the highest variance were used for the 2-dimensional representations. PCA, multivariate correlation analysis, and other calculations, as well as graphic representations, were performed with GraphPad Prism 9.0.2.

8. Ethical considerations

The present study was performed with surplus serum samples from routinely tested hospitalized COVID-19 patients, following protocols reviewed and approved by the HVH Institutional Review Board (Medical Research Ethics Committee, protocol number PR(AG)329-2020). Immunophenotyping studies of the peripheral blood cells underwent a separate review and approval process (protocol number PR(AG)242/2020). For the final dataset from the Vall d'Hebron prospective COVID-19 cohort database, clearance from the Institutional Review Board was obtained. To minimize risks of infection to the health staff, a written informed consent was waived, although all patients received proper study information and gave oral consent.

CHAPTER II: RESULTS

CHAPTER II - RESULTS

1. Baseline characteristics of the male and female study populations

As gender differences in response to infectious diseases are known and androgens are related to stress and critical illness, the baseline characteristics at entry-point were evaluated in both males and females to compare the severity of the disease.

Table 23. Baseline clinical characteristics of the male study population

	Mild-Moderate N=114	Severe-recovered N=97	Severe-deceased N=38	p-value ¹⁻²	p-value ¹⁻³	p-value ²⁻³
Age (y), median (IQR)	59(56-63)	56(53-59)	68(67-71)	0.1096	0.0001	<0.0001
Length of stay (days), median (IQR)	8(7-9)	30.5(27-34)	19(9-26)	<0.0001	<0.0001	0.0009
Comorbidity, n° (%)	54 (47.36)	57 (58.76)	28 (73.68)	0.1279	0.0051	0.1175
Hypertension	35 (30.70)	31 (31.96)	21 (55.26)	0.8822	0.0109	0.0178
Diabetes	20 (17.54)	15 (16.46)	11 (28.95)	0.7143	0.1630	0.0908
Cancer	6 (5.26)	3 (3.09)	3 (7.89)	0.5115	0.6915	0.3497
Cardiovascular diseases	9 (7.89)	12 (12.37)	3 (7.89)	0.3573	0.9999	0.5560
Chronic Lung diseases	10 (8.77)	6 (6.19)	5 (13.16)	0.6046	0.5297	0.2912
Obesity-Dyslipidaemia	16 (14.03)	33 (34.02)	11 (28.95)	0.0009	0.0497	0.6842
Chronic Kidney disease	6 (5.26)	2 (2.06)	1 (2.63)	0.2927	0.6808	0.6727
Others	9 (7.89)	13 (13.4)	7 (18.42)	0.2586	0.1220	0.5903
Biochemical parameters, median (IQR)						
Testosterone	144.3 (112.3-189.3)	52.91 (45.03-66.73)	58.48 (46.83-81.94)	<0.0001	<0.0001	0.9999
Leucocytes n°	6.32(5.78-6.88)	7.80(6.83-8.80)	8.70 (7.20-9.65)	<0.0001	0.0051	0.9999
Lymphocytes n°	1.20 (1.0 -1.4)	0.77 (0.70- 0.82)	0.8(0.65-0.90)	<0.0001	0.0001	0.9999
Lymphocytes %	18.55(16.15- 1.57)	9.20 (8.18- 11.28)	10.89 (7.95 -13.38)	<0.0001	<0.0001	0.9999
Neutrophils	4.57 (3.92-4.90)	6.26 (5.53 – 7.38)	6.39 (5.53-8.34)	<0.0001	0.0007	0.9999
Interleukine-6	42.30(25.33-53.46)	130.8(112.10-160.6)	215.30(117.6-996.4)	<0.0001	<0.0001	0.9999
C-reactive protein	9.57 (6.76-10.88)	17.47(12.17-0.72)	14.56(9.84 – 24.019)	<0.0001	0.0069	0.9999
LDH	324 (296.0-369.0)	472.5(440.0-506.0)	493.0(429.0-583.0)	<0.0001	<0.0001	0.9999
D-Dimer	236 (213.0 -311.0)	529.0 (361.0 -711.0)	421.5 (260.0-684.0)	<0.0001	0.0210	0.9999
Ferritin	934 (679.0 -1089.0)	1289 (1100.0-1574.0)	1443.0(554.9-1919.0)	0.0022	0.7403	0.6783

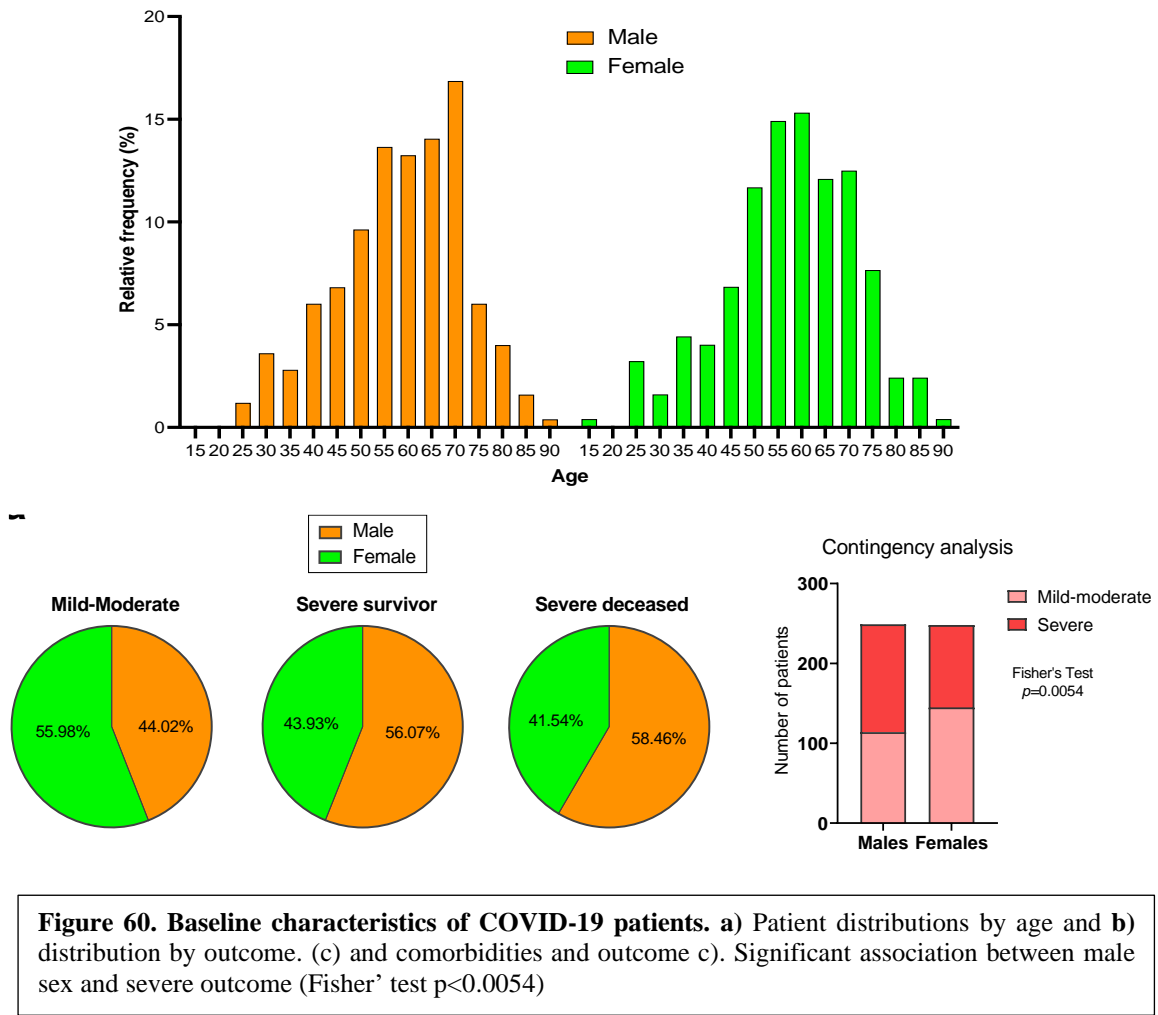
¹Mild-moderate group, ²Severe-recovered group, ³Severe-deceased group. The Fisher's exact test was used to compare comorbidities. The Kruskal-Wallis test with Dunn's Multiple comparison was used to analyze the length of stay and biochemical parameters.

Table 24. Baseline clinical characteristics of the female study population

	Mild-Moderate N=145	Severe-recovered N=76	Severe-deceased N=27	p-value ¹⁻²	p-value ¹⁻³	p-value ²⁻³
Age (y), median (IQR)	57(54-60)	55(53-62)	74(68-81)	0.9999	<0.0001	<0.0001
Length of stay (days), median (IQR)	7 (6 - 7)	25 (20.0- 33.0)	15 (8 – 19)	<0.0001	0.0033	0.0003
Comorbidity, n° (%)	89 (61.38)	47 (61.84)	22 (81.48)	0.9999	0.0503	0.0942
Hypertension	43 (29.65)	20 (26.31)	14 (51.85)	0.6408	0.0431	0.0190
Diabetes	20 (13.79)	6 (7.89)	2 (7.41)	0.2719	0.5343	>0.9999
Cancer	9 (6.21)	5 (6.58)	4 (14.81)	0.9999	0.1259	0.2366
Cardiovascular diseases	11 (7.58)	5 (6.58)	3 (11.11)	0.9999	0.4637	0.4290
Chronic Lung diseases	12 (8.27)	8 (10.53)	6 (22.22)	0.6249	0.0413	0.1877
Obesity-Dyslipidaemia	43 (29.65)	28 (36.84)	8 (29.63)	0.2916	0.9999	0.6396
Chronic Kidney disease	5 (3.49)	2 (2.63)	2 (7.41)	0.9999	0.3024	0.2805
Others	20 (13.79)	11 (14.47)	5 (18.52)	0.9999	0.5453	0.5461
Biochemical parameters, median (IQR)						
Leucocytes n°	5.95 (5.40-6.81)	6.28 (5.46- 7.02)	7.29 (5.74 – 9.07)	0.9999	0.2849	0.6427
Lymphocytes n°	1.18 (1.04-1.27)	1.00 (0.84-1.12)	0.89 (0.74 -1.21)	0.0008	0.0349	0.9999
Lymphocytes %	19.76 (17.96 – 22.16)	15.65 (16.62- 18.58)	13.40 (9.59- 19.18)	0.0009	0.0025	0.9999
Neutrophils n°	4.02 (3.6-4.78)	4.88 (4.23 – 5.43)	5.83 (4.37- 7.66)	0.2125	0.0649	0.9426
Interleukine-6	34.21 (26.81-38.60)	75.30 (50.26- 86.23)	65.36 (45.03 - 154.6)	<0.0001	<0.0001	0.9999
C-reactive protein	8.38 (4.78-10.44)	12.67 (10.44- 14.99)	14.47 (6.43 -21.89)	0.0042	0.0846	0.9999
LDH	304 (289.0-345.0)	420.0 (380.0 -486.0)	415.0 (283.0-539.0)	<0.0001	0.0855	0.9999
D-Dimer	258.0 (228.0 -275.0)	334.0 (258.0 - 422.0)	269.0 (207.0-424.0)	0.0379	0.7287	0.9999
Ferritin	378.0 (284.0 -437.0)	528.0 (445.0 - 729.0)	445.0 (387.0 – 730.0)	0.0023	0.3007	0.9999

¹Mild-moderate group, ²Severe-recovered group, ³Severe-deceased group. The Fisher's exact test was used to compare comorbidities. The Kruskal-Wallis test with Dunn's Multiple comparison was used to analyse the length of stay and biochemical parameters.

Tables 23 and 24 show the baseline characteristics in males and females, in order to ensure equal comparisons, patients were stratified by age (**Figure 60a**), no significant differences were observed, albeit a higher proportion of females older than 70 years was observed. It was observed a higher proportion of females developing a mild/moderate COVID-19 disease than males and on the other hand, there are more males with a severe (survivor or deceased) outcome (**Figure 60b**) and these differences were significant ($p=0.0054$, Fisher's test) (**Figure 60c**)



In both male and female patients, the median age in severe-deceased outcome groups was significantly older than those in mild or moderate outcome groups, as expected⁴¹⁰. However, women in the severe-deceased group were significantly older than males in the same outcome group (**Figure 61a**). To assess if differences between males and females were related to presence of comorbidities, we compared the proportions of comorbidities by outcome in both groups, however there were no significant differences (**Figure 61b**). Also, the treatment received in both groups by outcome was evaluated. In both groups, Corticoids, immunomodulators and anticoagulants were higher in patients with severe outcome than those with mild/moderate outcomes (**Table 25 and 26**).

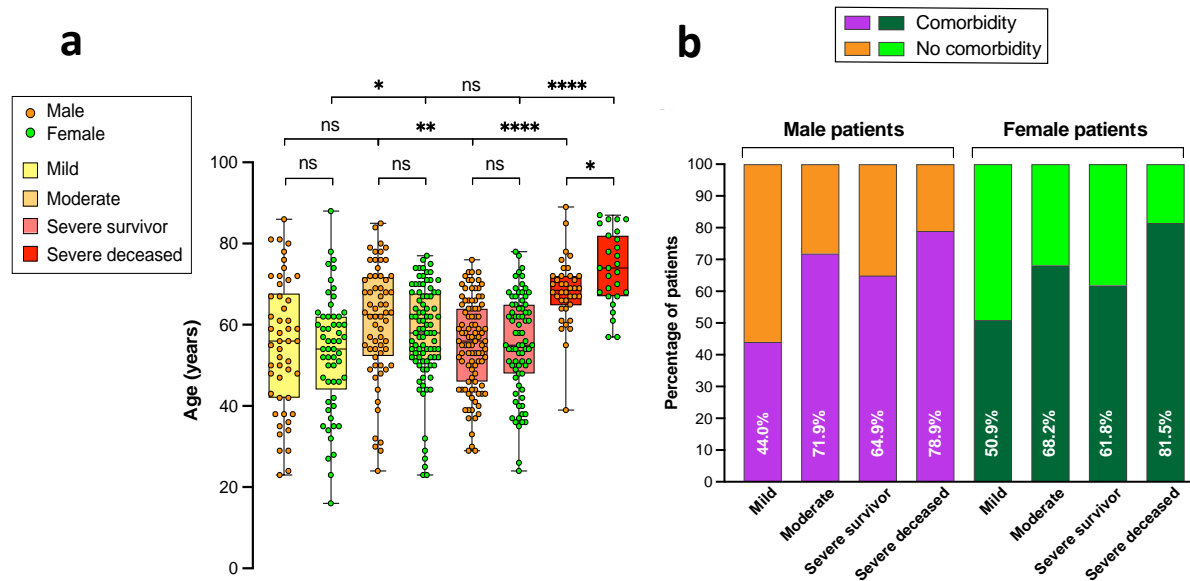


Table 25. Comparison between Mild-moderate and Severe outcomes in males

Treatments	Total 249 (%)	Mild-Moderate 114 (%)	Severe 135 (%)	p-value*
Hydroxychloroquine	241 (96.79)	112 (98.24)	129 (95.55)	0.2953
Antibiotics	238 (95.58)	104 (91.23)	134 (99.26)	0.0031
Antivirals	196 (78.71)	93 (81.58)	103 (76.30)	0.3528
Corticoids	66 (26.5)	13 (11.40)	53 (39.26)	<0.0001
Immunomodulators	130 (52.21)	23 (20.17)	107 (79.26)	<0.0001
Anticoagulants	123 (49.40)	34 (29.82)	89 (65.92)	<0.0001
Analgesics	28 (11.24)	13 (11.40)	15 (11.11)	0.9999

Table 26. Comparison between Mild-moderate and Severe outcomes in females

Treatments	Total 248 (%)	Mild-Moderate 145 (%)	Severe 103 (%)	P-value*
Hydroxychloroquine	228 (91.94)	133 (91.72)	95 (92.23)	0.9999
Antibiotics	231 (93.15)	128 (88.28)	103 (100.00)	0.0001
Antivirals	215 (86.69)	129 (88.97)	86 (83.5)	0.2557
Corticosteroids	41 (16.53)	11 (7.59)	30 (29.13)	<0.0001
Immunomodulators	95 (38.31)	23 (15.86)	72 (69.90)	<0.0001
Anticoagulants	70 (28.23)	10 (6.90)	60 (58.25)	<0.0001
Analgesics	65 (26.21)	40 (27.59)	25 (24.27)	0.6605

2. Biochemical and hematological predictors of outcome in male and female COVID-19 patients

2.1. Severe outcomes correlate with high neutrophils counts, IL-6, D-dimer and LDH in both males and females but are m

As an approach to capture global patterns of association between biochemical parameters and outcomes, a principal component analysis (PCA), was applied followed by Spearman multivariate correlation analysis (**Figure 62**). In male patients (**Figure 62a**), both PCA and multivariate analysis showed a clear correlation between mild or moderate outcomes with known predictors of good outcome, such as higher lymphocyte counts or hemoglobin levels, while severe outcome groups correlated with high neutrophil counts, and high IL-6, CRP, D-dimer, ferritin, or LDH levels, confirming prior evidence^{391,410,411}. Furthermore, older age presented a stronger correlation with a severe-deceased outcome than biochemical parameters predictive of poor outcome, such as D-dimer, ferritin, LDH, or IL-6. In female patients, PCA and multivariate analysis also highlight significant differences between mild-moderate and severe outcomes (**Figure 62b**). Similar to male patients, the mild outcome group of female patients showed strong correlations to lymphocyte counts and hemoglobin levels, while the severe outcome groups are correlated with high IL-6, CRP, D-dimer, ferritin, and LDH. Like in male patients, older age showed the strongest correlation to a severe-deceased group in female patients. Age, platelet counts, and fibrinogen levels significantly discriminated severe-survivor from severe-deceased female patients.

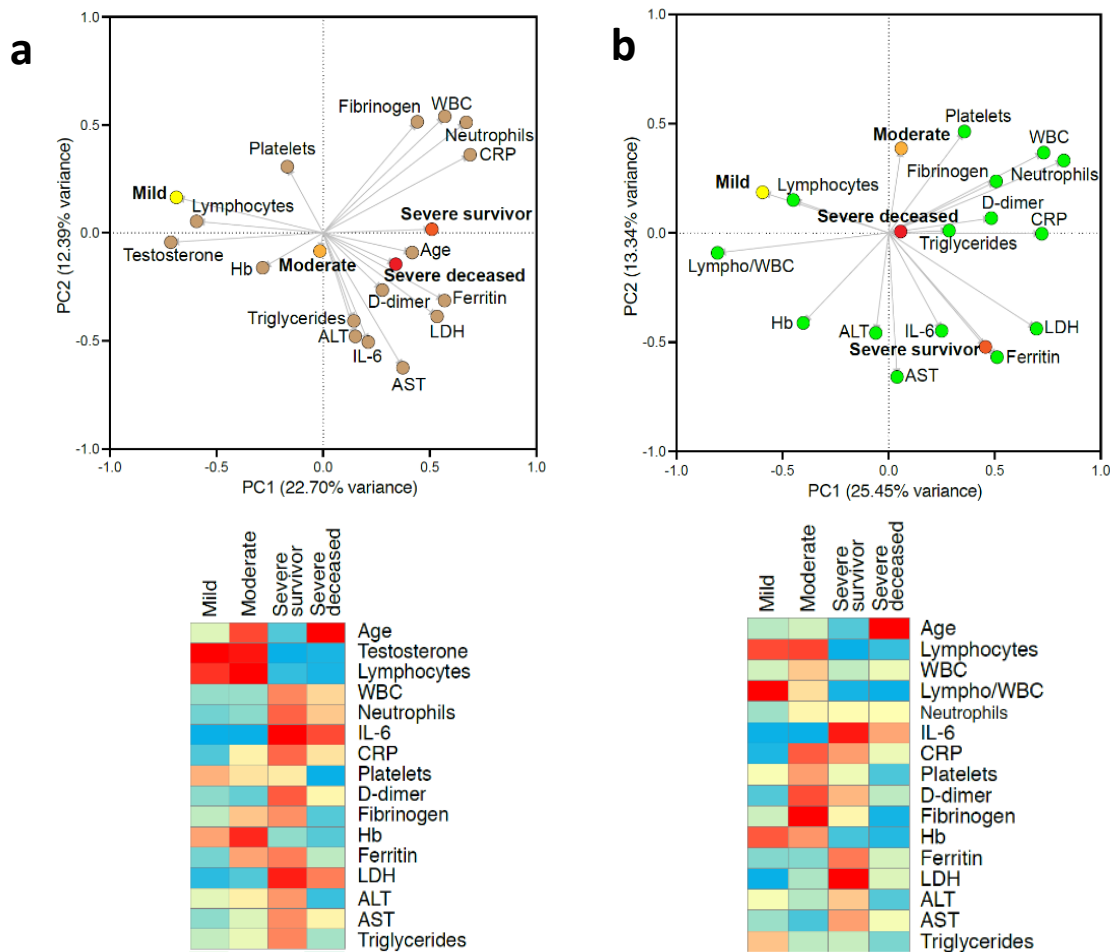


Figure 62. Association analyses between biochemical parameters and outcomes. Clinical biochemistry values were determined for samples collected at patient admission. **Top panels:** Principal component analysis (PCA) illustrating correlations between elevated levels of the indicated parameters and mild, moderate, severe survivor or severe deceased outcomes in male (a) or female (b) patients. **Bottom panels:** Heatmap of correlation coefficients between elevated levels of biochemical parameters and outcomes. Spearman multivariate correlation analyses were performed for all parameters vs. outcomes, the resulting coefficients normalized for each column (range, 0 to 1) and used to build heatmaps

Biochemical parameters collected at admission also were plotted according to outcomes, with separate plots for males (**Figure 63a**) and females (**Figure 63b**). In both genders, significant differences were observed between patients who developed mild to moderate disease and those who experienced severe outcomes. Notably, when we compared the biochemical values between males and females, we discovered that inflammatory markers such as Neutrophils, IL-6, D-dimer, and C-Reactive Protein were significantly elevated in males compared to females. Conversely, lymphocyte levels, which play a crucial role in adaptive immune responses, were significantly lower in males (**Figure 63c**).

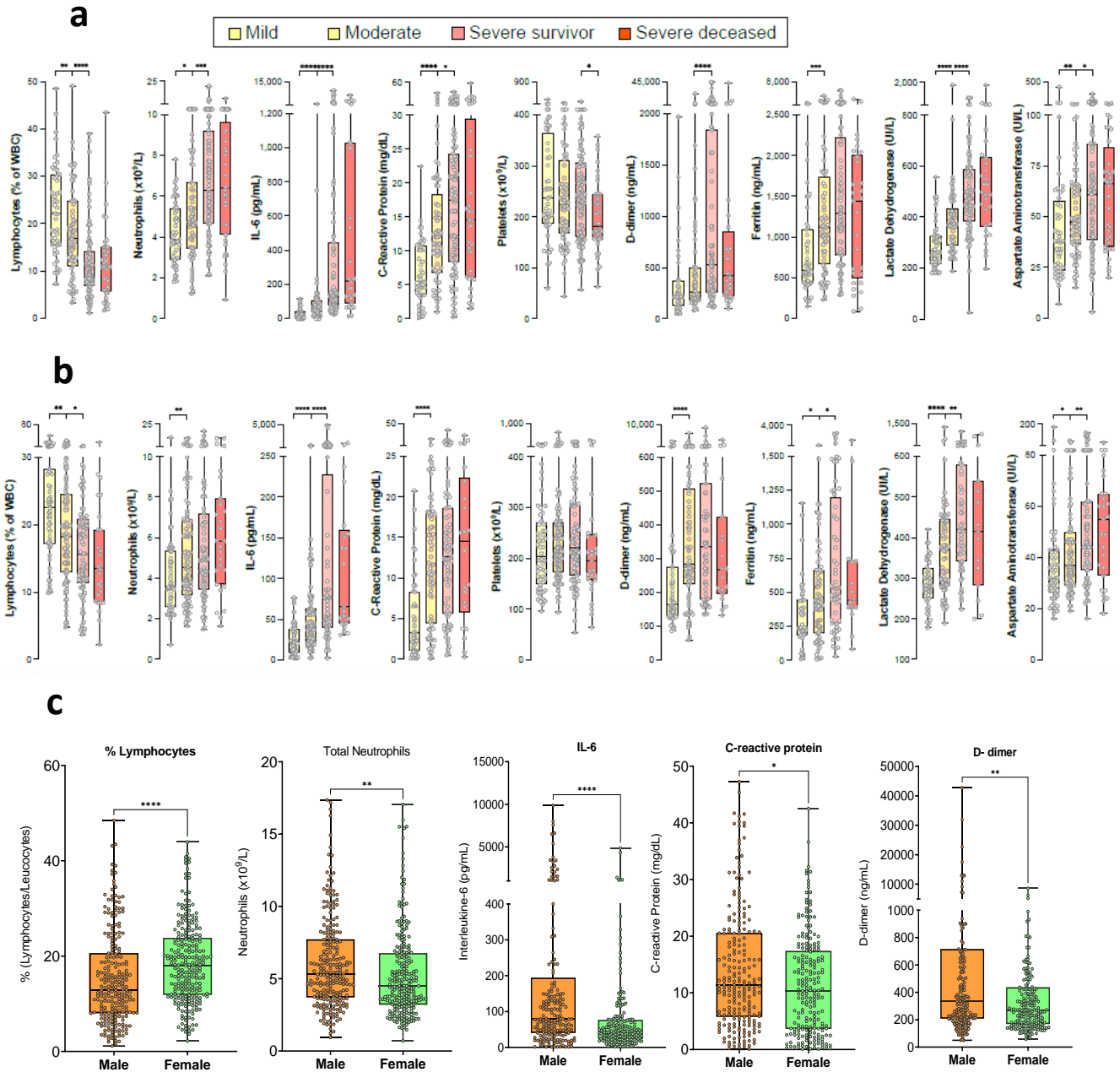


Figure 63. Clinical biochemistry features of male and female COVID-19 patients, associated with outcomes. Values of relevant clinical biochemistry parameters assessed for admission samples and grouped by eventual outcome for male (a) and female (b) patients. c) Relevant parameters grouped by sex. Asterisks denote significance of pairwise comparisons between samples grouped by outcome and between males and females.: * $p \leq 0.05$, ** $p \leq 0.01$, *** $p \leq 0.001$, and **** $p \leq 0.0001$. Non-significant comparisons ($p > 0.05$) are not shown.

2.2. Serum testosterone at admission point is significantly lower in severe patients and significantly correlates with lymphocytes

Patients with moderate or severe outcomes had significantly lower TST levels ($p < 0.0001$) compared to those with mild outcomes (Table 22, Figure 64a), in agreement with other studies. Notably, the low TST levels observed in the initial assessments at admission did not show significant differences between survivors and non-survivors (Figure 64a). Furthermore, a notable correlation emerged between TST levels and lymphocyte counts (both absolute counts, $r = 0.3122$, and fraction of white blood cells, $r = 0.4187$), as well as neutrophil counts ($r = -0.3586$), suggesting a potential interrelationship among these three parameters (Figure 64c). Interestingly, TST levels upon admission did not display a significant association with the occurrence of comorbidities in older men (Figure 64c)

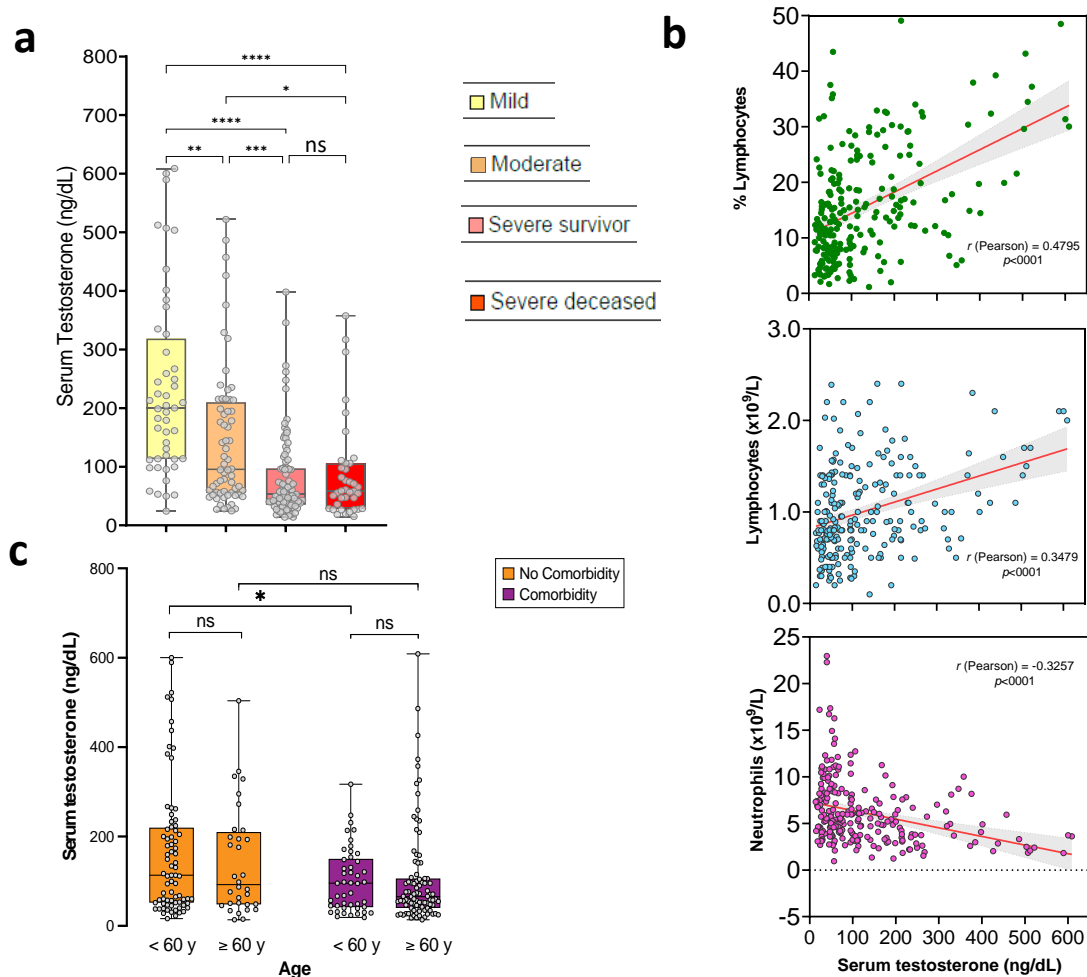


Figure 64. Serum Testosterone at admission in male patients with COVID-19. a) TST levels by outcome. **b)** Correlations of TST levels with lymphocytes percentage of WBC, lymphocytes counts and neutrophil counts. **c)** Distribution of male patients with comorbidities according to age. Asterisks denote significance of pairwise comparisons between samples grouped by outcome and between males and females.: * $p \leq 0.05$, ** $p \leq 0.01$, *** $p \leq 0.001$, and **** $p \leq 0.0001$. Non-significant comparisons: ns

2.3. IL-6 is the best risk predictors for severe disease at admission point in both females and males, whereas Testosterone and % lymphocytes are the best predictors for mild-moderate outcomes

The risk of ICU admission for patients with mild-moderate outcomes was assessed by odds ratio (OR) estimates and logistic regression analysis. In male patients, the most significant OR of ICU admission were found for IL-6 (OR 10.53, 95% CI 5.42 to 20.67), LDH (OR 6.62, 95% CI 3.62 to 11.79), lymphocyte fraction of WBC (OR 0.14, 95% CI 0.08 to 0.25) and neutrophilia (OR 3.95, 95% CI 2.30 to 6.78) (**Figure 65a**), in agreement with previous studies^{410,412}. A significant OR was also found for testosterone (0.17, 95% CI 0.09 to 0.31) also in line with other studies^{383,404,405}. In female patients, the most significant OR of ICU admission were for IL-6 (OR 7.77, 95% CI 3.48 to 16.9), LDH (OR 6.26, 95% CI 2.88 to 13.34), ferritin (OR 3.17, 95% CI 1.50 to 6.74), and lymphocyte fraction of WBC (OR 0.33, 95% CI 0.20 to 0.57) (**Figure 65a**). The power of these parameters to predict severe disease was corroborated by logistic regression analysis. The resulting receiver operating characteristic (ROC) curves yielded areas under the curve (AUC), which, in male patients, were > 0.7 ($p < 0.0001$) for IL-6, LDH, and neutrophilia, and < 0.23 for lymphopenia and testosterone. In females, AUC of ROC curves were > 0.7 ($p < 0.0001$) for IL-6 and LDH (**Figure 65c**).

The same parameters showed a weaker power to predict the risk of death from COVID-19 when comparing all survivors, including severe survivors, versus deceased patients, with the exception of serum IL-6 levels, in both male and female patients (OR 4.45, 95% CI 2.14 to 10.71 and AUC of ROC 0.7189, $p = 0.0002$ for males; and females had OR 4.21 and AUC of ROC 0.7123, $p = 0.0014$) (**Figure 65b, 65d**).

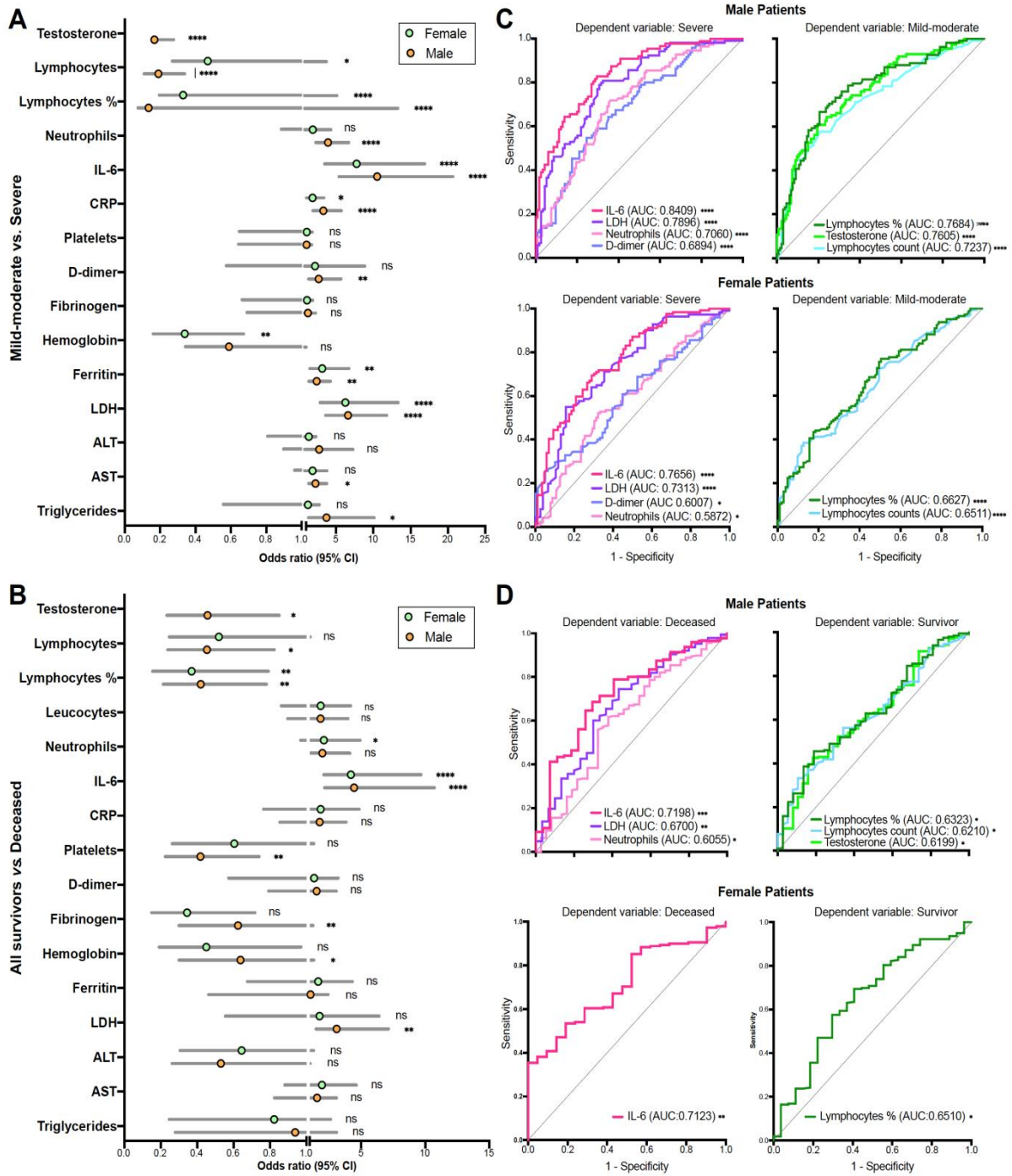
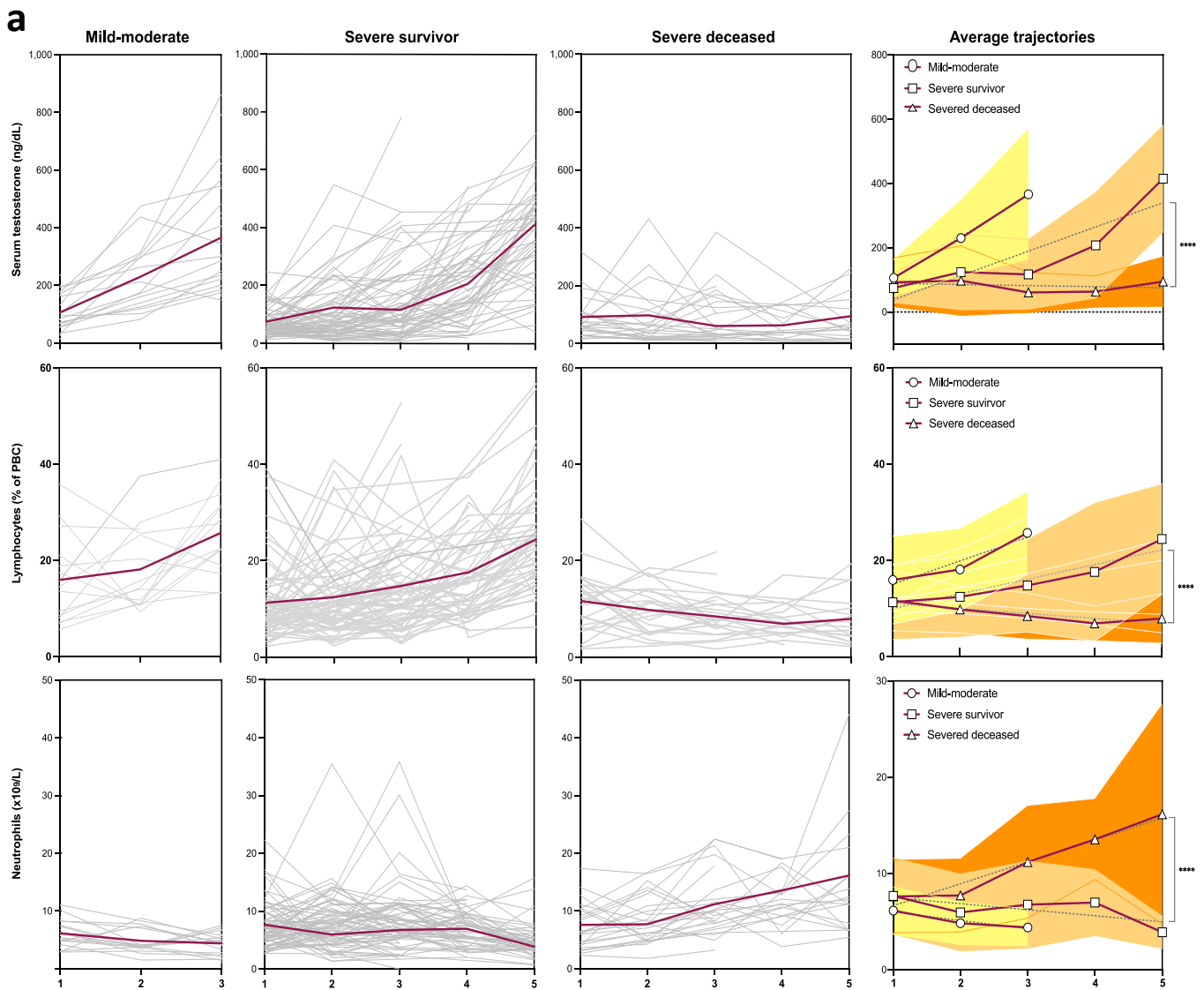


Figure 65 Assessment of clinical biochemistry parameters as predictors of risk of severe disease or death from COVID-19. Odds ratios (OR) of clinical biochemistry parameters and risk of severe disease (a) or death (b) in male and female patients. Receiver operating characteristic (ROC) curves and area under the curve (AUC) values of risk of severe disease (c) or death (d). Shown are only those parameters with significant AUC values ($p \leq 0.05$).

3. Serum testosterone as predictor of outcome in the longitudinal analysis

3.1. Evolutionary trajectories of biochemical parameters in males

To explore whether determinations in longitudinal samples could yield improved predictors of lethal disease, the trajectories for all biochemical and hematological parameters were evaluated and plotted for all patients grouped into mild-moderate, severe survivor, and severe deceased outcomes (**Figure 66a y 66b**). Trajectories of only three parameters: testosterone ($p = 0.0038$), lymphocyte counts (or fractions of WBC) ($p = 0.01$), and neutrophil counts ($p = 0.0023$), were significantly different (two-way ANOVA), comparing trajectories between the severe survivor and severe deceased groups (**Figure 66a**). No significant differences for any of these variables were observed between severe survivor and mild-moderate outcomes. None of the other parameters showed statistically significant different trajectories in comparisons between severe survivor vs. severe deceased outcomes (**Figure 65b**).



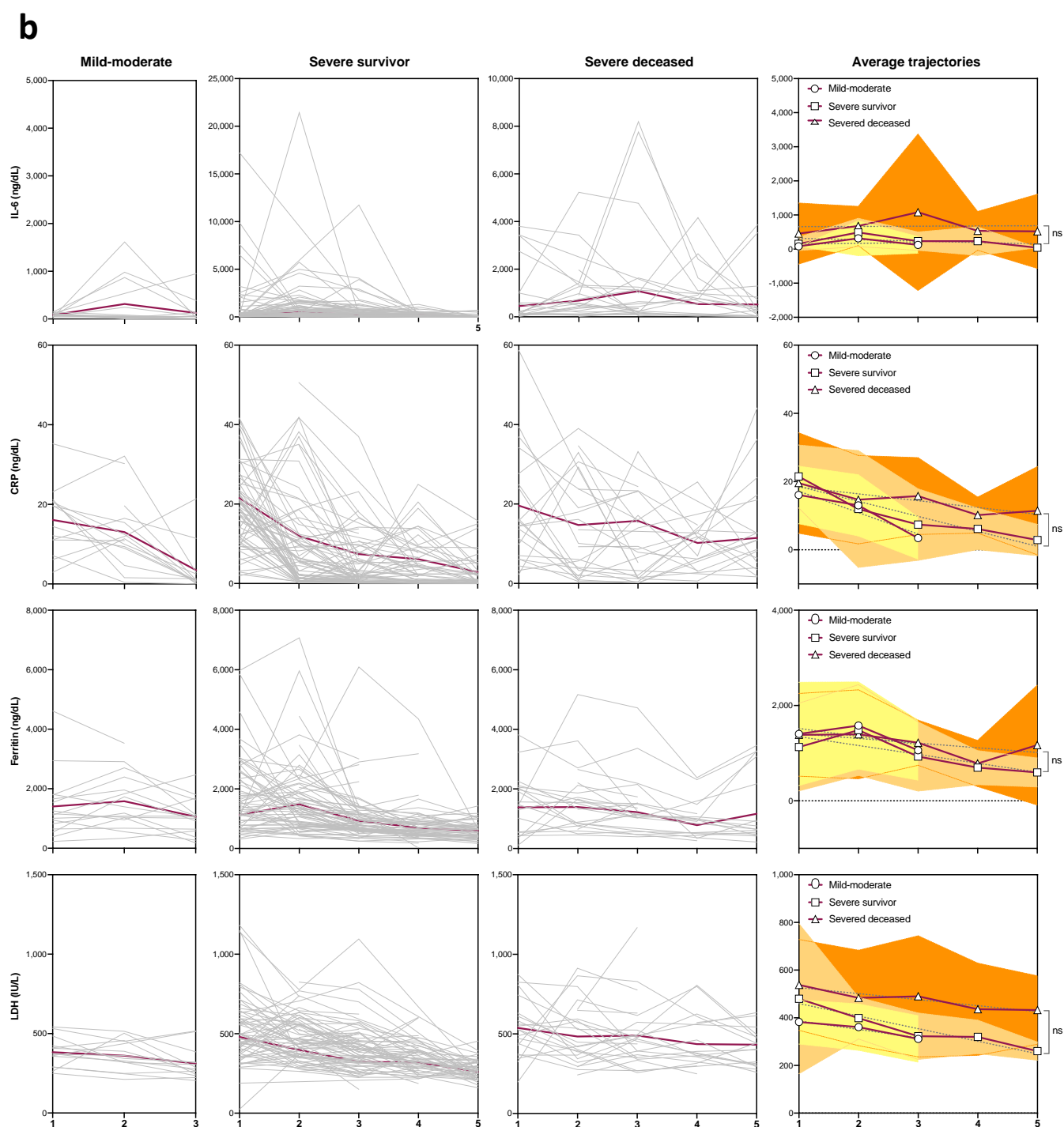


Figure 66. Longitudinal trajectories of biochemical parameters. a) longitudinal determinations (≥ 3 samples per patient collected on separate dates) of biochemical parameters were performed, and trajectories for individual patients (grey lines) and average values (red lines) plotted. A given time-point corresponds to a cluster of days post-admission (± 3 days). Linear regression was applied to average trajectories and the resulting slopes compared for significance between outcome groups by means of two-way ANOVA. **b)** Longitudinal analysis in male patients of serum levels of IL-6, C-reactive protein (CRP), ferritin and lactate dehydrogenase (LDH). For severe survivor and severe deceased outcomes, the trajectories of longitudinal determinations were submitted to linear regression analysis, and the resulting slopes compared for significance by two-way ANOVA. ns denotes not significant.

3.2. Recovery of serum testosterone levels accurately predicts survival in male COVID-19 patients

From the trajectories of each patient, a linear regression analysis was performed, and the slopes the resulting slope values were used in univariate logistic regression analysis to assess the outcome predictive power of the trajectories.

The resulting ROC curves and AUC values, calculated from the slopes of the trajectories, indicated that TST trajectories are remarkably accurate predictors of survival from COVID-19, both in all-survivor vs. deceased (AUC = 0.9281, 95% CI 0.8801 to 0.9761, $p < 0.0001$) and severe survivor vs. deceased (AUC = 0.9205, 95% CI 0.8664 to 0.9747, $p < 0.0001$) (**Figure 67**). Lymphocyte counts (or fractions of WBCs) were also highly accurate predictors of outcome, as were neutrophil counts (**Figure 67**). Interestingly, the trajectories of IL-6 or LDH, whose values on admission were predictive of severity and death from COVID-19 in male patients, were not significantly different in these longitudinal comparisons. These results suggest a role for testosterone in deregulation of the immune response in deceased patients, for the observed lymphopenia and neutrophilia.

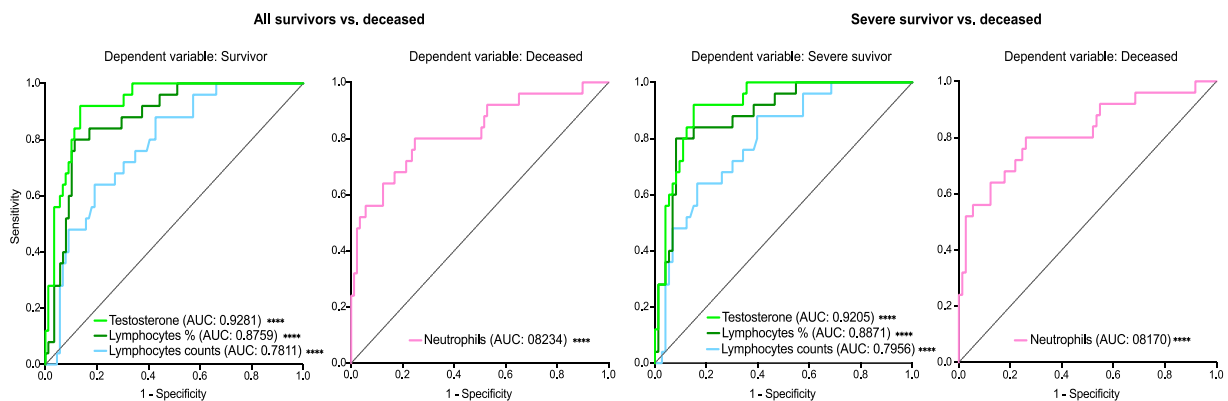


Figure 67. Recovery of serum testosterone levels and blood lymphocyte counts predict survival in male COVID-19 patients. ROC curves and AUC values for longitudinal trajectories (linear regression slopes) of serum testosterone, blood lymphocyte counts (number per mL and % of white blood cells), and blood neutrophils as predictors of survival in comparisons of all surviving vs. deceased.

3.3. TST trajectory slopes correlate with age in severe survivor patients

Age is a predictor of COVID-19 severity. In our cohort of male patients, the testosterone trajectory slopes significantly and inversely correlated with age ($r = -0.3801$, $p < 0.001$) (**Figure 67**). Consistently, most patients with severe deceased outcomes had low or negative testosterone trajectory slopes (**Figure 67**). However, and interestingly, the median age of

patients with severe deceased outcomes was not significantly different from the median age of patients with mild-moderate outcomes, and a substantial proportion of patients with severe survivor outcomes were aged older than 60 (**Figure 68**). Likewise, while the frequency of comorbidities was higher among patients with fatal outcomes as compared with those who survived severe disease, it was not significantly different from the frequency of the moderate outcome group (**Table 22, Figure 61b**).

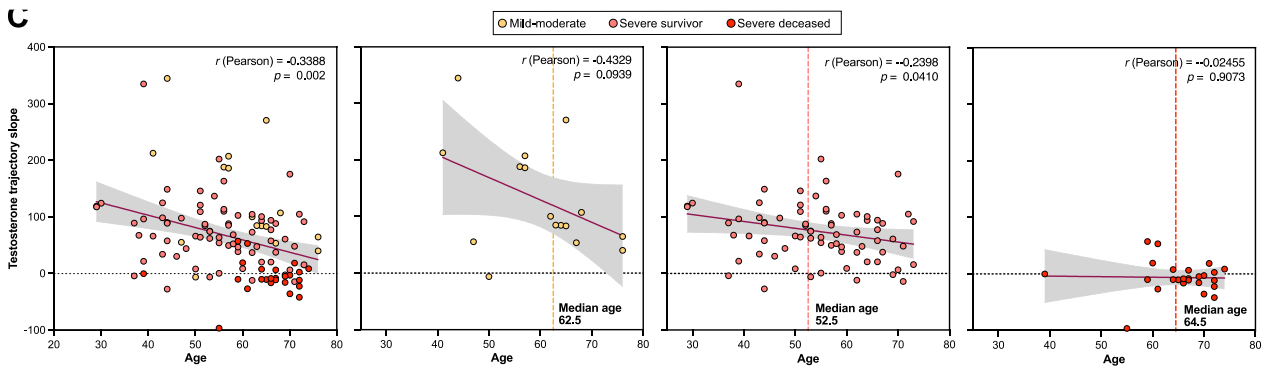


Figure 68. Correlations of age with testosterone trajectory slopes. In all patients with longitudinal analyses (leftmost panel) and in different outcome groups.

Since total serum testosterone (TST) was measured in this study, we asked if the available testosterone (free T) also had the same behavior of TST. Therefore, we were able to calculate the Free T using the Vermeulen method⁴⁰⁷. Similar to TST, free testosterone levels were significantly decreased in severe patients in comparison to the mild-moderate group (**Figure 69**). In addition, serum levels of sex hormone-binding globulin (SHBG), the most abundant circulating testosterone binding protein, showed a significant association of with older age in mild-moderate patients ($p = 0.0237$), but not in severe patients.

These observations suggest that old age, with or without accompanying comorbidities, may impact the ability of a subset of COVID-19 patients to reinstate testosterone production, coupled to a failure to recover from the disease.

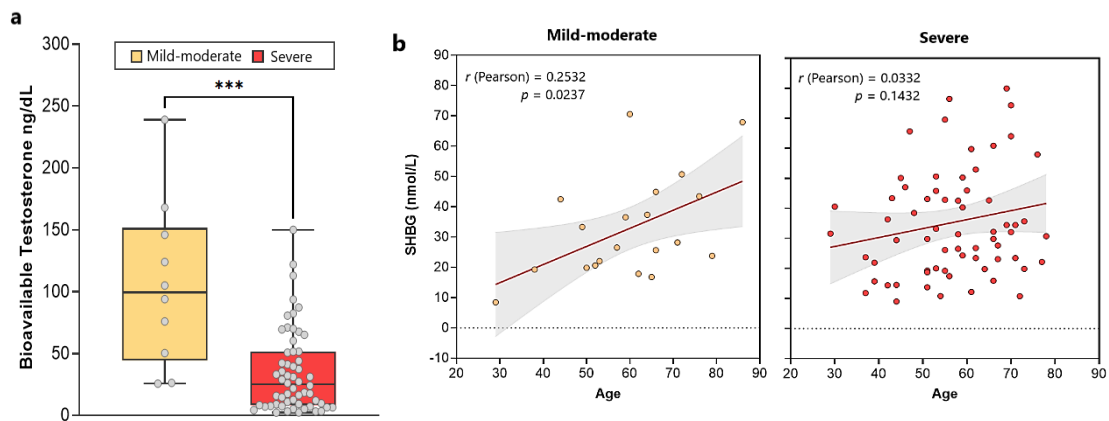


Figure 69. Bioavailable testosterone serum levels and correlation between Age and sex-hormone binding globulin (SHBG) . (a) bioavailable testosterone levels, inferred from SHBG and albumin levels. There is a significant difference ($p = 0.0002$, Mann-Whitney test) between severe and mild-moderate outcomes.) . (b) Values for serum SHBG levels from 86 male patients were plotted against age. Significant correlation was observed for patients with mild-moderate ($r^2=0.2532$ $p=0.0237$) but not severe outcomes

3.4. The LH-androstenedione axis is not significantly perturbed in male COVID-19 patients

Testosterone is synthesized from androstenedione in the Leydig cells of the testis under the stimulus of luteinizing hormone (LH), secreted from the anterior portion of the pituitary gland. The observed critical decline in circulating testosterone levels in male COVID-19 patients suggests the occurrence of a transient (survivor outcomes) or sustained (fatal outcomes) hypogonadism following the onset of COVID-19. To address potential mechanisms explaining the observed failure to recover circulating testosterone levels in fatal COVID-19, we determined circulating LH and androstenedione levels in a longitudinal series of samples in a patient subcohort for which the testosterone trajectories had been concomitantly determined. The median levels of LH fell within normal ranges, independent of patient outcome (**Figure 70a**). Similarly, longitudinal LH trajectories were not significantly different between patients in the survivor vs. deceased outcomes, in stark contrast with the strongly divergent testosterone trajectories (**Figure 70b**). Nevertheless, LH levels determined in the last of the longitudinal samples showed a decline in the deceased outcome group as compared to the severe survivor group, although without reaching the statistical significance. On the other hand, although androstenedione levels fell within normal ranges in the majority of patients in all outcome groups and throughout the longitudinal analysis (**Figure 70a, b**), deceased patients showed increased levels as compared to the survivor outcome groups, without a concomitant increase in testosterone

levels (**Figure 70a**). As such, the failure to recover physiological levels of testosterone in patients with fatal outcomes, in spite of LH and androstenedione levels within normal ranges, and the lack of rise in LH expected with low circulating testosterone, suggest the development of a combined central and peripheral (Leydig cell failure) malfunction in the biosynthesis of testosterone in these patients.

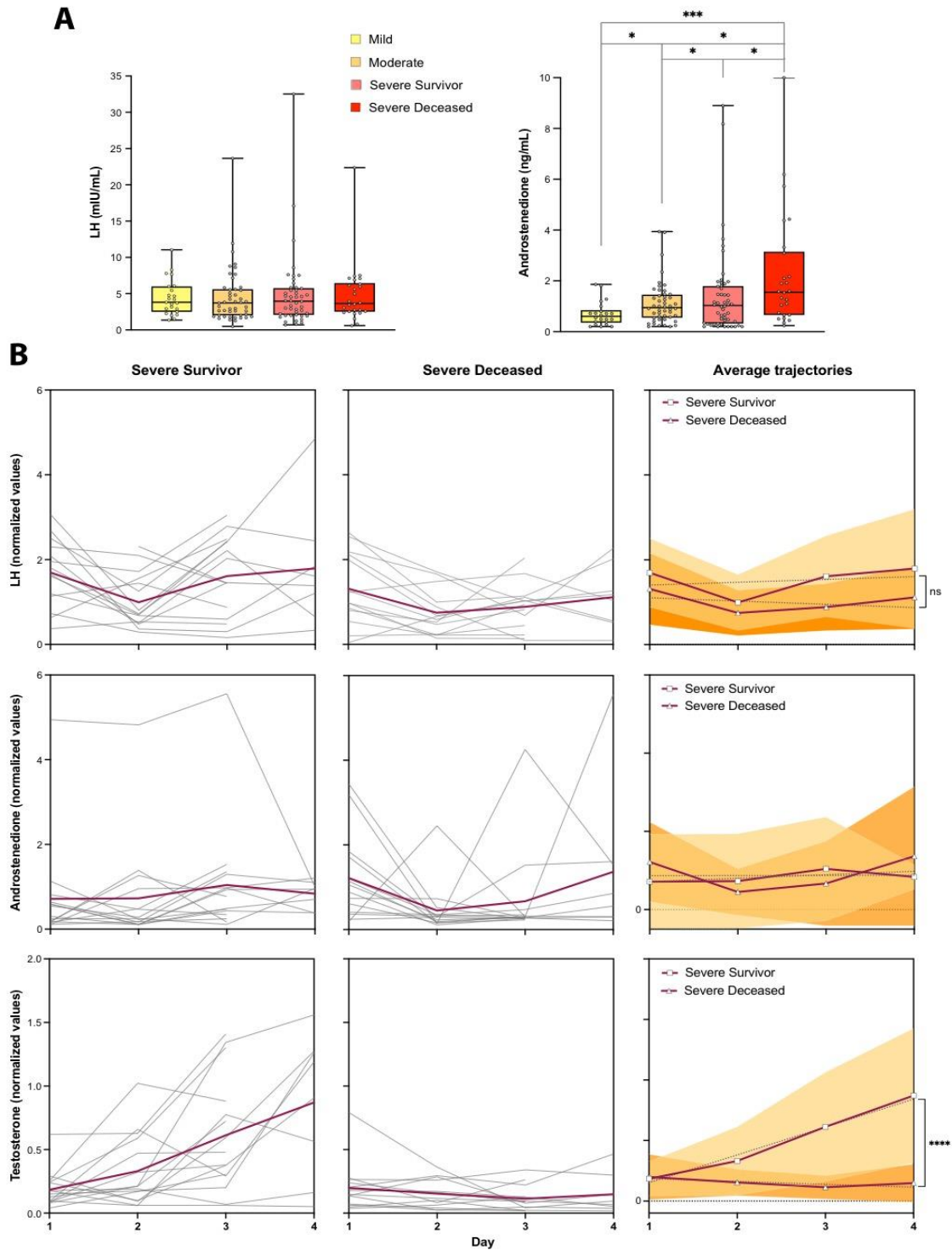


Figure 70. Description in the next page.

Figure 70. The luteinizing hormone (LH)-androstenedione axis is not significantly perturbed in male COVID-19 patients. a) Determinations of serum LH and androstenedione levels in samples collected at admission, grouped by eventual outcomes. Pair-way between-group comparisons were performed by t test. **b)** Longitudinal determinations (≥ 3 samples) of serum LH, androstenedione, and testosterone levels, analyzed as in Fig. 3. Comparisons of trajectories (linear regression slopes) were performed by two-way ANOVA

4. Immunophenotyping in COVID-19 male outcomes

4.1. Lethal male COVID-19 is associated with a depletion of circulating T helper cells

Several studies have found substantial differences in immune responses to SARS-CoV-2 between male and female patients^{413,414}, although the mechanisms underlying these differences are still unclear. In order to address the relationship between testosterone trajectories, outcome, and immune status in male patients, we analyzed circulating immune subpopulation repertoires in a subset of our patient cohort, in at least two independent determinations, separated by 5–20 days. These analyses point to a correlation between immune subpopulations, outcome, and testosterone levels both in a first determination near admission date (Sample 1) and a subsequent analysis of samples near discharge or death (Sample 2), with some subpopulations showing remarkable shifts between Sample 1 and Sample 2 in their correlations with outcome (**Figure 71a-b**). As such, Sample 1 determinations demonstrated relatively few changes in immune cell repertoires between surviving and deceased patients. In stark contrast, a subsequent determination (Sample 2) showed a coordinated depletion of T helper subpopulations in association with death, along with changes in natural killer (CD56+brightCD16- and CD56+dimCD16+) and monocyte subpopulations (**Figure 71a**). The subpopulations with the most significant changes in relative abundance as a function of outcome tended to correlate with serum testosterone levels sampled in the same period (1–3 days from sampling for immune repertoire analyses) (**Figure 71a**). These correlations were more evident in multivariate correlation analyses, particularly for Sample 2 (**Figure 71b**). These analyses show a generalized loss of representation of circulating differentiated and polarized T helper subpopulations in deceased patients (Th1, Th17, Th1- Th17, Th2, central memory CD4+, effector memory CD4+, CD4+ TEMRA) compared to surviving patients, accompanied with a reciprocal increased representation of undifferentiated CD4+ cells (recent thymus emigrant CD4+, naïve CD4+) (**Figure 71b-d**). They also point to an association of monocyte differentiation

with outcome, with a predominant correlation with non-classical monocytes in moderate and severe survivor patients and, conversely, with significantly more pro-inflammatory⁴¹⁵ classical monocytes in deceased patients (**Figure 71b-d**).

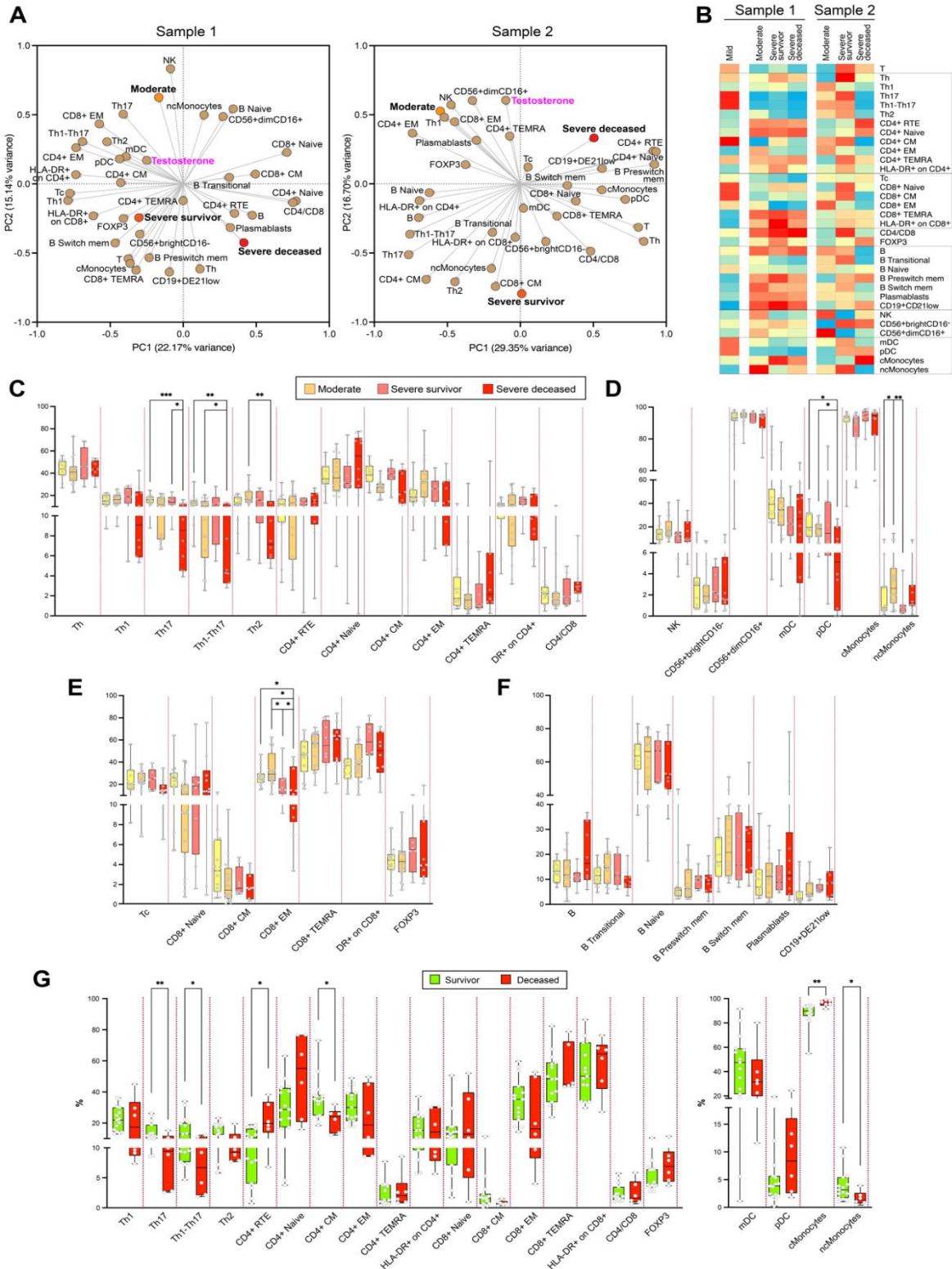


Figure 71. Description in the next page.

Figure 71. Immune switch during the course of disease in severe and deceased patients, as determined by multiparameter profiling of circulating immune cells. **A)** PCA of samples analyzed near admission (Sample 1, left panel) and near discharge or death (Sample 2, right panel). Mild, moderate, severe survivor, and severe deceased outcomes were assigned values 1, 2, 3, and 4, respectively. Serum testosterone values of samples collected in the same or nearby dates (± 3 days) were included in the analysis. The indicated immune subpopulations are defined by cell-surface markers and determined by spectral flow cytometry (Materials and methods). **B)** Heatmap of correlation coefficients between immune subpopulation values and outcomes, for near-admission (Sample 1, left Heatmap) and near-discharge/death (Sample 2, right Heatmap) samples. Spearman multivariate correlation analyses were performed for all parameters vs. outcomes, the resulting coefficients normalized for each column (range, 0 to 1) and used to build heatmaps. **C–F)** Between-outcome comparisons of immune cell subpopulation: CD4+ (**C**); natural killer, dendritic, and monocyte (**D**); CD8+ (**E**); and B (**F**) cell subpopulations. **G)** Survivor (mild, moderate, severe survivor) vs. deceased patient comparisons for T cell (CD4+ and CD8+) and dendritic cells and monocytes. Such comparisons were not significant for other immune subpopulations (B cells, NK cells)

There are additional associations of cytotoxic T cell or B cell subpopulations with lethal COVID-19 (**Figure 71d-f**), albeit without reaching statistical significance. These correlations were made more evident when comparing all surviving patients (moderate and severe survivor) with deceased patients (**Figure 71g**) and further illustrated by flow cytometry histograms of representative cases (**Figure 72**).

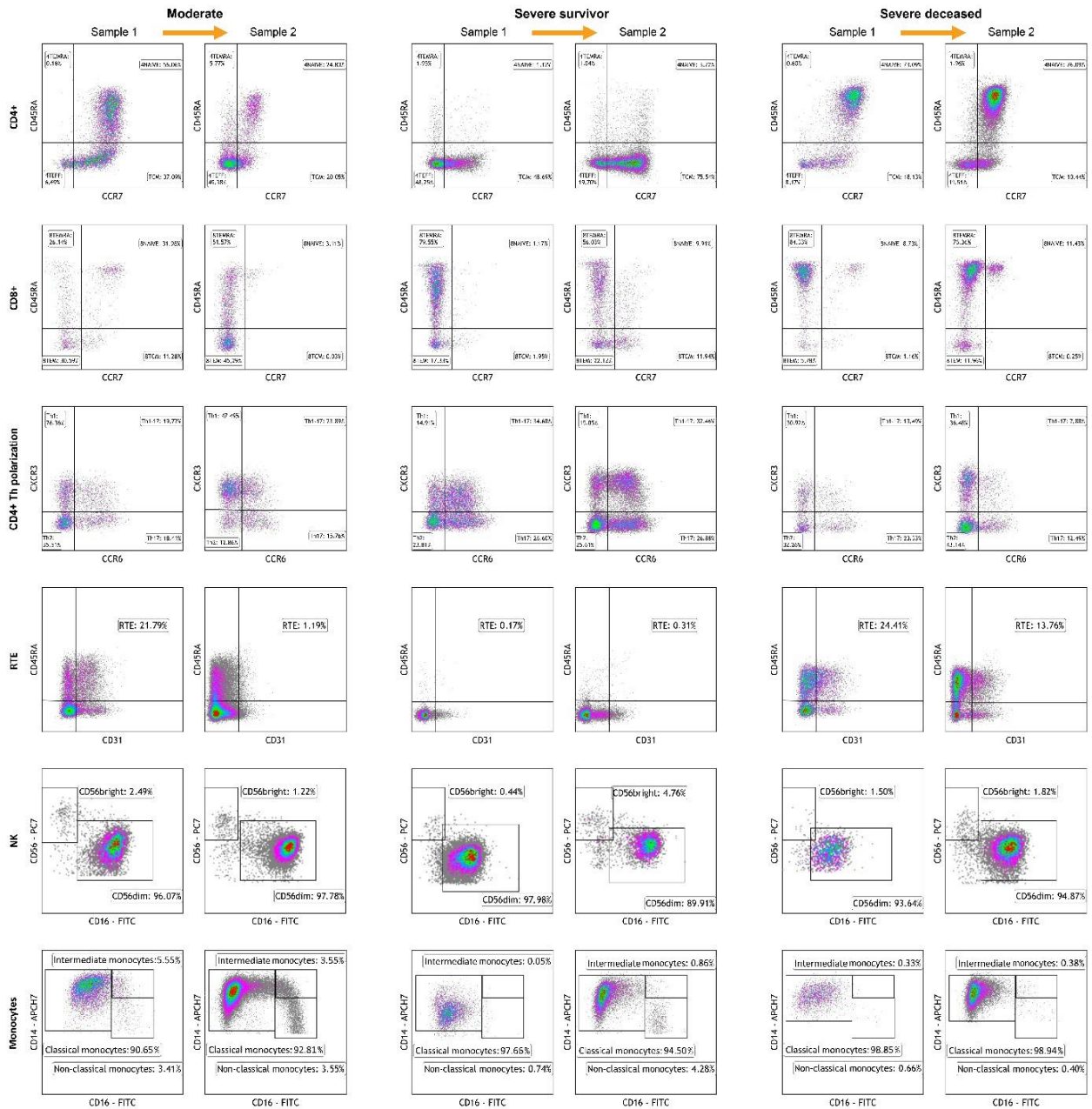


Figure 72. Flow cytometry of representative cases of male patients with COVID-19. For each case, Sample 1 corresponds to the first available analysis post-admission, and Sample 2 corresponds to a subsequent analysis, separated from Sample 1 by 6-12 days. CD4+ and CD8+ subpopulations were further segmented into the indicated subpopulations by analyzing for CD45RA and CCR7 expression. CD3+ subpopulations were further segmented into subpopulations by analyzing the expression of the polarization markers CXCR3 and CCR6. Recent thymic emigrant (RTE) populations were identified and scored through the expression of CD3, CD45RA and CD31. Natural killer (NK) cell subpopulations were segmented by analyzing the expression of CD56 and CD16. Monocyte subpopulations were segmented by analyzing the expression of CD14 and CD16. Not shown are B cell and dendritic cell subpopulations, which did not show significant shifts in repertoire between outcomes and longitudinal sampling. 4TEFF, 4TCM, 4TEMRA, 8TEFF, 8TCM, 8TEMRA: CD4+ or CD8+ effector, central memory or T effector memory re- expressing CD45RA, respectively.

CHAPTER II: DISCUSSION

CHAPTER II - DISCUSSION

Numerous studies have identified prognostic markers able to discern severe COVID-19 patients, including older age, male sex, co-morbidities such as obesity, diabetes, or cardiovascular disease, elevated circulating markers of inflammation, lymphopenia, neutrophilia^{391,410–412,416} or the presence of autoantibodies to class-I interferons⁴¹⁷. Nomograms or scores that combine several independent parameters have been proposed as predictors of COVID-19 outcome^{392,410}. However, relatively few studies have addressed sex differences in predictive markers of disease outcome^{404,410,418–420}.

Interestingly, inflammation markers, but not co-morbidities, BMI, or age, have been found to be associated with outcome differences between male and female COVID-19 patients⁴²⁰. Our comparative analysis of biochemical and hematological parameters has revealed that both sexes share markers with significant predictive power of disease outcome, including IL-6, LDH, D-dimer, lymphopenia, and neutrophilia. Nevertheless, the levels of these markers, and the strength of their predictive power, are consistently higher in male patients as compared to female patients. This becomes more evident when evaluating predictive markers of lethal COVID-19, which yields IL-6 and lymphocyte (percentage of total WBC) as the only two significantly predictive markers shared in both male and female patients. Other significant markers predictive of lethal COVID-19 in male but not female patients are LDH levels, neutrophilia, and absolute lymphocyte counts, in addition to testosterone levels, which are exclusively masculine in our patient cohorts. Furthermore, we found significant and direct correlations between testosterone levels, lymphocytes, and neutrophils, suggesting a role for testosterone in aberrant immune responses in deceased patients. These observations suggest that male COVID-19 patients with severe and lethal disease suffer from more deleterious underlying pathogenic and inflammatory processes than female patients with comparable clinical severity³⁹², a situation also observed in other respiratory viral infections^{397,421}. Our baseline analysis reveals that critically low serum testosterone levels in male patients are a risk factor for severe COVID-19, along with other factors predictive of severity that are in line with prior evidence^{410–412}. We have also found that male COVID-19 patients with a higher risk of progression to a severe critical disease present higher level of inflammatory markers (serum IL-6, blood neutrophil counts) and tissue damage (LDH), and more marked lymphopenia³⁹², as compared to age-matched female patients. Interestingly, markers of inflammation (IL-6, CRP) or tissue damage (LDH), with good outcome predictive power in admission sample determinations, lost their

predictive power in longitudinal analyses in male patients, collected up to the time of discharge or death. In contrast, testosterone levels, whose determinations on admission provided a relatively modest outcome predictive power, corroborating other studies^{404,405,422}, gained remarkable levels of significance when analyzed longitudinally. The AUC values of ROC curves in logistic regression analyses (mild-moderate vs. severe: 0.9281, 95% CI 0.7216 to 0.9252, $p < 0.0001$; severe survivor vs. deceased: 0.9205, 95% CI 0.8664 to 0.9747, $p < 0.0001$) indicate that serum testosterone trajectories in longitudinal determinations constitute, to the best of our knowledge, the most accurate independent predictors of disease outcome in male COVID-19 patients described thus far. Furthermore, longitudinal trajectories of lymphocyte and neutrophil counts also yield highly significant predictions of disease outcome. Other biochemical parameters indicative of pathological inflammatory or pro-coagulant states, such as elevated IL-6, CRP, or D-dimer levels, eventually return to near-physiological levels in both survivors and patients with fatal outcomes. This has been observed in other studies^{420,423} and suggests that the normalization of these factors is insufficient, per se, to abate the pathological hyperinflammation and hypercoagulation accompanying severe COVID-19 with a fatal outcome, which might require the concomitant alleviation of lymphopenia and neutrophilia. On the other hand, although different stimuli and conditions such as mechanical ventilation, muscle immobilization, severe sepsis, and multiple organ dysfunction as well as neuro/myotoxic agents may contribute to a critical status among patients admitted to ICU⁴²⁴, all severe patients in our study, with either survivor or deceased outcomes, were under comparable pharmacological and physical management (Tables T3 A and B), and thus, these factors are unlikely to contribute to the differential outcomes in this study.

We have found that testosterone trajectories are not paralleled by changes in circulating LH or androstenedione trajectories expected in the presence of functioning physiological feedback loops. This could be explained by an inhibition of the LH-androstenedione axis, which has been associated with non-specific critical illness⁹ and the deleterious action on the hypophysis of inflammatory cytokines⁴²⁵. A second possible mechanism may involve infection and damage by SARS-CoV-2 of ACE2- expressing testicular cells, mainly Leydig cells^{426,427}. In the first scenario, acute declines in LH and androstenedione levels would be expected, while in the latter scenario, they would be either unaffected or increased for LH due to a negative feedback loop with testosterone⁹. However, we observed that LH levels showed a slight decline in deceased patients, while androstenedione levels were

increased. It should be noted that circulating androstenedione is produced mostly by adrenal glands²⁵⁸ and its synthesis might be affected by the corticosteroids used to treat these patients (Table T3B), which may block the endogenous production of cortisol, corticosterone, and aldosterone²⁵⁸. Therefore, a likely mechanism to explain the failure of patients with fatal outcomes to recover their physiological levels of testosterone, combined with normal androstenedione levels and a lack of rise in LH, suggests a malfunction of the testosterone-LH feedback loop. As such, an irreversible damage of Leydig cells⁴²⁸ in patients with fatal outcomes could explain these observations, while a resolution of viral infection would explain the recovery of a normal production of testosterone in survivors. Another relevant factor associated with late-onset hypogonadism⁴²⁹, as well as with an irreversible failure to reinstate testosterone production after critical situations that may compromise the LH-androstenedione axis, is old age⁴³⁰, which has been linked to senescent dysfunction of Leydig cells⁴³¹. The fact that a majority of non-survivor patients in our study who failed to reinstate testosterone levels are older than 60 years of age would be consistent with the senescence hypothesis. However, our cohort has more patients older than 60 who reinstated their testosterone levels and survived severe COVID-19. Therefore, either Leydig cell senescence only affects a small subset of older patients or other mechanisms may be invoked to explain failure to restore testosterone production. Conversely, these observations also suggest that while the reinstatement of physiological testosterone levels may be mechanistically linked to a return to lymphocyte and neutrophil homeostasis, it may not be required for the relative normalization of other inflammatory pathways, arguably driven by an unmitigated production of IL-6 and other pro-inflammatory cytokines triggered by acute viral infection⁴³². Our observations suggest that sufficient and timely resolution of pathogenic hyperinflammation to prevent a lethal outcome may require the additional return to homeostasis of innate and/or adaptive immune cell dynamics and function, possibly assisted in male patients by the reinstatement of testosterone production.

There is now a wealth of studies describing the dynamics of immune responses to acute and subacute infection with SARS-CoV-2, including multiparameter and functional analyses of circulating and tissue-associated innate and adaptive immune subpopulations^{433,434}. Some of these studies have addressed sex differences in such responses^{383,422}. Our analysis in male patients indicates an association of specific immune subpopulations with COVID-19 outcome and a shift of such associations from early (Sample 1) to late (Sample 2) time-points in the course of the disease. For example, the relative representation of differentiated (CD8+

TEMRA, CD4+TEMRA) and activated (HLA-DR+ on CD4+and onCD8+) T cell subpopulations and differentiating B cells modestly correlated with all outcomes except mild disease in Sample 1. This indicates an ongoing early immune response of similar nature and magnitude, regardless of final outcome, as reported by others⁴³³. In this phase, non-classical monocytes are more prevalent than classical monocytes in patients with a moderate outcome, while patients with severe survivor and severe deceased outcomes show a predominance of more inflammatory classical monocytes⁴³⁵, in support of a more inflammatory state of these patients, as also evidenced by the clinical biochemical and hematological parameters discussed above. However, later in the course of disease (Sample 2), a remarkable shift takes place, in particular regarding correlations with severe survivor as compared to severe deceased patients. As such, while patients with severe survivor outcomes show positive correlations with differentiated (CD4+TEMRA, CD8+TEMRA), activated (HLA-DR+ on CD4+ and on CD8+), and memory (CD4+ central memory, CD8+ central memory) T cell subpopulations, patients with eventual fatal outcomes evidence a depletion of these subpopulations, along with an accumulation of undifferentiated T helper cells (recent thymic emigrant CD4+ and naïve CD4+).

This late shift also affects innate immune populations, as severe survivor patients correlate with non-classical monocytes over classical monocytes, while the reverse is the case for severe deceased patients. Similar observations have been made by others in studies correlating innate⁴³³ and adaptive⁴³⁶ immune cell subpopulations to COVID-19 outcome. Importantly, our study additionally correlates relative representations of immune subpopulations to testosterone levels. Thus, higher testosterone levels in Sample 1 are correlated to polarized (Th1, Th17, Th1-17, Th2) and differentiated (effector memory CD4+, central memory CD4+, CD8+ TEMRA) T cell subpopulations. In Sample 2, testosterone levels correlate to a similar range of subpopulations, along with plasmablasts and mature NK cells (CD16+dimCD16+). These temporal switches in the differentiation profiles of distinct immune subpopulations may suggest that in patients with lethal outcomes, there may be a defective differentiation of T helper cells⁴³⁷ and monocytes. A second possible explanation of the apparent depletion of circulating differentiated and polarized cells may be an enhanced clearance or migration from circulation to peripheral tissues⁴³⁸. Finally, specific subpopulations may become exhausted in late stages of the disease⁴³⁹⁻⁴⁴¹. These three putative mechanisms are not mutually exclusive and may take place either simultaneously or dynamically at different time points along the clinical course of the

patients. Notably, very recent studies recognize T cell apoptosis and depletion as a feature defining severe COVID-19⁴⁴¹. The observed concordance of lethal outcome in male COVID-19 patients with (i) persistent lymphopenia and neutrophilia, (ii) depletion of circulating differentiated T helper and T cytotoxic cells and non-classical monocytes, (iii) accumulation of undifferentiated immune counterparts, and (iv) failure to reinstate physiological levels of testosterone, mirrored by converse phenotypes in severe survivor patients who have undergone equivalent critical illness and management, makes it appealing to hypothesize a mechanistic relationship bonding these coincident phenotypes. Relevantly, sex hormones have a profound influence on innate and adaptive immune system development, differentiation, and response to challenge^{383,442,413,436,414}. More specifically, androgens have a global anti-inflammatory effect^{443,444}, reflected in higher frequencies of autoimmune diseases in women or in acquired or genetically determined hypogonadism³⁹⁹, as compared to men with a normal XY chromosome complement. On the other hand, testosterone replacement therapy in hypogonadal men attenuates inflammation⁴⁴⁵ and androgens suppress thymic precursor development⁴⁴⁶ and promote the terminal differentiation of T cell subpopulations⁴⁴⁷ and monocyte precursors⁴⁴⁸. Conversely, androgen deprivation through surgical or pharmacological castration in animal models prompts the regeneration of the thymus in aged mice, leading to a relative accumulation of undifferentiated T cell populations (RTE and naïve T cells)⁴⁴⁹ and classical monocytes⁴⁵⁰. A similar effect of androgen deprivation on T cell development and differentiation has been observed in prostate cancer patients, with an expansion of RTE and naïve T cells, particularly among CD4+ cells^{451,449}.

CHAPTER II: CONCLUSIONS

CHAPTER II – CONCLUSIONS

1. The recovery of serum testosterone in male patients with COVID-19 strongly associates with patient survival, making it an accurate predictor of COVID-19 progression.
2. Lethal outcome in males correlates with (i) lymphopenia and neutrophilia (ii) depletion of circulating differentiated T helper - T cytotoxic cells and non-classical monocytes (iii) accumulation of undifferentiated immune counterparts.
3. The tight association observed between reinstatement of testosterone and survival from COVID-19 in male patients, along with a reversal of signs of excessive inflammation and immune dysfunction, suggests potential functional role for testosterone

REFERENCES

REFERENCES

1. Tilley, S. K. & Fry, R. C. Chapter 10 - Hormone Response Pathways as Responders to Environmental Contaminants and Their Roles in Disease. in *Systems Biology in Toxicology and Environmental Health* (ed. Fry, R. C.) 225–238 (Academic Press, 2015). doi:10.1016/B978-0-12-801564-3.00010-9.
2. Aleksandrova, K. V. *et al.* Biochemistry of Hormones. (Module 2, IV Semester). (2015).
3. Rezzani, R., Franco, C., Hardeland, R. & Rodella, L. Thymus-Pineal Gland Axis: Revisiting Its Role in Human Life and Ageing. *International Journal of Molecular Sciences* **21**, 8806 (2020).
4. Nussey, S. & Whitehead, S. *Endocrinology: An Integrated Approach*. (BIOS Scientific Publishers, 2001).
5. Micevych, P. E. & Kelly, M. J. Membrane Estrogen Receptor Regulation of Hypothalamic Function. *Neuroendocrinology* **96**, 103–110 (2012).
6. Soltysik, K. & Czekaj, P. Membrane estrogen receptors - is it an alternative way of estrogen action? *J Physiol Pharmacol* **64**, 129–142 (2013).
7. Prossnitz, E. R., Arterburn, J. B. & Sklar, L. A. GPR30: a G protein-coupled receptor for estrogen. *Mol Cell Endocrinol* **265–266**, 138–142 (2007).
8. Kleine, B. & Rossmannith, W. G. *Hormones and the Endocrine System: Textbook of Endocrinology*. (Springer International Publishing, 2016). doi:10.1007/978-3-319-15060-4.
9. Téblick, A., Langouche, L. & Van den Berghe, G. Anterior pituitary function in critical illness. *Endocr Connect* **8**, R131–R143 (2019).
10. Luis, D. & Annane, D. The neuroendocrine response to critical illness. in *Brain Disorders in Critical Illness: Mechanisms, Diagnosis, and Treatment* (eds. Ely, E. W., Stevens, R. D. & Sharshar, T.) 181–191 (Cambridge University Press, 2013). doi:10.1017/CBO9781139248822.022.
11. Preiser, J.-C., Ichai, C., Orban, J.-C. & Groeneveld, A. B. J. Metabolic response to the stress of critical illness. *British Journal of Anaesthesia* **113**, 945–954 (2014).
12. Boonen, E. & Van den Berghe, G. Endocrine Responses to Critical Illness: Novel Insights and Therapeutic Implications. *The Journal of Clinical Endocrinology & Metabolism* **99**, 1569–1582 (2014).
13. Somasundaram, N. P. & Gunatilake, S. S. C. Infections in Endocrinology: Viruses. in *Endotext* (eds. Feingold, K. R. *et al.*) (MDText.com, Inc., 2000).
14. Harding, A. T. & Heaton, N. S. The Impact of Estrogens and Their Receptors on Immunity and Inflammation during Infection. *Cancers (Basel)* **14**, 909 (2022).
15. Faurschou, M. & Borregaard, N. Neutrophil granules and secretory vesicles in inflammation. *Microbes and Infection* **5**, 1317–1327 (2003).
16. Hampton, M. B., Kettle, A. J. & Winterbourn, C. C. Inside the neutrophil phagosome: oxidants, myeloperoxidase, and bacterial killing. *Blood* **92**, 3007–3017 (1998).
17. Josefsson, E., Tarkowski, A. & Carsten, H. Anti-inflammatory properties of estrogen: I. In vivo suppression of leukocyte production in bone marrow and redistribution of peripheral blood neutrophils. *Cellular Immunology* **142**, 67–78 (1992).
18. Delyani, J. A., Murohara, T., Nossuli, T. O. & Lefer, A. M. Protection from Myocardial Reperfusion Injury by Acute Administration of 17 β -Estradiol. *Journal of Molecular and Cellular Cardiology* **28**, 1001–1008 (1996).

19. Gagliano-Jucá, T. *et al.* Differential effects of testosterone on circulating neutrophils, monocytes, and platelets in men: Findings from two trials. *Andrology* **8**, 1324–1331 (2020).
20. Chuang, K.-H. *et al.* Neutropenia with impaired host defense against microbial infection in mice lacking androgen receptor. *J Exp Med* **206**, 1181–1199 (2009).
21. Miller, L. & Hunt, J. S. Sex steroid hormones and macrophage function. *Life Sci* **59**, 1–14 (1996).
22. Cutolo, M. *et al.* Androgen and estrogen receptors are present in primary cultures of human synovial macrophages. *J Clin Endocrinol Metab* **81**, 820–827 (1996).
23. Chatterton, R. T. Functions of dehydroepiandrosterone in relation to breast cancer. *Steroids* **179**, 108970 (2022).
24. Takeda, K. & Akira, S. Toll-like receptors. *Curr Protoc Immunol* **109**, 14.12.1-14.12.10 (2015).
25. Rettew, J. A., Huet, Y. M. & Marriott, I. Estrogens Augment Cell Surface TLR4 Expression on Murine Macrophages and Regulate Sepsis Susceptibility in Vivo. *Endocrinology* **150**, 3877–3884 (2009).
26. Calippe, B. *et al.* 17Beta-estradiol promotes TLR4-triggered proinflammatory mediator production through direct estrogen receptor alpha signaling in macrophages in vivo. *J Immunol* **185**, 1169–1176 (2010).
27. Wichmann, M. W., Ayala, A. & Chaudry, I. H. Male sex steroids are responsible for depressing macrophage immune function after trauma-hemorrhage. *Am J Physiol* **273**, C1335-1340 (1997).
28. Rettew, J. A., Huet-Hudson, Y. M. & Marriott, I. Testosterone reduces macrophage expression in the mouse of toll-like receptor 4, a trigger for inflammation and innate immunity. *Biol Reprod* **78**, 432–437 (2008).
29. Zhang, X. *et al.* Estrogen inhibits lipopolysaccharide-induced tumor necrosis factor-alpha release from murine macrophages. *Methods Find Exp Clin Pharmacol* **23**, 169–173 (2001).
30. Carruba, G. *et al.* Estrogen regulates cytokine production and apoptosis in PMA-differentiated, macrophage-like U937 cells. *J Cell Biochem* **90**, 187–196 (2003).
31. Wilcoxon, S. C., Kirkman, E., Dowdell, K. C. & Stohlman, S. A. Gender-dependent IL-12 secretion by APC is regulated by IL-10. *J Immunol* **164**, 6237–6243 (2000).
32. Straub, R. H. *et al.* Hormone replacement therapy and interrelation between serum interleukin-6 and body mass index in postmenopausal women: a population-based study. *J Clin Endocrinol Metab* **85**, 1340–1344 (2000).
33. Girasole, G. *et al.* 17 beta-estradiol inhibits interleukin-6 production by bone marrow-derived stromal cells and osteoblasts in vitro: a potential mechanism for the antiosteoporotic effect of estrogens. *J Clin Invest* **89**, 883–891 (1992).
34. Su, C., Chen, M., Huang, H. & Lin, J. Testosterone enhances lipopolysaccharide-induced interleukin-6 and macrophage chemotactic protein-1 expression by activating the extracellular signal-regulated kinase 1/2/nuclear factor- κ B signalling pathways in 3T3-L1 adipocytes. *Molecular Medicine Reports* **12**, 696–704 (2015).
35. Karpuzoglu, E., Phillips, R. A., Gogal, R. M. & Ansar Ahmed, S. IFN-gamma-inducing transcription factor, T-bet is upregulated by estrogen in murine splenocytes: role of IL-27 but not IL-12. *Mol Immunol* **44**, 1808–1814 (2007).
36. Kissick, H. T. *et al.* Androgens alter T-cell immunity by inhibiting T-helper 1 differentiation. *Proc Natl Acad Sci U S A* **111**, 9887–9892 (2014).

37. Henze, L., Schwinge, D. & Schramm, C. The Effects of Androgens on T Cells: Clues to Female Predominance in Autoimmune Liver Diseases? *Front Immunol* **11**, 1567 (2020).
38. Cai, Y., Zhou, J. & Webb, D. C. Estrogen Stimulates Th2 Cytokine Production and Regulates the Compartmentalisation of Eosinophils during Allergen Challenge in a Mouse Model of Asthma. *International Archives of Allergy and Immunology* **158**, 252–260 (2012).
39. Hepworth, M. R., Hardman, M. J. & Grecis, R. K. The role of sex hormones in the development of Th2 immunity in a gender-biased model of *Trichuris muris* infection. *Eur J Immunol* **40**, 406–416 (2010).
40. Cattrini, C. *et al.* Sex Hormones and Hormone Therapy during COVID-19 Pandemic: Implications for Patients with Cancer. *Cancers* **12**, 2325 (2020).
41. Hanahan, D. & Weinberg, R. A. The Hallmarks of Cancer. *Cell* **100**, 57–70 (2000).
42. Hornberg, J. J., Bruggeman, F. J., Westerhoff, H. V. & Lankelma, J. Cancer: A Systems Biology disease. *Biosystems* **83**, 81–90 (2006).
43. Key, T. J. A. Hormones and cancer in humans. *Mutation Research/Fundamental and Molecular Mechanisms of Mutagenesis* **333**, 59–67 (1995).
44. Israel, L. & Band, P. HORMONES AS CANCER GROWTH FACTORS. *The Lancet* **324**, 843–844 (1984).
45. Ahmad, N. & Kumar, R. Steroid hormone receptors in cancer development: A target for cancer therapeutics. *Cancer Letters* **300**, 1–9 (2011).
46. Arnesen, S. *et al.* Estrogen Receptor Alpha Mutations in Breast Cancer Cells Cause Gene Expression Changes through Constant Activity and Secondary Effects. *Cancer Res* **81**, 539–551 (2021).
47. Dai, Z. *et al.* Genetic polymorphisms of estrogen receptor genes are associated with breast cancer susceptibility in Chinese women. *Cancer Cell Int* **19**, 11 (2019).
48. Allahloubi, N. M. A. *et al.* Estrogen Receptor Gene Polymorphism as a Possible Genetic Risk Factor for Treatment Response in ER-Positive Breast Cancer Patients. *Biochem Genet* **60**, 1963–1985 (2022).
49. Han, R. *et al.* Estrogen promotes progression of hormone-dependent breast cancer through CCL2-CCR2 axis by upregulation of Twist via PI3K/AKT/NF- κ B signaling. *Sci Rep* **8**, 9575 (2018).
50. Watts, E. L. *et al.* Circulating free testosterone and risk of aggressive prostate cancer: Prospective and Mendelian randomisation analyses in international consortia. *International Journal of Cancer* **151**, 1033–1046 (2022).
51. Hanahan, D. & Weinberg, R. A. Hallmarks of Cancer: The Next Generation. *Cell* **144**, 646–674 (2011).
52. Faubert, B., Solmonson, A. & DeBerardinis, R. J. Metabolic reprogramming and cancer progression. *Science* **368**, eaaw5473 (2020).
53. Nong, S. *et al.* Metabolic reprogramming in cancer: Mechanisms and therapeutics. *MedComm* **4**, e218 (2023).
54. Anderson, N. M. & Simon, M. C. Tumor Microenvironment. *Curr Biol* **30**, R921–R925 (2020).
55. de Visser, K. E. & Joyce, J. A. The evolving tumor microenvironment: From cancer initiation to metastatic outgrowth. *Cancer Cell* **41**, 374–403 (2023).
56. Seyfried, T. N. & Shelton, L. M. Cancer as a metabolic disease. *Nutr Metab (Lond)* **7**, 7 (2010).
57. Liberti, M. V. & Locasale, J. W. The Warburg Effect: How Does it Benefit Cancer Cells? *Trends Biochem Sci* **41**, 211–218 (2016).

58. Beloribi-Djefafia, S., Vasseur, S. & Guillaumond, F. Lipid metabolic reprogramming in cancer cells. *Oncogenesis* **5**, e189–e189 (2016).
59. Harwood, J. L. & Gurr, M. I. *Lipid Biochemistry: An Introduction*. (Springer Science & Business Media, 2013).
60. Jeong, D.-W., Lee, S. & Chun, Y.-S. How cancer cells remodel lipid metabolism: strategies targeting transcription factors. *Lipids in Health and Disease* **20**, 163 (2021).
61. Menendez, J. A. & Lupu, R. Fatty acid synthase and the lipogenic phenotype in cancer pathogenesis. *Nat Rev Cancer* **7**, 763–777 (2007).
62. N, Z., Jv, S. & K, S. ATP-citrate lyase: a key player in cancer metabolism. *Cancer research* **72**, (2012).
63. Kumar, V. L. & Majumder, P. K. Prostate gland: Structure, functions and regulation. *International Urology and Nephrology* **27**, 231–243 (1995).
64. Reeves, F., Everaerts, W., Murphy, D. G. & Costello, A. Chapter 29 - The Surgical Anatomy of the Prostate. in *Prostate Cancer (Second Edition)* (eds. Mydlo, J. H. & Godec, C. J.) 253–263 (Academic Press, 2016). doi:10.1016/B978-0-12-800077-9.00029-3.
65. Oelke, M. Physiology and Pharmacology of the Prostate. in *Urologic Principles and Practice* (eds. Chapple, C. R., Steers, W. D. & Evans, C. P.) 127–150 (Springer International Publishing, 2020). doi:10.1007/978-3-030-28599-9_8.
66. Aaron, L., Franco, O. E. & Hayward, S. W. Review of Prostate Anatomy and Embryology and the Etiology of Benign Prostatic Hyperplasia. *Urol Clin North Am* **43**, 279–288 (2016).
67. Kelly, K. Profiling prostate biology. *Science* **368**, 467–468 (2020).
68. Choi, N., Zhang, B., Zhang, L., Ittmann, M. & Xin, L. Adult murine prostate basal and luminal cells are self-sustained lineages that can both serve as targets for prostate cancer initiation. *Cancer Cell* **21**, 253–265 (2012).
69. Weiner, A. B. *et al.* A novel prostate cancer subtyping classifier based on luminal and basal phenotypes. *Cancer* **129**, 2169–2178 (2023).
70. Karthaus, W. R. *et al.* Regenerative potential of prostate luminal cells revealed by single cell analysis. *Science* **368**, 497–505 (2020).
71. Parimi, V., Goyal, R., Poropatich, K. & Yang, X. J. Neuroendocrine differentiation of prostate cancer: a review. *Am J Clin Exp Urol* **2**, 273–285 (2014).
72. De Torres, I. *et al.* PTOV-1 overexpression in neuroendocrine tumors: a new molecular marker. in *NEUROENDOCRINOLOGY* vol. 92 6–6 (KARGER ALLSCHWILERSTRASSE 10, CH-4009 BASEL, SWITZERLAND, 2010).
73. Beltran, H. *et al.* Molecular characterization of neuroendocrine prostate cancer and identification of new drug targets. *Cancer Discov* **1**, 487–495 (2011).
74. van Leenders, G. J. L. H. *et al.* Intermediate Cells in Human Prostate Epithelium Are Enriched in Proliferative Inflammatory Atrophy. *Am J Pathol* **162**, 1529–1537 (2003).
75. Wang, Y., Hayward, S., Cao, M., Thayer, K. & Cunha, G. Cell differentiation lineage in the prostate. *Differentiation* **68**, 270–279 (2001).
76. Flint, M., McAlister, D., Agarwal, A. & Du Plessis, S. Male accessory sex glands: structure and function. in *Mammalian Endocrinology and Male Reproductive Biology* (CRC Press, 2015).
77. Hayward, S. W. & Cunha, G. R. THE PROSTATE: DEVELOPMENT AND PHYSIOLOGY. *Radiologic Clinics of North America* **38**, 1–14 (2000).

78. Ferlay, J. *et al.* Global Cancer Observatory: Cancer Today. <http://gco.iarc.fr/today/home> (2020).
79. Wang, L. *et al.* Prostate Cancer Incidence and Mortality: Global Status and Temporal Trends in 89 Countries From 2000 to 2019. *Frontiers in Public Health* **10**, (2022).
80. Prostate Cancer - Statistics. *Cancer.Net* <https://www.cancer.net/cancer-types/prostate-cancer/statistics> (2023).
81. Rawla, P. Epidemiology of Prostate Cancer. *World J Oncol* **10**, 63–89 (2019).
82. Crawford, E. D. Understanding the epidemiology, natural history, and key pathways involved in prostate cancer. *Urology* **73**, S4-10 (2009).
83. Rebello, R. J. *et al.* Prostate cancer. *Nat Rev Dis Primers* **7**, 1–27 (2021).
84. Leibovici, D. *et al.* Prostate cancer progression in the presence of undetectable or low serum prostate-specific antigen level. *Cancer* **109**, 198–204 (2007).
85. Liu, T. T. *et al.* Modeling human prostate cancer progression in vitro. *Carcinogenesis* **40**, 893–902 (2019).
86. Coussens, L. M. & Werb, Z. Inflammation and cancer. *Nature* **420**, 860–867 (2002).
87. Nakai, Y. & Nonomura, N. Inflammation and prostate carcinogenesis. *International Journal of Urology* **20**, 150–160 (2013).
88. Shen, M. M. & Abate-Shen, C. Molecular genetics of prostate cancer: new prospects for old challenges. *Genes Dev.* **24**, 1967–2000 (2010).
89. Nguyen, D. P., Li, J. & Tewari, A. K. Inflammation and prostate cancer: the role of interleukin 6 (IL-6). *BJU International* **113**, 986–992 (2014).
90. Udensi, U. K. & Tchounwou, P. B. Oxidative stress in prostate hyperplasia and carcinogenesis. *J Exp Clin Cancer Res* **35**, 139 (2016).
91. Lee, N. K. L. & MacLean, H. E. Polyamines, androgens, and skeletal muscle hypertrophy. *Journal of Cellular Physiology* **226**, 1453–1460 (2011).
92. Mehraein-Ghomi, F., Basu, H. S., Church, D. R., Hoffmann, F. M. & Wilding, G. Androgen Receptor Requires JunD as a Coactivator to Switch on an Oxidative Stress Generation Pathway in Prostate Cancer Cells. *Cancer Research* **70**, 4560–4568 (2010).
93. Gupta-Elera, G., Garrett, A. R., Robison, R. A. & O'Neill, K. L. The role of oxidative stress in prostate cancer. *European Journal of Cancer Prevention* **21**, 155–162 (2012).
94. Tomlins, S. A. *et al.* Recurrent fusion of TMPRSS2 and ETS transcription factor genes in prostate cancer. *Science* **310**, 644–648 (2005).
95. Barbieri, C. E. *et al.* Exome sequencing identifies recurrent SPOP, FOXA1 and MED12 mutations in prostate cancer. *Nat Genet* **44**, 685–689 (2012).
96. Baca, S. C. *et al.* Punctuated evolution of prostate cancer genomes. *Cell* **153**, 666–677 (2013).
97. Cancer Genome Atlas Research Network. The Molecular Taxonomy of Primary Prostate Cancer. *Cell* **163**, 1011–1025 (2015).
98. Robinson, D. *et al.* Integrative clinical genomics of advanced prostate cancer. *Cell* **161**, 1215–1228 (2015).
99. Qiu, X. *et al.* MYC drives aggressive prostate cancer by disrupting transcriptional pause release at androgen receptor targets. *Nat Commun* **13**, 2559 (2022).
100. Grasso, C. S. *et al.* The mutational landscape of lethal castration-resistant prostate cancer. *Nature* **487**, 239–243 (2012).

101. Stopsack, K. H. *et al.* Oncogenic Genomic Alterations, Clinical Phenotypes, and Outcomes in Metastatic Castration-Sensitive Prostate Cancer. *Clinical Cancer Research* **26**, 3230–3238 (2020).
102. Soares, S. C. M., de Camargo Cancela, M., Migowski, A. & de Souza, D. L. B. Digital rectal examination and its associated factors in the early detection of prostate cancer: a cross-sectional population-based study. *BMC Public Health* **19**, 1573 (2019).
103. Izawa, J. I. & Babaian, R. J. Chapter 14 - Prostate Cancer: Detection and Biopsy Strategies. in *Prostate Cancer* (eds. Mydlo, J. H. & Godec, C. J.) 129–136 (Academic Press, 2003). doi:10.1016/B978-012286981-5/50016-1.
104. Duffy, M. J. Biomarkers for prostate cancer: prostate-specific antigen and beyond. *Clin Chem Lab Med* **58**, 326–339 (2020).
105. Malm, J. & Lilja, H. Biochemistry of prostate specific antigen, PSA. *Scand J Clin Lab Invest Suppl* **221**, 15–22 (1995).
106. Zhong, J.-G. *et al.* Predicting prostate cancer in men with PSA levels of 4–10 ng/mL: MRI-based radiomics can help junior radiologists improve the diagnostic performance. *Sci Rep* **13**, 4846 (2023).
107. Scherr, D., Swindle, P. W., Scardino, P. T., & National Comprehensive Cancer Network. National Comprehensive Cancer Network guidelines for the management of prostate cancer. *Urology* **61**, 14–24 (2003).
108. Epstein, J. I. *et al.* The 2014 International Society of Urological Pathology (ISUP) Consensus Conference on Gleason Grading of Prostatic Carcinoma: Definition of Grading Patterns and Proposal for a New Grading System. *Am J Surg Pathol* **40**, 244–252 (2016).
109. Khauli, R. *et al.* Treatment of Localized and Locally Advanced, High-Risk Prostate Cancer: A Report From the First Prostate Cancer Consensus Conference for Developing Countries. *JCO Global Oncology* 530–537 (2021) doi:10.1200/GO.20.00421.
110. Posdzich, P. *et al.* Metastatic Prostate Cancer—A Review of Current Treatment Options and Promising New Approaches. *Cancers (Basel)* **15**, 461 (2023).
111. Clarke, N. W. *et al.* Addition of docetaxel to hormonal therapy in low- and high-burden metastatic hormone sensitive prostate cancer: long-term survival results from the STAMPEDE trial. *Ann Oncol* **30**, 1992–2003 (2019).
112. Teo, M. Y., Rathkopf, D. E. & Kantoff, P. Treatment of Advanced Prostate Cancer. *Annual Review of Medicine* **70**, 479–499 (2019).
113. Liu, H.-H. *et al.* Evolving Personalized Therapy for Castration-Resistant Prostate Cancer. *BioMed* **4**, 2 (2014).
114. Khan, M., Maker, A. V. & Jain, S. The Evolution of Cancer Immunotherapy. *Vaccines (Basel)* **9**, 614 (2021).
115. Kantoff, P. W. *et al.* Sipuleucel-T Immunotherapy for Castration-Resistant Prostate Cancer. *New England Journal of Medicine* **363**, 411–422 (2010).
116. Chandrasekar, T., Yang, J. C., Gao, A. C. & Evans, C. P. Mechanisms of resistance in castration-resistant prostate cancer (CRPC). *Transl Androl Urol* **4**, 365–380 (2015).
117. Huang, Y., Jiang, X., Liang, X. & Jiang, G. Molecular and cellular mechanisms of castration resistant prostate cancer. *Oncol Lett* **15**, 6063–6076 (2018).
118. Shiota, M. *et al.* Androgen receptor mutations for precision medicine in prostate cancer. *Endocrine-Related Cancer* **29**, R143–R155 (2022).

119. Chen, C. D. *et al.* Molecular determinants of resistance to antiandrogen therapy. *Nat Med* **10**, 33–39 (2004).
120. Mostaghel, E. A. Steroid hormone synthetic pathways in prostate cancer. *Translational Andrology and Urology* **2**, 21227–21227 (2013).
121. Lee, H. G. & Kim, C. J. Classic and backdoor pathways of androgen biosynthesis in human sexual development. *Ann Pediatr Endocrinol Metab* **27**, 83–89 (2022).
122. Lubik, A. A. *et al.* Insulin Increases De Novo Steroidogenesis in Prostate Cancer Cells. *Cancer Research* **71**, 5754–5764 (2011).
123. Cai, C. *et al.* Intratumoral De Novo Steroid Synthesis Activates Androgen Receptor in Castration Resistant Prostate Cancer and is Upregulated by Treatment with CYP17A1 Inhibitors. *Cancer Res* **71**, 6503–6513 (2011).
124. Pfeiffer, M. J., Smit, F. P., Sedelaar, J. P. M. & Schalken, J. A. Steroidogenic Enzymes and Stem Cell Markers Are Upregulated during Androgen Deprivation in Prostate Cancer. *Mol Med* **17**, 657–664 (2011).
125. Buttiglieri, C. *et al.* Understanding and overcoming the mechanisms of primary and acquired resistance to abiraterone and enzalutamide in castration resistant prostate cancer. *Cancer Treatment Reviews* **41**, 884–892 (2015).
126. Zadra, G. *et al.* Inhibition of de novo lipogenesis targets androgen receptor signaling in castration-resistant prostate cancer. *Proc Natl Acad Sci U S A* **116**, 631–640 (2019).
127. Mostaghel, E. A. *et al.* Resistance to CYP17A1 Inhibition with Abiraterone in Castration-Resistant Prostate Cancer: Induction of Steroidogenesis and Androgen Receptor Splice Variants. *Clinical Cancer Research* **17**, 5913–5925 (2011).
128. Armandari, I., Hamid, A. R., Verhaegh, G. & Schalken, J. Intratumoral steroidogenesis in castration-resistant prostate cancer: a target for therapy. *Prostate Int* **2**, 105–113 (2014).
129. Adamiecki, R. *et al.* In Vivo Models for Prostate Cancer Research. *Cancers (Basel)* **14**, 5321 (2022).
130. Shappell, S. B. *et al.* Prostate pathology of genetically engineered mice: definitions and classification. The consensus report from the Bar Harbor meeting of the Mouse Models of Human Cancer Consortium Prostate Pathology Committee. *Cancer Res* **64**, 2270–2305 (2004).
131. Grabowska, M. M. *et al.* Mouse models of prostate cancer: picking the best model for the question. *Cancer Metastasis Rev* **33**, 377–397 (2014).
132. Oliveira, D. S. M. *et al.* The mouse prostate: a basic anatomical and histological guideline. *Biomolecules and Biomedicine* **16**, 8–13 (2016).
133. Ittmann, M. *et al.* Animal Models of Human Prostate Cancer: The Consensus Report of the New York Meeting of the Mouse Models of Human Cancers Consortium Prostate Pathology Committee. *Cancer Research* **73**, 2718–2736 (2013).
134. Singh, M. & Johnson, L. Using genetically engineered mouse models of cancer to aid drug development: an industry perspective. *Clin Cancer Res* **12**, 5312–5328 (2006).
135. Sailer, V. *et al.* Experimental in vitro, ex vivo and in vivo models in prostate cancer research. *Nat Rev Urol* **20**, 158–178 (2023).
136. Barretina, J. *et al.* The Cancer Cell Line Encyclopedia enables predictive modelling of anticancer drug sensitivity. *Nature* **483**, 603–607 (2012).
137. Ellem, S. J., De-Juan-Pardo, E. M. & Risbridger, G. P. In vitro modeling of the prostate cancer microenvironment. *Advanced Drug Delivery Reviews* **79–80**, 214–221 (2014).

138. Jensen, K. B. & Little, M. H. Organoids are not organs: Sources of variation and misinformation in organoid biology. *Stem Cell Reports* **18**, 1255–1270 (2023).
139. Hayflick, L. & Moorhead, P. S. The serial cultivation of human diploid cell strains. *Exp Cell Res* **25**, 585–621 (1961).
140. Shtutman, M., Chang, B.-D., Schools, G. P. & Broude, E. V. Cellular Model of p21-Induced Senescence. *Methods Mol Biol* **1534**, 31–39 (2017).
141. Collado, M. & Serrano, M. Senescence in tumours: evidence from mice and humans. *Nat Rev Cancer* **10**, 51–57 (2010).
142. Campisi, J. Aging, Cellular Senescence, and Cancer. *Annual Review of Physiology* **75**, 685–705 (2013).
143. Yang, J., Liu, M., Hong, D., Zeng, M. & Zhang, X. The Paradoxical Role of Cellular Senescence in Cancer. *Front. Cell Dev. Biol.* **9**, 722205 (2021).
144. Da Silva-Álvarez, S. *et al.* The development of cell senescence. *Experimental Gerontology* **128**, 110742 (2019).
145. Antelo-Iglesias, L., Picallos-Rabina, P., Estévez-Souto, V., Da Silva-Álvarez, S. & Collado, M. The role of cellular senescence in tissue repair and regeneration. *Mechanisms of Ageing and Development* **198**, 111528 (2021).
146. Milanovic, M. *et al.* Senescence-associated reprogramming promotes cancer stemness. *Nature* **553**, 96–100 (2018).
147. Chen, Z. *et al.* Crucial role of p53-dependent cellular senescence in suppression of Pten-deficient tumorigenesis. *Nature* **436**, 725–730 (2005).
148. Guccini, I. *et al.* Senescence Reprogramming by TIMP1 Deficiency Promotes Prostate Cancer Metastasis. *Cancer Cell* **39**, 68-82.e9 (2021).
149. Hodges, C. V. & Kirchheim, D. Hormone Treatment of Cancer of the Prostate. in *New Trends in the Treatment of Cancer* (eds. Manuila, L., Moles, S. & Rentchnick, P.) 133–142 (Springer, 1967). doi:10.1007/978-3-642-87620-2_7.
150. Huggins, C. The Hormone-Dependent Cancers. *JAMA* **186**, 481–483 (1963).
151. Sharifi, N., Gulley, J. L. & Dahut, W. L. Androgen Deprivation Therapy for Prostate Cancer. *JAMA* **294**, 238–244 (2005).
152. Harris, W. P., Mostaghel, E. A., Nelson, P. S. & Montgomery, B. Androgen deprivation therapy: progress in understanding mechanisms of resistance and optimizing androgen depletion. *Nat Clin Pract Urol* **6**, 76–85 (2009).
153. Karantanos, T., Corn, P. G. & Thompson, T. C. Prostate cancer progression after androgen deprivation therapy: mechanisms of castrate-resistance and novel therapeutic approaches. *Oncogene* **32**, 5501–5511 (2013).
154. Wadosky, K. M. & Koochekpour, S. Molecular mechanisms underlying resistance to androgen deprivation therapy in prostate cancer. *Oncotarget* **7**, 64447–64470 (2016).
155. Ferrari, N. *et al.* Adaptive phenotype drives resistance to androgen deprivation therapy in prostate cancer. *Cell Communication and Signaling* **15**, 51 (2017).
156. Locke, J. A. *et al.* Androgen Levels Increase by Intratumoral De novo Steroidogenesis during Progression of Castration-Resistant Prostate Cancer. *Cancer Research* **68**, 6407–6415 (2008).
157. Lubik, A. A. *et al.* IGF2 increases de novo steroidogenesis in prostate cancer cells. *Endocrine-Related Cancer* **20**, 173–186 (2013).

158. Sakai, M., Martinez-Arguelles, D. B., Aprikian, A. G., Magliocco, A. M. & Papadopoulos, V. De novo steroid biosynthesis in human prostate cell lines and biopsies. *The Prostate* **76**, 575–587 (2016).
159. Devlies, W., Handle, F., Devos, G., Joniau, S. & Claessens, F. Preclinical Models in Prostate Cancer: Resistance to AR Targeting Therapies in Prostate Cancer. *Cancers (Basel)* **13**, 915 (2021).
160. Risbridger, G. P., Toivanen, R. & Taylor, R. A. Preclinical Models of Prostate Cancer: Patient-Derived Xenografts, Organoids, and Other Explant Models. *Cold Spring Harb Perspect Med* **8**, a030536 (2018).
161. Flores-Téllez, T. del N. J. & Baena, E. Experimental challenges to modeling prostate cancer heterogeneity. *Cancer Letters* **524**, 194–205 (2022).
162. Cheng, J., Wu, Y., Mohler, J. L. & Ip, C. The Transcriptomics of de novo Androgen Biosynthesis in Prostate Cancer Cells Following Androgen Reduction. *Cancer Biol Ther* **9**, 1033–1042 (2010).
163. Abdolahi, S. *et al.* Patient-derived xenograft (PDX) models, applications and challenges in cancer research. *Journal of Translational Medicine* **20**, 206 (2022).
164. Pamarthy, S. & Sabaawy, H. E. Patient derived organoids in prostate cancer: improving therapeutic efficacy in precision medicine. *Molecular Cancer* **20**, 125 (2021).
165. Ryabov, V. M., Baryshev, M. M., Voskresenskiy, M. A. & Popov, B. V. Early Cell Cultures from Prostate Cancer Tissue Express Tissue Specific Epithelial and Cancer Markers. *International Journal of Molecular Sciences* **24**, 2830 (2023).
166. Loop, S. M., Rozanski, T. A. & Ostenson, R. C. Human primary prostate tumor cell line, ALVA-31: a new model for studying the hormonal regulation of prostate tumor cell growth. *Prostate* **22**, 93–108 (1993).
167. Nanni, S. *et al.* Epithelial-Restricted Gene Profile of Primary Cultures from Human Prostate Tumors: A Molecular Approach to Predict Clinical Behavior of Prostate Cancer. *Molecular Cancer Research* **4**, 79–92 (2006).
168. Bühler, P. *et al.* Primary prostate cancer cultures are models for androgen-independent transit amplifying cells. *Oncology Reports* **23**, 465–470 (2010).
169. Horoszewicz, J. S. *et al.* LNCaP model of human prostatic carcinoma. *Cancer Res* **43**, 1809–1818 (1983).
170. Veldscholte, J., Berrevoets, C. A. & Mulder, E. Studies on the human prostatic cancer cell line LNCaP. *The Journal of Steroid Biochemistry and Molecular Biology* **49**, 341–346 (1994).
171. Cunningham, D. & You, Z. In vitro and in vivo model systems used in prostate cancer research. *J Biol Methods* **2**, e17 (2015).
172. Stone, K. R., Mickey, D. D., Wunderli, H., Mickey, G. H. & Paulson, D. F. Isolation of a human prostate carcinoma cell line (DU 145). *International Journal of Cancer* **21**, 274–281 (1978).
173. Alimirah, F., Chen, J., Basrawala, Z., Xin, H. & Choubey, D. DU-145 and PC-3 human prostate cancer cell lines express androgen receptor: Implications for the androgen receptor functions and regulation. *FEBS Letters* **580**, 2294–2300 (2006).
174. Men, A. E., Wilson, P., Siemering, K. & Forrest, S. Sanger DNA Sequencing. in *Next Generation Genome Sequencing* 1–11 (John Wiley & Sons, Ltd, 2008). doi:10.1002/9783527625130.ch1.
175. Ali, N., Rampazzo, R. de C. P., Costa, A. D. T. & Krieger, M. A. Current Nucleic Acid Extraction Methods and Their Implications to Point-of-Care Diagnostics. *Biomed Res Int* **2017**, 9306564 (2017).

176. Fleige, S. & Pfaffl, M. W. RNA integrity and the effect on the real-time qRT-PCR performance. *Mol Aspects Med* **27**, 126–139 (2006).
177. Lightfoot, S. Quantitation comparison of total RNA using the Agilent. (2002).
178. Meister, G. & Tuschl, T. Mechanisms of gene silencing by double-stranded RNA. *Nature* **431**, 343–349 (2004).
179. Chendrimada, T. P. *et al.* TRBP recruits the Dicer complex to Ago2 for microRNA processing and gene silencing. *Nature* **436**, 740–744 (2005).
180. Ohto, U. *et al.* Crystal Structure of Human β -Galactosidase. *J Biol Chem* **287**, 1801–1812 (2012).
181. Lee, B. Y. *et al.* Senescence-associated β -galactosidase is lysosomal β -galactosidase. *Aging Cell* **5**, 187–195 (2006).
182. Safwan-Zaiter, H., Wagner, N. & Wagner, K.-D. P16INK4A—More Than a Senescence Marker. *Life (Basel)* **12**, 1332 (2022).
183. Rayess, H., Wang, M. B. & Srivatsan, E. S. Cellular senescence and tumor suppressor gene p16. *Int J Cancer* **130**, 1715–1725 (2012).
184. McCann, J. J. *et al.* Mutant p53 elicits context-dependent pro-tumorigenic phenotypes. *Oncogene* **41**, 444–458 (2022).
185. Arora, K. & Barbieri, C. E. Molecular Subtypes of Prostate Cancer. *Curr Oncol Rep* **20**, 58 (2018).
186. Maxwell, K. N. *et al.* Inherited TP53 Variants and Risk of Prostate Cancer. *European Urology* **81**, 243–250 (2022).
187. T, B., Jld, P. & Me, M. Common genetic variants in the TP53 pathway and their impact on cancer. *Journal of molecular cell biology* **11**, (2019).
188. Marin, M. C. *et al.* A common polymorphism acts as an intragenic modifier of mutant p53 behaviour. *Nat Genet* **25**, 47–54 (2000).
189. Günal, S., Hardman, R., Kopriva, S. & Mueller, J. W. Sulfation pathways from red to green. *Journal of Biological Chemistry* **294**, 12293–12312 (2019).
190. Weiss, R. H. *et al.* p21 is a Prognostic Marker for Renal Cell Carcinoma: Implications for Novel Therapeutic Approaches. *The Journal of Urology* **177**, 63–69 (2007).
191. Galanos, P. *et al.* Chronic p53-independent p21 expression causes genomic instability by deregulating replication licensing. *Nat Cell Biol* **18**, 777–789 (2016).
192. Al-Sharaky, D. R. *et al.* ROC-1, P21 and CAIX as markers of tumor aggressiveness in bladder carcinoma in Egyptian patients. *Diagnostic Pathology* **15**, 33 (2020).
193. Blagosklonny, M. V., Wu, G. S., Omura, S. & el-Deiry, W. S. Proteasome-dependent regulation of p21WAF1/CIP1 expression. *Biochem Biophys Res Commun* **227**, 564–569 (1996).
194. Jascur, T. *et al.* Regulation of p21WAF1/CIP1 Stability by WISp39, a Hsp90 Binding TPR Protein. *Molecular Cell* **17**, 237–249 (2005).
195. Jung, Y.-S., Qian, Y. & Chen, X. Examination of the expanding pathways for the regulation of p21 expression and activity. *Cell Signal* **22**, 1003–1012 (2010).
196. Ohtani, N. The roles and mechanisms of senescence-associated secretory phenotype (SASP): can it be controlled by senolysis? *Inflammation and Regeneration* **42**, 11 (2022).
197. Takasugi, M., Yoshida, Y., Hara, E. & Ohtani, N. The role of cellular senescence and SASP in tumour microenvironment. *The FEBS Journal* **290**, 1348–1361 (2023).

198. Brzozowa-Zasada, M. *et al.* Notch and its oncogenic activity in human malignancies. *Eur Surg* **49**, 199–209 (2017).
199. Gharaibeh, L., Elmadany, N., Alwosaibai, K. & Alshaer, W. Notch1 in Cancer Therapy: Possible Clinical Implications and Challenges. *Mol Pharmacol* **98**, 559–576 (2020).
200. Kunnimalaiyaan, M. & Chen, H. Tumor Suppressor Role of Notch-1 Signaling in Neuroendocrine Tumors. *The Oncologist* **12**, 535–542 (2007).
201. Hanlon, L. *et al.* Notch1 Functions as a Tumor Suppressor in a Model of K-ras–Induced Pancreatic Ductal Adenocarcinoma. *Cancer Research* **70**, 4280–4286 (2010).
202. Alaña, L. *et al.* Prostate tumor OVerexpressed-1 (PTOV1) down-regulates HES1 and HEY1 notch targets genes and promotes prostate cancer progression. *Molecular Cancer* **13**, 74 (2014).
203. Hoare, M. & Narita, M. NOTCH and the 2 SASPs of senescence. *Cell Cycle* **16**, 239–240 (2017).
204. Teo, Y. V. *et al.* Notch Signaling Mediates Secondary Senescence. *Cell Reports* **27**, 997–1007.e5 (2019).
205. Li, D., Xu, D., Zhang, Y., Chen, P. & Xie, J. Effect of Notch1 signaling on cellular proliferation and apoptosis in human laryngeal carcinoma. *World Journal of Surgical Oncology* **20**, 262 (2022).
206. Laubach, K. N. *et al.* p73 α 1, a p73 C-terminal isoform, regulates tumor suppression and the inflammatory response via Notch1. *Proceedings of the National Academy of Sciences* **119**, e2123202119 (2022).
207. Tolkach, Y. & Kristiansen, G. The Heterogeneity of Prostate Cancer: A Practical Approach. *Pathobiology* **85**, 108–116 (2018).
208. Centenera, M. M. *et al.* Harnessing the Heterogeneity of Prostate Cancer for Target Discovery Using Patient-Derived Explants. *Cancers* **14**, 1708 (2022).
209. Taylor, R. A., Lawrence, M. G. & Risbridger, G. P. Advances in preclinical models of prostate cancer for research discovery. *Journal of Endocrinology* **257**, (2023).
210. Maggio, V. Novel tools to study aggressive prostate cancer. *TDX (Tesis Doctorals en Xarxa)* (Universitat Autònoma de Barcelona, 2019).
211. Boquest, A. C. *et al.* Isolation and Transcription Profiling of Purified Uncultured Human Stromal Stem Cells: Alteration of Gene Expression after In Vitro Cell Culture. *MBoC* **16**, 1131–1141 (2005).
212. Zaitseva, M., Vollenhoven, B. J. & Rogers, P. A. W. In vitro culture significantly alters gene expression profiles and reduces differences between myometrial and fibroid smooth muscle cells. *Molecular Human Reproduction* **12**, 187–207 (2006).
213. Kim, S. W., Kim, S.-J., Langley, R. R. & Fidler, I. J. Modulation of the cancer cell transcriptome by culture media formulations and cell density. *International Journal of Oncology* **46**, 2067–2075 (2015).
214. Ledur, P. F., Onzi, G. R., Zong, H. & Lenz, G. Culture conditions defining glioblastoma cells behavior: what is the impact for novel discoveries? *Oncotarget* **8**, 69185–69197 (2017).
215. Cox, M. C., Deng, C., Naler, L. B., Lu, C. & Verbridge, S. S. Effects of culture condition on epigenomic profiles of brain tumor cells. *ACS Biomater Sci Eng* **5**, 1544–1552 (2019).
216. Mehrian Shai, R. *et al.* Robustness of gene expression profiling in glioma specimen samplings and derived cell lines. *Molecular Brain Research* **136**, 99–103 (2005).
217. Pan, C., Kumar, C., Bohl, S., Klingmueller, U. & Mann, M. Comparative Proteomic Phenotyping of Cell Lines and Primary Cells to Assess Preservation of Cell Type-specific Functions. *Mol Cell Proteomics* **8**, 443–450 (2009).

218. Cifola, I. *et al.* Renal cell carcinoma primary cultures maintain genomic and phenotypic profile of parental tumor tissues. *BMC Cancer* **11**, 244 (2011).
219. Ghani, F. I. *et al.* An Ex-Vivo Culture System of Ovarian Cancer Faithfully Recapitulating the Pathological Features of Primary Tumors. *Cells* **8**, 644 (2019).
220. Brooks, L. A. *et al.* Preferential retention of codon 72 arginine p53 in squamous cell carcinomas of the vulva occurs in cancers positive and negative for human papillomavirus. *Cancer Res* **60**, 6875–6877 (2000).
221. Schneider-Stock, R. *et al.* Retention of the arginine allele in codon 72 of the p53 gene correlates with poor apoptosis in head and neck cancer. *Am J Pathol* **164**, 1233–1241 (2004).
222. Schneider-Stock, R. *et al.* Selective Loss of Codon 72 Proline p53 and Frequent Mutational Inactivation of the Retained Arginine Allele in Colorectal Cancer. *Neoplasia* **6**, 529–535 (2004).
223. Papadakis, E. D., Soultziz, N. & Spandidos, D. A. Association of p53 codon 72 polymorphism with advanced lung cancer: the Arg allele is preferentially retained in tumours arising in Arg/Pro germline heterozygotes. *Br J Cancer* **87**, 1013–1018 (2002).
224. De Souza, C. *et al.* Effect of the p53 P72R Polymorphism on Mutant TP53 Allele Selection in Human Cancer. *J Natl Cancer Inst* **113**, 1246–1257 (2021).
225. Basu, S. *et al.* Mutant p53 controls tumor metabolism and metastasis by regulating PGC-1 α . *Genes & Development* **32**, 230 (2018).
226. Shen, H. *et al.* p53 Codon 72 Arg Homozygotes Are Associated with an Increased Risk of Cutaneous Melanoma. *J Invest Dermatol* **121**, 1510–1514 (2003).
227. Volodko, N. *et al.* TP53 codon 72 Arg/Arg polymorphism is associated with a higher risk for inflammatory bowel disease development. *World J Gastroenterol* **21**, 10358–10366 (2015).
228. Dia, Y. *et al.* Arg Allele of P53 Gene Codon72 is a Risk Factor for Breast Cancer in Senegalese Women. *Journal of Molecular and Genetic Medicine* **11**, (2017).
229. Doosti, A. & Dehkordi, P. G. The p53 codon 72 polymorphism and association to prostate cancer in Iranian patients. *African Journal of Biotechnology* **10**, 12821–12825 (2011).
230. Ezzikouri, S. *et al.* The Pro variant of the p53 codon 72 polymorphism is associated with hepatocellular carcinoma in Moroccan population. *Hepatology Research* **37**, 748–754 (2007).
231. Mohana Devi, S. *et al.* Analysis of Genetic Damage and Gene Polymorphism in Hepatocellular Carcinoma (HCC) Patients in a South Indian Population. *Dig Dis Sci* **58**, 759–767 (2013).
232. Son, M. S. *et al.* Promoter polymorphisms of pri-miR-34b/c are associated with hepatocellular carcinoma. *Gene* **524**, 156–160 (2013).
233. Tang, N.-P., Wu, Y.-M., Wang, B. & Ma, J. Systematic review and meta-analysis of the association between P53 codon 72 polymorphism and colorectal cancer. *European Journal of Surgical Oncology (EJSO)* **36**, 431–438 (2010).
234. Weng, Y. *et al.* p53 codon 72 polymorphism and Hematological Cancer Risk: An Update Meta-Analysis. *PLOS ONE* **7**, e45820 (2012).
235. Ye, J., Li, X.-F., Wang, Y.-D. & Yuan, Y. Arg72Pro Polymorphism of TP53 Gene and the Risk of Skin Cancer: a Meta-Analysis. *PLOS ONE* **8**, e79983 (2013).
236. Zhang, L. *et al.* Association between p53 Pro72Arg polymorphism and prostate cancer risk: a meta-analysis. *J Biomed Res* **25**, 25–32 (2011).
237. Xu, T., Xu, Z.-C., Zou, Q., Yu, B. & Huang, X.-E. P53 Arg72Pro polymorphism and bladder cancer risk--meta-analysis evidence for a link in Asians but not Caucasians. *Asian Pac J Cancer Prev* **13**, 2349–2354 (2012).

238. Krüger, S. *et al.* The p53 codon 72 variation is associated with the age of onset of hereditary non-polyposis colorectal cancer (HNPCC). *Journal of Medical Genetics* **42**, 769–773 (2005).
239. Henner, W. D. *et al.* Association of codon 72 polymorphism of p53 with lower prostate cancer risk. *Prostate* **49**, 263–266 (2001).
240. Suzuki, K. *et al.* A p53 codon 72 polymorphism associated with prostate cancer development and progression in Japanese. *J Biomed Sci* **10**, 430–435 (2003).
241. Li, M. S., Liu, J. L., Wu, Y., Wang, P. & Teng, H. Meta-analysis demonstrates no association between p53 codon 72 polymorphism and prostate cancer risk. *Genet Mol Res* **10**, 2924–2933 (2011).
242. Lu, Y. *et al.* Association of p53 codon 72 polymorphism with prostate cancer: an update meta-analysis. *Tumor Biol.* **35**, 3997–4005 (2014).
243. Sivoňová, M. K. *et al.* Association of p53 and p21 polymorphisms with prostate cancer. *Biomedical Reports* **3**, 707–714 (2015).
244. Duncan, A. *et al.* Association of TP53 Single Nucleotide Polymorphisms with Prostate Cancer in a Racially Diverse Cohort of Men. *Biomedicines* **11**, 1404 (2023).
245. Gunaratna, R. T. *et al.* Dynamic role of the codon 72 p53 single-nucleotide polymorphism in mammary tumorigenesis in a humanized mouse model. *Oncogene* **38**, 3535–3550 (2019).
246. Kung, C.-P., Liu, Q. & Murphy, M. E. The codon 72 polymorphism of p53 influences cell fate following nutrient deprivation. *Cancer Biology & Therapy* **18**, 484–491 (2017).
247. Babaei, F. *et al.* The TP53 Codon 72 Polymorphism and Risk of Sporadic Prostate Cancer among Iranian Patients. *Iran J Public Health* **43**, 453–459 (2014).
248. Aydin, M. *et al.* Lack of evidence of HPV etiology of prostate cancer following radical surgery and higher frequency of the Arg/Pro genotype in Turkish men with prostate cancer. *Int Braz J Urol* **43**, 36–46 (2017).
249. Shen, T., Lu, Y. & Zhang, Q. High Squalene Epoxidase in Tumors Predicts Worse Survival in Patients With Hepatocellular Carcinoma: Integrated Bioinformatic Analysis on NAFLD and HCC. *Cancer Control* **27**, 1073274820914663 (2020).
250. Kim, N. I., Park, M. H., Kweon, S.-S., Cho, N. & Lee, J. S. Squalene epoxidase expression is associated with breast tumor progression and with a poor prognosis in breast cancer. *Oncology Letters* **21**, 1–1 (2021).
251. Li, C. *et al.* Squalene epoxidase drives cancer cell proliferation and promotes gut dysbiosis to accelerate colorectal carcinogenesis. *Gut* **71**, 2253–2265 (2022).
252. Zhang, Z. *et al.* Squalene epoxidase promotes hepatocellular carcinoma development by activating STRAP transcription and TGF- β /SMAD signalling. *British Journal of Pharmacology* **180**, 1562–1581 (2023).
253. Liu, Y., Fang, L. & Liu, W. High SQLE Expression and Gene Amplification Correlates with Poor Prognosis in Head and Neck Squamous Cell Carcinoma. *Cancer Management and Research* **13**, 4709–4723 (2021).
254. You, W. *et al.* SQLE, A Key Enzyme in Cholesterol Metabolism, Correlates With Tumor Immune Infiltration and Immunotherapy Outcome of Pancreatic Adenocarcinoma. *Frontiers in Immunology* **13**, (2022).
255. Xu, R. *et al.* SQLE promotes pancreatic cancer growth by attenuating ER stress and activating lipid rafts-regulated Src/PI3K/Akt signaling pathway. *Cell Death Dis* **14**, 1–16 (2023).

256. Kalogirou, C. *et al.* MiR-205-driven downregulation of cholesterol biosynthesis through SQLE-inhibition identifies therapeutic vulnerability in aggressive prostate cancer. *Nat Commun* **12**, 5066 (2021).
257. Zou, Y., Zhang, H., Bi, F., Tang, Q. & Xu, H. Targeting the key cholesterol biosynthesis enzyme squalene monooxygenase for cancer therapy. *Frontiers in Oncology* **12**, (2022).
258. Hu, J., Zhang, Z., Shen, W.-J. & Azhar, S. Cellular cholesterol delivery, intracellular processing and utilization for biosynthesis of steroid hormones. *Nutrition & Metabolism* **7**, 47 (2010).
259. Stigliano, A. *et al.* Increased metastatic lymph node 64 and CYP17 expression are associated with high stage prostate cancer. *Journal of Endocrinology* **194**, 55–61 (2007).
260. Vassilev, B. *et al.* Elevated Levels of StAR-Related Lipid Transfer Protein 3 Alter Cholesterol Balance and Adhesiveness of Breast Cancer Cells: Potential Mechanisms Contributing to Progression of HER2-Positive Breast Cancers. *The American Journal of Pathology* **185**, 987–1000 (2015).
261. Sui, L. *et al.* PTU-68 The Expression and Clinical Significance of MLN64 in Human Pancreatic Cancer. *Gut* **70**, A145–A146 (2021).
262. Fararjeh, A., Kaddumi, E., Al-Khader, A. & Aburayyan, W. The significance of StAR-related lipid transfer protein-3 expression in breast cancer. *Pol J Pathol* **73**, 215–222 (2023).
263. Asif, K. *et al.* STARD3: A Prospective Target for Cancer Therapy. *Cancers (Basel)* **13**, 4693 (2021).
264. Thul, P. J. *et al.* A subcellular map of the human proteome. *Science* **356**, eaal3321 (2017).
265. Zhang, M. *et al.* MLN64 mediates mobilization of lysosomal cholesterol to steroidogenic mitochondria. *J Biol Chem* **277**, 33300–33310 (2002).
266. Charman, M., Kennedy, B. E., Osborne, N. & Karten, B. MLN64 mediates egress of cholesterol from endosomes to mitochondria in the absence of functional Niemann-Pick Type C1 protein. *J Lipid Res* **51**, 1023–1034 (2010).
267. Nelles, J. L., Hu, W.-Y. & Prins, G. S. Estrogen action and prostate cancer. *Expert Rev Endocrinol Metab* **6**, 437–451 (2011).
268. Li, F., Zhu, W. & Gonzalez, F. J. Potential role of CYP1B1 in the development and treatment of metabolic diseases. *Pharmacol Ther* **178**, 18–30 (2017).
269. Sissung, T. M. *et al.* Association of the CYP1B1*3 allele with survival in patients with prostate cancer receiving docetaxel. *Mol Cancer Ther* **7**, 19–26 (2008).
270. Sissung, T. M. *et al.* Estrogen receptor α and aromatase polymorphisms affect risk, prognosis, and therapeutic outcome in men with castration-resistant prostate cancer treated with docetaxel-based therapy. *J Clin Endocrinol Metab* **96**, E368-372 (2011).
271. Wilson, E. M. & French, F. S. Binding properties of androgen receptors. Evidence for identical receptors in rat testis, epididymis, and prostate. *Journal of Biological Chemistry* **251**, 5620–5629 (1976).
272. GRINO, P. B., GRIFFIN, J. E. & WILSON, J. D. Testosterone at High Concentrations Interacts with the Human Androgen Receptor Similarly to Dihydrotestosterone*. *Endocrinology* **126**, 1165–1172 (1990).
273. Chang, K.-H., Ercole, C. E. & Sharifi, N. Androgen metabolism in prostate cancer: from molecular mechanisms to clinical consequences. *Br J Cancer* **111**, 1249–1254 (2014).
274. Fiandalo, M. V. *et al.* Inhibition of dihydrotestosterone synthesis in prostate cancer by combined frontdoor and backdoor pathway blockade. *Oncotarget* **9**, 11227–11242 (2018).

275. Miller, W. L. & Auchus, R. J. The 'backdoor pathway' of androgen synthesis in human male sexual development. *PLoS Biol.* **17**, e3000198 (2019).
276. Liu, C. *et al.* Inhibition of AKR1C3 Activation Overcomes Resistance to Abiraterone in Advanced Prostate Cancer. *Molecular Cancer Therapeutics* **16**, 35–44 (2017).
277. Uhlén, M. *et al.* Tissue-based map of the human proteome. *Science* **347**, 1260419 (2015).
278. Sun, P.-M. *et al.* An estrogen receptor alpha-dependent regulation of estrogen receptor-related receptor alpha in the proliferation of endometrial carcinoma cells. *Int J Gynecol Cancer* **16 Suppl 2**, 564–568 (2006).
279. Sun, P. *et al.* Expression of estrogen receptor-related receptors, a subfamily of orphan nuclear receptors, as new tumor biomarkers in ovarian cancer cells. *J Mol Med (Berl)* **83**, 457–467 (2005).
280. Stein, R. A., Gaillard, S. & McDonnell, D. P. Estrogen-related receptor alpha induces the expression of vascular endothelial growth factor in breast cancer cells. *J Steroid Biochem Mol Biol* **114**, 106–112 (2009).
281. Cheung, C. P. *et al.* Expression and functional study of estrogen receptor-related receptors in human prostatic cells and tissues. *J Clin Endocrinol Metab* **90**, 1830–1844 (2005).
282. Xu, Z. *et al.* Nuclear receptor ERR α contributes to castration-resistant growth of prostate cancer via its regulation of intratumoral androgen biosynthesis. *Theranostics* **10**, 4201–4216 (2020).
283. Chlenski, A., Nakashiro, K., Ketels, K. V., Korovaitseva, G. I. & Oyasu, R. Androgen receptor expression in androgen-independent prostate cancer cell lines. *Prostate* **47**, 66–75 (2001).
284. Fialova, B. *et al.* Epigenetic modulation of AR gene expression in prostate cancer DU145 cells with the combination of sodium butyrate and 5'-Aza-2'-deoxycytidine. *Oncology Reports* **36**, 2365–2374 (2016).
285. Fujita, K. & Nonomura, N. Role of Androgen Receptor in Prostate Cancer: A Review. *World J Mens Health* **37**, 288–295 (2019).
286. Formaggio, N., Rubin, M. A. & Theurillat, J.-P. Loss and revival of androgen receptor signaling in advanced prostate cancer. *Oncogene* **40**, 1205–1216 (2021).
287. Liu, T., Wu, L. Y., Fulton, M. D., Johnson, J. M. & Berkman, C. E. Prolonged androgen deprivation leads to downregulation of androgen receptor and prostate-specific membrane antigen in prostate cancer cells. *International Journal of Oncology* **41**, 2087–2092 (2012).
288. Fialova, B., Smesny Trtkova, K., Paskova, L., Langova, K. & Kolar, Z. Effect of histone deacetylase and DNA methyltransferase inhibitors on the expression of the androgen receptor gene in androgen-independent prostate cancer cell lines. *Oncol Rep* **29**, 2039–2045 (2013).
289. Thomas, P., Converse, A. & Berg, H. A. ZIP9, a novel membrane androgen receptor and zinc transporter protein. *General and Comparative Endocrinology* **257**, 130–136 (2018).
290. Converse, A. & Thomas, P. Androgens promote vascular endothelial cell proliferation through activation of a ZIP9-dependent inhibitory G protein/PI3K-Akt/Erk/cyclin D1 pathway. *Molecular and Cellular Endocrinology* **538**, 111461 (2021).
291. Takagi, K., Yamaguchi, M., Miyashita, M., Sasano, H. & Suzuki, T. Diverse role of androgen action in human breast cancer. *Endocrine Oncology* **2**, R102–R111 (2022).
292. Fukada, T. & Kambe, T. Molecular and genetic features of zinc transporters in physiology and pathogenesis. *Metallomics* **3**, 662–674 (2011).

293. Sugiyama, M. G., Fairn, G. D. & Antonescu, C. N. Akt-ing Up Just About Everywhere: Compartment-Specific Akt Activation and Function in Receptor Tyrosine Kinase Signaling. *Frontiers in Cell and Developmental Biology* **7**, (2019).
294. el-Deiry, W. S. *et al.* WAF1, a potential mediator of p53 tumor suppression. *Cell* **75**, 817–825 (1993).
295. el-Deiry, W. S. *et al.* WAF1/CIP1 is induced in p53-mediated G1 arrest and apoptosis. *Cancer Res* **54**, 1169–1174 (1994).
296. Deng, C., Zhang, P., Harper, J. W., Elledge, S. J. & Leder, P. Mice Lacking p21CIP1/WAF1 undergo normal development, but are defective in G1 checkpoint control. *Cell* **82**, 675–684 (1995).
297. El-Deiry, W. S. p21(WAF1) Mediates Cell-Cycle Inhibition, Relevant to Cancer Suppression and Therapy. *Cancer Research* **76**, 5189–5191 (2016).
298. Roninson, I. B. Oncogenic functions of tumour suppressor p21(Waf1/Cip1/Sdi1): association with cell senescence and tumour-promoting activities of stromal fibroblasts. *Cancer Lett* **179**, 1–14 (2002).
299. Dupont, J., Karas, M. & LeRoith, D. The cyclin-dependent kinase inhibitor p21CIP/WAF is a positive regulator of insulin-like growth factor I-induced cell proliferation in MCF-7 human breast cancer cells. *J Biol Chem* **278**, 37256–37264 (2003).
300. Pellikainen, M. J. *et al.* p21WAF1 expression in invasive breast cancer and its association with p53, AP-2, cell proliferation, and prognosis. *Journal of Clinical Pathology* **56**, 214–220 (2003).
301. Ohkoshi, S., Yano, M. & Matsuda, Y. Oncogenic role of p21 in hepatocarcinogenesis suggests a new treatment strategy. *World J Gastroenterol* **21**, 12150–12156 (2015).
302. Lu, S., Tsai, S. Y. & Tsai, M. J. Molecular mechanisms of androgen-independent growth of human prostate cancer LNCaP-AI cells. *Endocrinology* **140**, 5054–5059 (1999).
303. Yanase, T. & Fan, W. Modification of androgen receptor function by IGF-1 signaling implications in the mechanism of refractory prostate carcinoma. *Vitam Horm* **80**, 649–666 (2009).
304. Wang, Y. *et al.* Change of the cell cycle after flutamide treatment in prostate cancer cells and its molecular mechanism. *Asian J Androl* **7**, 375–380 (2005).
305. Huang, S.-B. *et al.* Androgen deprivation-induced elevated nuclear SIRT1 promotes prostate tumor cell survival by reactivation of AR signaling. *Cancer Letters* **505**, 24–36 (2021).
306. Di Nardo, G. & Gilardi, G. Human aromatase: perspectives in biochemistry and biotechnology. *Biotechnol Appl Biochem* **60**, 92–101 (2013).
307. Chinnam, M. *et al.* MDM2 E3 ligase activity is essential for p53 regulation and cell cycle integrity. *PLoS Genet* **18**, e1010171 (2022).
308. The UniProt Consortium. UniProt: the Universal Protein Knowledgebase in 2023. *Nucleic Acids Research* **51**, D523–D531 (2023).
309. Gartel, A. L. & Tyner, A. L. Transcriptional regulation of the p21((WAF1/CIP1)) gene. *Exp Cell Res* **246**, 280–289 (1999).
310. Nag, S., Qin, J., Srivenugopal, K. S., Wang, M. & Zhang, R. The MDM2-p53 pathway revisited. *J Biomed Res* **27**, 254–271 (2013).
311. Broude, E. V. *et al.* p21 (CDKN1A) is a negative regulator of p53 stability. *Cell Cycle* **6**, 1468–1471 (2007).

312. Shi, D. & Gu, W. Dual Roles of MDM2 in the Regulation of p53: Ubiquitination Dependent and Ubiquitination Independent Mechanisms of MDM2 Repression of p53 Activity. *Genes Cancer* **3**, 240–248 (2012).
313. Zhang, Z. *et al.* MDM2 is a negative regulator of p21WAF1/CIP1, independent of p53. *J Biol Chem* **279**, 16000–16006 (2004).
314. Wang, B. *et al.* 14-3-3 τ Regulates Ubiquitin-Independent Proteasomal Degradation of p21, a Novel Mechanism of p21 Downregulation in Breast Cancer. *Molecular and Cellular Biology* **30**, 1508–1527 (2010).
315. Xu, H., Zhang, Z., Li, M. & Zhang, R. MDM2 promotes proteasomal degradation of p21Waf1 via a conformation change. *J Biol Chem* **285**, 18407–18414 (2010).
316. Enge, M. *et al.* MDM2-dependent downregulation of p21 and hnRNP K provides a switch between apoptosis and growth arrest induced by pharmacologically activated p53. *Cancer Cell* **15**, 171–183 (2009).
317. Van Waes, C. Nuclear factor-kappaB in development, prevention, and therapy of cancer. *Clin Cancer Res* **13**, 1076–1082 (2007).
318. Xia, L. *et al.* Role of the NF κ B-signaling pathway in cancer. *Onco Targets Ther* **11**, 2063–2073 (2018).
319. Jana, A. *et al.* NF κ B is essential for activin-induced colorectal cancer migration via upregulation of PI3K-MDM2 pathway. *Oncotarget* **8**, 37377–37393 (2017).
320. Busuttill, V. *et al.* NF- κ B inhibits T-cell activation-induced, p73-dependent cell death by induction of MDM2. *Proceedings of the National Academy of Sciences of the United States of America* **107**, 18061–18066 (2010).
321. Thomasova, D., Mulay, S. R., Bruns, H. & Anders, H.-J. p53-Independent Roles of MDM2 in NF- κ B Signaling: Implications for Cancer Therapy, Wound Healing, and Autoimmune Diseases. *Neoplasia* **14**, 1097–1101 (2012).
322. Kim, Y. K. TGF- β 1 induction of p21WAF1/cip1 requires smad-independent protein kinase C signaling pathway. *Arch Pharm Res* **30**, 739–742 (2007).
323. Abbas, T. & Dutta, A. p21 in cancer: intricate networks and multiple activities. *Nat Rev Cancer* **9**, 400–414 (2009).
324. Koo, B.-H., Kim, Y., Je Cho, Y. & Kim, D.-S. Distinct roles of transforming growth factor- β signaling and transforming growth factor- β receptor inhibitor SB431542 in the regulation of p21 expression. *European Journal of Pharmacology* **764**, 413–423 (2015).
325. Freudlsperger, C. *et al.* TGF- β and NF- κ B signal pathway cross-talk is mediated through TAK1 and SMAD7 in a subset of head and neck cancers. *Oncogene* **32**, 1549–1559 (2013).
326. Chetty, A., Cao, G.-J. & Nielsen, H. C. Insulin-like Growth Factor-I signaling mechanisms, type I collagen and alpha smooth muscle actin in human fetal lung fibroblasts. *Pediatr Res* **60**, 389–394 (2006).
327. De Luca, F. Regulatory role of NF- κ B in growth plate chondrogenesis and its functional interaction with Growth Hormone. *Mol Cell Endocrinol* **514**, 110916 (2020).
328. Hofland, J. *et al.* Activin A Stimulates AKR1C3 Expression and Growth in Human Prostate Cancer. *Endocrinology* **153**, 5726–5734 (2012).
329. Koster, R. *et al.* Cytoplasmic p21 expression levels determine cisplatin resistance in human testicular cancer. *J Clin Invest* **120**, 3594–3605 (2010).

330. Moussa, R. S., Kovacevic, Z. & Richardson, D. R. Differential targeting of the cyclin-dependent kinase inhibitor, p21CIP1/WAF1, by chelators with anti-proliferative activity in a range of tumor cell-types. *Oncotarget* **6**, 29694–29711 (2015).
331. Zamagni, A. *et al.* CDKN1A upregulation and cisplatin-pemetrexed resistance in non-small cell lung cancer cells. *International Journal of Oncology* **56**, 1574–1584 (2020).
332. Choi, K.-W., Suh, H., Oh, H. L., Ryou, C. & Lee, C.-H. p21CIP1 Induces Apoptosis via Binding to BCL2 in LNCaP Prostate Cancer Cells Treated with MCS-C3, A Novel Carbocyclic Analog of Pyrrolopyrimidine. *Anticancer Research* **36**, 213–220 (2016).
333. Zhou, B. P. *et al.* Cytoplasmic localization of p21Cip1/WAF1 by Akt-induced phosphorylation in HER-2/neu-overexpressing cells. *Nat Cell Biol* **3**, 245–252 (2001).
334. Vincent, A. J. *et al.* Cytoplasmic translocation of p21 mediates NUPR1-induced chemoresistance: NUPR1 and p21 in chemoresistance. *FEBS Letters* **586**, 3429–3434 (2012).
335. Renty, C. de, DePamphilis, M. L. & Ullah, Z. Cytoplasmic Localization of p21 Protects Trophoblast Giant Cells from DNA Damage Induced Apoptosis. *PLOS ONE* **9**, e97434 (2014).
336. Kreis, N.-N., Louwen, F. & Yuan, J. The Multifaceted p21 (Cip1/Waf1/CDKN1A) in Cell Differentiation, Migration and Cancer Therapy. *Cancers (Basel)* **11**, 1220 (2019).
337. Georgakilas, A. G., Martin, O. A. & Bonner, W. M. p21: A Two-Faced Genome Guardian. *Trends Mol Med* **23**, 310–319 (2017).
338. Zhou, Y. *et al.* Cytoplasmic p21 induced by p65 prevents doxorubicin-induced cell death in pancreatic carcinoma cell line. *Journal of Biomedical Science* **19**, 15 (2012).
339. Luo, Y., Hurwitz, J. & Massagué, J. Cell-cycle inhibition by independent CDK and PCNA binding domains in p21Cip1. *Nature* **375**, 159–161 (1995).
340. Rodríguez-Vilarrupla, A. *et al.* Identification of the nuclear localization signal of p21(cip1) and consequences of its mutation on cell proliferation. *FEBS Lett* **531**, 319–323 (2002).
341. Gawriluk, T. R. *et al.* Comparative analysis of ear-hole closure identifies epimorphic regeneration as a discrete trait in mammals. *Nat Commun* **7**, 11164 (2016).
342. Singh, S. K., Banerjee, S., Acosta, E. P., Lillard, J. W. & Singh, R. Resveratrol induces cell cycle arrest and apoptosis with docetaxel in prostate cancer cells via a p53/ p21 WAF1/CIP1 and p27 KIP1 pathway. *Oncotarget* **8**, 17216–17228 (2017).
343. Gartel, A. L. & Tyner, A. L. The role of the cyclin-dependent kinase inhibitor p21 in apoptosis. *Mol Cancer Ther* **1**, 639–649 (2002).
344. Dong, C., Li, Q., Lyu, S.-C., Krensky, A. M. & Clayberger, C. A novel apoptosis pathway activated by the carboxyl terminus of p21. *Blood* **105**, 1187–1194 (2005).
345. Baba, A. B. *et al.* Transforming Growth Factor-Beta (TGF- β) Signaling in Cancer-A Betrayal Within. *Front Pharmacol* **13**, 791272 (2022).
346. Romanov, V. S. & Rudolph, K. L. p21 shapes cancer evolution. *Nat Cell Biol* **18**, 722–724 (2016).
347. Romanov, V. S., Pospelov, V. A. & Pospelova, T. V. Cyclin-dependent kinase inhibitor p21(Waf1): contemporary view on its role in senescence and oncogenesis. *Biochemistry (Mosc)* **77**, 575–584 (2012).
348. Herbig, U. & Sedivy, J. M. Regulation of growth arrest in senescence: telomere damage is not the end of the story. *Mech Ageing Dev* **127**, 16–24 (2006).
349. Beauséjour, C. M. *et al.* Reversal of human cellular senescence: roles of the p53 and p16 pathways. *EMBO J* **22**, 4212–4222 (2003).

350. Rayess, H., Wang, M. B. & Srivatsan, E. S. Cellular senescence and tumor suppressor gene p16. *International Journal of Cancer* **130**, 1715–1725 (2012).
351. Liu, J.-Y. *et al.* Cells exhibiting strong p16INK4a promoter activation in vivo display features of senescence. *Proceedings of the National Academy of Sciences* **116**, 2603–2611 (2019).
352. Wagner, K.-D. & Wagner, N. The Senescence Markers p16INK4A, p14ARF/p19ARF, and p21 in Organ Development and Homeostasis. *Cells* **11**, 1966 (2022).
353. Gorgoulis, V. *et al.* Cellular Senescence: Defining a Path Forward. *Cell* **179**, 813–827 (2019).
354. López-Otín, C., Blasco, M. A., Partridge, L., Serrano, M. & Kroemer, G. Hallmarks of aging: An expanding universe. *Cell* **186**, 243–278 (2023).
355. Fischer, C. A. *et al.* Co-overexpression of p21 and Ki-67 in head and neck squamous cell carcinoma relative to a significantly poor prognosis. *Head Neck* **33**, 267–273 (2011).
356. Barney, L. E. *et al.* Tumor cell-organized fibronectin maintenance of a dormant breast cancer population. *Science Advances* **6**, eaaz4157 (2020).
357. Sun, X. *et al.* Ki-67 Contributes to Normal Cell Cycle Progression and Inactive X Heterochromatin in p21 Checkpoint-Proficient Human Cells. *Molecular and Cellular Biology* **37**, e00569-16 (2017).
358. Kumar, S. *et al.* Cyclin-dependent kinase inhibitor p21 and proliferative marker ki67 in colonic carcinoma. *J Cancer Res Ther* **18**, 915–920 (2022).
359. Childs, B. G. *et al.* Senescent cells: an emerging target for diseases of ageing. *Nat Rev Drug Discov* **16**, 718–735 (2017).
360. Admasu, T. D., Rae, M. J. & Stolzing, A. Dissecting primary and secondary senescence to enable new senotherapeutic strategies. *Ageing Research Reviews* **70**, 101412 (2021).
361. Wang, L., Zuo, X., Xie, K. & Wei, D. The Role of CD44 and Cancer Stem Cells. in *Cancer Stem Cells: Methods and Protocols* (eds. Papaccio, G. & Desiderio, V.) 31–42 (Springer, 2018). doi:10.1007/978-1-4939-7401-6_3.
362. Shen, Y.-A. *et al.* CD44 and CD24 coordinate the reprogramming of nasopharyngeal carcinoma cells towards a cancer stem cell phenotype through STAT3 activation. *Oncotarget* **7**, 58351–58366 (2016).
363. Guo, L. *et al.* TDP43 promotes stemness of breast cancer stem cells through CD44 variant splicing isoforms. *Cell Death Dis* **13**, 1–11 (2022).
364. Kim, Y.-D. *et al.* ESRP1-Induced CD44 v3 Is Important for Controlling Pluripotency in Human Pluripotent Stem Cells. *STEM CELLS* **36**, 1525–1534 (2018).
365. De Blander, H., Morel, A.-P., Senaratne, A. P., Ouzounova, M. & Puisieux, A. Cellular Plasticity: A Route to Senescence Exit and Tumorigenesis. *Cancers (Basel)* **13**, 4561 (2021).
366. Milanovic, M. *et al.* Senescence-associated reprogramming promotes cancer stemness. *Nature* **553**, 96–100 (2018).
367. Mosteiro, L., Pantoja, C., de Martino, A. & Serrano, M. Senescence promotes in vivo reprogramming through p16INK4a and IL-6. *Aging Cell* **17**, e12711 (2018).
368. Geneva: World Health Organization. WHO COVID-19 Dashboard. <https://covid19.who.int/more-resources> (2020).
369. Yan, Y. *et al.* The First 75 Days of Novel Coronavirus (SARS-CoV-2) Outbreak: Recent Advances, Prevention, and Treatment. *Int J Environ Res Public Health* **17**, 2323 (2020).
370. Holmes, E. C. *et al.* The origins of SARS-CoV-2: A critical review. *Cell* **184**, 4848–4856 (2021).

371. Hardenbrook, N. J. & Zhang, P. A structural view of the SARS-CoV-2 virus and its assembly. *Current Opinion in Virology* **52**, 123–134 (2022).
372. Mariano, G., Farthing, R. J., Lale-Farjat, S. L. M. & Bergeron, J. R. C. Structural Characterization of SARS-CoV-2: Where We Are, and Where We Need to Be. *Frontiers in Molecular Biosciences* **7**, (2020).
373. Luring, A. S., Frydman, J. & Andino, R. The role of mutational robustness in RNA virus evolution. *Nat Rev Microbiol* **11**, 327–336 (2013).
374. Wong, A. H. M. *et al.* Receptor-binding loops in alphacoronavirus adaptation and evolution. *Nature Communications* **8**, 1–10 (2017).
375. Isabel, S. *et al.* Evolutionary and structural analyses of SARS-CoV-2 D614G spike protein mutation now documented worldwide. *Sci Rep* **10**, 14031 (2020).
376. Thakur, V. *et al.* Waves and variants of SARS-CoV-2: understanding the causes and effect of the COVID-19 catastrophe. *Infection* **50**, 309–325 (2022).
377. Hu, B., Guo, H., Zhou, P. & Shi, Z.-L. Characteristics of SARS-CoV-2 and COVID-19. *Nat Rev Microbiol* **19**, 141–154 (2021).
378. Kim, G. -u. *et al.* Clinical characteristics of asymptomatic and symptomatic patients with mild COVID-19. *Clinical Microbiology and Infection* **26**, 948.e1-948.e3 (2020).
379. Song, J.-W. *et al.* Immunological and inflammatory profiles in mild and severe cases of COVID-19. *Nat Commun* **11**, 3410 (2020).
380. Epidemiology Working Group for NCIP Epidemic Response, Chinese Center for Disease Control and Prevention. [The epidemiological characteristics of an outbreak of 2019 novel coronavirus diseases (COVID-19) in China]. *Zhonghua Liu Xing Bing Xue Za Zhi* **41**, 145–151 (2020).
381. Gebhard, C., Regitz-Zagrosek, V., Neuhauser, H. K., Morgan, R. & Klein, S. L. Impact of sex and gender on COVID-19 outcomes in Europe. *Biol Sex Differ* **11**, 29 (2020).
382. Qi, S. *et al.* Sex differences in the immune response to acute COVID-19 respiratory tract infection. *Biology of Sex Differences* **12**, 66 (2021).
383. Takahashi, T. *et al.* Sex differences in immune responses that underlie COVID-19 disease outcomes. *Nature* **588**, 315–320 (2020).
384. Jin, H.-J., Kim, J. & Yu, J. Androgen receptor genomic regulation. *Translational Andrology and Urology* **2**, 15877–15177 (2013).
385. Cao, W., Feng, Q. & Wang, X. Computational analysis of TMPRSS2 expression in normal and SARS-CoV-2-infected human tissues. *Chemico-Biological Interactions* **346**, 109583 (2021).
386. Wang, Q. *et al.* A Hierarchical Network of Transcription Factors Governs Androgen Receptor-Dependent Prostate Cancer Growth. *Molecular Cell* **27**, 380–392 (2007).
387. Clinckemalie, L. *et al.* Androgen Regulation of the TMPRSS2 Gene and the Effect of a SNP in an Androgen Response Element. *Mol Endocrinol* **27**, 2028–2040 (2013).
388. Matsuyama, S. *et al.* Efficient Activation of the Severe Acute Respiratory Syndrome Coronavirus Spike Protein by the Transmembrane Protease TMPRSS2. *Journal of Virology* **84**, 12658–12664 (2010).
389. Glowacka, I. *et al.* Evidence that TMPRSS2 Activates the Severe Acute Respiratory Syndrome Coronavirus Spike Protein for Membrane Fusion and Reduces Viral Control by the Humoral Immune Response. *Journal of Virology* **85**, 4122–4134 (2011).

390. Hoffmann, M. *et al.* SARS-CoV-2 Cell Entry Depends on ACE2 and TMPRSS2 and Is Blocked by a Clinically Proven Protease Inhibitor. *Cell* (2020) doi:10.1016/j.cell.2020.02.052.
391. Jin, J.-M. *et al.* Gender Differences in Patients With COVID-19: Focus on Severity and Mortality. *Front. Public Health* **8**, (2020).
392. Peckham, H. *et al.* Male sex identified by global COVID-19 meta-analysis as a risk factor for death and ICU admission. *Nat Commun* **11**, 6317 (2020).
393. Grasselli, G. *et al.* Baseline Characteristics and Outcomes of 1591 Patients Infected With SARS-CoV-2 Admitted to ICUs of the Lombardy Region, Italy. *JAMA* **323**, 1574–1581 (2020).
394. Zhu, N. *et al.* Morphogenesis and cytopathic effect of SARS-CoV-2 infection in human airway epithelial cells. *Nat Commun* **11**, 3910 (2020).
395. Scully, E. P., Haverfield, J., Ursin, R. L., Tannenbaum, C. & Klein, S. L. Considering how biological sex impacts immune responses and COVID-19 outcomes. *Nature Reviews Immunology* **20**, 442–447 (2020).
396. The Sex, Gender and COVID-19 Project. The COVID-19 Sex-Disaggregated Data Tracker | Global Health 50/50. <https://globalhealth5050.org/the-sex-gender-and-covid-19-project/the-data-tracker/> (2021).
397. Karlberg, J., Chong, D. S. Y. & Lai, W. Y. Y. Do Men Have a Higher Case Fatality Rate of Severe Acute Respiratory Syndrome than Women Do? *American Journal of Epidemiology* **159**, 229–231 (2004).
398. Price-Haywood, E. G., Burton, J., Fort, D. & Seoane, L. Hospitalization and Mortality among Black Patients and White Patients with Covid-19. *N Engl J Med* **382**, 2534–2543 (2020).
399. Klein, S. L. & Flanagan, K. L. Sex differences in immune responses. *Nat Rev Immunol* **16**, 626–638 (2016).
400. Cephus, J. *et al.* Testosterone attenuates group 2 innate lymphoid cell-mediated airway inflammation. *Cell Rep* **21**, 2487–2499 (2017).
401. Laffont, S. & Guéry, J.-C. Chapter Two - Deconstructing the sex bias in allergy and autoimmunity: From sex hormones and beyond. in *Advances in Immunology* (ed. Alt, F.) vol. 142 35–64 (Academic Press, 2019).
402. Oliva, M. *et al.* The impact of sex on gene expression across human tissues. *Science* **369**, eaba3066 (2020).
403. Baratchian, M. *et al.* Androgen regulation of pulmonary AR, TMPRSS2 and ACE2 with implications for sex-discordant COVID-19 outcomes. *Sci Rep* **11**, 11130 (2021).
404. Rastrelli, G. *et al.* Low testosterone levels predict clinical adverse outcomes in SARS-CoV-2 pneumonia patients. *Andrology* **9**, 88–98 (2021).
405. Salonia, A. *et al.* Severely low testosterone in males with COVID-19: A case-control study. *Andrology* **9**, 1043–1052 (2021).
406. Grein, J. *et al.* Compassionate Use of Remdesivir for Patients with Severe Covid-19. *New England Journal of Medicine* **382**, 2327–2336 (2020).
407. Vermeulen, A., Verdonck, L. & Kaufman, J. M. A critical evaluation of simple methods for the estimation of free testosterone in serum. *J Clin Endocrinol Metab* **84**, 3666–3672 (1999).
408. Maecker, H. T., McCoy, J. P. & Nussenblatt, R. Standardizing immunophenotyping for the Human Immunology Project. *Nat Rev Immunol* **12**, 191–200 (2012).
409. Garcia-Prat, M. *et al.* Extended immunophenotyping reference values in a healthy pediatric population. *Cytometry Part B: Clinical Cytometry* **96**, 223–233 (2019).

410. Zhang, J., Yu, M., Tong, S., Liu, L.-Y. & Tang, L.-V. Predictive factors for disease progression in hospitalized patients with coronavirus disease 2019 in Wuhan, China. *Journal of Clinical Virology* **127**, 104392 (2020).
411. Huang, C. *et al.* Clinical features of patients infected with 2019 novel coronavirus in Wuhan, China. *The Lancet* **395**, 497–506 (2020).
412. Laguna-Goya, R. *et al.* IL-6–based mortality risk model for hospitalized patients with COVID-19. *J Allergy Clin Immunol* **146**, 799–807.e9 (2020).
413. Kreutmair, S. *et al.* Distinct immunological signatures discriminate severe COVID-19 from non-SARS-CoV-2-driven critical pneumonia. *Immunity* **54**, 1578–1593.e5 (2021).
414. Lucas, C. *et al.* Longitudinal analyses reveal immunological misfiring in severe COVID-19. *Nature* **584**, 463–469 (2020).
415. Kvedaraitė, E. *et al.* Major alterations in the mononuclear phagocyte landscape associated with COVID-19 severity. *Proceedings of the National Academy of Sciences* **118**, e2018587118 (2021).
416. Kuri-Cervantes, L. *et al.* Comprehensive mapping of immune perturbations associated with severe COVID-19. *Science Immunology* **5**, eabd7114 (2020).
417. Bastard, P. *et al.* Autoantibodies against type I IFNs in patients with life-threatening COVID-19. *Science* **370**, eabd4585 (2020).
418. Chakravarty, D. *et al.* Sex differences in SARS-CoV-2 infection rates and the potential link to prostate cancer. *Communications Biology* **3**, 1–12 (2020).
419. Meng, Y. *et al.* Sex-specific clinical characteristics and prognosis of coronavirus disease-19 infection in Wuhan, China: A retrospective study of 168 severe patients. *PLOS Pathogens* **16**, e1008520 (2020).
420. ten-Caten, F. *et al.* In-depth analysis of laboratory parameters reveals the interplay between sex, age, and systemic inflammation in individuals with COVID-19. *International Journal of Infectious Diseases* **105**, 579–587 (2021).
421. Noymer, A. & Garenne, M. The 1918 Influenza Epidemic’s Effects on Sex Differentials in Mortality in the United States. *Population and Development Review* **26**, 565–581 (2000).
422. Dhindsa, S. *et al.* Association of Circulating Sex Hormones With Inflammation and Disease Severity in Patients With COVID-19. *JAMA Network Open* **4**, e2111398 (2021).
423. Venet, F. *et al.* Longitudinal assessment of IFN-I activity and immune profile in critically ill COVID-19 patients with acute respiratory distress syndrome. *Critical Care* **25**, 140 (2021).
424. Friedrich, O. *et al.* The Sick and the Weak: Neuropathies/Myopathies in the Critically Ill. *Physiological Reviews* **95**, 1025–1109 (2015).
425. Malkin, C. J. *et al.* The Effect of Testosterone Replacement on Endogenous Inflammatory Cytokines and Lipid Profiles in Hypogonadal Men. *The Journal of Clinical Endocrinology & Metabolism* **89**, 3313–3318 (2004).
426. Hikmet, F., Méar, L., Uhlén, M. & Lindskog, C. The protein expression profile of ACE2 in human tissues. *bioRxiv* 2020.03.31.016048 (2020) doi:10.1101/2020.03.31.016048.
427. Guo, J. *et al.* The adult human testis transcriptional cell atlas. *Cell Res* **28**, 1141–1157 (2018).
428. Yang, M. *et al.* Pathological Findings in the Testes of COVID-19 Patients: Clinical Implications. *European Urology Focus* **6**, 1124–1129 (2020).
429. Wu, F. C. W. *et al.* Identification of Late-Onset Hypogonadism in Middle-Aged and Elderly Men. *New England Journal of Medicine* **363**, 123–135 (2010).

430. Mulligan, T., Iranmanesh, A. & Veldhuis, J. D. Pulsatile iv Infusion of Recombinant Human LH in Leuprolide-Suppressed Men Unmasks Impoverished Leydig-Cell Secretory Responsiveness to Midphysiological LH Drive in the Aging Male. *The Journal of Clinical Endocrinology & Metabolism* **86**, 5547–5553 (2001).
431. Zhang, C. *et al.* FOXO4-DRI alleviates age-related testosterone secretion insufficiency by targeting senescent Leydig cells in aged mice. *Aging* **12**, 1272–1284 (2020).
432. Velazquez-Salinas, L., Verdugo-Rodriguez, A., Rodriguez, L. L. & Borca, M. V. The Role of Interleukin 6 During Viral Infections. *Frontiers in Microbiology* **10**, (2019).
433. Carsetti, R. *et al.* Different Innate and Adaptive Immune Responses to SARS-CoV-2 Infection of Asymptomatic, Mild, and Severe Cases. *Frontiers in Immunology* **11**, (2020).
434. Zhang, J.-Y. *et al.* Single-cell landscape of immunological responses in patients with COVID-19. *Nat Immunol* **21**, 1107–1118 (2020).
435. Kapellos, T. S. *et al.* Human Monocyte Subsets and Phenotypes in Major Chronic Inflammatory Diseases. *Frontiers in Immunology* **10**, (2019).
436. Kuri-Cervantes, L. *et al.* Comprehensive mapping of immune perturbations associated with severe COVID-19. *Science Immunology* **5**, eabd7114 (2020).
437. Brooks, D. G., Teyton, L., Oldstone, M. B. A. & McGavern, D. B. Intrinsic Functional Dysregulation of CD4 T Cells Occurs Rapidly following Persistent Viral Infection. *Journal of Virology* **79**, 10514–10527 (2005).
438. Chen, Z. & John Wherry, E. T cell responses in patients with COVID-19. *Nat Rev Immunol* **20**, 529–536 (2020).
439. Diao, B. *et al.* Reduction and Functional Exhaustion of T Cells in Patients With Coronavirus Disease 2019 (COVID-19). *Frontiers in Immunology* **11**, (2020).
440. Kusnadi, A. *et al.* Severely ill patients with COVID-19 display impaired exhaustion features in SARS-CoV-2–reactive CD8+ T cells. *Science Immunology* **6**, eabe4782 (2021).
441. André, S. *et al.* T cell apoptosis characterizes severe Covid-19 disease. *Cell Death Differ* **29**, 1486–1499 (2022).
442. Liva, S. M. & Voskuhl, R. R. Testosterone Acts Directly on CD4+ T Lymphocytes to Increase IL-10 Production. *The Journal of Immunology* **167**, 2060–2067 (2001).
443. Furman, D. *et al.* Systems analysis of sex differences reveals an immunosuppressive role for testosterone in the response to influenza vaccination. *Proceedings of the National Academy of Sciences* **111**, 869–874 (2014).
444. Gubbels Bupp, M. R. & Jorgensen, T. N. Androgen-Induced Immunosuppression. *Frontiers in Immunology* **9**, (2018).
445. Corrales, J. J. *et al.* Enhanced immunological response by dendritic cells in male hypogonadism. *European Journal of Clinical Investigation* **42**, 1205–1212 (2012).
446. Lai, J.-J. *et al.* Androgen Receptor Influences on Body Defense System via Modulation of Innate and Adaptive Immune Systems: Lessons from Conditional AR Knockout Mice. *The American Journal of Pathology* **181**, 1504–1512 (2012).
447. Brown, M. A. & Su, M. A. An Inconvenient Variable: Sex Hormones and Their Impact on T Cell Responses. *The Journal of Immunology* **202**, 1927–1933 (2019).
448. Consiglio, C. R. & Gollnick, S. O. Androgen Receptor Signaling Positively Regulates Monocytic Development. *Frontiers in Immunology* **11**, (2020).

449. Sutherland, J. S. *et al.* Activation of Thymic Regeneration in Mice and Humans following Androgen Blockade. *The Journal of Immunology* **175**, 2741–2753 (2005).
450. van Dommelen, S. L. *et al.* Regeneration of dendritic cells in aged mice. *Cell Mol Immunol* **7**, 108–115 (2010).
451. Morse, M. D. & McNeel, D. G. Prostate cancer patients on androgen deprivation therapy develop persistent changes in adaptive immune responses. *Human Immunology* **71**, 496–504 (2010).

ANNEX: PUBLICATIONS

1. **C1 esterase inhibitor and the contact system in COVID-19**

Timothy M. Thomson, **Emily Toscano-Guerra**, Ernesto Casis & Rosanna Paciucci. *British Journal of Haematology* 2020. 190: 520-524. <https://doi.org/10.1111/bjh.16938>

2. **Recovery of serum testosterone levels is an accurate predictor of survival from COVID-19 in male patients.**

Emily Toscano-Guerra, Mónica Martínez-Gallo, Iria Arrese-Muñoz, Anna Giné, Noelia Díaz-Troyano, Pablo Gabriel-Medina, Mar Riveiro-Barciela, Moisés Labrador-Horrillo, Fernando Martinez-Valle, Adrián Sánchez Montalvá, Manuel Hernández-González, Ricardo Pujol Borrell, Francisco Rodríguez-Frias, Roser Ferrer, Timothy M. Thomson & Rosanna Paciucci. *BMC Medicine* 2022. 20:129. <https://doi.org/10.1186/s12916-022-02345-w>